N79 27532 UNC

MICROCOPY RESOLUTION TEST CHART
NATIONAL BUREAU OF STANDARDS-1963-A

NASA

National Aeronautics and
Space Administration

ENERGY EFFICIENT ENGINE
FAN TEST HARDWARE DETAILED DESIGN REPORT

by

T.J. Sullivan, G.W. Luebering, and R.D. Gravitt

General Electric Company
Aircraft Engine Business Group

MAR 1981
RECEIVED
NASA STI FACILITY
ACCESS DEPT.

Prepared for

National Aeronautics and Space Administration

RELEASE DATE:

PUBLICLY RELEASE ON JANUARY 31, 1983

1. Report No. NASA CR-165148	2. Government Accession No.	3. Recipient's Catalog No.
4. Title and Subtitle Energy Efficient Engine Fan Test Hardware Detailed Design Report		5. Report Date October 1980
		6. Performing Organization Code
7. Author(s) T.J. Sullivan, G.W. Luebering, and R.D. Gravitt		8. Performing Organization Report No R80-AEG-417
		10. Work Unit No.
9. Performing Organization Name and Address General Electric Company Aircraft Engine Business Group Cincinnati, Ohio 45215		
		11. Contract or Grant No. NAS3-20643
		13. Type of Report and Period Covered Topical Report
12. Sponsoring Agency Name and Address NASA-Lewis Research Center 21000 Brookpark Road Cleveland, Ohio 44135		
		14. Sponsoring Agency Code

15. Supplementary Notes

NASA Project Manager - Carl C. Ciepluch
GE Project Manager - Thomas L. Hampton

16. Abstract

A single-stage fan and quarter-stage booster were designed for the Energy Efficient Engine. The fan has an inlet radius ratio of 0.342 and a specific flow rate of 208.9 Kg/S-M^2 (42.8 lbm/sec ft^2). The fan rotor has 32 medium-aspect-ratio (2.597) titanium blades with a part-span shroud at 55% blade height. The design corrected fan tip speed is 411.5 M/S (1350 ft/sec). The quarter-stage island splits the total fan flow with approximately 22% of the flow being supercharged by the quarter-stage rotor. The fan bypass ratio is 6.8. The core flow total pressure ratio is 1.67 and the fan bypass pressure ratio is 1.65. This report contains the design details of the fan and booster blading, and the fan frame and static structure for the E^3 fan configuration.

17. Key Words (Suggested by Author(s)) Single Stage Fan and Booster Turbofan Engine Energy Efficient Engine		18. Distribution Statement	
19. Security Classif. (of this report) Unclassified	20. Security Classif. (of this page) Unclassified	21. No. of Pages 138	22. Price*

Foreword

This report presents the results of the fan aerodynamic and mechanical design performed by the General Electric Company for the National Aeronautics and Space Administration, Lewis Research Center, under Contract NAS3-20643. This work was performed as part of the Aircraft Energy Efficiency (ACEE) Program, Energy Efficient Engine (E^3) Project. Mr. Carl C. Ciepluch is the NASA Project Manager and Mr. Lawrence E. Macioce is the NASA Assistant Project Manager. Mr. Roy D. Hager is the NASA Project Engineer responsible for managing the effort associated with the fan component design presented in this report. Mr. T.L. Hampton is the Manager of the Energy Efficient Engine Project for the General Electric Company. This report was prepared by Messrs. T.J. Sullivan, G.W. Luebering, and R.D. Gravitt of the General Electric Company, Evendale, Ohio.

TABLE OF CONTENTS

TABLE OF CONTENTS (Concluded)

iv

LIST OF ILLUSTRATIONS

LIST OF ILLUSTRATIONS (Continued)

LIST OF ILLUSTRATIONS (Concluded)

LIST OF TABLES

INTRODUCTION AND SUMMARY

The detailed aerodynamic and mechanical design of the fan and quarter-stage configuration for the Energy Efficient Engine (E[3]) is described herein. The fan design was initiated following an extensive preliminary design study of alternate fan configurations. The selected fan configuration (Figure 1) uses a quarter-stage booster to provide the required core supercharging. This design was chosen over a single-stage rotor with a higher tip speed and a more highly loaded hub due to its higher core-stream efficiency potential and an easier growth path for future engine development. The fan bypass stream also has a higher efficiency potential by reason of the lower fan speed. Additionally, the quarter-stage island arrangement provides an excellent means for separating foreign objects from the core flow. The flowpath was made to be nearly optimum for the flight propulsion cycle, with some provisions to accommodate a potential growth application. The aerodynamic design point corresponds to the maximum climb power setting at Mach 0.80 and 35,000-feet altitude.

The fan has an inlet radius ratio of 0.342 and a specific flow rate of 208.9 kg/s-m^2 (42.8 lbm/sec-ft^2). The fan rotor has 32 medium aspect-ratio (AR) titanium blades with a part-span shroud at 55% blade height. The design corrected fan tip speed is 411.5 m/s (1350 ft/sec). The quarter-stage island splits the total fan flow so that approximately 22% of the total flow is supercharged by the quarter-stage rotor. Downstream of the booster rotor, the flow is further split with 42% of the booster flow reentering the bypass duct and the remaining flow directed through the core duct into the 10-stage compressor. The total bypass ratio is 6.8. The core flow total-pressure ratio is 1.67 and the fan bypass total-pressure ratio is 1.65.

The rotor structure features an aluminum nonstructural spinner with the latest ice-resistant configuration, a titanium high-bore ring disk for coupled blade-disk mode stiffness and internal fan-structure accessibility, a one-piece titanium quarter-stage spool, and a steel fan shaft arrangement that allows for disassembly of either the shaft, the entire fan rotor, or the fan module (rotor and stator) from the high pressure compressor forward face.

The containment ring for the ICLS fan is a slave design consisting of a modified CF6 steel outercasing with bolted-in wooden flowpath panels. A steel slave integral vane-frame supports the casing and ultimately the rotor, through an attached bearing support cone and bearing.

The axial spacing between the fan rotor trailing edge and the bypass outlet guide vanes (which also serve as the fan frame structural members) is approximately 1.8 rotor-tip chords. made large in order to minimize fan noise generation. The bypass vane-frame airfoils are grouped into five different camber types positioned circumferentially to minimize the distortion of the flow field, recognizing the presence of the pylon at the top of the engine. .
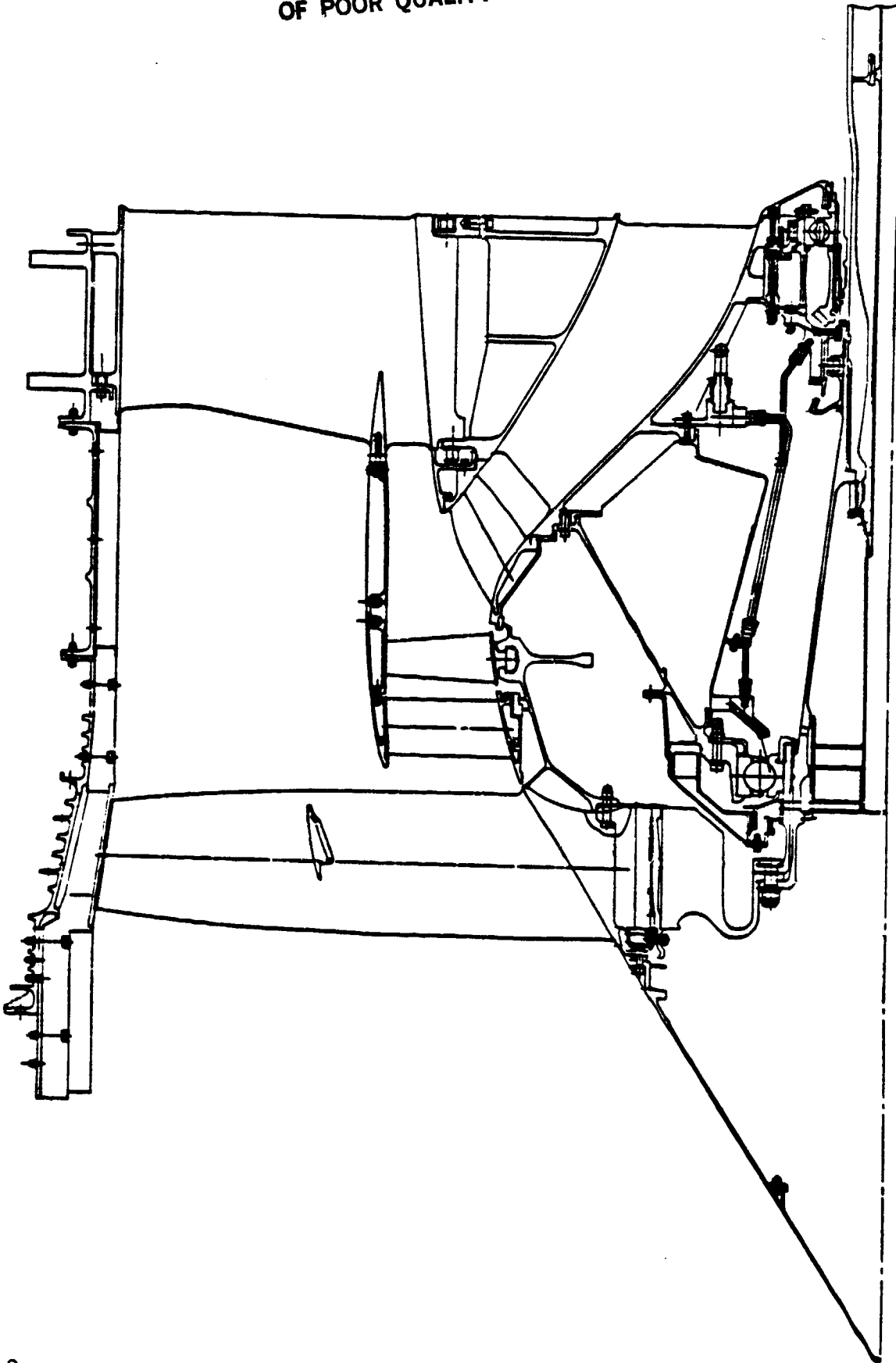
Figure 1. ICLS Fan Configuration.

The airfoils and rotor structure have been designed for a service life of 36,000 missions with two stress cycles per mission. The fan structure is designed to be capable of sustaining stall events with no mechanical damage, and there are no coupled-mode resonances predicted in the operating-speed range between the rotor and fan case. All material-properties data in the fan design are based on average minus three standard deviations properties, including section size considerations.

AERODYNAMIC DESIGN

I. FLOWPATH AND VECTOR DIAGRAM DESIGN

A. Aerodynamic Design Requirements and Growth Considerations

The principal aerodynamic characteristics of the fan at three key operating points are shown in Table I. The aerodynamic design point coincides with the maximum climb condition of the Flight Propulsion System (FPS) cycle. The selected flowpath is shown in Figure 2 with the pertinent aerodynamic design parameters indicated. The fan tip diameter at the rotor inlet is 2.108 meters (83 inches) and the inlet hub-to-tip radius ratio is 0.342. The fan operates at a design tip speed of 411.5 m/s (1350 ft/sec) with a specific flow rate of 208.9 $kg/s-m^2$ (42.8 $lbm/sec-ft^2$) of rotor inlet annulus area. A quarter stage, or booster, is added to increase the fan hub pressure ratio and help separate foreign objects from the core flow. The fan rotor has 32 medium-aspect-ratio blades with a part-span shroud at 55% blade height based on the stacking axis. The spinner cone half angle is 32°, and the slightly contoured fan hub approximately follows that angle.

The total fan flow is split by the quarter-stage island with 22.3% of the flow passing under the island and supercharged by the quarter-stage rotor. Before entering the core duct, the flow is further split with approximately 42% of the quarter-stage flow reentering the bypass stream. The flow that enters the core duct has a total-pressure ratio of 1.67. After 1.8% duct pressure loss is sustained, the flow enters the core compressor with a corrected airflow of 54.4 kg/s (120 lbm/sec). The airflow that passes over the upper surface of the island rejoins the flow that is spilled from the quarter stage to give an average total-pressure ratio of 1.65 at the bypass vane-frame exit plane. The total bypass ratio is 6.8 at the aerodynamic design point.

Since it is planned to ultimately provide for 20% growth of the E^3 engine by increasing fan speed and quarter-stage aerodynamic loading, the growth fan aerodynamics were considered in a preliminary manner. Table II gives the growth fan requirements as they are currently foreseen. The core stream pressure ratio of 2.05 is substantially higher than the bypass-stream pressure ratio. The design of the fan for the FPS engine has taken into account some design considerations that will allow easy adaptation of the fan to the growth configuration. In the FPS design, the hub radii through the quarter stage are slightly oversized to allow for growth. This introduces a slight weight penalty but without any performance penalty. Hence,

Table I. FPS Fan Aerodynamic Design Requirements.

	Maximum Climb	Maximum Cruise	Takeoff
Corrected Tip Speed, m/sec (ft/sec)	411.5 (1350)	399.6 (1311)	365.2 (1198)
Corrected Airflow, kg/sec (lbm/sec)	643.6 (1419)	634.1 (1398)	577.9 (1274)
Flow/Annulus Area, kg/sec-m^2 (lbm/sec-ft^2)	209.0 (42.8)	206.0 (42.1)	187.0 (38.4)
Bypass Stream Pressure Ratio	1.65	1.61	1.50
Bypass Stream Adiabatic Efficiency, percent	87.9	88.7	90.0
Core Stream Pressure Ratio	1.67	1.63	1.51
Core Stream Adiabatic Efficiency, percent	88.5	89.2	89.7
Bypass Ratio	6.8	6.9	7.3

4
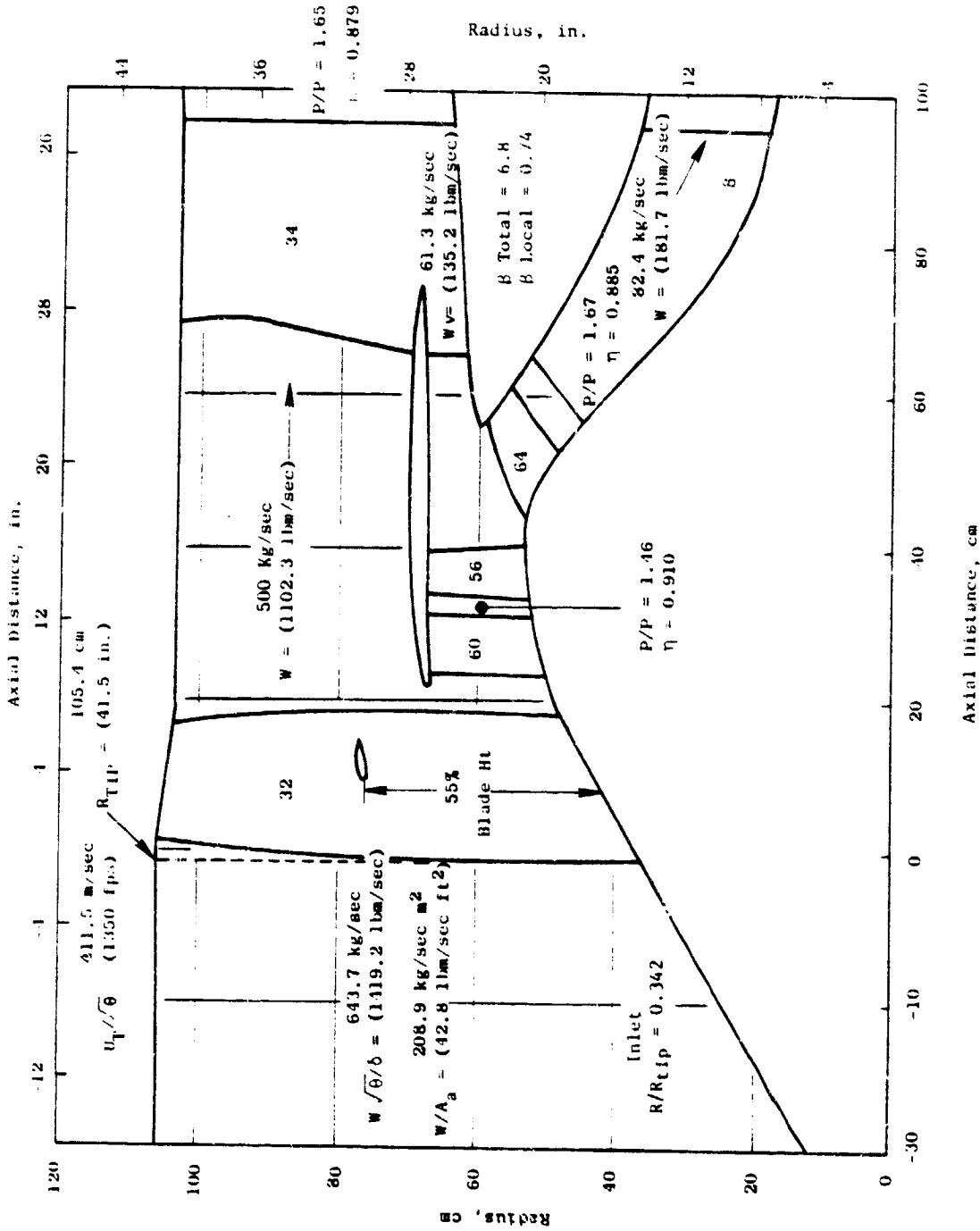
Figure 2. Selected Fan Configuration Flowpath.

Table II. Growth Fan Requirements.

	Maximum Climb	Maximum Cruise	Takeoff
Corrected Tip Speed, m/sec (ft/sec)	457.2 (1500)	446.8 (1466)	420.9 (1381)
Corrected Airflow, kg/sec (lbm/sec)	659.1 (1453)	647.7 (1428)	612.8 (1351)
Flow/Annulus Area, kg/sec-m^2 (lbm/sec-ft^2)	214.0 (43.8)	210.0 (43.0)	198.0 (40.6)
Bypass Stream Pressure Ratio	1.75	1.71	1.60
Bypass Stream Adiabatic Efficiency, percent	86.4	87.2	88.6
Core Stream Pressure Ratio	2.05	2.01	1.90
Core Stream Adiabatic Efficiency, percent	87.6	88.3	88.9
Bypass Ratio	5.5	5.6	6.0

this is thought to be a desirable compromise. It is intended that the bypass vane-frame and inner OGV and core duct hardware will remain the same for both engines. In the growth version, the quarter-stage island moves radially outward approximately 1.0 cm (0.4 in.) at the leading edge to accommodate the larger core flow and mates with the FPS vane-frame at the island trailing edge. The FPS engine casing and hub flowpaths remain the same for the growth engine. The total bypass ratio is reduced to 5.5 for the growth fan. The fan rotor and booster stator and rotor will necessarily be new airfoil designs.

The total pressure ratio profile for the FPS fan is shown in Figure 3. The rotor exit profile as well as the stage exit profiles are shown. The booster rotor turns the tip-strong pressure coming out of the fan hub to the radially constant pressure ratio value of 1.683. In the growth fan, Figure 4, the booster rotor is running approximately 11% faster and produces a substantially higher pressure rise in the region of the flow which enters the core. The hub pressure is made significantly greater than the tip pressure in order to supercharge the core with a 2.05 pressure ratio. The tip pressure is kept low in order to minimize the discontinuity of total pressure coming off the island trailing edge. Experience with similar designs has indicated that the resulting ring vortex sheet does not create downstream instabilities or unexpected losses. The circulation gradient implied by the skewed total pressure profile at the rotor exit will set up substantial secondary flows. These have been estimated, and the mixing that they represent has also been estimated. It was concluded that the rotor blade could be satisfactorily designed for the growth conditions, taking account of the secondary flows, and producing the total-pressure profile shown in Figure 4.

B. Design Point Calculation Procedure and Results

Circumferential-average flow calculations were made at the FPS engine fan aerodynamic design point, which coincides with the maximum climb cycle condition, using the General Electric Circumferential-Average Flow Determination (CAFD) computer program. The calculation procedure of this program is described in Reference 1. Briefly, the flow solution is a radial equilibrium solution including the effects of streamline curvature together with axial gradients of blockage, enthalpy, and entropy. The velocity vector diagrams for the fan and quarter stage were calculated at numerous streamlines from tip to hub throughout the entire flowpath. Calculation stations were used at the leading and trailing edges of each blade row and in the upstream and downstream duct areas to ensure an accurate representation of the flow. In addition to the leading and trailing edge stations, seven calculation stations were located within the fan rotor blade and three within each of the other blade rows. Boundary layer displacement thicknesses on the flowpath walls based on General Electric experience were used. At the internal blade calculation stations, the blockage due to the thickness of the blades or vanes was also included. Flowpath contours, loss coefficients, chordwise work distributions, and spanwise total-pressure distributions were specified; and aerodynamic loadings, velocity diagrams, and fluid properties were calculated for the fan and quarter-stage blade rows.
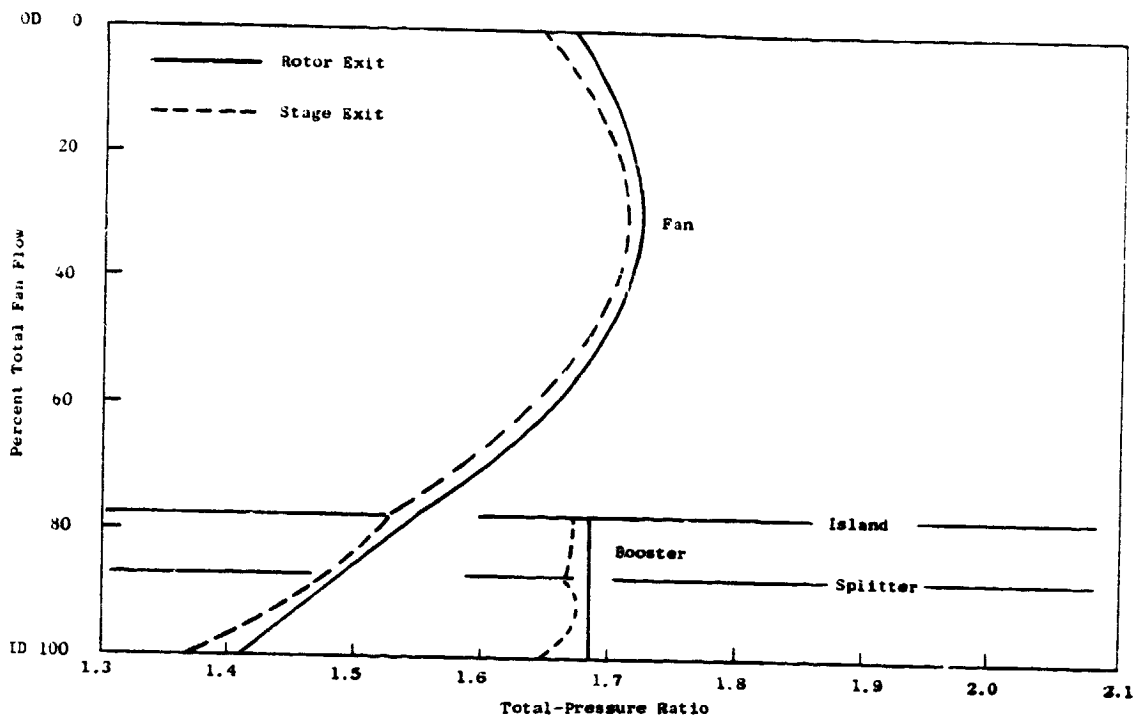
Figure 3. Aerodynamic Design Point Total-Pressure Ratio.
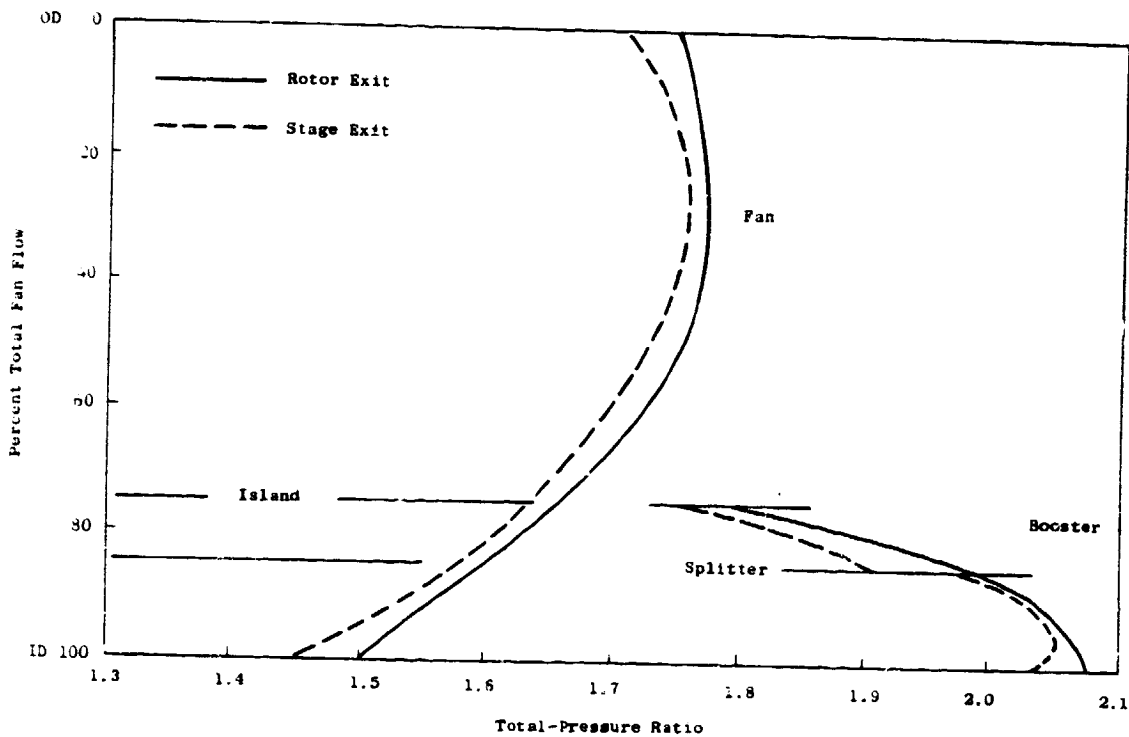
Figure 4. Growth Fan Total-Pressure Ratio.

8

Figures 5 through 9 show the aerodynamic design point parameters. Figure 5 is concerned with the fan rotor and displays the blade inlet and exit relative Mach numbers and flow angles and the blade row total-loss coefficients and diffusion factors. The loss coefficients employed were based on General Electric correlations and experience. The FPS booster rotor loss coefficients are shown in Figure 6 along with the calculated diffusion factors. The booster rotor inlet and exit Mach numbers and flow angles are also shown in Figure 6. These figures show that booster rotor aerodynamic loading is light for the FPS engine, allowing (with an 11% blade speed increase) the booster pressure ratio to be increased substantially for the growth engine.

The booster stator aerodynamic design parameters for the FPS configuration are shown in Figure 7. The inlet and exit Mach numbers and flow angles are shown along with the loss coefficients and diffusion factors. The swirl angle exiting the stator varies from 12° at the tip to 8° at hub; this was specified to give a good loading balance between this vane row and the inner OGV. Similar design point parameters for the inner OGV and bypass OGV are presented in Figures 8 and 9.

The calculated vector diagram quantities are also tabulated in Appendix A.

II. AIRFOIL DESIGN

A. Fan Rotor Blade

The aerodynamic design of the E^3 fan rotor at the maximum climb cycle condition included the definition of airfoil sections which are transonic in the outer region and subsonic near the hub. The fan rotor blade airfoil shapes were specifically tailored for each streamline section using General Electric's Streamsurface Blade Section computer program. In general, the airfoils were shaped in an attempt to minimize shock losses since the inlet Mach numbers are supersonic for all streamlines above the quarter-stage island. Below the island streamline location, the Mach numbers range from 1.02 at 78% flow value to 0.70 at the hub streamline. The airfoils on the hub streamline were patterned after other advanced fan hub airfoil shapes that have shown excellent performance. The designs of the rotor blade sections were performed along 12 axisymmetric streamsurfaces with the surfaces viewed along a radial blade axis using the Streamsurface Blade Section program. The considerations which guide and influence the design of high transonic Mach number cascades such as the E^3 fan rotor are presented and discussed in References 1, 2, and 3.

The fan rotor incidence angles at the aerodynamic design point are approximately 5° all along the span. For sections which have supersonic inlet Mach numbers, the blade inlet region sets the amount of flow the cascade can pass, provided the throat area is not limiting. The blade suction surface upstream of the Mach wave which intersects the leading edge of the adjacent blade was offset a small amount from the "free-flow" streamline to account for the effects of leading edge thickness, bow wave losses, and boundary layer buildup. The free-flow streamline is the direction of the flow if

9
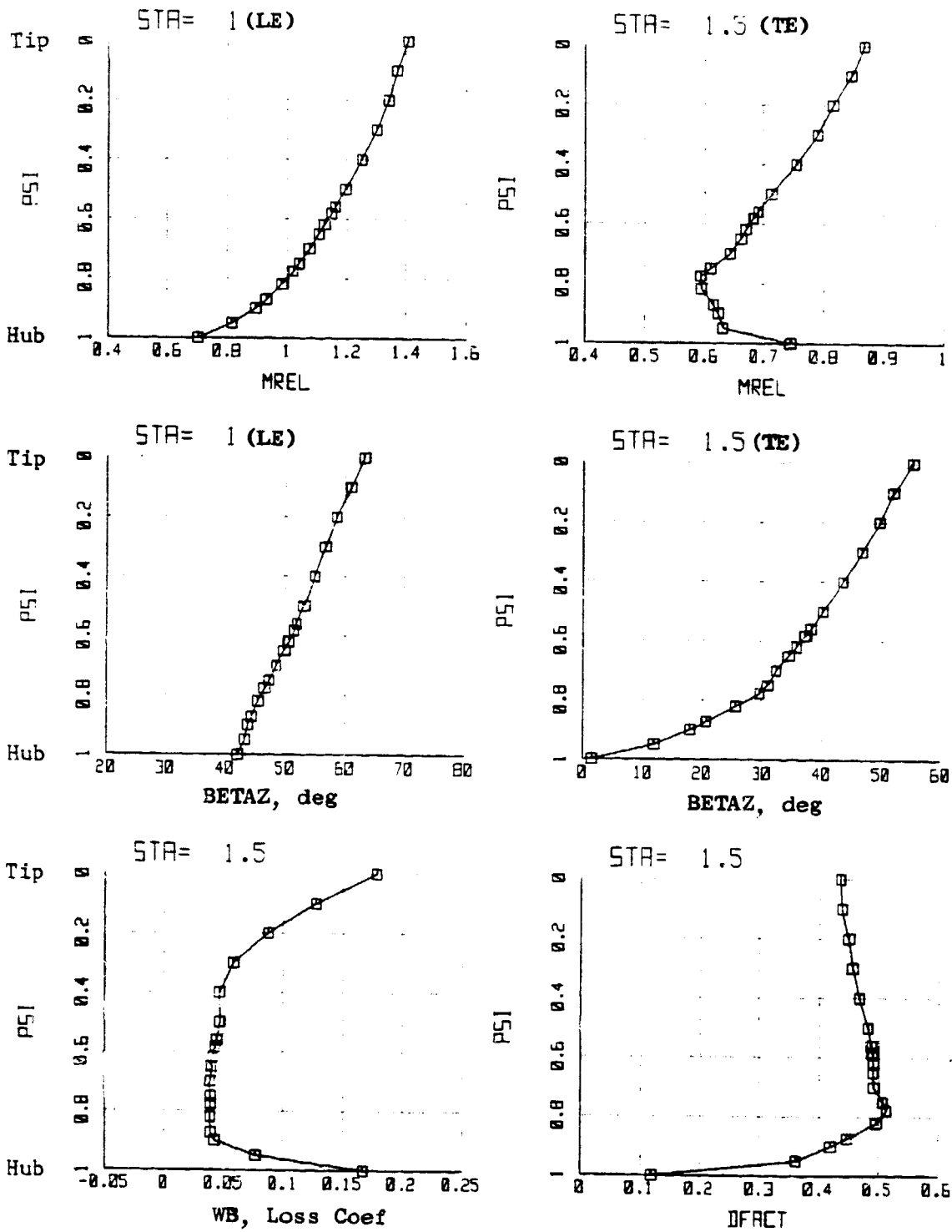
Figure 5. Aerodynamic Design Parameters - Fan Rotor.
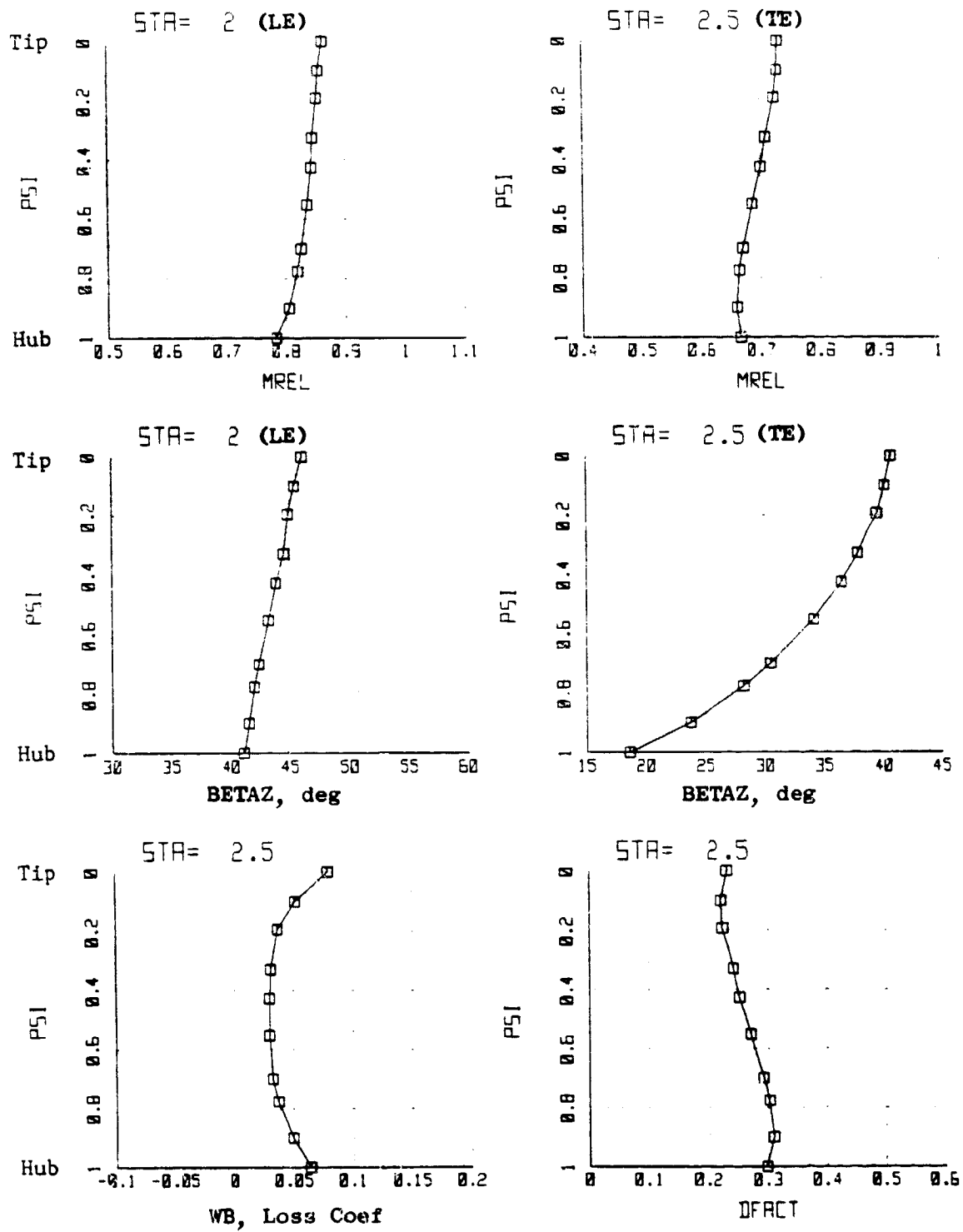
Figure 6. Aerodynamic Design Parameters - Quarter-Stage Rotor.

11
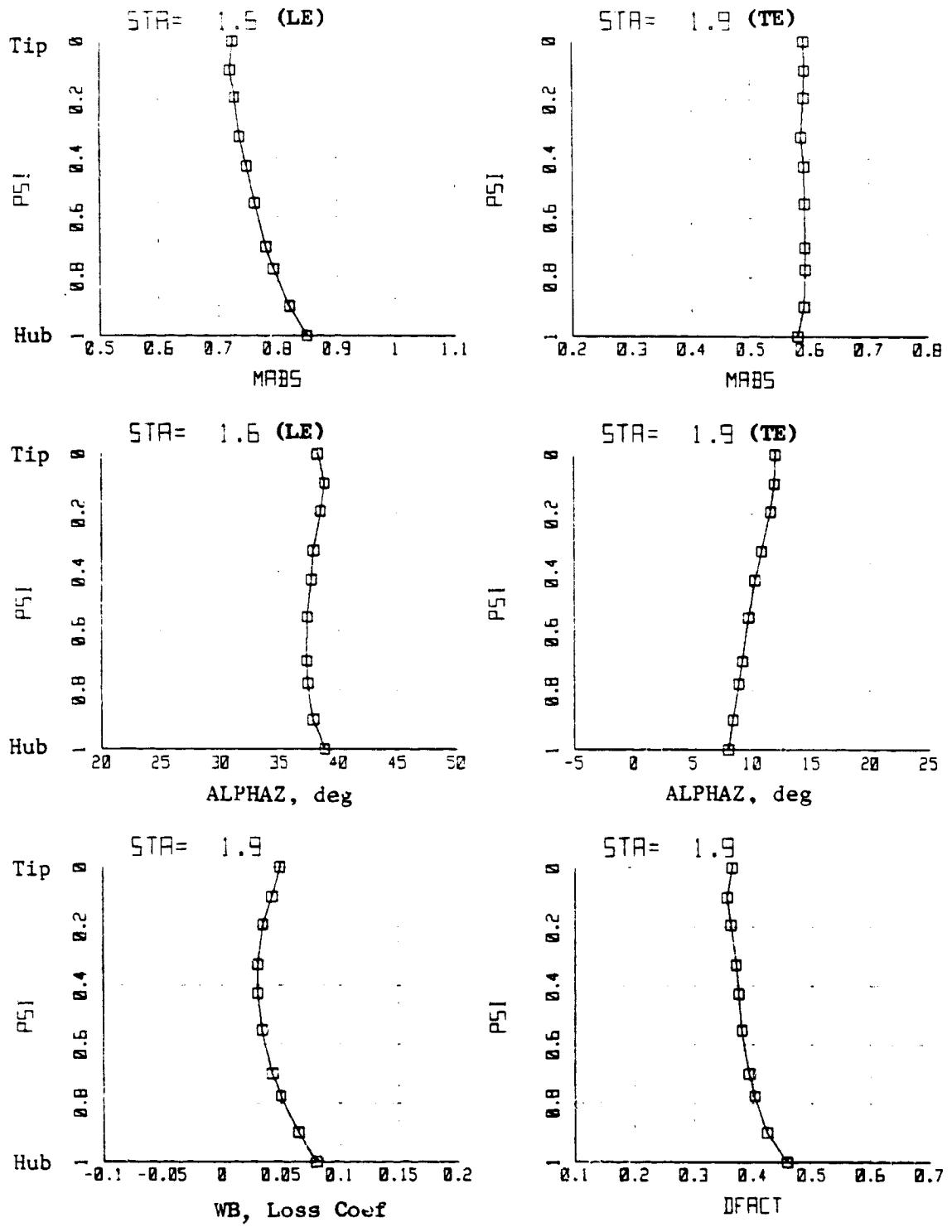
Figure 7. Aerodynamic Design Parameters - Stator 1.
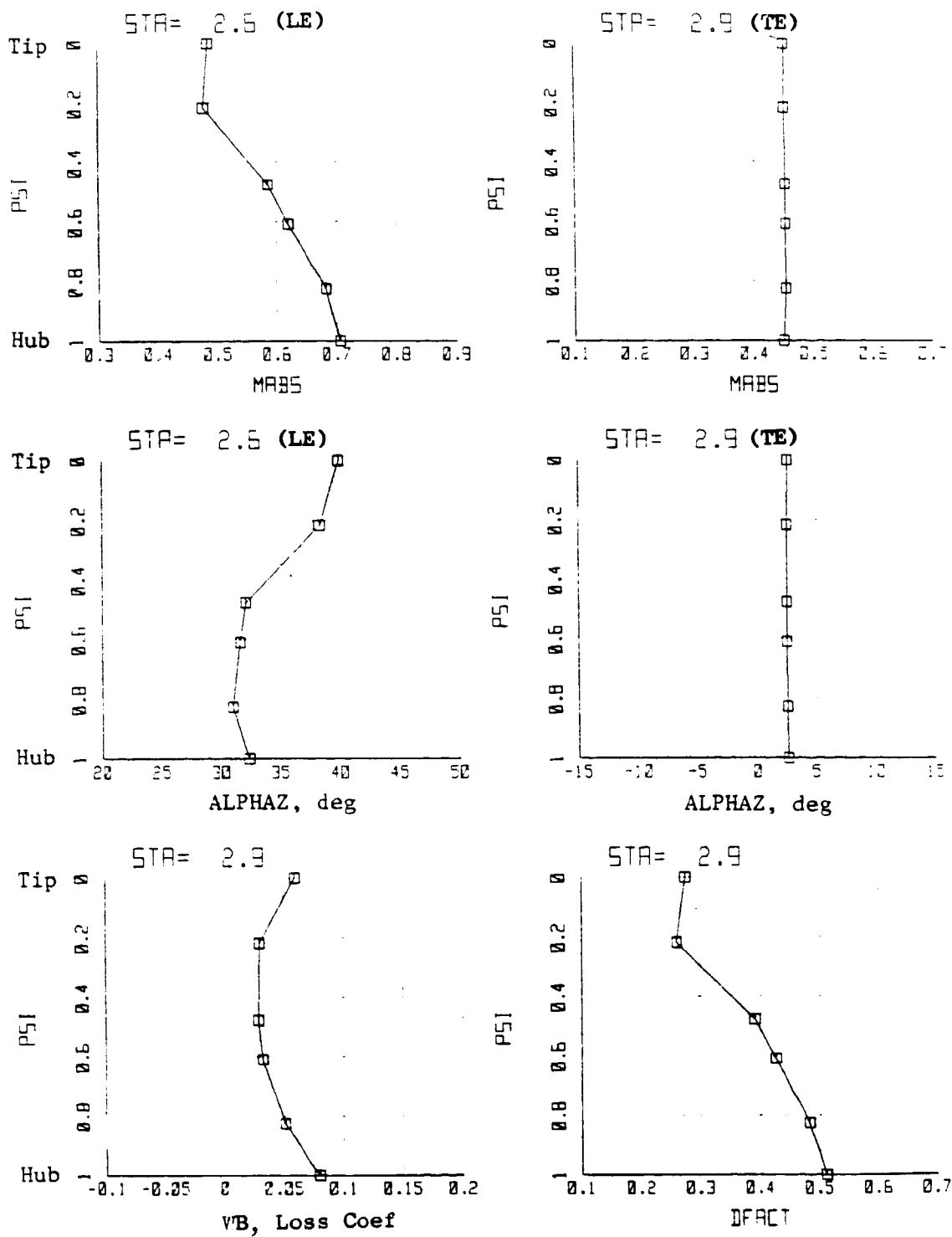
Figure 8.   Aerodynamic Design Parameters - Inner OGV.
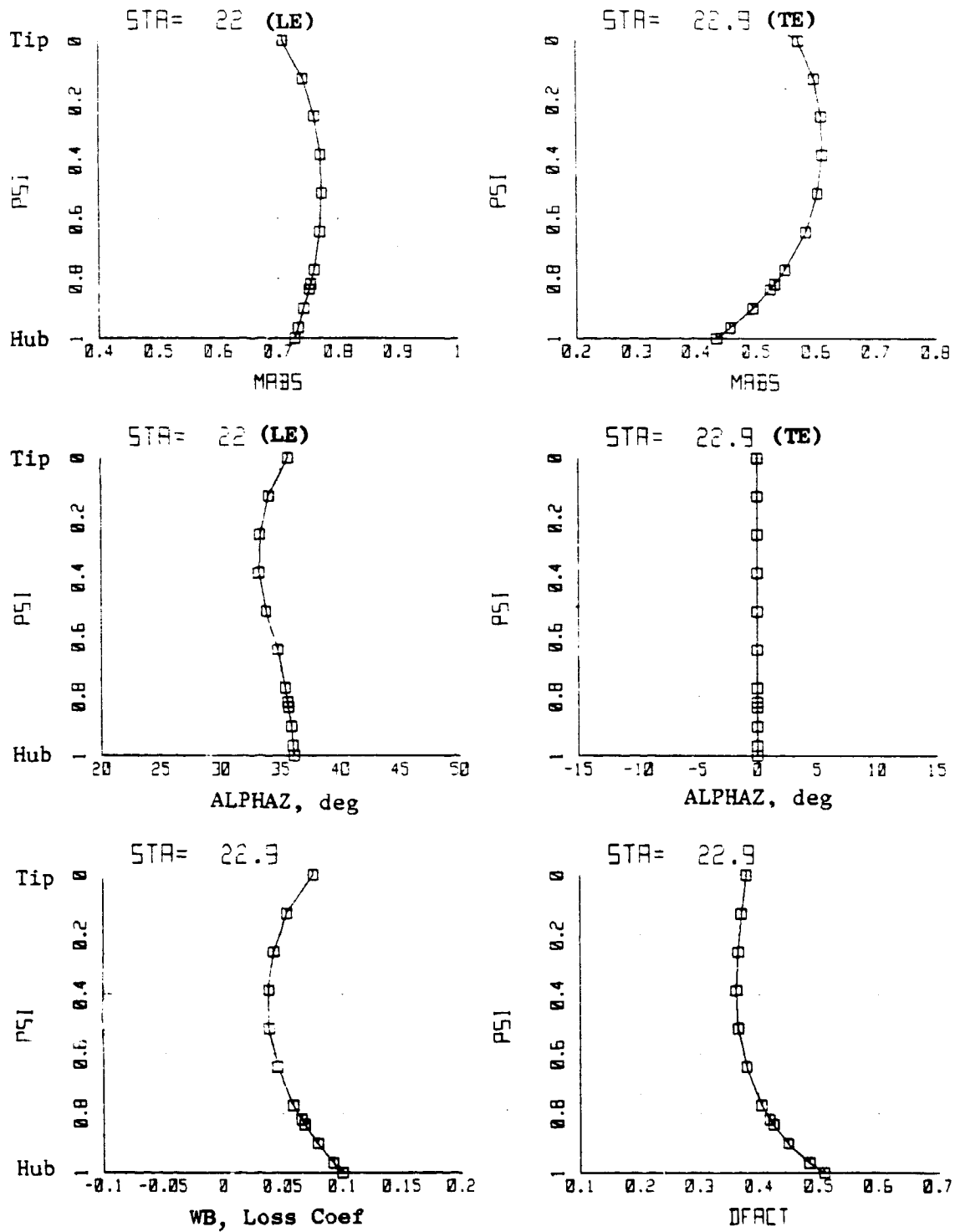
Figure 9. Aerodynamic Design Parameters – Bypass OGV.

14

there were no disturbances or blade forces but with the flow confined to stay in the axisymmetric laminae generated by the CAFD full solution. Figure 10 shows the location of the free-flow streamline for the tip streamline airfoil section. Figure 11 shows the streamline at the location of the part-span shroud and Figure 12 shows the rotor hub streamline airfoil section. Other information on Figures 10 through 12 will be discussed later. The difference between the average free-flow streamline angle and the average suction surface blade angle defines an average suction surface incidence angle; these values are approximately 0.5° at the tip and 2° to 3° in the hub region. These values were selected based on General Electric experience with similar designs. After establishing the suction surface of the airfoil for the outer portion of the blade in this manner, relatively little freedom remained for selecting the incidence angle, although there was some latitude in the selection of the meanline angle distribution from the leading edge to the first captured wave.

In the extreme hub region (10% flow) where the inlet Mach numbers are less than 0.90, the leading and trailing edge blade angles plus the meanline angle distribution were selected with the aid of General Electric's Cascade Analysis by Streamline Curvature (CASC) computer program. This program is capable of calculating surface velocity distributions for subsonic inlet flow sections, although low-supersonic flow regions are allowed. To analyze the supersonic airfoil sections in the outer part of the fan blade, the program was still used, recognizing the fact that the solution was incorrect for the inlet supersonic portion of the airfoil. For these tip sections, however, the exit flow was well subsonic and the cascade analysis program was used to predict the exit flow angles. The exit flow angles predicted by the CASC program for all sections were related to the design exit air angles from the axisymmetric flow solution through an empirical adjustment factor. The radial distributions of this empirical factor were derived from data analyses of high speed fans for which the rotor geometry was somewhat similar to that of the E^3 fan, and also from calculations of secondary flow effects expected for this fan rotor.

Figures 13 and 14 show the airfoil shape and the calculation-grid network and the resultant surface Mach number distribution for the hub streamline. Meanline angle distributions were adjusted to give velocity distributions of this type, believed from experience to produce low losses. The hub streamline has an inlet relative Mach number of 0.70 and an exit Mach number of 0.75. Except for an initial diffusion that is small enough to avoid boundary layer distress, the suction surface Mach number is nearly constant.

To avoid a choking condition, the passage throat areas for most fan blade sections were set such that the effective throat-to-capture area ratio exceeded the critical area ratio by approximately 5% after accounting for the loss due to one normal shock at the leading edge Mach number. Near the extreme ends of the blade, the throat margins were allowed to be slightly larger than this, resulting in 7.5% at the OD and 8.8% at the ID. In order to ensure operation with an oblique leading edge shock which was desired at the maximum climb design point, the ratio of the contraction from the cascade mouth to the throat must not exceed the critical contraction ratio after sustaining one

15
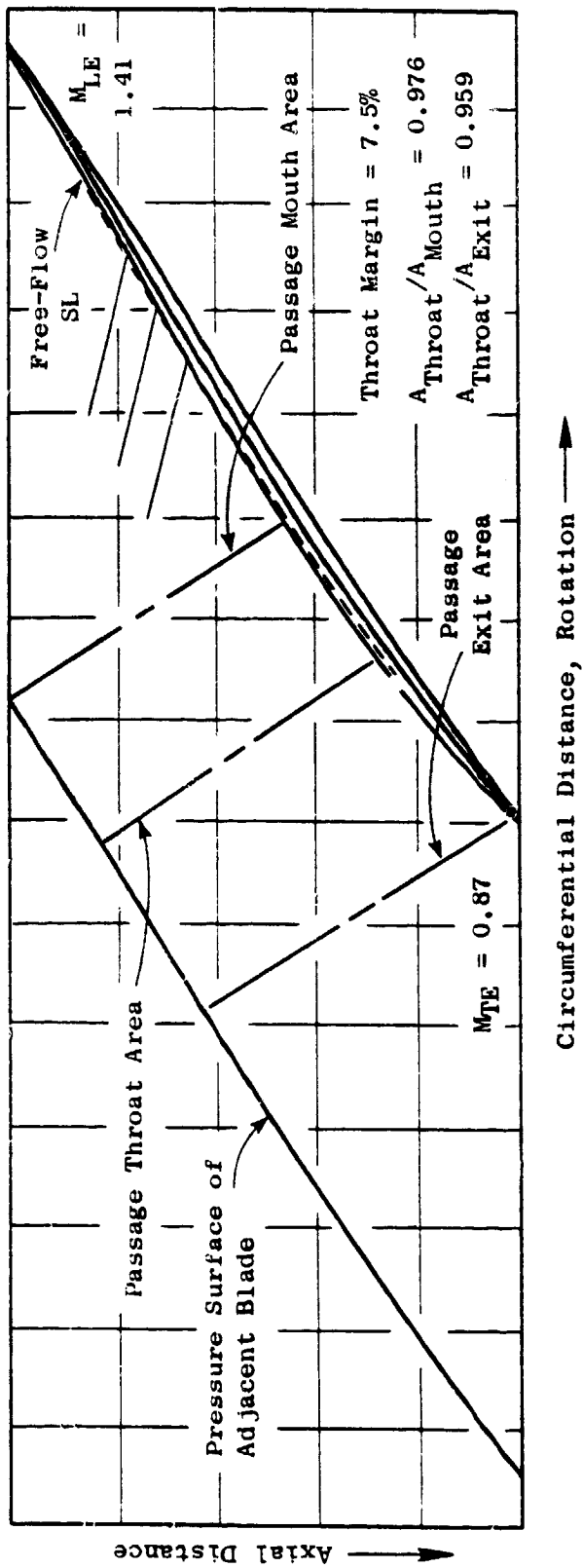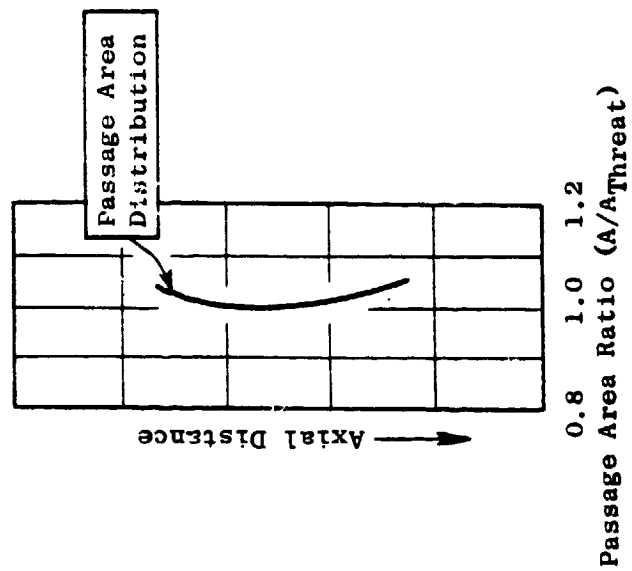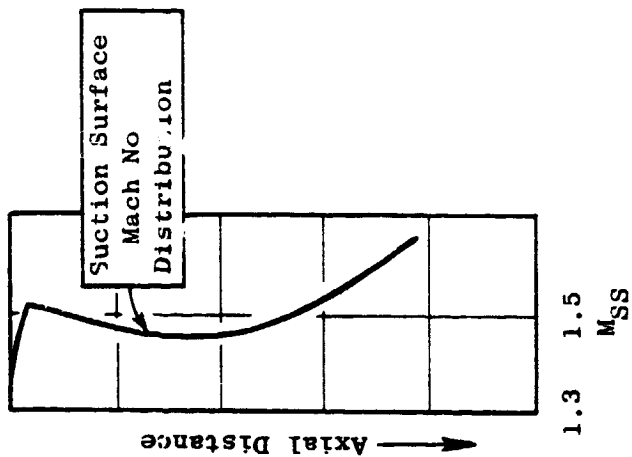
Figure 10. Fan Rotor Tip Streamline Airfoil Section.
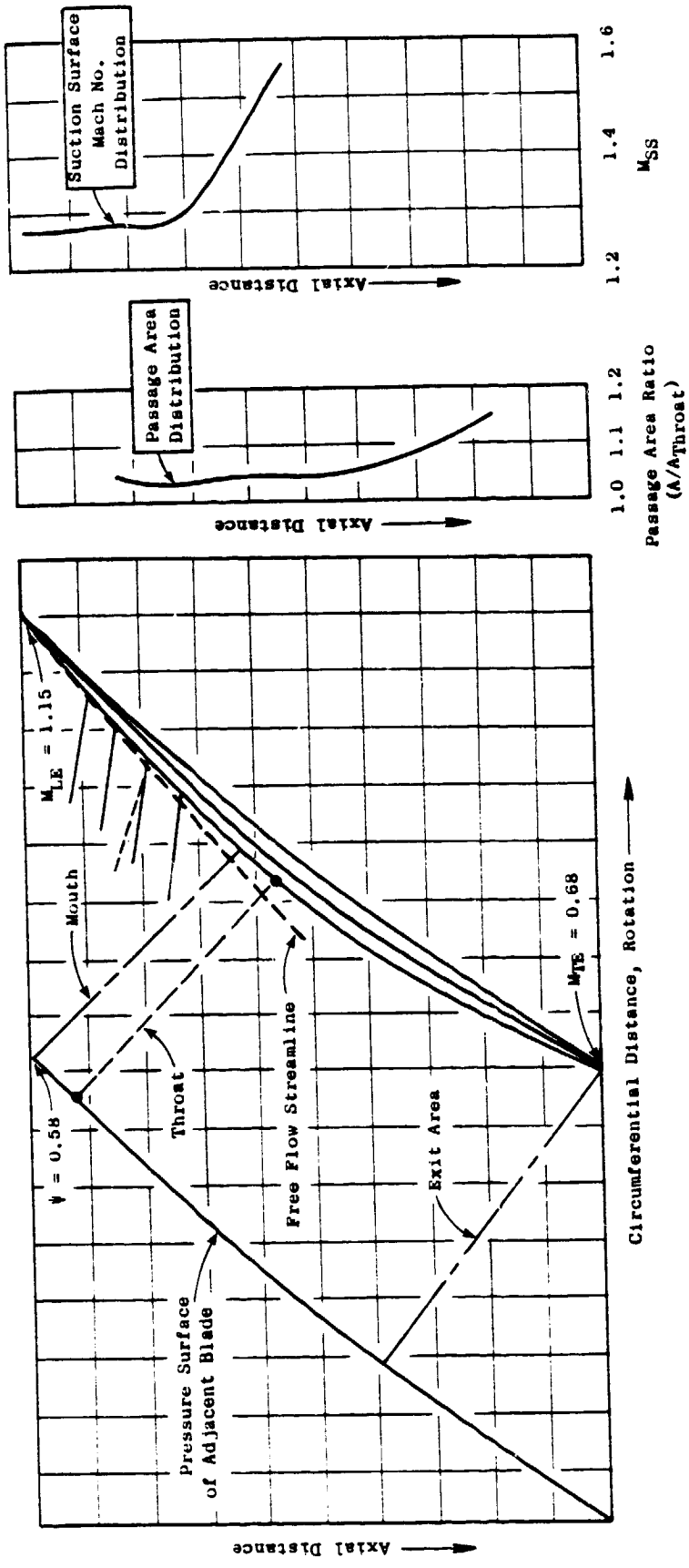
Figure 11. Fan Rotor Shroud - Streamline Airfoil Section.

17
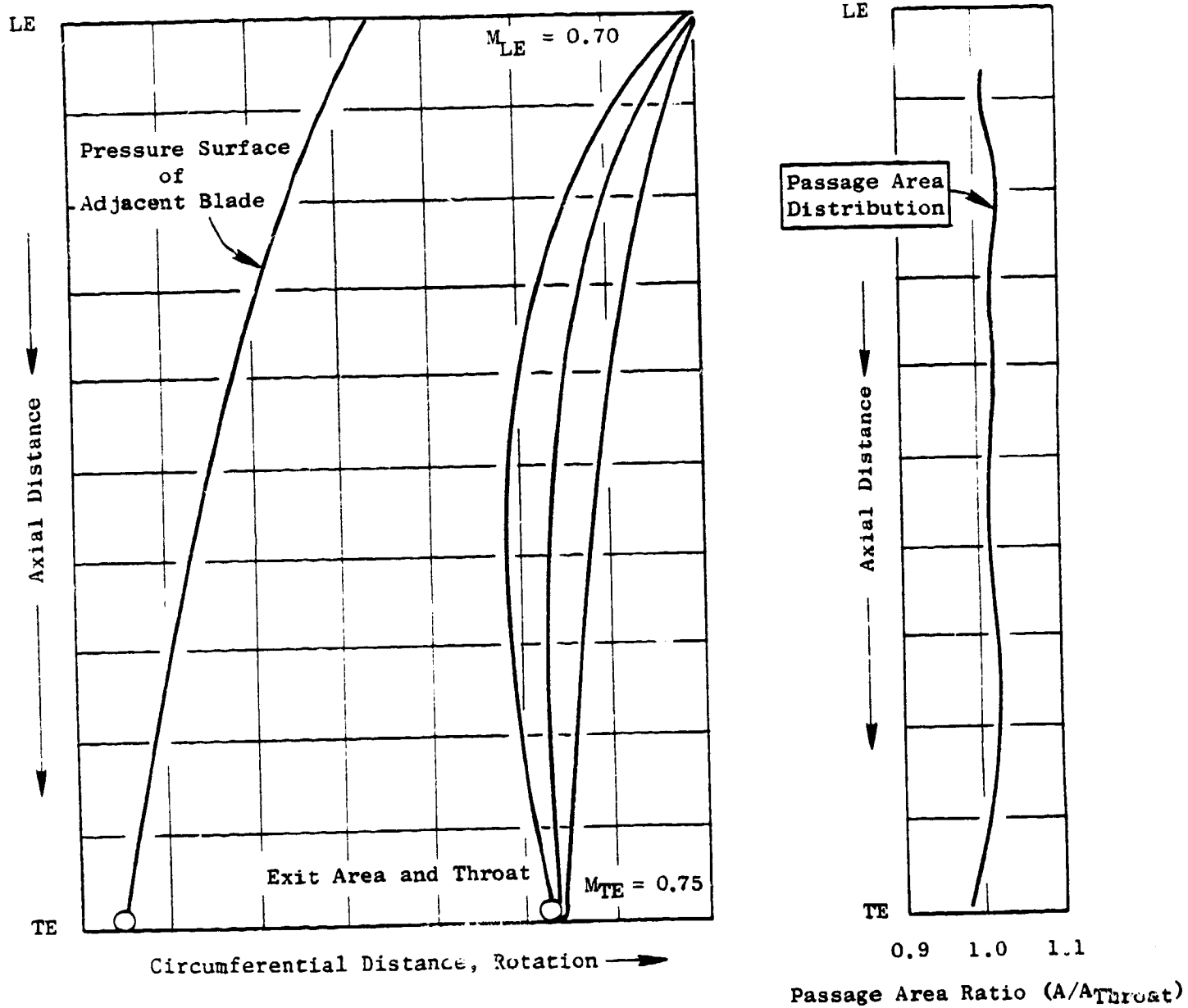
Figure 12.   Fan Rotor Hub - Streamline Airfoil Section.
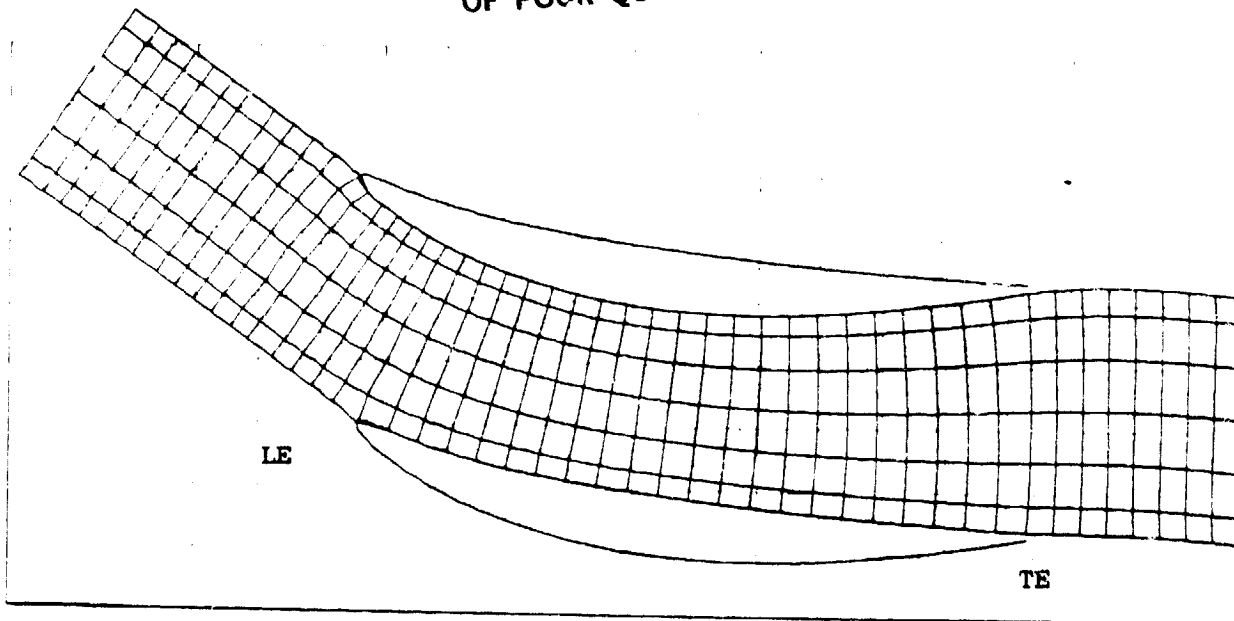
Figure 13.   Fan Rotor Hub Streamline Cascade.
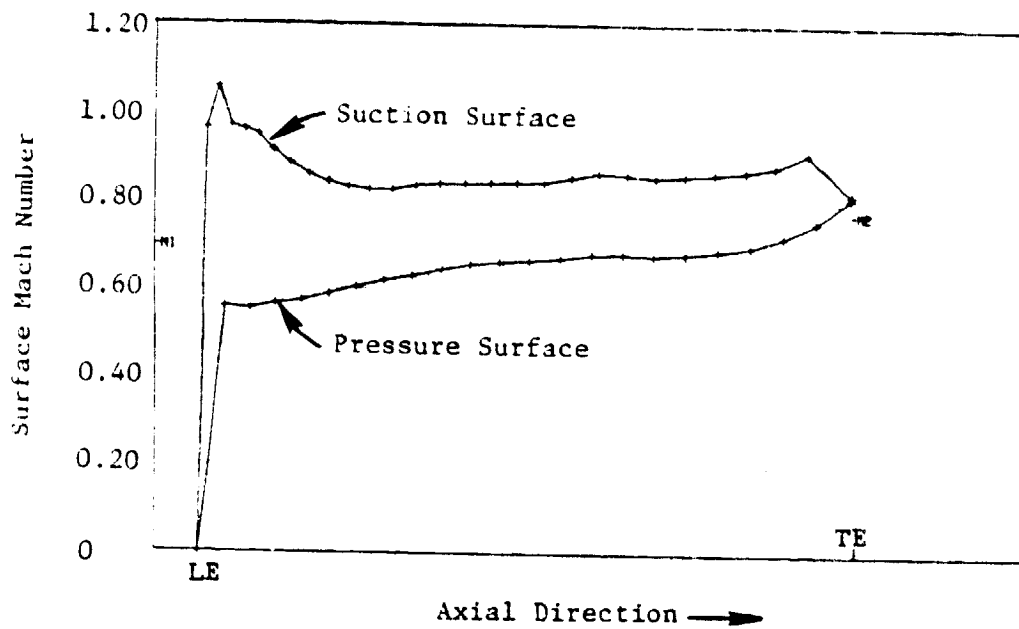
Figure 14.   Fan Rotor Hub Streamline Surface
Mach Number Distribution.

19

normal shock loss at the mouth Mach number. The amount by which the passage throat area exceeds this limiting contraction ratio is referred to as starting margin. The amount of passage area contraction from the mouth to the throat for all rotor streamline is approximately 2% to 2.5%. The passage throat, mouth, and exit areas are indicated on Figures 10, 11, and 12 for streamline sections at the tip, shroud, and hub locations.

The airfoil shape for each streamline section is dependent upon the chordwise thickness distribution and meanline blade angles. For the fan rotor, the level and radial distribution of the maximum thickness-to-chord ratio is primarily dependent upon mechanical and aeromechanical considerations. The chord, solidity, and tm/c distributions in manufacturing planes are shown in Figures 15 and 16. The location of maximum thickness along the blade chord was specified at 59% chord at the tip streamline. Above the island, this location stays aft of 55% chord and then moves forward somewhat at lower radii toward the hub streamline where the maximum thickness occurs at 42% chord. In the part-span shroud region, the maximum thickness of the airfoil is at 58% chord. The part-span shroud, as previously mentioned, is positioned at 55% blade height. The axial position of a point on the shroud stacking axis is at 65% axial blade chord. The shroud leading edge is at 48% and trailing edge is at approximately 82% axial blade chord. It has a nearly elliptical thickness distribution with a maximum thickness of 0.89 centimeter (0.35 inch).

The blade chordwise thickness varies from leading edge to the point of maximum thickness according to a quarter-sine wave curve and then reverses the distribution from the maximum thickness point to the trailing edge. This distribution holds for all streamlines down to the region just below the island. Here the airfoils are slightly thicker in the leading edge region than the quarter-sine distribution would imply.

The geometric properties of the manufacturing plane blade sections are tabulated in Appendix B.

B. Stator 1

The design of the Stage 1 stator vanes was performed similar to the design of the fan rotor. That is, the vector diagrams were calculated along several streamlines at the leading and trailing edge stations as well as at a number of intrablade stations. Airfoil sections were defined for each streamline by specifying the thickness and meanline angle distributions. Each streamline cascade was then analyzed with the cascade analysis computer program.

The Stator 1 vanes have a chordwise thickness distribution that varies from tip to hub. At the OD where the inlet Mach number is 0.73, a 65-Series thickness distribution was selected. At the ID where the inlet Mach number is 0.85, the thickness distribution is thinner in the leading edge region as it follows the first-quarter cycle of a sine wave to the maximum thickness location at 38% chord and then follows a 65-Series distribution to the trailing edge. A linear blend of these thickness distributions from the OD to the ID is used to define the intermediate airfoil sections. Slightly modified

20

$\overline{R}$ (SA O.D.) = 40.9061 in.

$\overline{R}$ (SA I.D.) = 16.4399 in.

Z (SA) = 3.2253 in.

Blade Ht. = 24.4662 in.

AR = 2.597

NB = 32
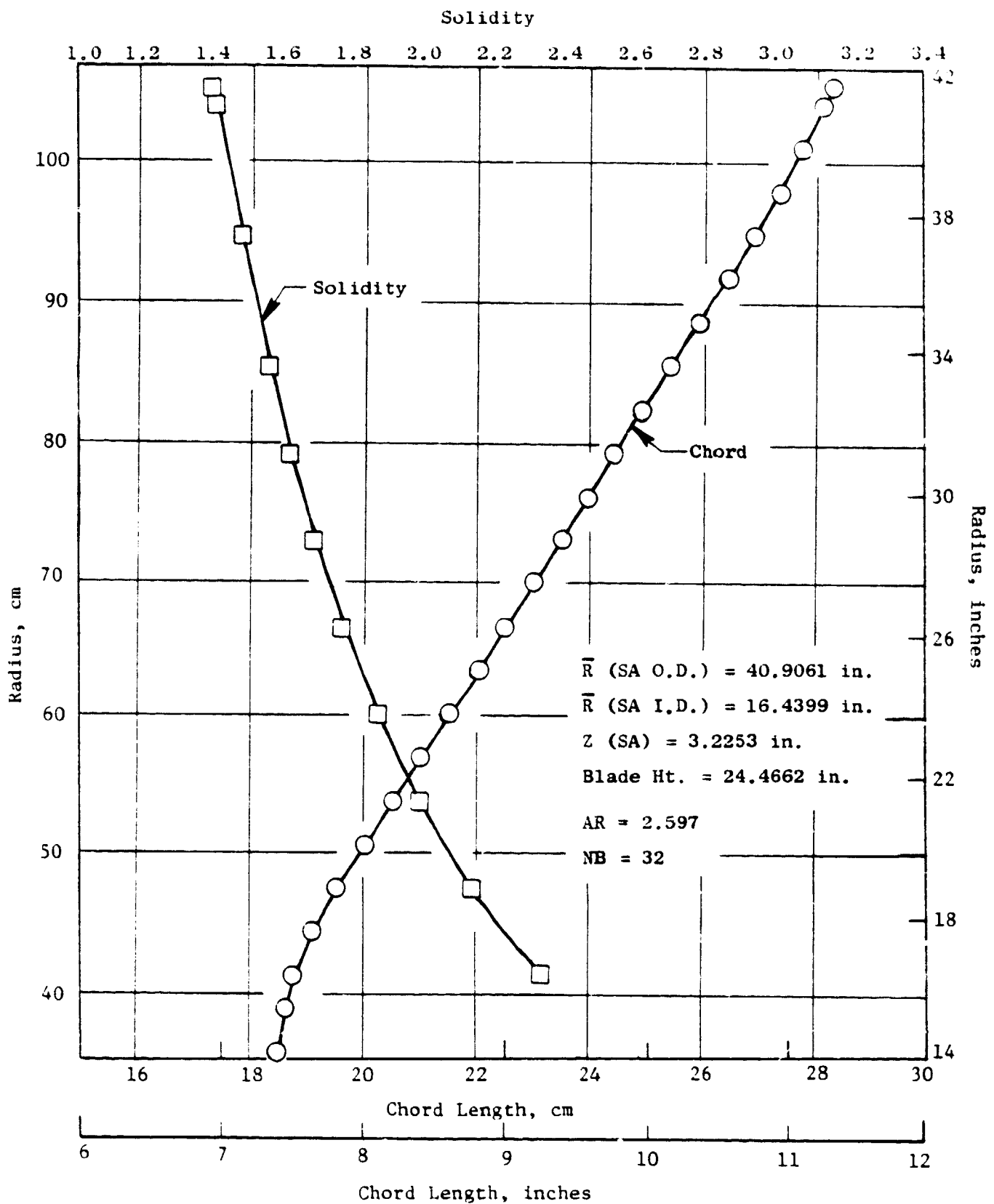
Figure 15.   Fan Rotor Chord and Solidity.

21
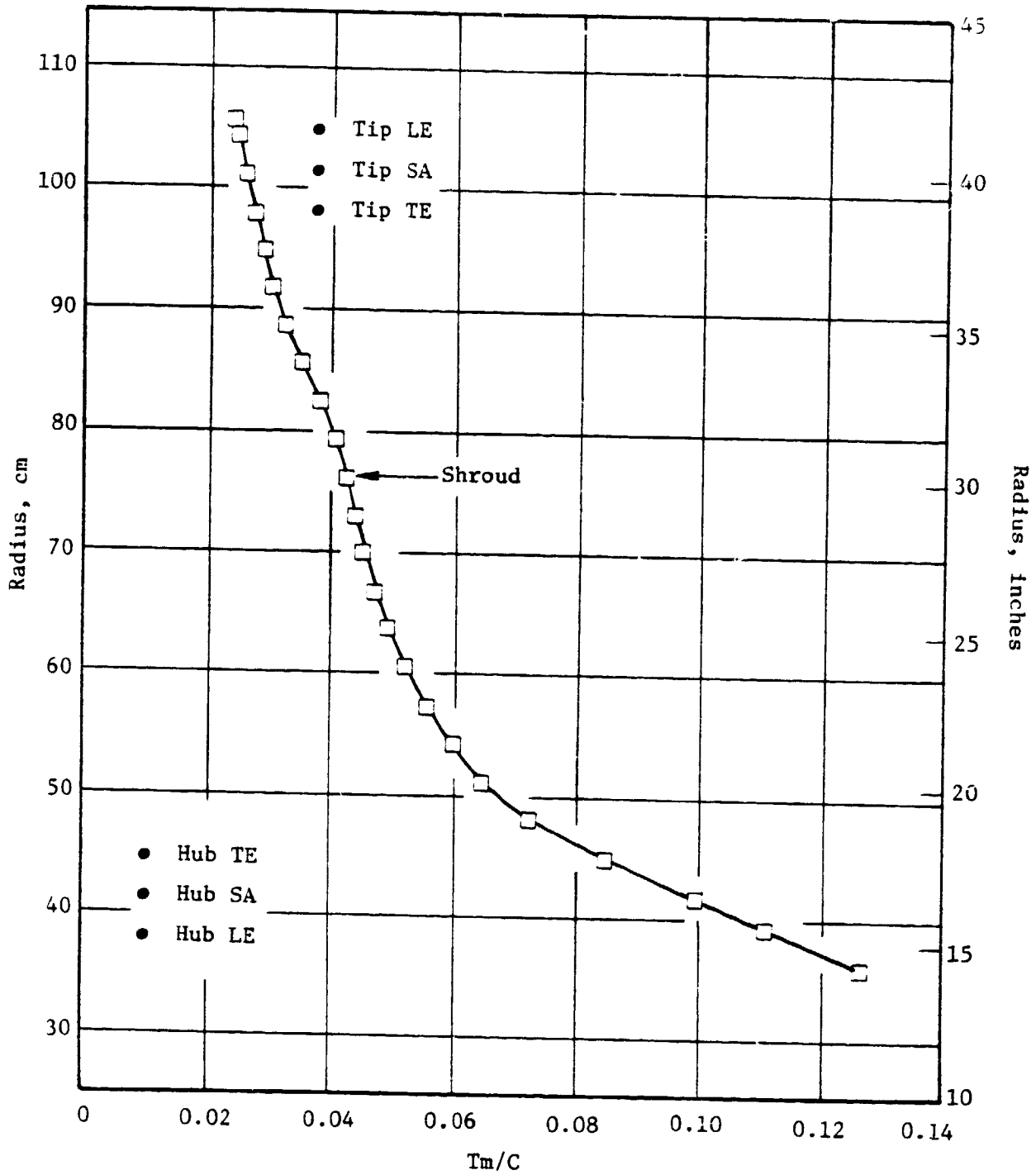
Figure 16. Fan Rotor Tm/C.

circular-arc meanline angle distributions are employed for all streamline sections. The vanes have a constant chord of 8.10 cm (3.19 in.) and a maximum thickness-to-chord ratio that varies from 0.062 at the OD to 0.049 at the ID.

The cascade analysis computer program was used as a guide in shaping the airfoil meanlines. Each streamline was analyzed to obtain a desirable incidence angle and surface velocity distribution. The cascade grid and resultant surface Mach number distributions for streamline sections at the tip and near the hub are shown in Figures 17 through 20. The deviation angles resulted from using the cascade analysis to predict the exit flow angles. These angles were then related to the design exit air angles of the CAFD solution through an empirical factor.

The incidence angles were specified slightly less than 1° for all streamlines except the hub. At the hub streamline, a 3° high inflow angle was intentionally specified to account for the higher swirl anticipated from the rotor hub due to secondary flow effects.

With the passage throat area occurring at the mouth of the cascade, there is approximately 6% to 8% throat margin above the critical area ratio.

The streamline airfoil sections were stacked at 50% chord and plane section cuts were made to define manufacturing sections. The geometric properties of these sections are tabulated in Appendix C.

C. Quarter-Stage Rotor

The quarter-stage rotor airfoils were specified similar to the other blade rows using the stramline section and cascade analysis computer programs. Initially, the vector diagrams are defined for several streamlines at axial stations including the leading edge, trailing edge, and intrablade region.

The rotor airfoil sections have a chordwise thickness distribution for all streamlines which is a quarter-sine wave from the leading edge to maximum thickness and then a 65-Series thickness distribution to the trailing edge. The meanline angle distribution for all streamlines is a modified circular arc. The maximum thickness-to-chord ratio varies from 0.049 at the tip to 0.081 at the hub. There are 56 blades with an aspect ratio of 2.09. The blade chord is linear from 6.35 cm (2.50 in.) at the tip to 7.11 cm (2.80 in.) at the hub. The solidity is fairly low since the design point aerodynamic loading is quite moderate. The passage throat areas for all streamlines were set with approximately 5% to 6% throat margin.

Cascade flow analyses were made for all streamline sections and the tip and hub results are presented in Figures 21 through 24. Figures 21 and 22 show the cascade calculation grid and surface Mach number distributions for the tip streamline, respectively. Only a slight amount of turning is required at the tip and hence the low value of solidity. The Mach number distribution shows the suction surface value skirting just above Mach 1.0 near maximum thickness before diffusing to the trailing edge Mach 0.73. The pressure

23
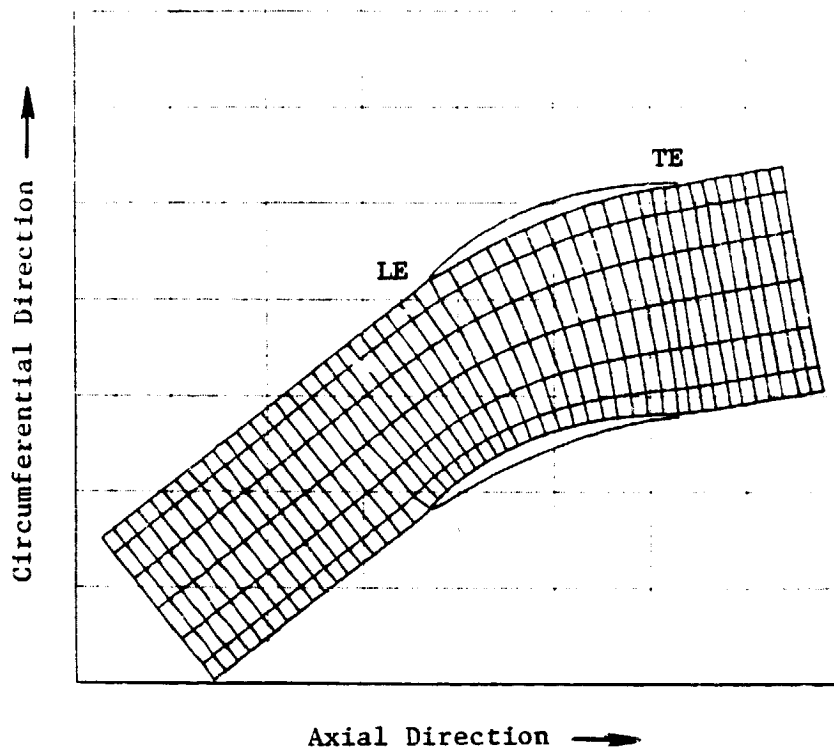
Figure 17. Stator 1 Tip Streamline Cascade.
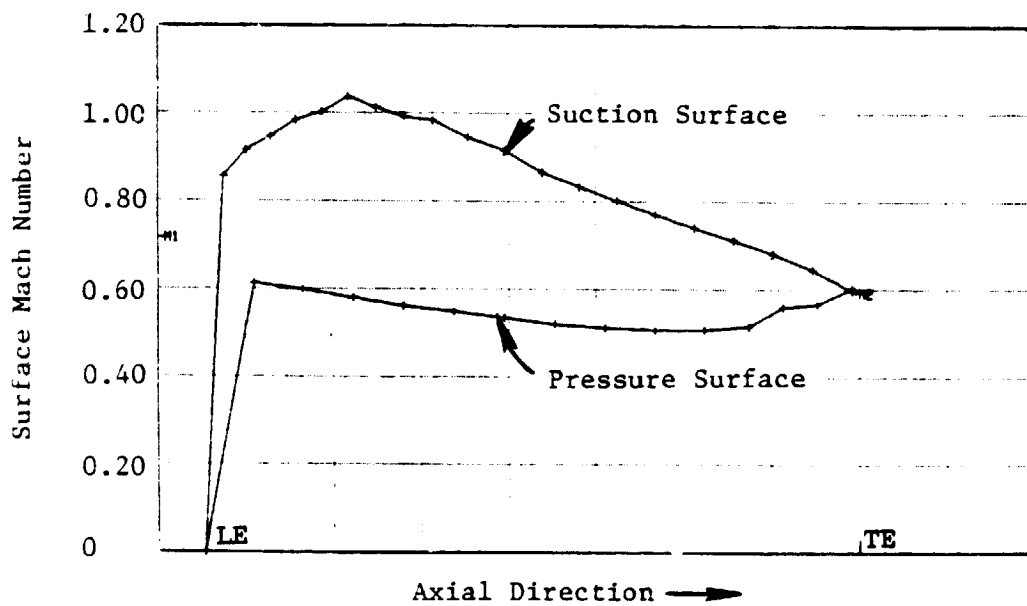
Figure 18. Stator 1 Tip Streamline Surface Mach Number.

24
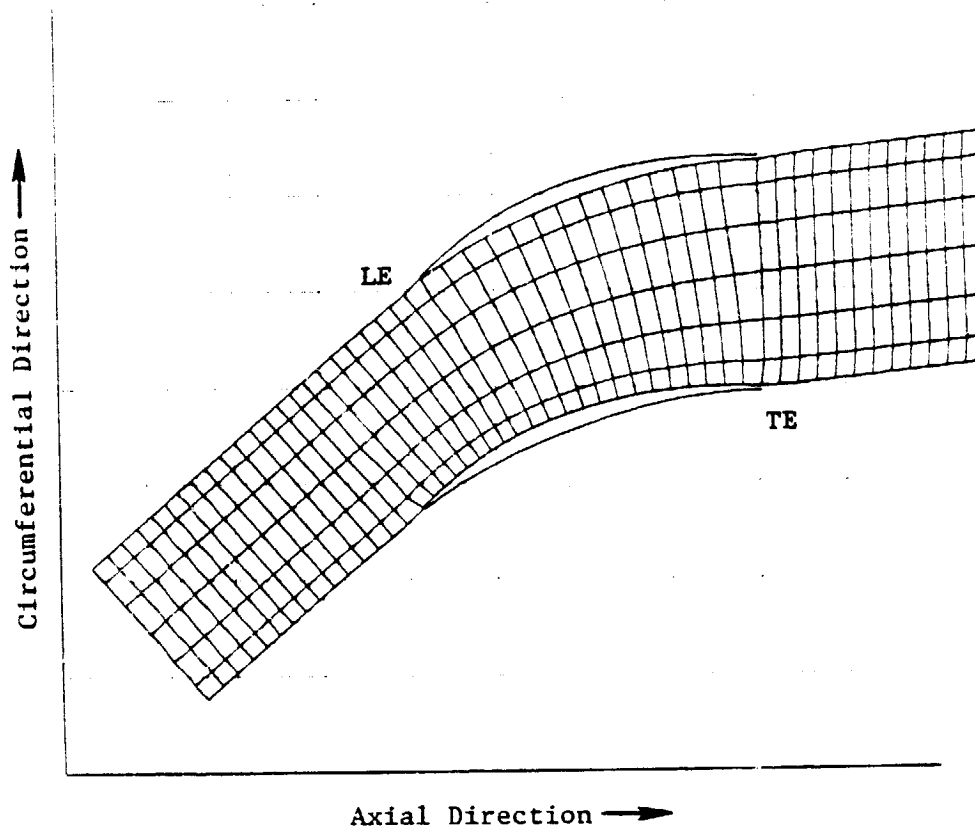
Figure 19. Stator 1 Hub Streamline Cascade.
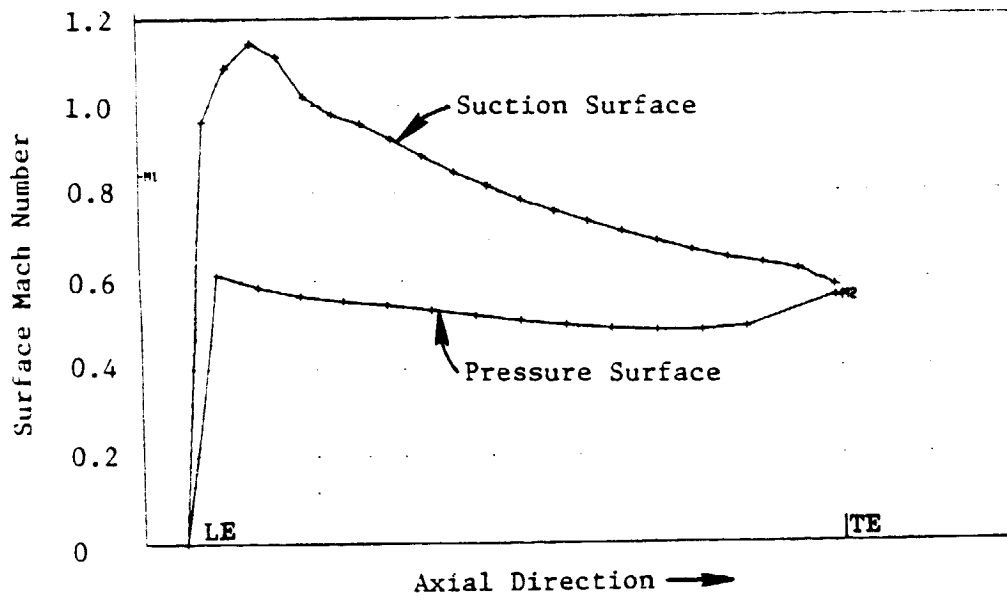
Figure 20. Stator 1 Hub Streamline Surface Mach Number.
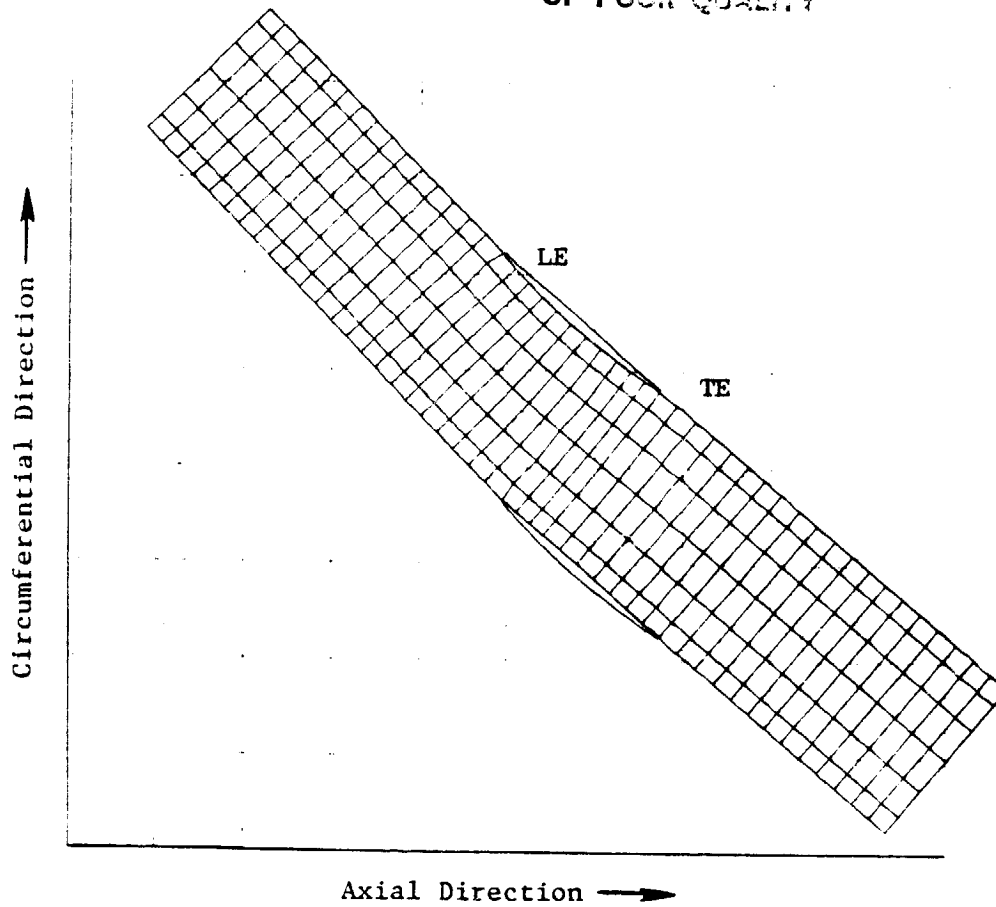
Figure 21.   Quarter-Stage Rotor Tip Streamline Cascade.
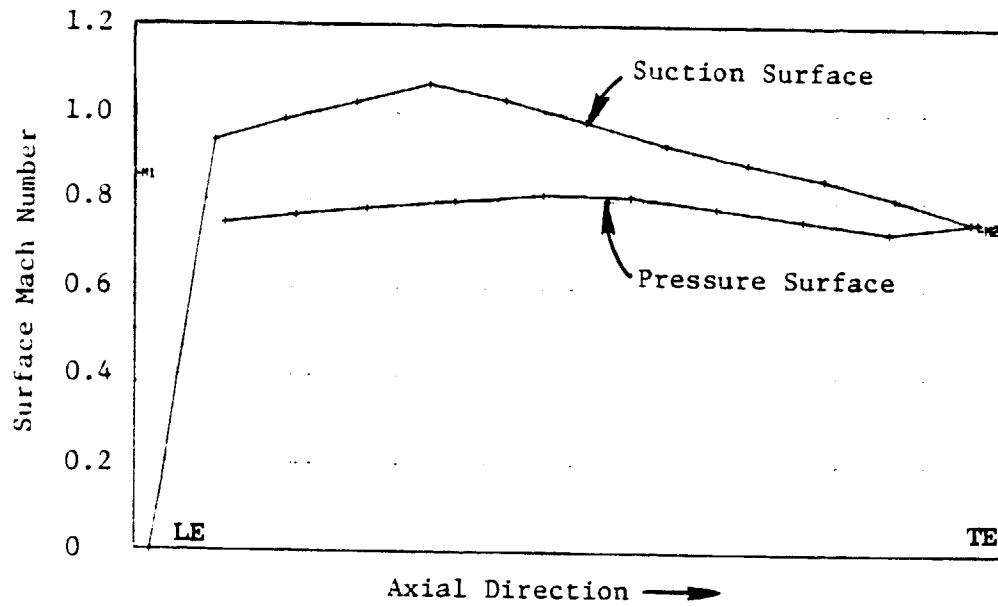
Figure 22.   Quarter-Stage Rotor Tip Streamline
Surface Mach Number.
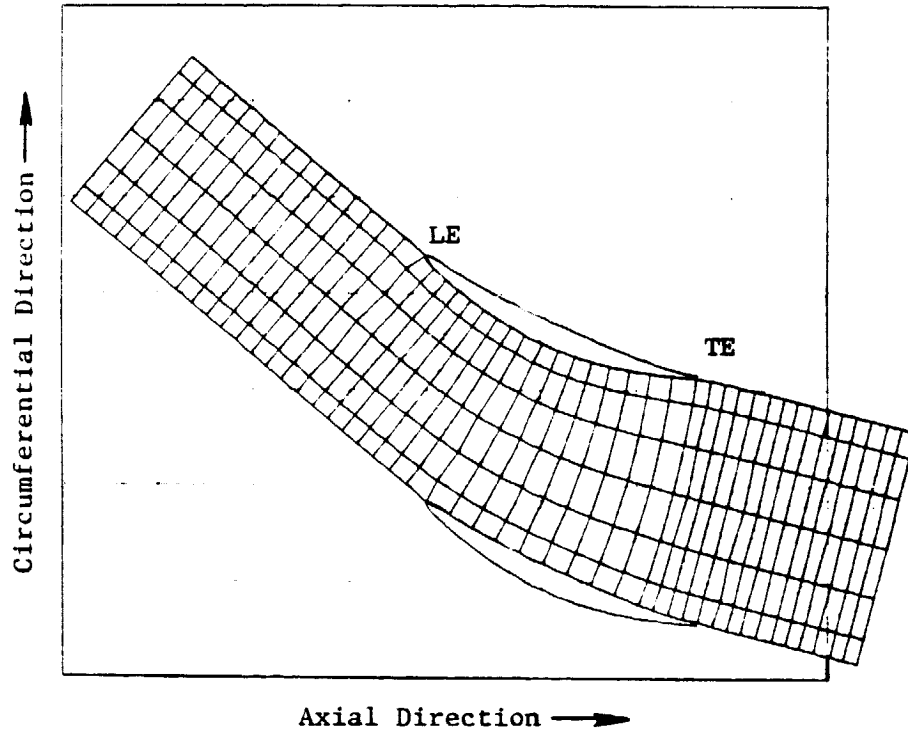
Figure 23. Quarter-Stage Rotor Hub Streamline
Cascade.
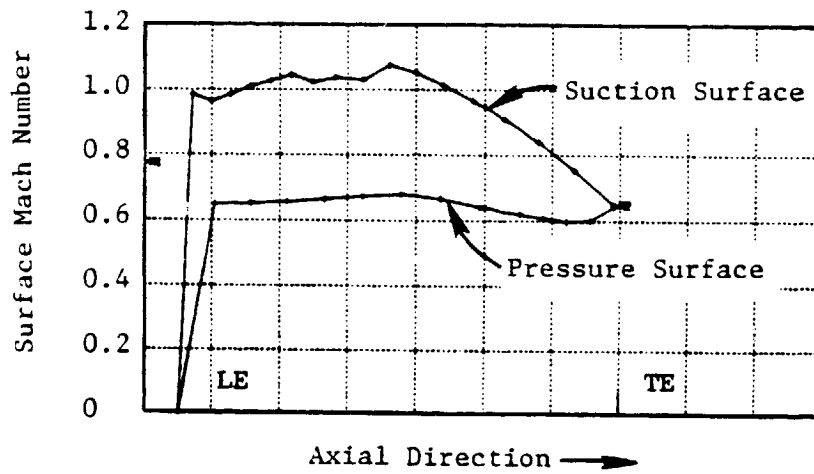
Figure 24. Quarter-Stage Rotor Hub Streamline
Surface Mach Number.

surface Mach number remains nearly constant along the chord. In the hub region, where the blade must raise the low fan hub total-pressure to a 1.68 pressure ratio, a solidity of 1.2 and 32° of camber are required. Figures 23 and 24 show the hub streamline cascade and Mach number distributions. Again, the peak suction surface Mach number is slightly larger than 1.0 but here the diffusion is delayed until the last 40% of the chord.

The deviation angles were again calculated using the CASC predicted exit flow angles. The empirical adjustment included a compensation for the secondary flow that results from the nonuniform loading of this blade row and its incoming free-stream absolute vorticity.

The rotor blade streamline sections were stacked so that the plane section centers of gravity were aligned along the radial stacking axis. Plane section cuts defined the blade for the purpose of manufacturing. The blade geometry for these plane sections is tabulated in Appendix D.

D. Inner OGV

The inner outlet guide vane (OGV) blade row shown in Figure 25 was designed to remove the swirl received from the booster rotor and direct the flow into the core duct. To do this efficiently, the 64 vanes were swept aft and leaned with the pressure side facing the fan axis of rotation. The aerodynamic design of this blade row was performed using the procedure described in Reference 4. This procedure consists of cutting the airfoil along streamlines and viewing the sections along the blade axis. The blade axis is a curved line in space, swept aft by 60° from a radial line and leaned circumferentially in an amount that varies from 0° (no lean) at the OD to 20° at the ID. The stacking axis for viewing the cascade projection and for defining manufacturing sections is a straight line between the intersection of the blade axis with the OD flowpath and the intersection of the blade axis with the ID flowpath. The flow and airfoil meanline angles that are observed in this projection are referred to as cascade angles.

The sweep angle (60°) of the stacking axis was selected to be compatible with the shape of the flowpath in the region entering the core duct. The degree of lean was chosen primarily to control and minimize the level of Mach number in the hub region as the flow enters the core duct. At the entrance to the stator, the downward radial force on the flow imposed by the 20° of lean increases the static pressure, and thereby reduces the inlet Mach number. This eventually leads to a lower hub diffusion rate. The lean angle drops off sharply to 0° at the OD in order to avoid an undesirable acute angle between the vane suction surface and the outer flowpath. Even though there is no lean at the tip, the radial gradient of lean tends to increase the Mach numbers slightly at the tip streamline. The reduced Mach numbers and aerodynamic loadings in the hub, where the flow is the most sensitive because of the flowpath shape, makes the total lean effect favorable.

The airfoil shapes were defined using the quarter-sine wave/65-Series thickness distribution described earlier. The 64 vanes have a chord varying

28
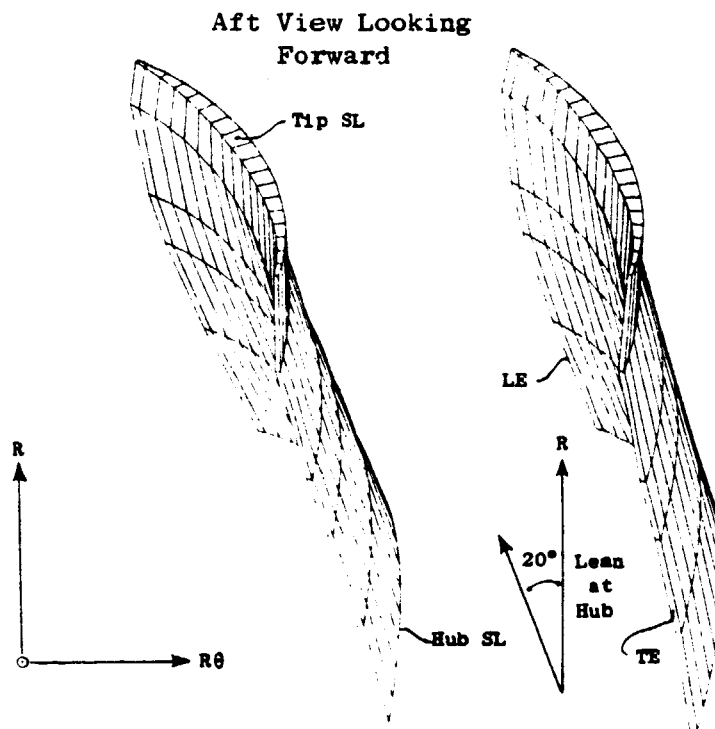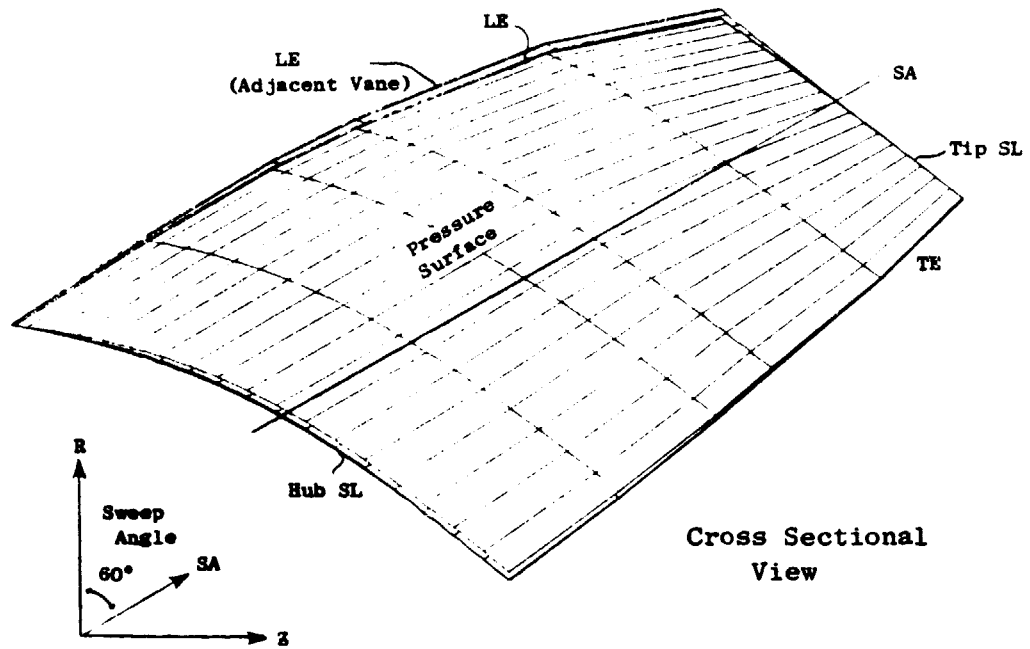
Figure 25. Inner Outlet Guide Vane.

from 5.44 cm (2.14 in.) at the OD to 9.25 cm (3.64 in.) at the ID. The maxi-
mum thickness-to-chord ratio is 0.066 locally at the OD, decreasing to a 0.053
value which is then held constant over the inner 50% of the span.

Cascade flow analyses were made with the sections viewed looking down
the leaned and swept axis. Figures 26 through 29 present the cascade projec-
tion and surface Mach number distribution for the tip and hub streamlines.
The inlet and exit Mach numbers used for calculation purposes and shown on
these plots are the perpendicular components of the full Mach numbers that
exist in planes perpendicular to the swept and leaned airfoil stacking axis.
The surface Mach number plots indicate that most of the turning is accom-
plished in the front portion of the cascade. The peak Mach number of both
streamline sections shown, occurs on the suction surface at approximately
30% of the chord. Uniform diffusion is carried out in the remaining cascade
passage.

End-effect adjustments to the camberline shape were calculated using
the method of Reference 4, but were attenuated somewhat in application.
The maximum adjustment at the tip streamline amounted to a camberline angle
increase of 7.8°, occurring at 50% chord. At the hub, the adjustment was a
camberline angle decrease of 4.7°, occurring at 40% chord.

Airfoil section coordinates were defined on planes perpendicular to the
swept and leaned stacking axis. A summary of the geometry for this vane is
tabulated in Appendix E.

E. Bypass OGV Vane-Frame

The aerodynamic design of the bypass vane-frame was complicated by the
presence of a pylon having a maximum thickness of 40.6 cm (16 in.) and located
at the top of the engine (0°) just downstream of the vane trailing edges. In
addition, the overall engine system design required the bottom (180°) vane or
strut to be substantially thicker than the rest of the vanes to provide space
for a radial drive shaft and accessory pipes. The presence of these bodies
relative to the rotor and OGV planes, as shown schematically in Figure 30,
sets up a nonaxisymmetric flow field which required circumferentially nonuni-
form airfoil geometry to be defined using a special computer program analysis.

Initially, the circumferential-average flow solution was carried out as
usual. This flow solution recognizes the vane and pylon blockages and the
island trailing edge static pressure match. Next, a two-dimensional stream
surface analysis was employed to establish the magnitudes of static pressure
and flow angle variations. This two-dimensional analysis was performed at
the pitch streamline and the resulting circumferential distributions of pres-
sure and flow angle are shown in Figures 31 and 32. The calculations show a
significant circumferential variation at the OGV inlet and exit planes but
essentially no distortion at the fan rotor exit plane. A coarse three-dimen-
sional, finite-element analysis was then employed to establish the radial
trend of the vane exit flow angles. This analysis was conducted using the
five streamline sections: tip (T), near-tip (P-T), pitchline (P), island (I),

30
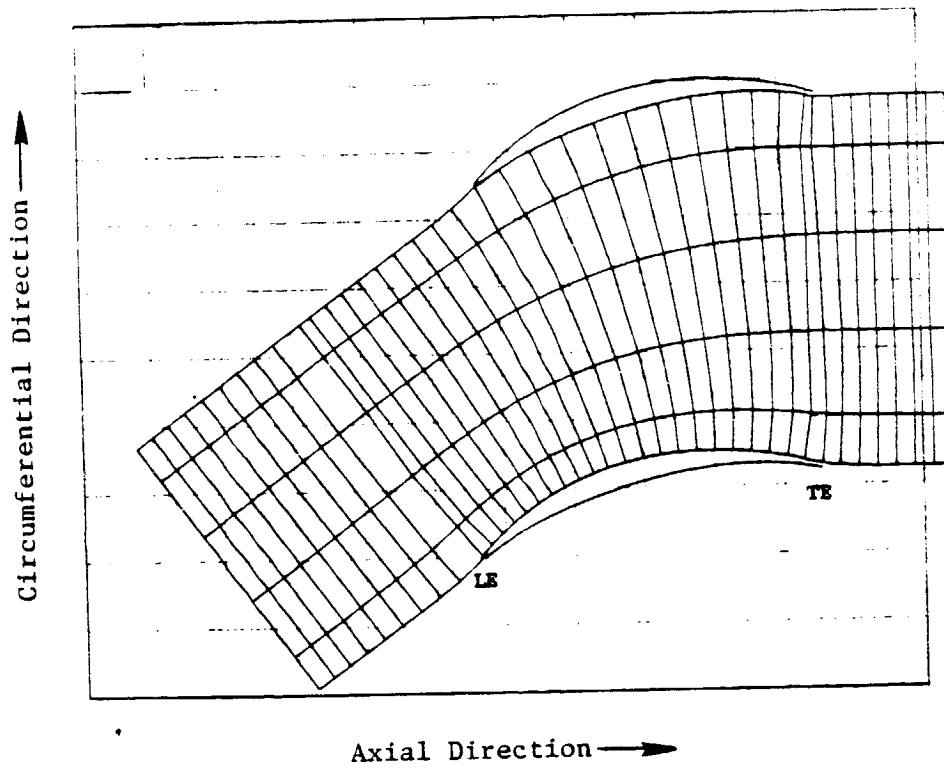
Figure 26.   Inner OGV Tip Streamline Cascade.
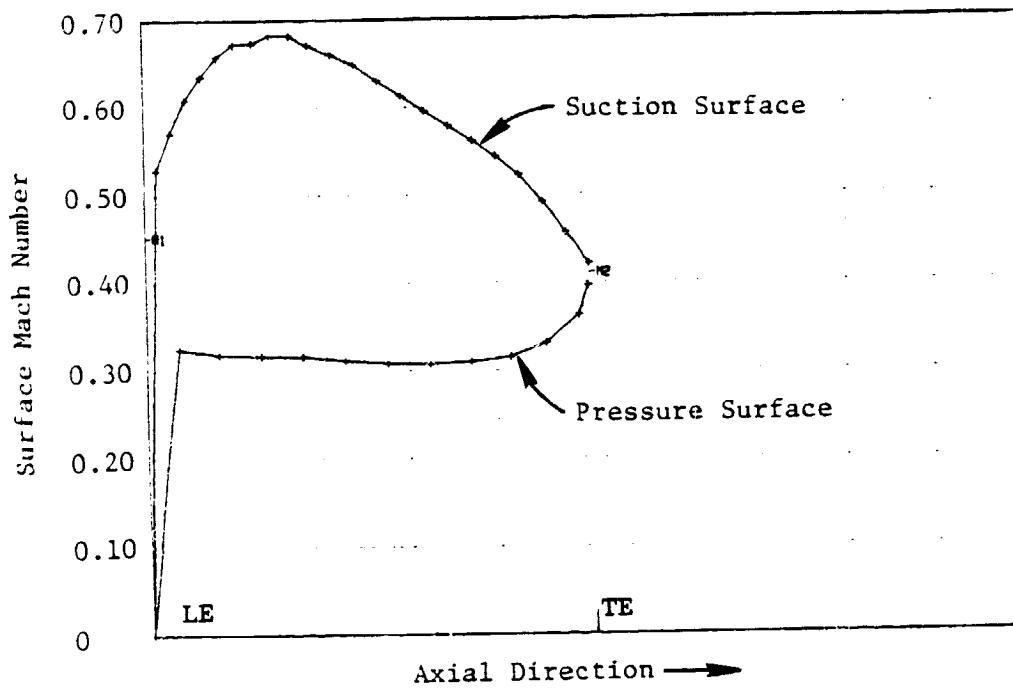
Figure 27.   Inner OGV Tip Streamline Surface Mach Number.
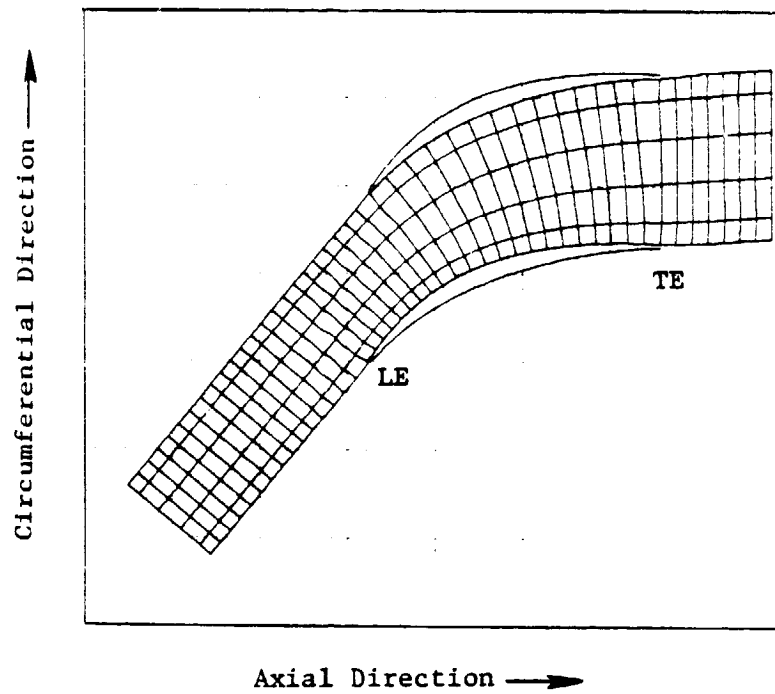
Figure 28.   Inner OGV Hub Streamline Cascade.
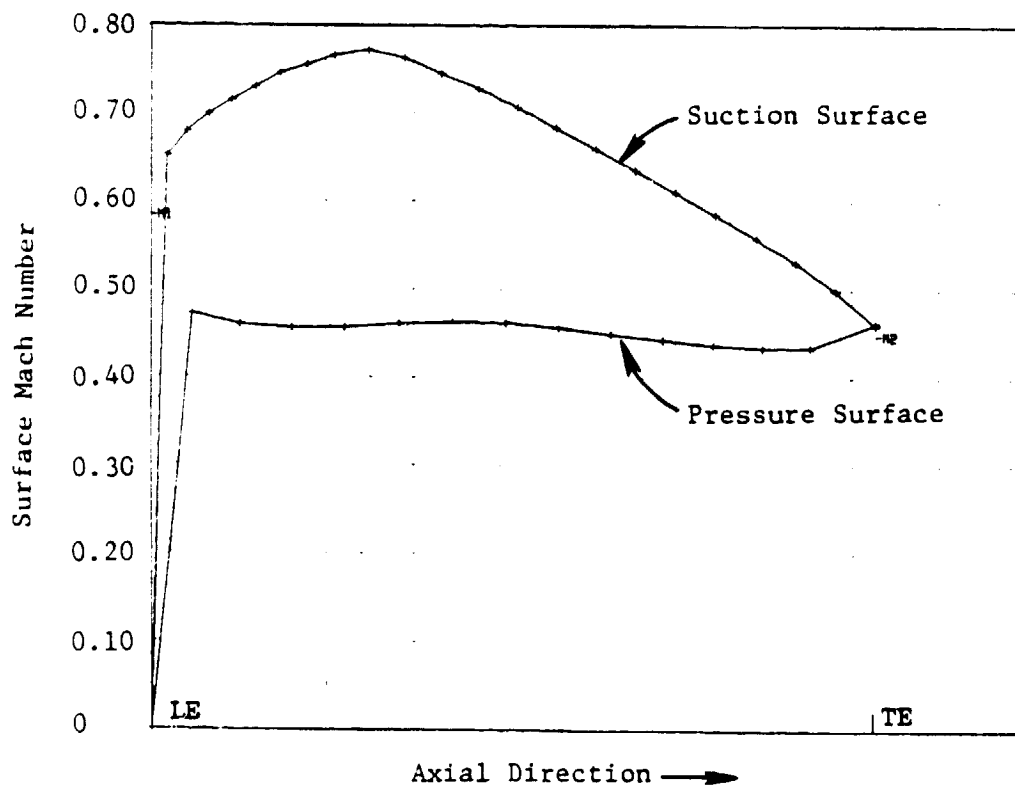
Figure 29.   Inner OGV Hub Streamline Surface Mach Number.
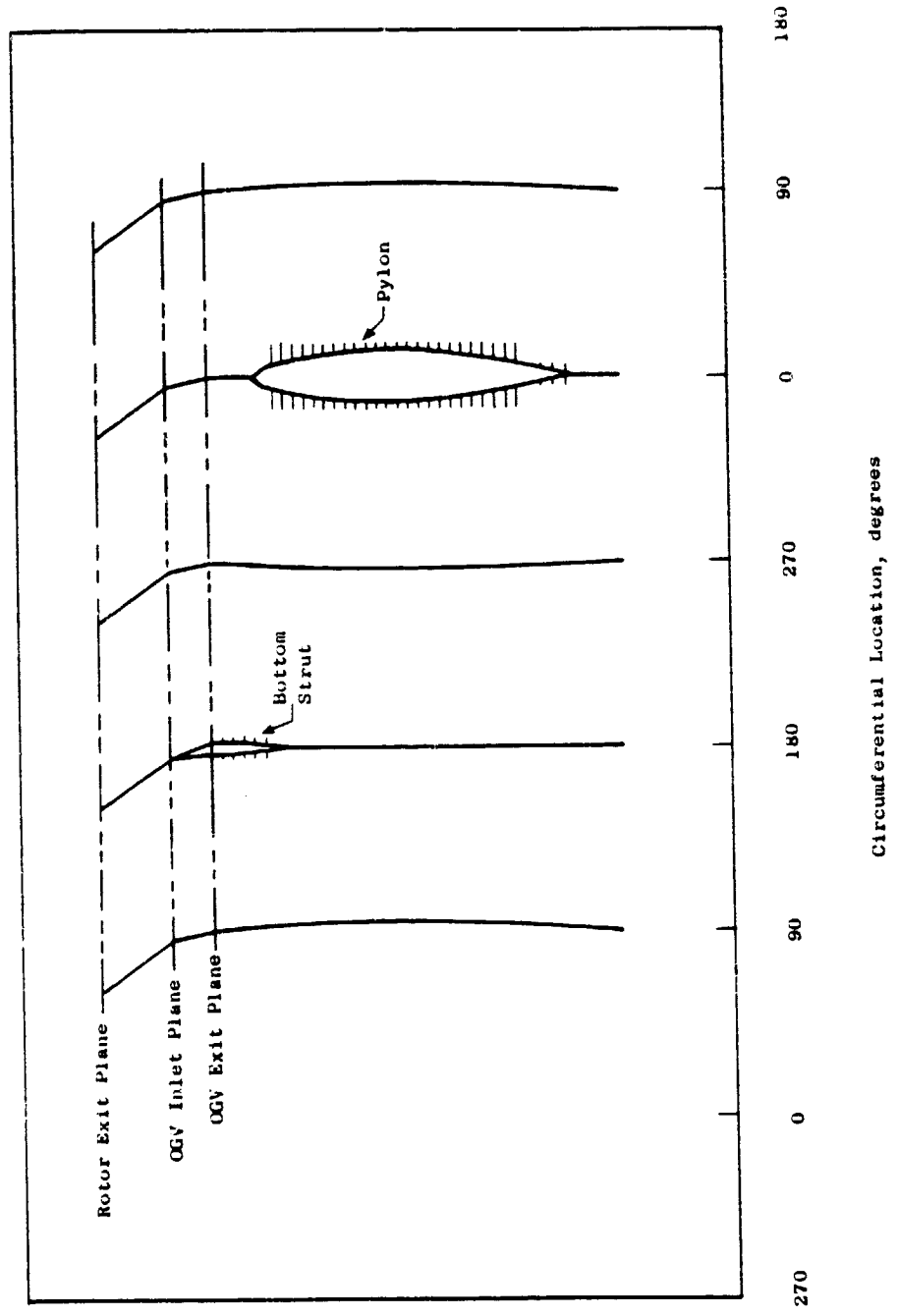
Figure 30. Two-Dimensional Stream Surface Geometry, Section P.

33
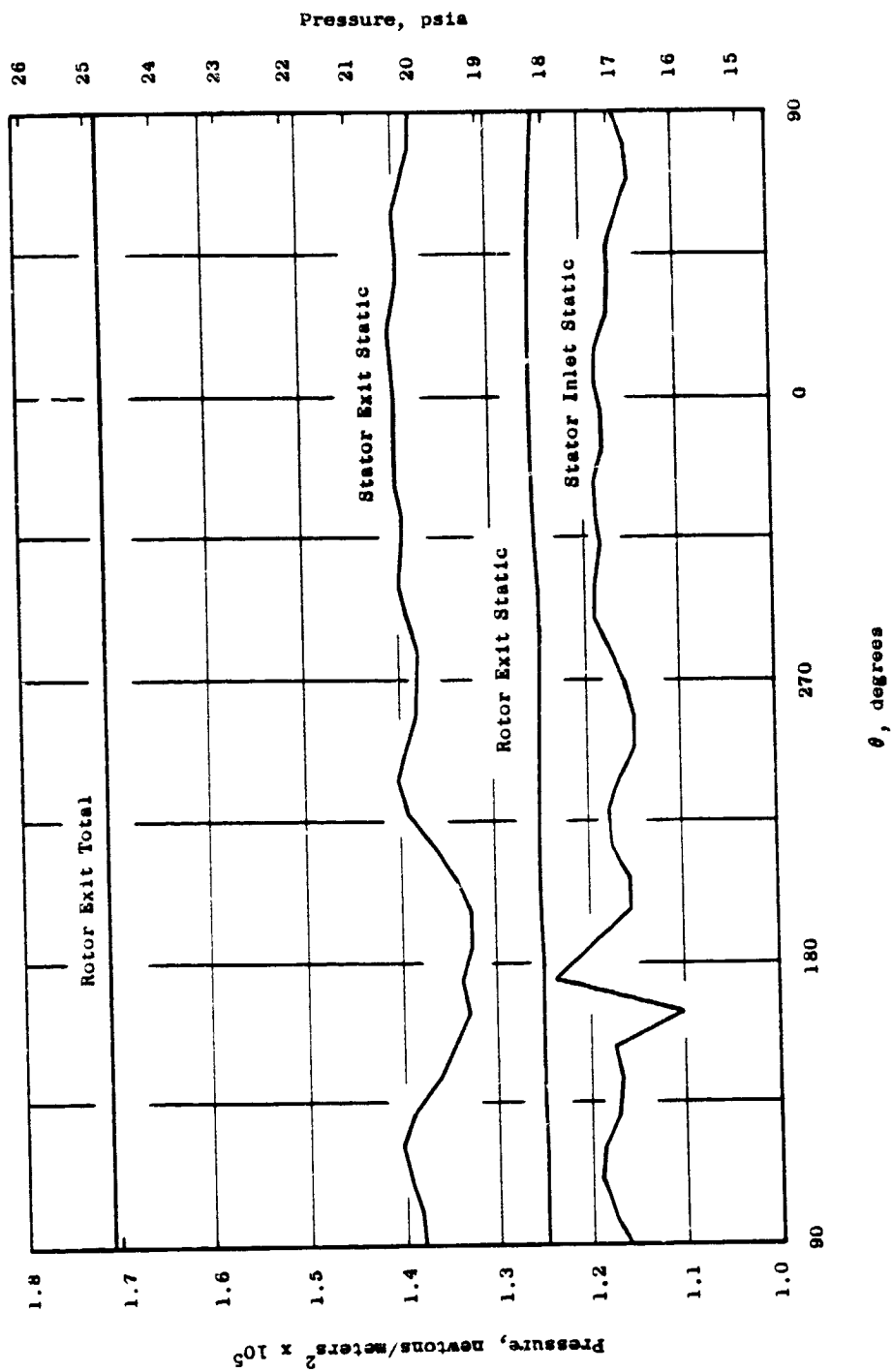
Figure 31. Circumferential Distribution of Pressure, Section P.
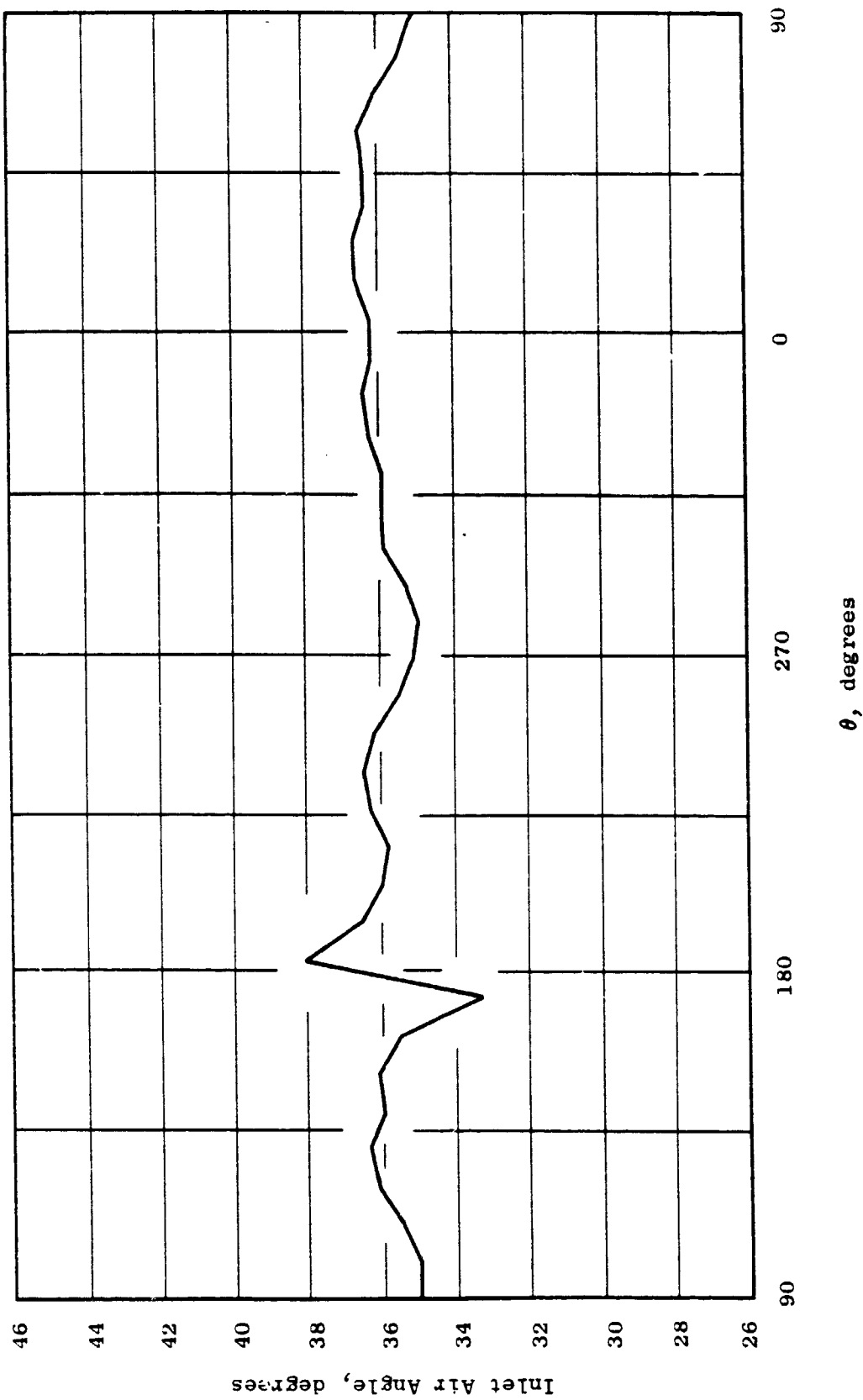
Figure 32. Circumferential Distribution of OGV Inlet Air Angle, Section P.

35

and hub (H). The three-dimensional program calculated the OGV exit flow angles which would be required to circumferentially shift the flow around the pylon and bottom strut bodies. The maximum circumferential variation of these angles was on either side of the pylon location where the calculated flow angles varied from +7° to -7°. At the horizontal locations, 90° and 270° clockwise aft looking forward, the calculated flow angles are approximately +3° and -3°, respectively. At the bottom of the engine (180°), the calculated flow angle is near zero. The vanes were then grouped into five sets, each of a different camber. With the inlet spacing between vanes held constant, the resulting vane geometry for sections near the tip (T) and near the island (I) at the top of the engine is shown in Figures 33 and 34. The position of the pylon relative to the vanes is also shown. In the bottom segment of the engine, the vanes adjacent to the thick strut and fairing are the nominal type vanes with the chords cut back to minimize the blockage in the passages. This configuration is shown schematically in Figure 35.

Cascade flow analyses were made of airfoil sections with nominal vane passage area distributions and also the airofil types on either side of the upper pylon where the maximum and minimum cambers occur. The results of the surface Mach number calculations for the nominal vane passages are shown for streamlines at the tip (T) and the island upper (I) and lower (H-I) surfaces in Figures 36 through 38. A 3° high inflow angle was intentionally specified at the tip streamline to account for the higher swirl in the boundary layer flow adjacent to the casing. The Mach number distribution for this streamline is shown in Figure 36. The Mach number distributions at the (I) and (H-I) sections show opposite trends; this is a consequence of the need to match static pressures at the island trailing edge with the different total pressures of the two streams. The circumferential-average solutions that dominate this effect are also shown.

The airfoil geometry for the five groups of vanes is tabulated in Appendix F.

MECHANICAL DESIGN

III. FAN ROTOR DESIGN

Figure 39 shows a cross section of the fan design to be used in the integrated core/low speed (ICLS) test. The rotor features a 32-blade fan stage shrouded at 55% span, and a 56-blade booster stage for core supercharging. The reduced aspect ratio improves the fan blade's ruggedness and the lowered shroud position improves aerodynamic efficiency to offset the greater weight of the fan rotor.

Included in the rotor mechanical features are the drop down dovetail slot that permits individual blade replacement and an anticlank system that prevents dovetail wear by limiting blade movement in the slot. Integrated with the anticlank spring, the blade axial retention system prevents fore or aft movement; the toal system is designed so there is no restriction on individual blade replacement.

36
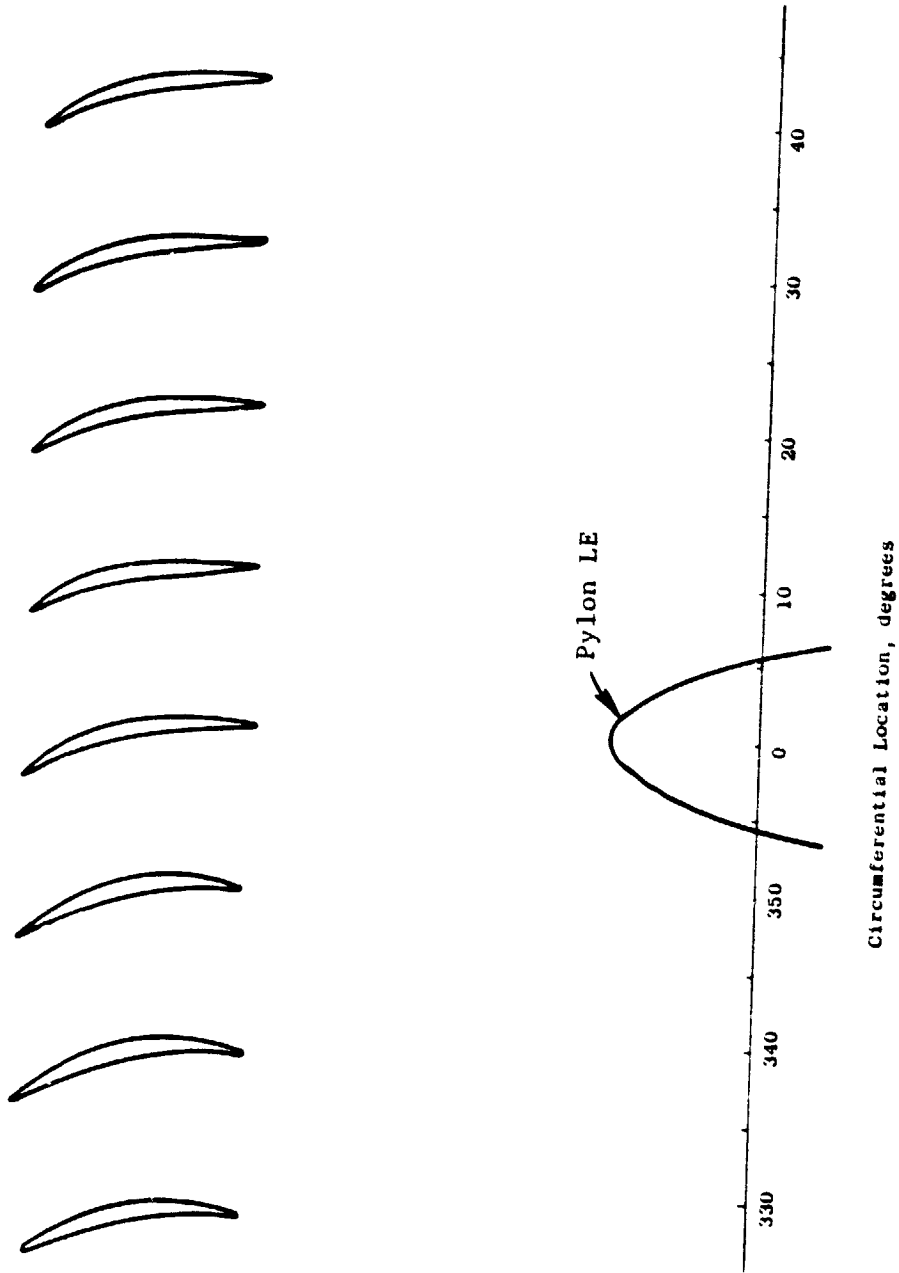
Figure 33. Vane Geometry Near Upper Pylon, Section T.
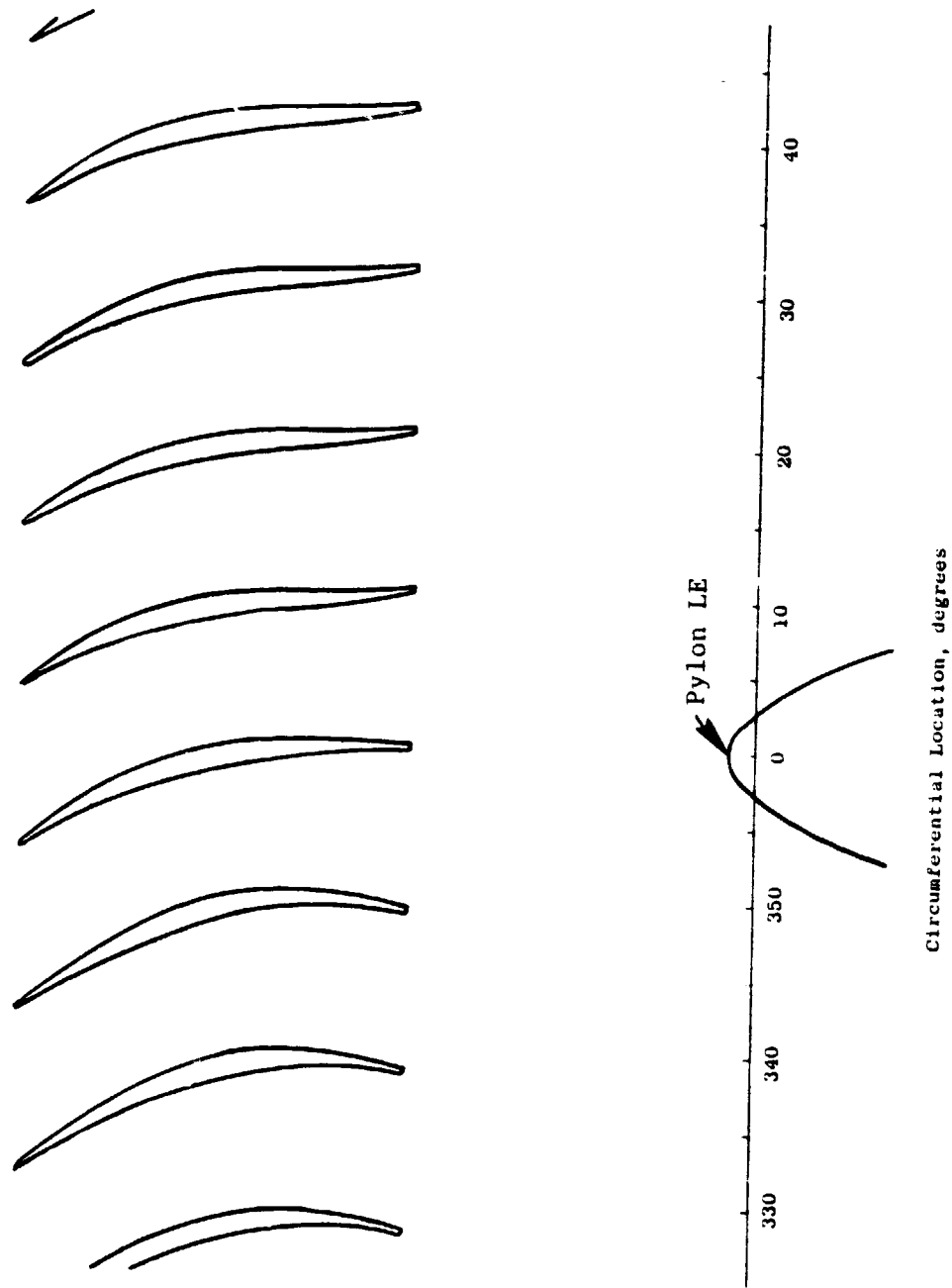
Figure 34. Vane Geometry Near Upper Pylon, Section I.

Nominal Vane
Type III

Nominal Vane
Type III

Circumferential Location, degrees

190 185 180 175 170
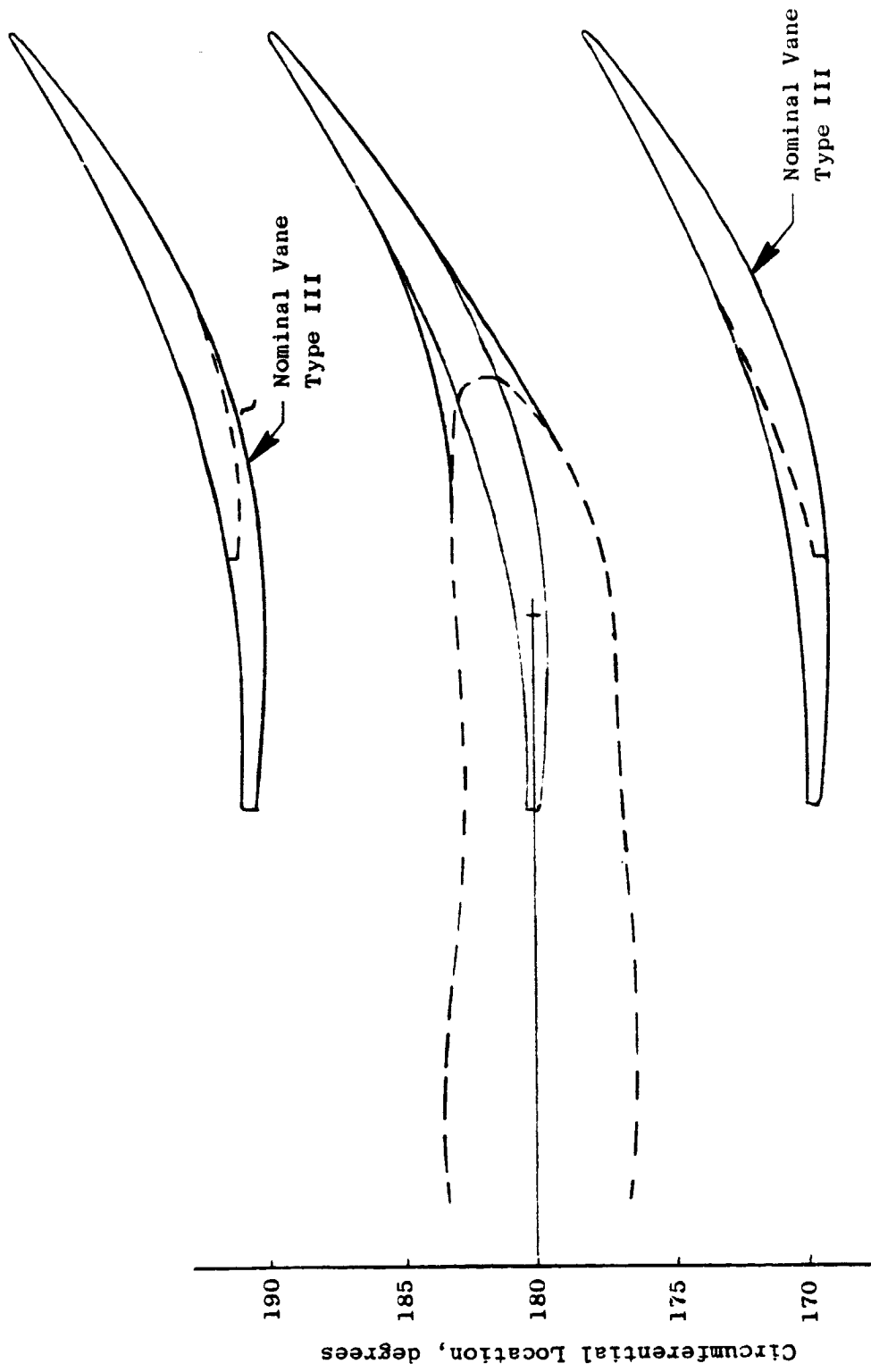
Figure 35. Modified Strut Fairing and Cutback Airfoils.
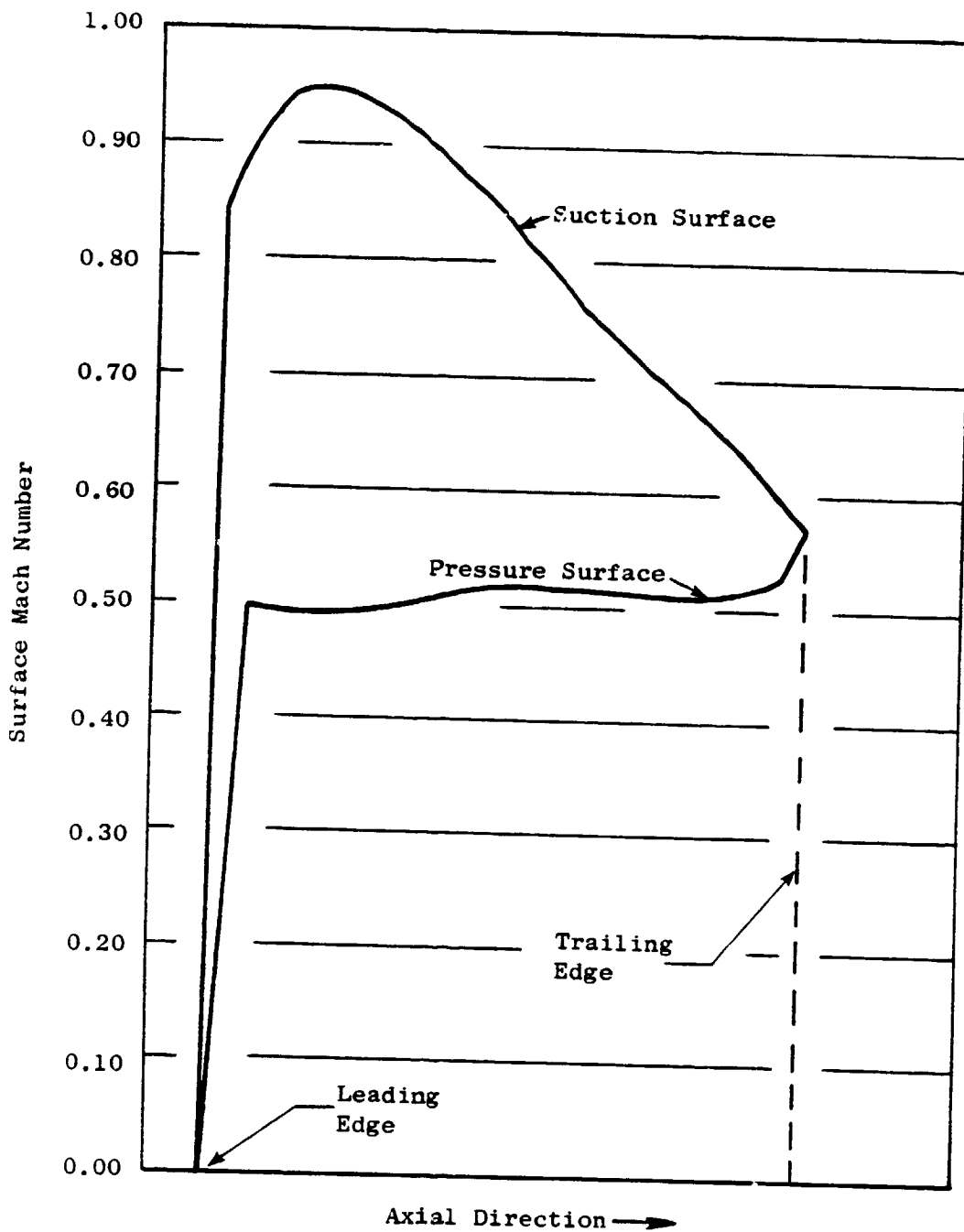
Figure 36.   OGV Mach Number Distribution, Section T.
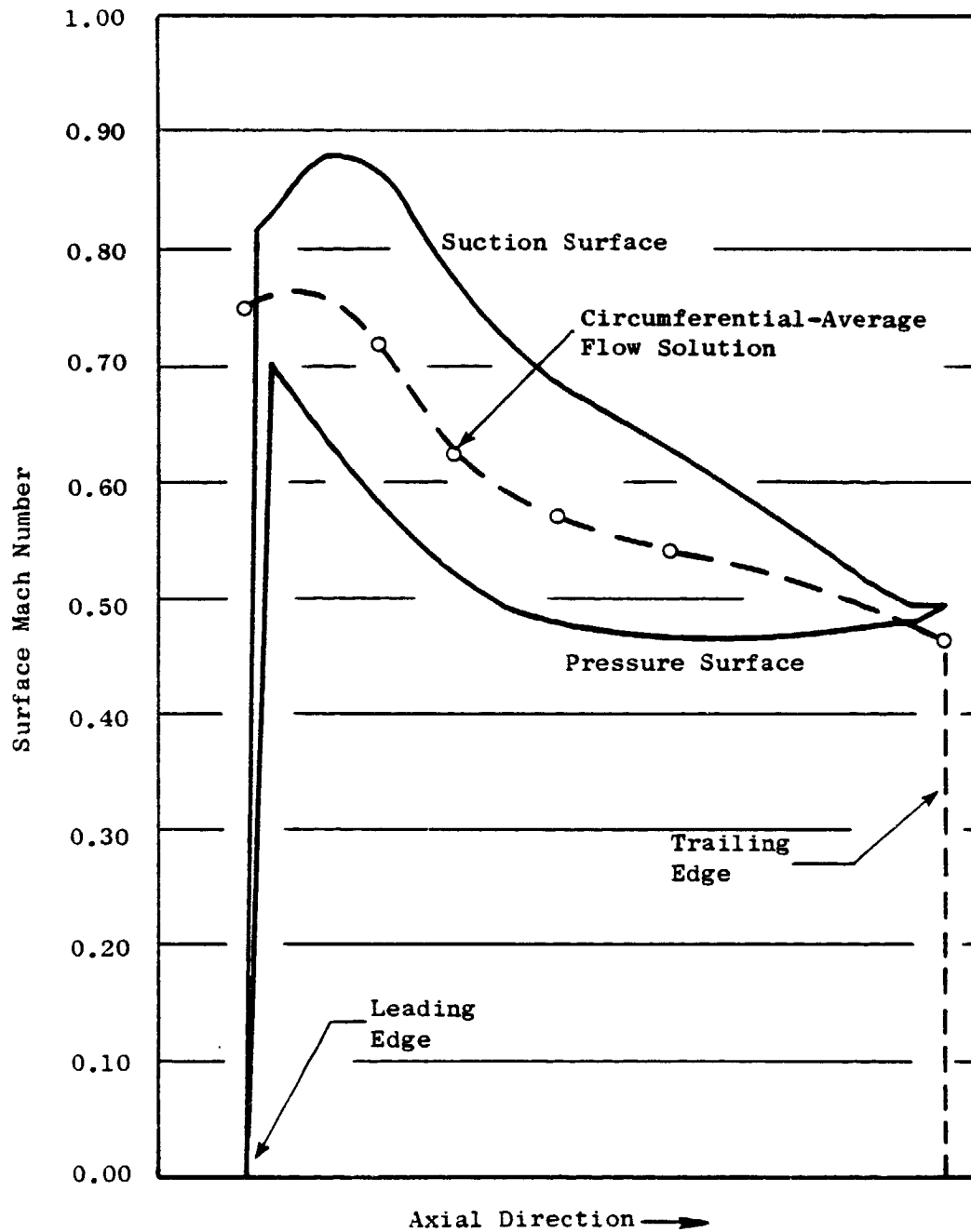
Figure 37. OGV Mach Number Distribution, Section I.
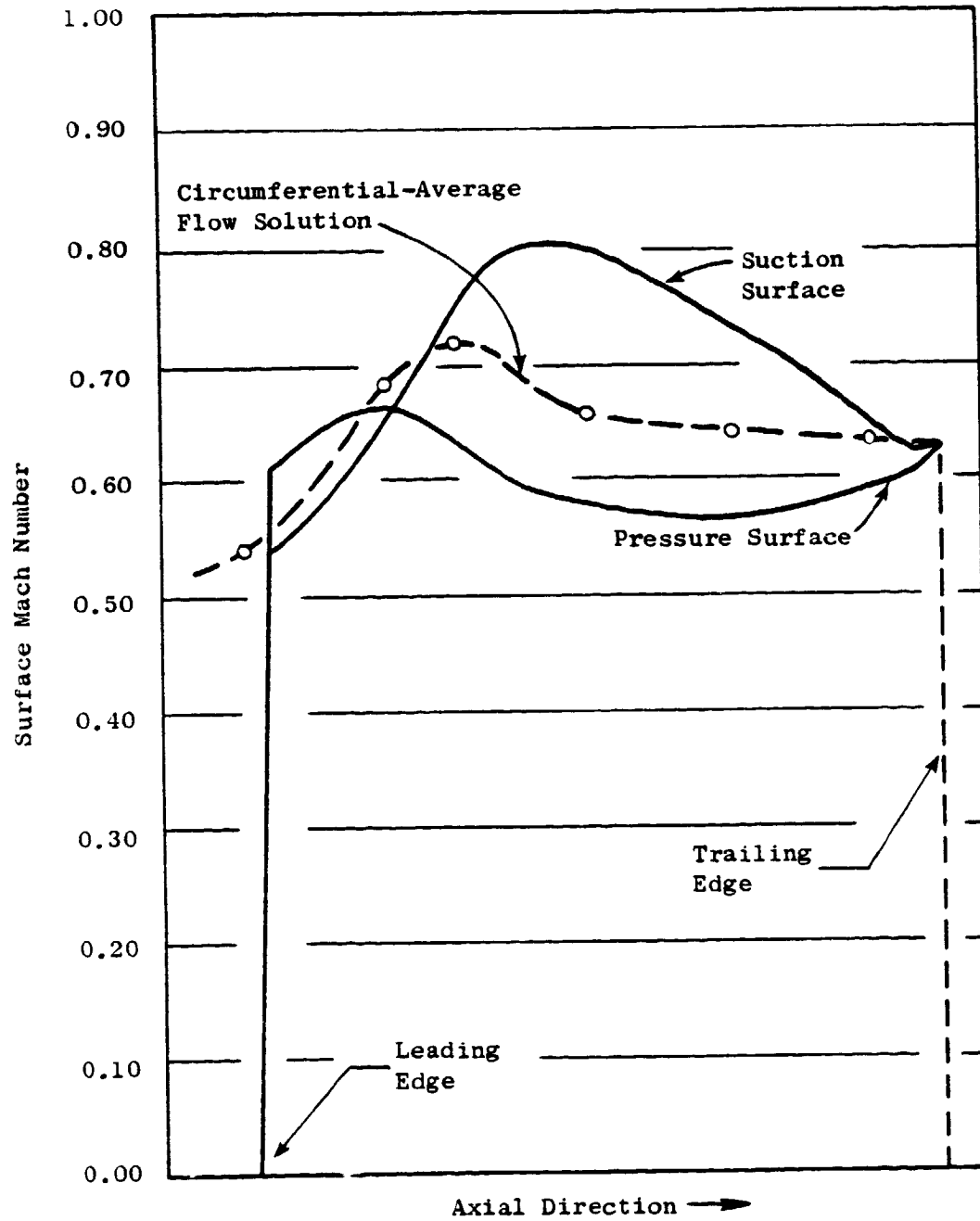
Figure 38. OGV Mach Number Distribution, Section H-I.
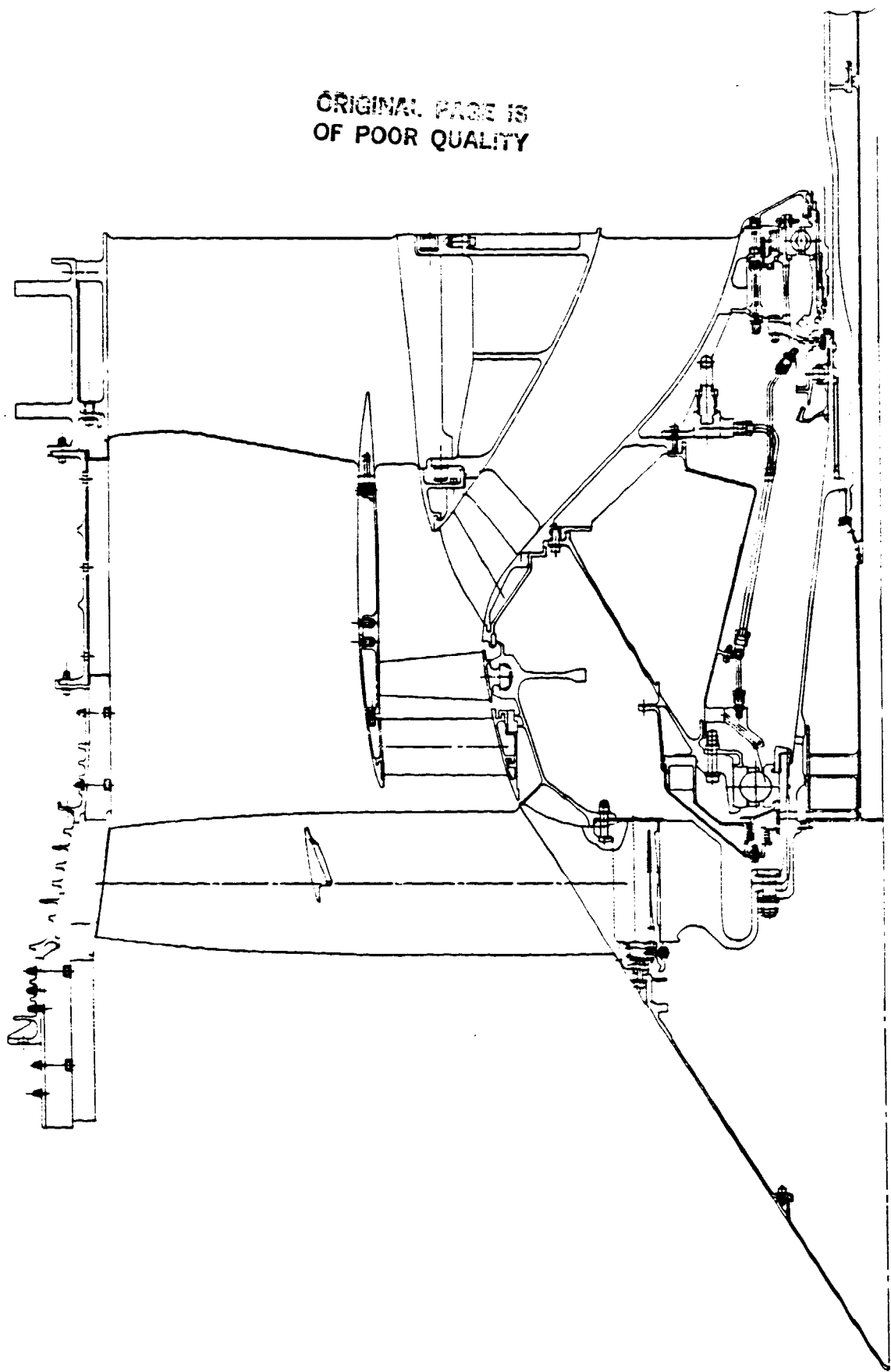
Figure 39. ICLS Fan Configuration.

The shafting arrangement connects the fan disk to the forward fan shaft and, through the support shaft, to the No. 1 thrust bearing. The remote connection of the bolted joint to the bearing permits the disk bearing and joint to be designed independently and has these advantages.

- The design of the disk, bearing, and joint are more nearly optimized by not having to be compromised by one another

- Oversizing the bearing or undersizing the flange would be required if the conventional flange under bearing configuration were used

- The bolted joint can accommodate more and smaller size bolts for a lighter design and yet have sufficient torque driving capacity

- With the smaller bearing and eccentric design of the disk, the two can be fitted more closely together to minimize fan overhang.

With the flange of the fan shaft on the forward side of the joint, the shaft can be removed without disturbing the fan rotor thus allowing access to the interior of the engine and making possible modular disassembly of the engine.

The conical shape of the spinner is resistant to ice buildup or damage from bird impact. The production spinner will be a one-piece structure directly mounted to the fan disk.

The Stage 1 stator inner shroud passes over the Stage 2 disk forward sealing element at buildup and thus permits the shroud to be a 360° continuous ring for greater stator stiffness and reduced wear.

The full-scale fan test vehicle (Figure 40) has all of the mechanical design features of the ICLS fan rotor except the connecting shafting which has been modified to conform to facility requirements.

A. Design Loads and Limits

The mechanical loads and limits to which the fan rotor is designed are defined in the technical requirements and are supplemented by GE design practices. Loads are given in cycle cases covering the aero design point and maximum rotor speed (Table III). The fan test vehicle and the ICLS engine hardware are designed to meet FPS conditions in the airfoils and growth case conditions in the supporting structure. Should it be required to demonstrate growth conditions, only the airfoils would require modification. Aerodynamic input to the blading design is shown in Table IV.

Design stresses are limited to minus 3 sigma deviations from average material properties for elastic conditions. In high cycle fatigue, the Goodman diagram indicates an allowable vibratory stress for infinite life. Low cycle fatigue stress levels are based on 36,000 aircraft missions with two stress cycles per mission for a total of 72,000 stress cycles. The disks must show a residual life of 6000 cycles with a 0.01 x 0.03-inch defect.
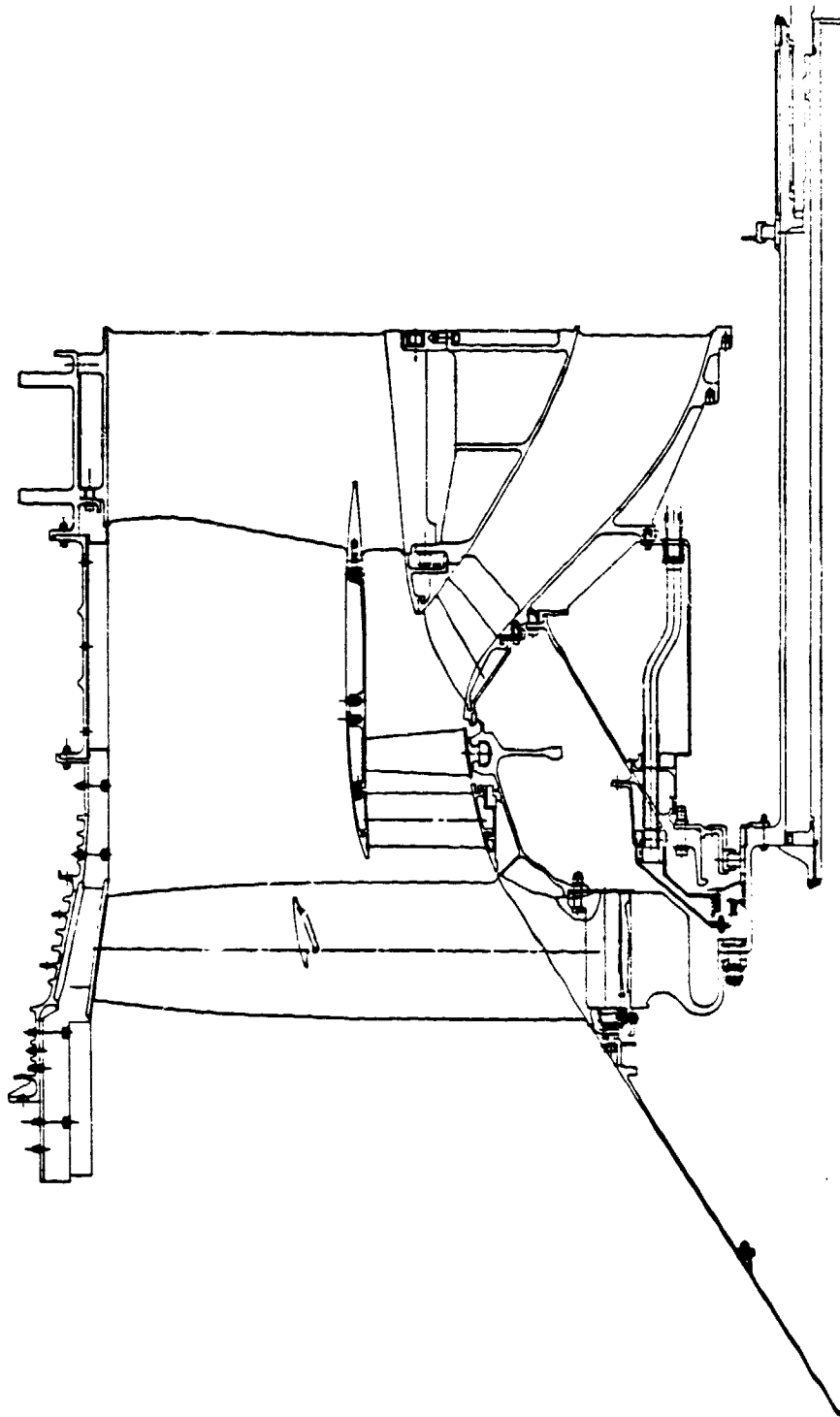
Figure 40. Full-Scale Fan Test Vehicle.

Table III. Fan Design - Cycle Performance Parameters.

	FPS	Growth
Flowpath and Clearance Calculation		
• Cycle Case No. 41		
Altitude	10,668 m (35,000 ft)	10,668 m (35,000 ft)
M_o	0.80	0.80
ΔT_o	+10° C (+18° F)	+10° C (+18° F)
Rating	Max Climb	Max Climb
Fan Physical Speed	3539 rpm	3939 rpm
Maximum Stress Calculation		
• Cycle Case No. 72		
Altitude	5791 m (19,000 ft)	5791 m (19,000 ft)
M_o	0.30	0.30
ΔT_o	+15° C (+27° F)	+15° C (+27° F)
Rating	Takeoff	Takeoff
Fan Physical Speed	3611 rpm	4079 rpm
(at 1.2% Overspeed)	(3653 rpm)	(4126 rpm)

Table IV. Fan Design - Aerodynamic Parameters.

	Fan Stage 1	Booster Stage
Tip Diameter	210.8 cm (83.0 in.)	133.8 cm (52.66 in.)
Tip Speed	411.5 m/sec (1350.0 ft/sec)	261.1 m/sec (856.5 ft/sec)
Airflow	643.7 kg/sec (1419.16 lb/sec)	143.7 kg/sec (316.90 lb/sec)
Radius Ratio (Inlet)	0.342	0.782
Aspect Ratio	2.597	2.12
P_R	1.650	1.129
T_R	1.1757	1.0475
Number of Blades	32	56

B. Design Goals

Fan rotor improved durability and ruggedness, and reduction of maintenance were design goals established for the fan rotor. These were to be accomplished by incorporating in the rotor design the following features for greater mechanical reliability.

● Improved vibratory characteristics

- 15% vibratory margin over 2/rev at maximum rotor speed

- Improved rotor stiffness to maintain frequency margins in the coupled disk/blade modes

- Blade attachments stronger than airfoils in the lower vibratory modes.

● Improved mechanical characteristics

- Good bird strike capability

- Low dovetail stress for improved life

- Design dovetail posts to withstand blade loss without further failure

- Anticlank system to prevent dovetail wear

- Improved torque transmitting capability of the disk/shaft bolted joint.

● Improved system characteristics of the fan rotor

- Reduce rotor overhang to minimize unbalance moment

- Configure shafting to allow modular disassembly of the engine.

Materials

Table V lists the materials selected for the fan test and ICLS rotors; 4340 steel was selected for the forward fan shaft demonstrator because of the unavailability at this time of the primary shaft material (MARAGE 250). Tradeoff studies may show greater advantages in a higher strength titanium in the growth version of the rotor in terms of weight savings and improved fatigue life.

C. Fan Blade Design

Figure 41a and 41b illustrate configuration parameters of the fan blade design. In Figure 41a, the effect of shroud placement can be seen having its effect on the thickness distribution in the blade. The midspan thickening was necessary to obtain flexural frequency margin over 2/rev excitation. The weight penalty associated with the thicker blade and lower shroud is counterbalanced by improved blade efficiency and better resistance to birdstrike.

48

Table V. Fan Rotor List of Materials.

Fan Blades	Titanium 6Al-4V
Fan Disk	Titanium 6Al-4V
Spinner	7075 Aluminum
Spinner Cover	7075 Aluminum
Anticlank Spring	Titanium 6Al-4V
Blade Retention Key	Inco 718
Booster Spool	Titanium 6Al-4V
Booster Blade	Titanium 6Al-4V
Fan Shaft 5/8-inch Bolts	Inco 718
Forward Fan Shaft	4340 Stainless Steel
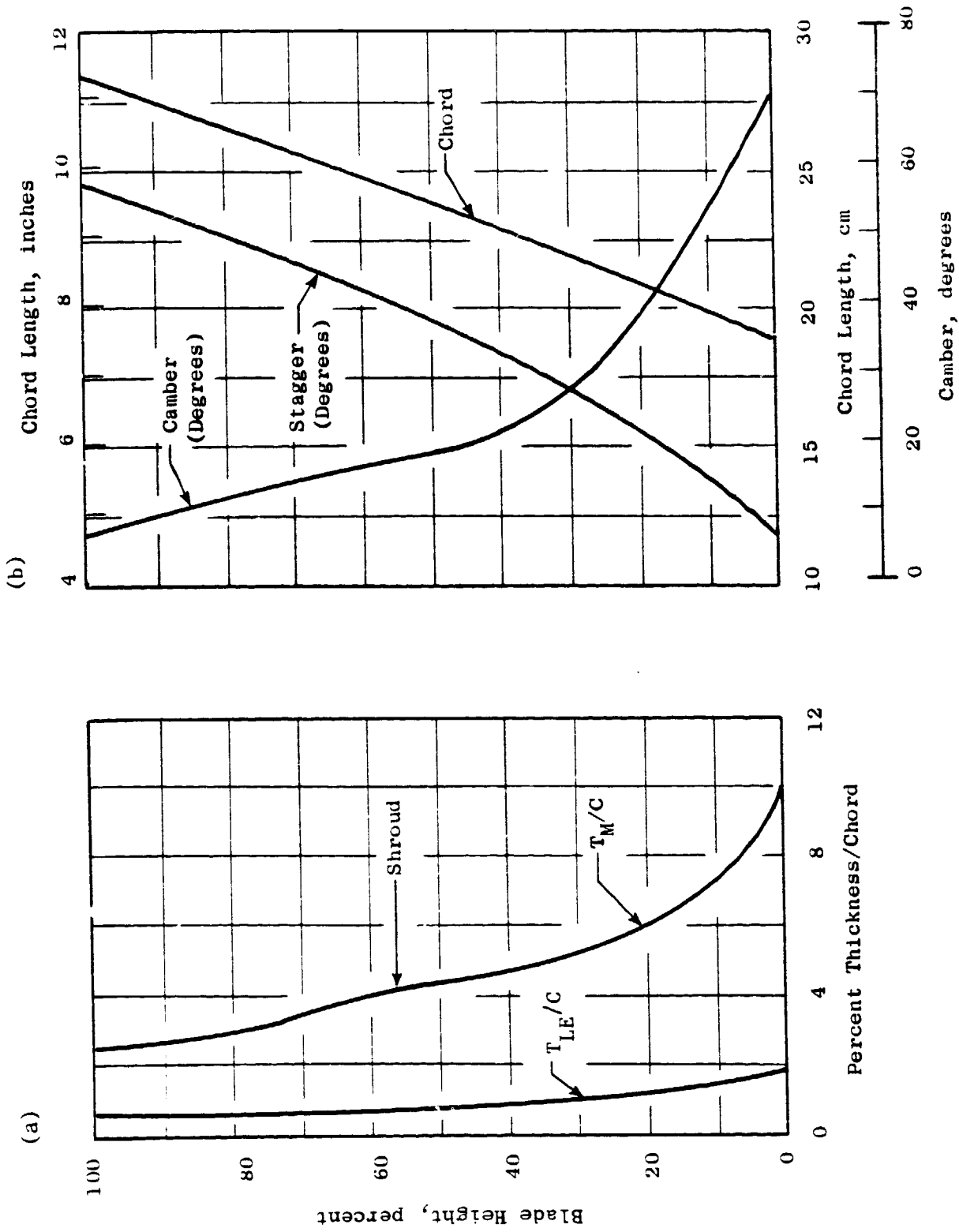
Figure 41. Fan Blade Geometry.

Figure 42 shows the contour plots of blade surface effective stress at steady state conditions derived from the finite element (TAMP-MASS) analysis. These values were in reasonably good agreement with the Twisted Blade (beam) results. Untwist of the blade (shown in Figure 43) was calculated by TAMP-MASS and was used to pretwist the blade to obtain correct aerodynamic incidence at operating conditions. The stress plot of Figure 44 shows the stress around the root of the blade at the platform as derived from the Twisted Blade program using scaled CF6 end effects. The stress levels shown in Figures 42 and 44 allow adequate high cycle fatigue capability and are well under the allowable low cycle fatigue stress. These stress levels and distribution will be verified by test as hardware becomes available.

Figure 45 shows the Campbell diagram for the fan blade with the first three modes plotted. The spread of frequencies at each mode indicates the frequency range between the lowest disk/blade combined frequency and the highest or fixed blade out-of-phase frequency. In first flex, the frequency margin between the lowest in-phase frequency and 2/rev is 14.6% which meets the design goal of providing adequate frequency margin at maximum speed. In addition, the first flex crossing of other per rev lines occurs at low enough speeds to be out of the operating range, or precludes a significant response. The fan blade is stall protected from torsional instability at all operating speeds. Using data from a similar blade and previously developed correlations, the fan blade platform corner frequency was calculated to be well above the stator passing frequency.

Figure 46 presents a summary of geometry and stress and deflection data on the fan blade shroud. Bending stresses at the shroud fillet are approximately 46.9 kN/cm^2 (68 ksi) as obtained by the TAMP-MASS finite element program. Shroud tip deflections calculated by this program were used to establish predroop of the shroud so that at speed, the shroud deflections match and surface-to-surface contact takes place between each pair of mating shrouds. Shroud cross sections are aerodynamic shapes modified to provide adequate contact surface so that contact stress will be low enough [1324 N/cm^2 (1920 psi) in this case] to ensure long life for the tungsten carbide hard facing. Line of action of the blade deflection in the flexural modes was checked to ensure it would not be along the contact face of the shroud.

Figure 47 shows a cross section of the fan blade and disk at the dovetail/post interface, the cross section taken through the blade stacking axis. Due to the steep flowpath, the shank is very short at the front of the blade requiring disk relief to clear the blade platform. This view also shows the depth of the slot that is required to drop the blade, clearing the shroud interlock for individual blade removal. In normal assembly, the space under the blade is occupied by the anticlank spring which preloads the blade outward to take play out of the disk/blade interface.

Figure 48 is a summary of the blade dovetail and disk post steady-state stresses. The 10° orientation angle and blade stacking axis offsets were done to balance dovetail corner stresses. A Goodman diagram (Figure 49) shows the relative strength between the fan blade airfoil and its dovetail

Convex Face   Concave Face

- N = 3653 rpm
- Stress in kN/cm^2 (ksi)

Figure 42. Fan Blade Effective Stress Contour Plots.
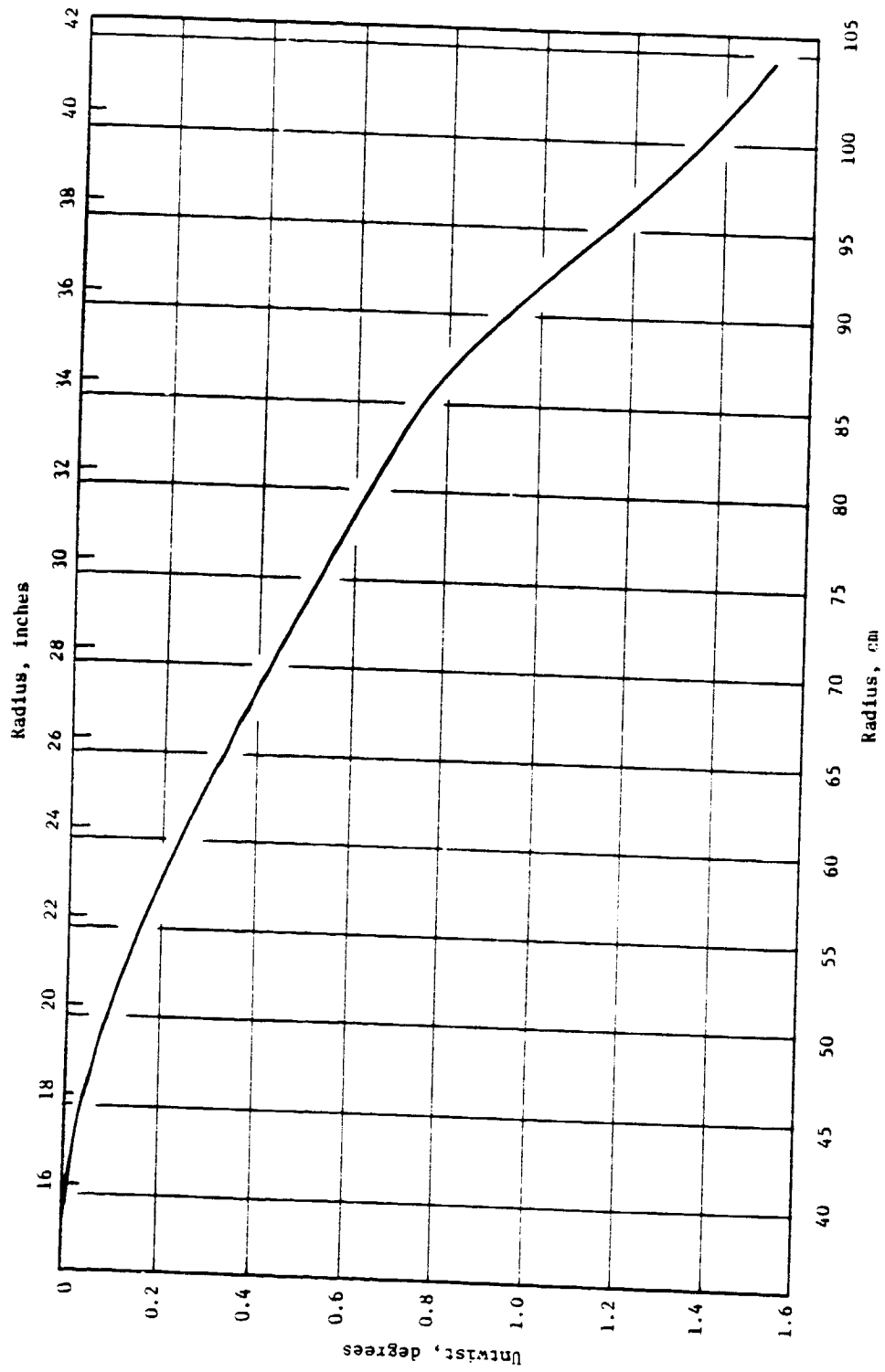
Figure 43. Fan Rotor Blade Untwist.
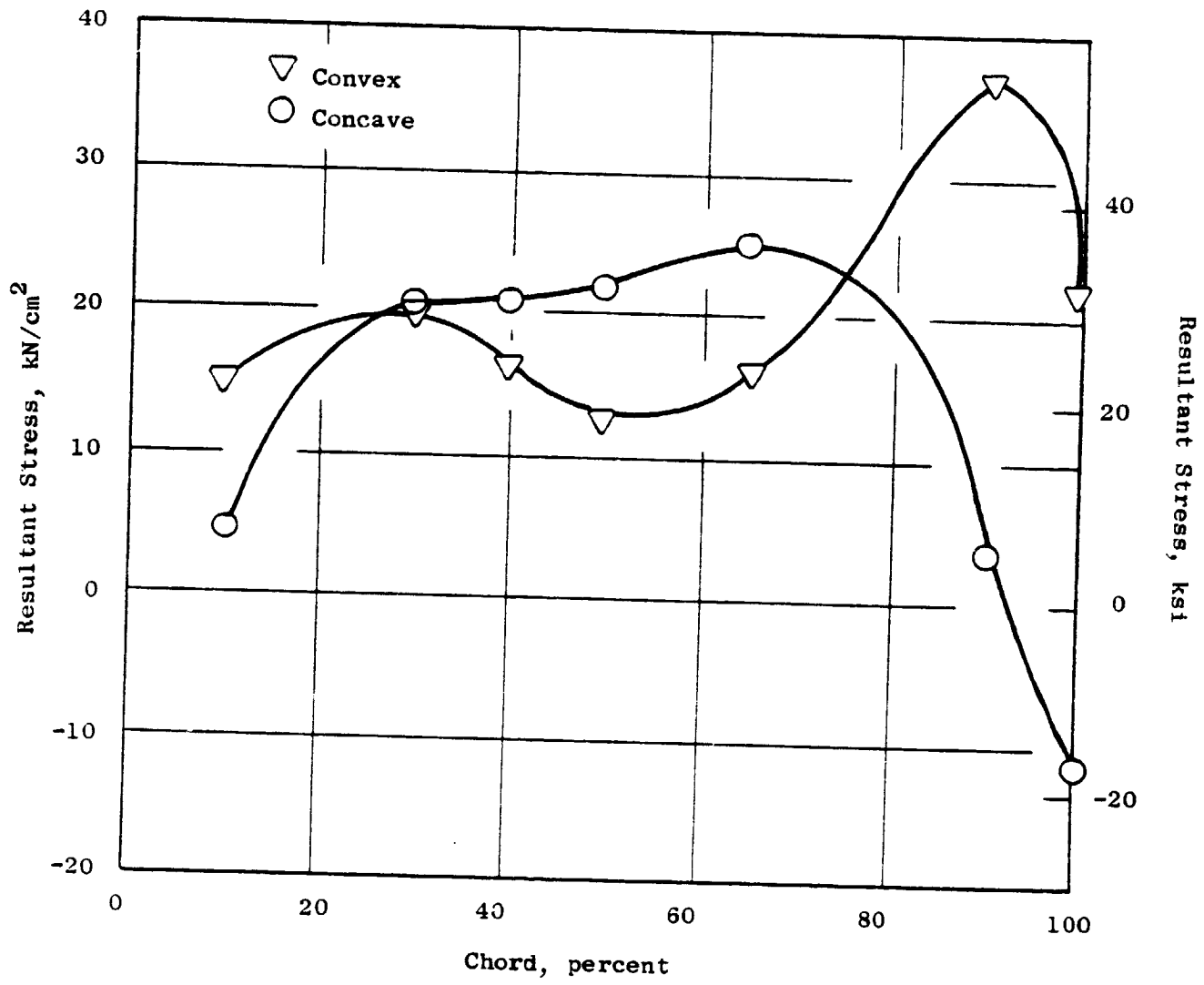
Figure 44.   Fan Blade Root Stress.
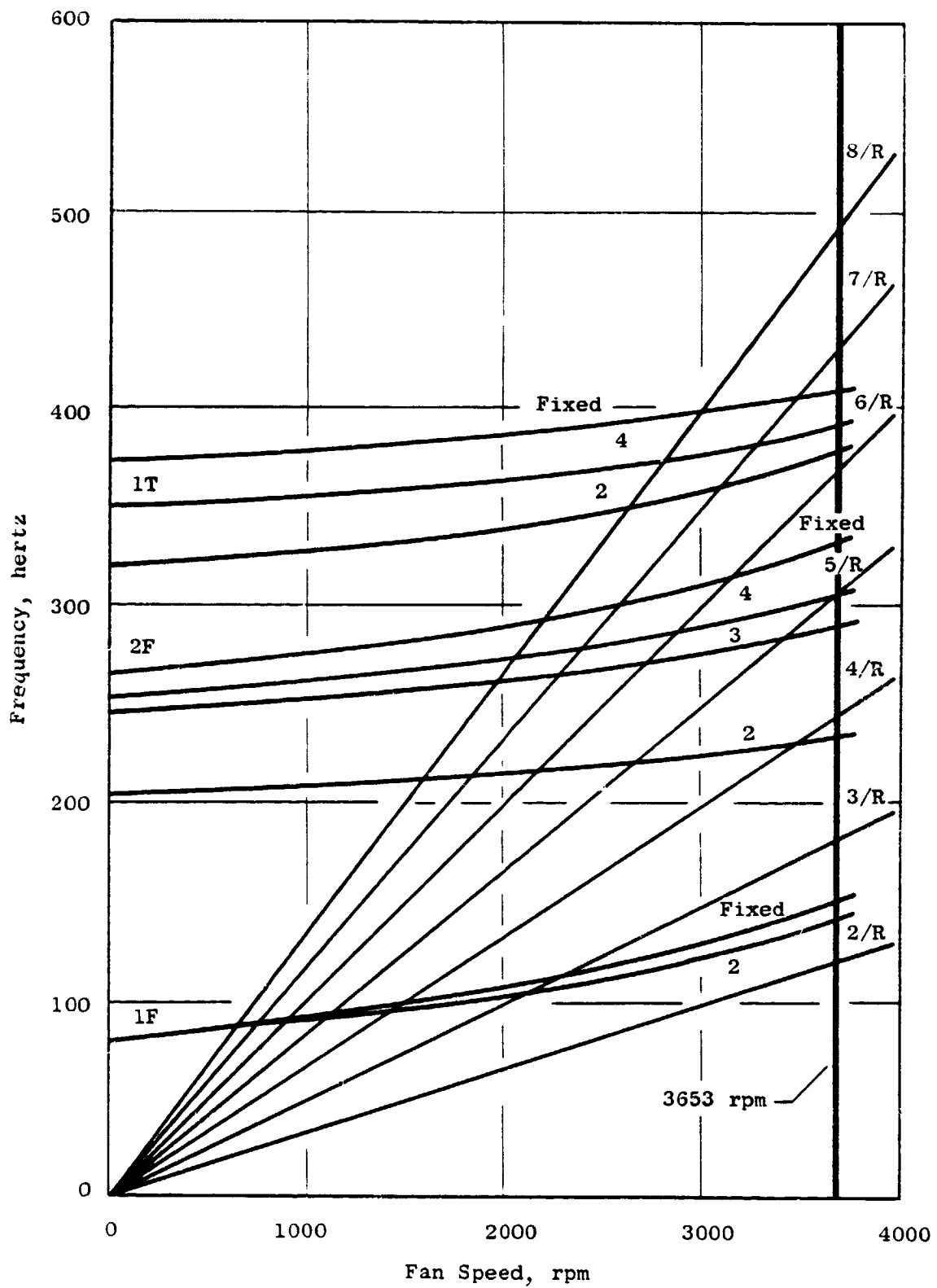
Figure 45. Fan Blade System and Fixed Blade Frequencies.

46.9 kN/cm^2 (68 ksi) ————
    Fillet Stress

• 3653 rpm
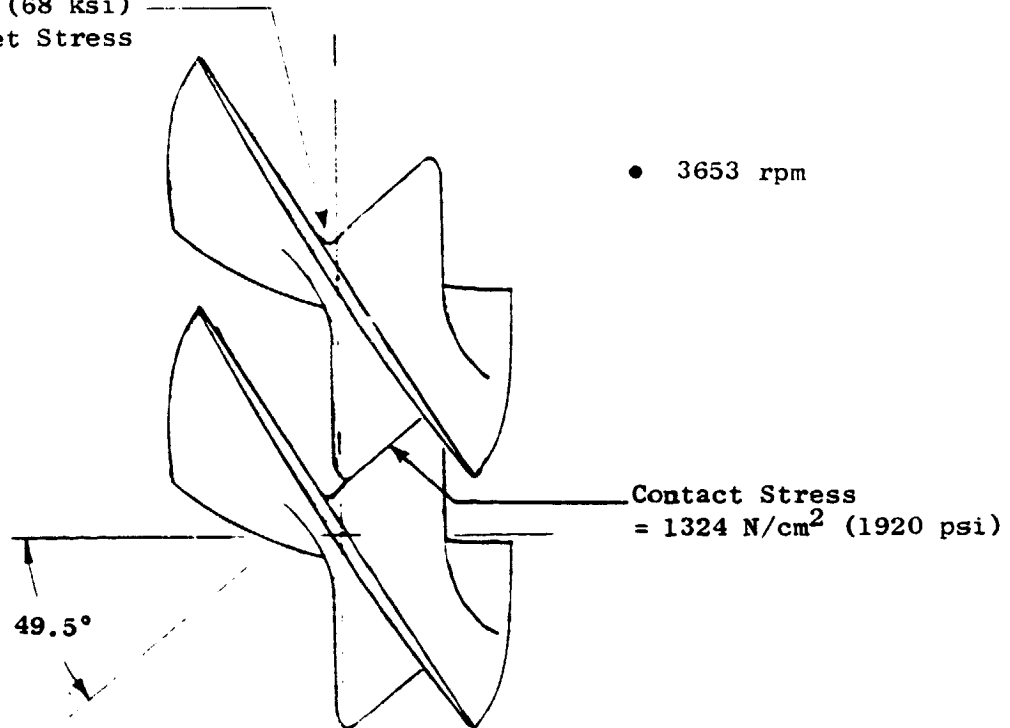
Contact Stress
= 1324 N/cm^2 (1920 psi)

49.5°

Flexural Displacement Vector Relative
to Shroud Angle:
1st Flex = 48.6°
2nd Flex = 50.0°

Shroud Tip Deflection
Left Wing = 0.180 cm (0.071 in.)
Right Wing = 0.150 cm (0.059 in.)
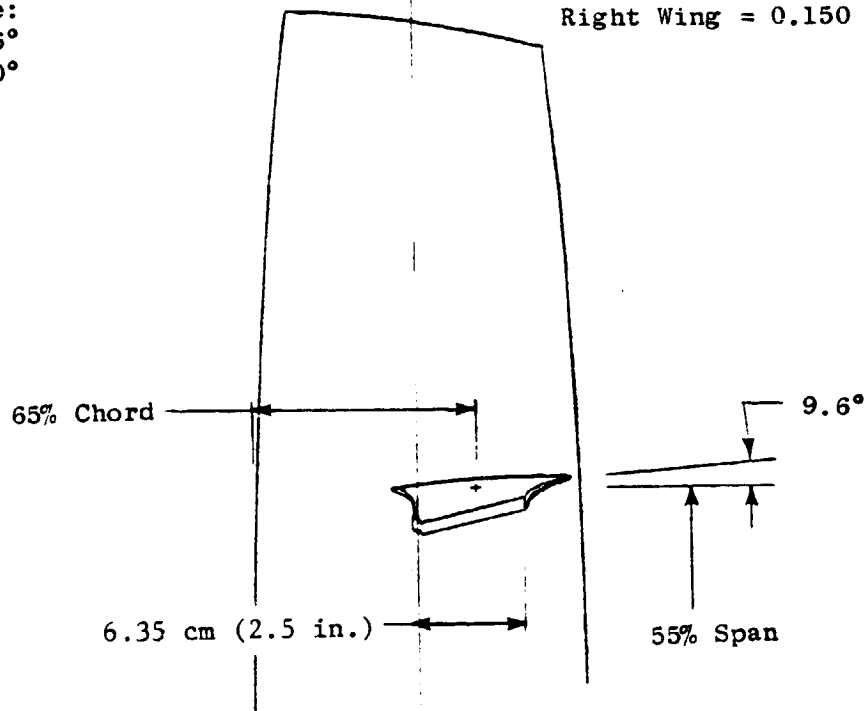
65% Chord

9.6°

6.35 cm (2.5 in.)

55% Span

Figure 46.   Fan Blade Shroud.
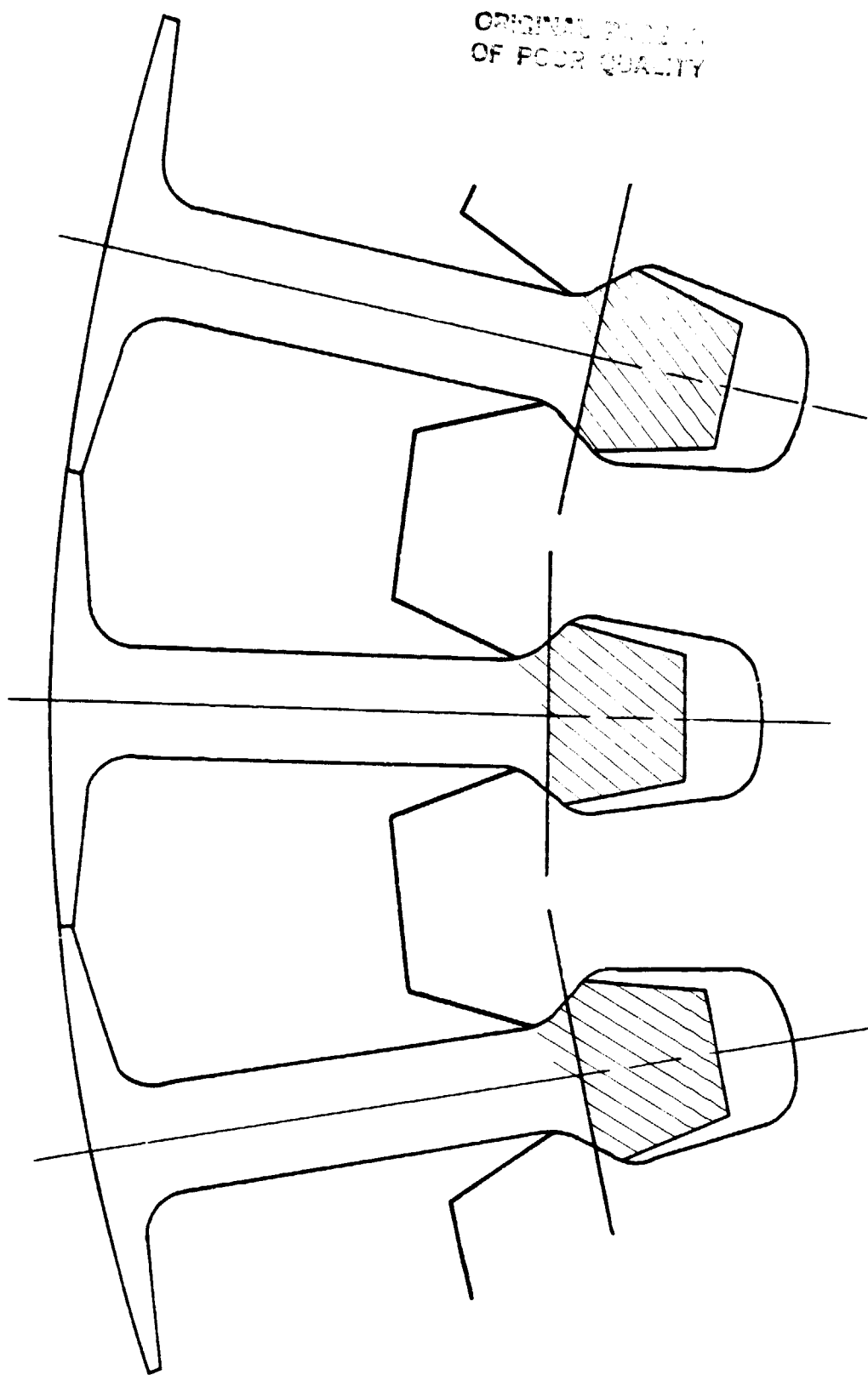
Figure 47. Fan Dovetail and Post Cross Section.

31.0 kN/cm^2 24.1 kN/cm^2
(44.9 ksi)   (35.0 ksi)

Forward

28.1 kN/cm^2
(40.8 ksi)

Aft

31.9 kN/cm^2
(46.2 ksi)

27.1 kN/cm^2
(39.3 ksi)

23.0 kN/cm^2
(33.3 ksi)

35.9 kN/cm^2
(52.0 ksi)

38.5 kN/cm^2 29.0 kN/cm^2
(55.8 ksi)   (42.1 ksi)

Forward

36.8 kN/cm^2
(53.4 ksi)

Aft

39.3 kN/cm^2
(57.0 ksi)

27.8 kN/cm^2
(40.3 ksi)

Disk Post

Axial Length	16.3 cm	(6.4 in.)
Minimum Post Width	2.890 cm	(1.137 in.)
Orientation	10°	
Flank Angle	55°	
Flank Width	0.803 cm	(0.316 in.)
Crush Stress	30.4 kN/cm^2	(44.1 ksi)
LCF Limit	46.9 kN/cm^2	(68 ksi)
(72,000 Cycles)		

Blade Dovetail

Axial Length	16.3 cm	(6.4 in.)
Shank Thickness	1.94 cm	(0.764 in.)
Orientation	10°	
Flank Angle	55°	
Flank Width	0.803 cm	(0.316 in.)
Blade Offsets		
Axial	0.295 cm	(0.116 in.)
Tangential	0.119 cm	(0.047 in.)
Crush Stress	30.4 kN/cm^2	(44.1 ksi)
LCF Limit	50.3 kN/cm^2	(73 ksi)
(72,000 Cycles)		

Figure 48.   Fan Blade Dovetail and Disk Post Stresses.

58
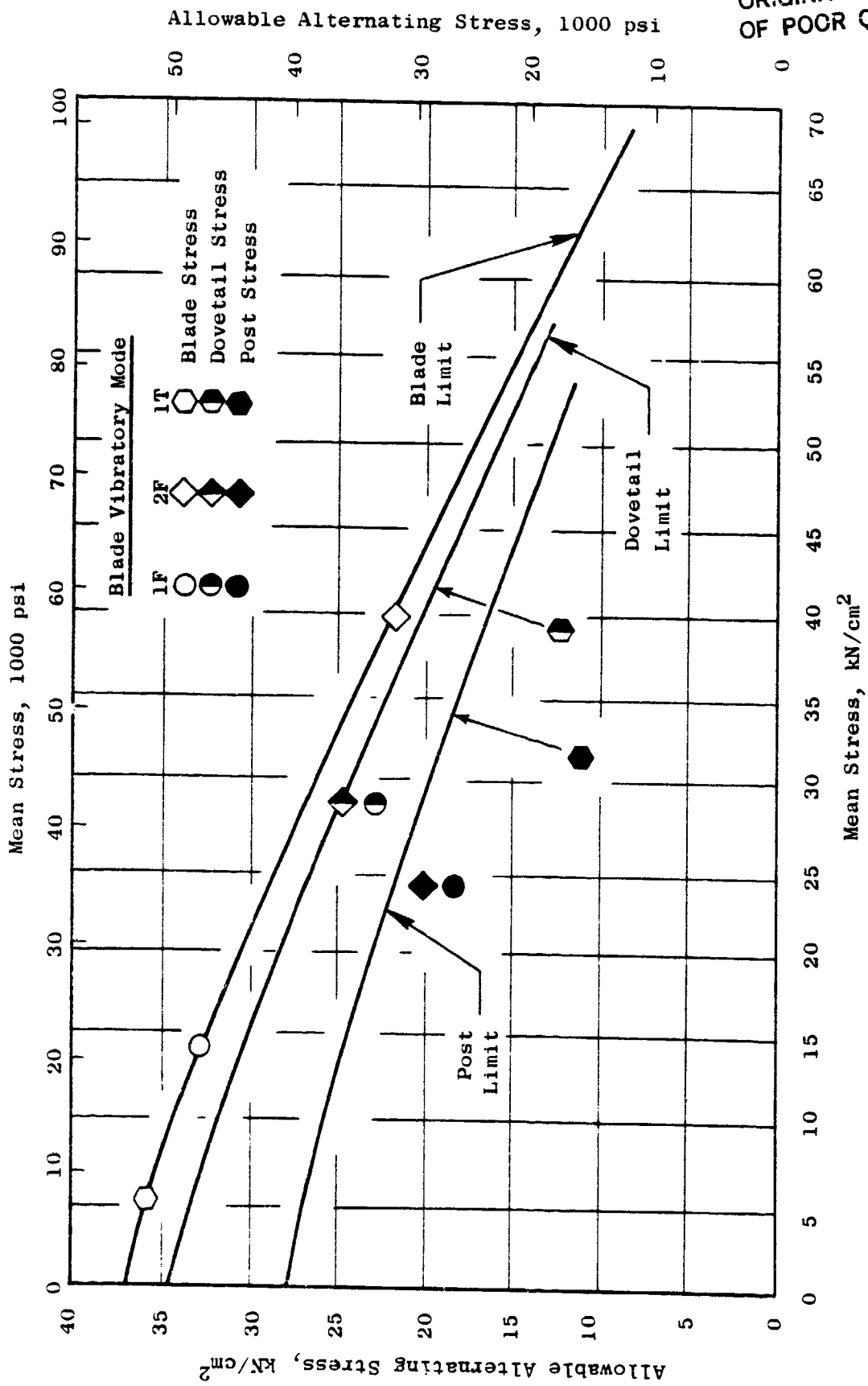
Figure 49. Fan Blade Goodman Diagram.

for the primary vibratory modes. If it is assumed that the airfoil is oper-
ating at its maximum vibratory limit (upper curve and points), then the
scaled resulting attachment loads should be below their allowable limits
(lower curves and associated points). Different property level curves in
Figure 49 have to do with property reduction due to forging size.

Figure 50 is an indicator of birdstrike capability as compared to the
advanced CF6-50 fan blade. A measure of resistance to damage is the calcu-
lated shear stress in the blade resulting from a strike. The dashed curve
is the ratio of E^3 calculated shear stress compared to CF6-50 shear stress
taken as a level of 1. For comparison, the X points indicate test strikes
that the CF5-50 blade has successfully withstood. Aft positioning of the
blade shroud ($\approx 65\%$ of chord) is one of the measures employed by the CF6
and E^3 to enhance birdstrike capability.

Figure 51 shows an exploded view of the blade retention/anticlank system.
The system is completely interlocking so that all pieces are held by each
other, with the complete assembly finally secured by a bolt. The sequence of
assembly is as follows: the blade is inserted in the slot and held outward
against the dovetail pressure faces; the spring is inserted under the blade
and the retainer pins into their slots; the spring is depressed and the key
inserted to maintain the spring load, and the whole assembly is held in place
by a bolt through the spring and into the key. Radial movement of the re-
tainer is restricted by notches engaging the key; axial movement of the
assembly is prevented by the retainer pins engaging notches in the spring.
The strength of the retention system is based on birdstrike induced inter-
action with the casing of a level derived from past experience. Forward
plane balance weights may be added under the retention bolts.

D. Booster Blade Design

Figure 52a and 52b illustrate the configuration parameters of the final
booster blade design. The tm/c plot in Figure 52a shows the result of
thickening the blade tip to avoid stripe mode coincidence with a starter
passing frequency. The blade is approximately constant chord with relatively
little twist or camber reflecting the low work level designed into this stage.

Airfoil stresses and frequencies were calculated by the TAMP-MASS finite
element program. Steady state stresses are shown on Figure 53 and are seen
to be very low. Scaling of end effects data from a similar CF6 blade and
applying to the Twisted Blade program yielded the airfoil root stresses shown
in Figure 54. Maximum stress is on the convex side of the airfoil root and is
less than 30 ksi. The Campbell diagram in Figure 55 shows the calculated fre-
quencies of the blade and indicates adequate margin between first flex and two
per rev, and between 60/rev (stator passing) and the two stripe blade mode.

Figure 56 gives dovetail geometry and shows the low level of stresses
on the dovetail. A Goodman diagram for the booster blade and dovetail for the
three lowest vibratory modes (Figure 57), shows that the blade attachment is
stronger than the airfoil for a given level of airfoil vibratory stress. The

60

• Calculated for 0.68 kg (1.5 lb) Bird at 3600 rpm

✕ Test Strikes – Advanced CF6-50 – No Fragmentation
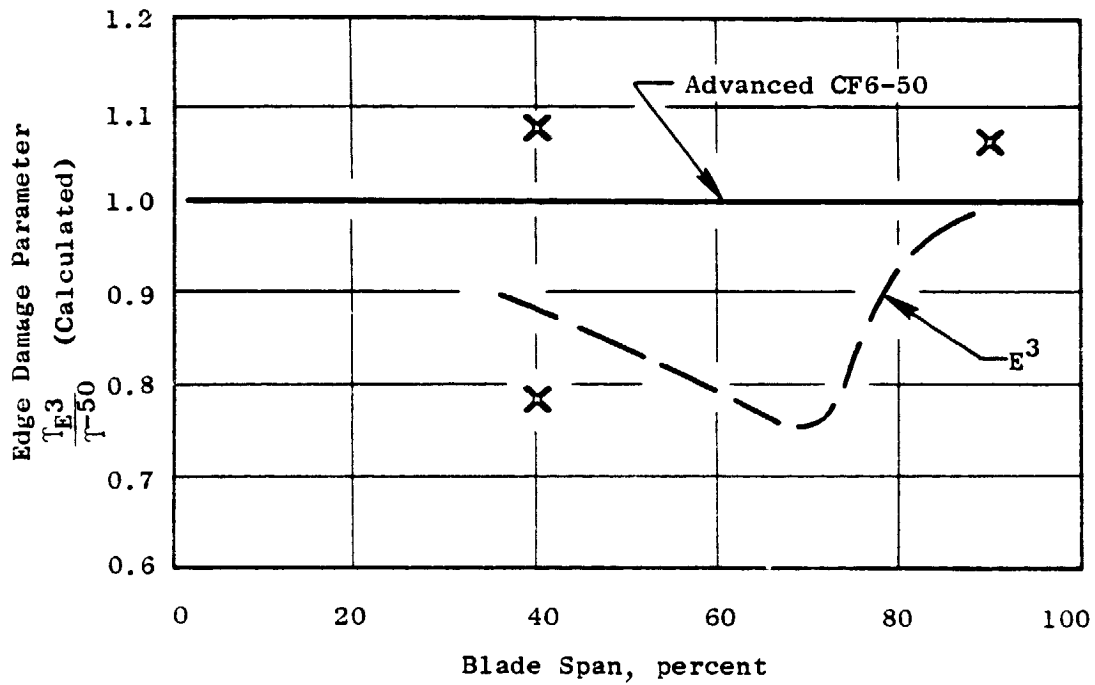
Figure 50. Fan Blade Bird Strike Stress Level.
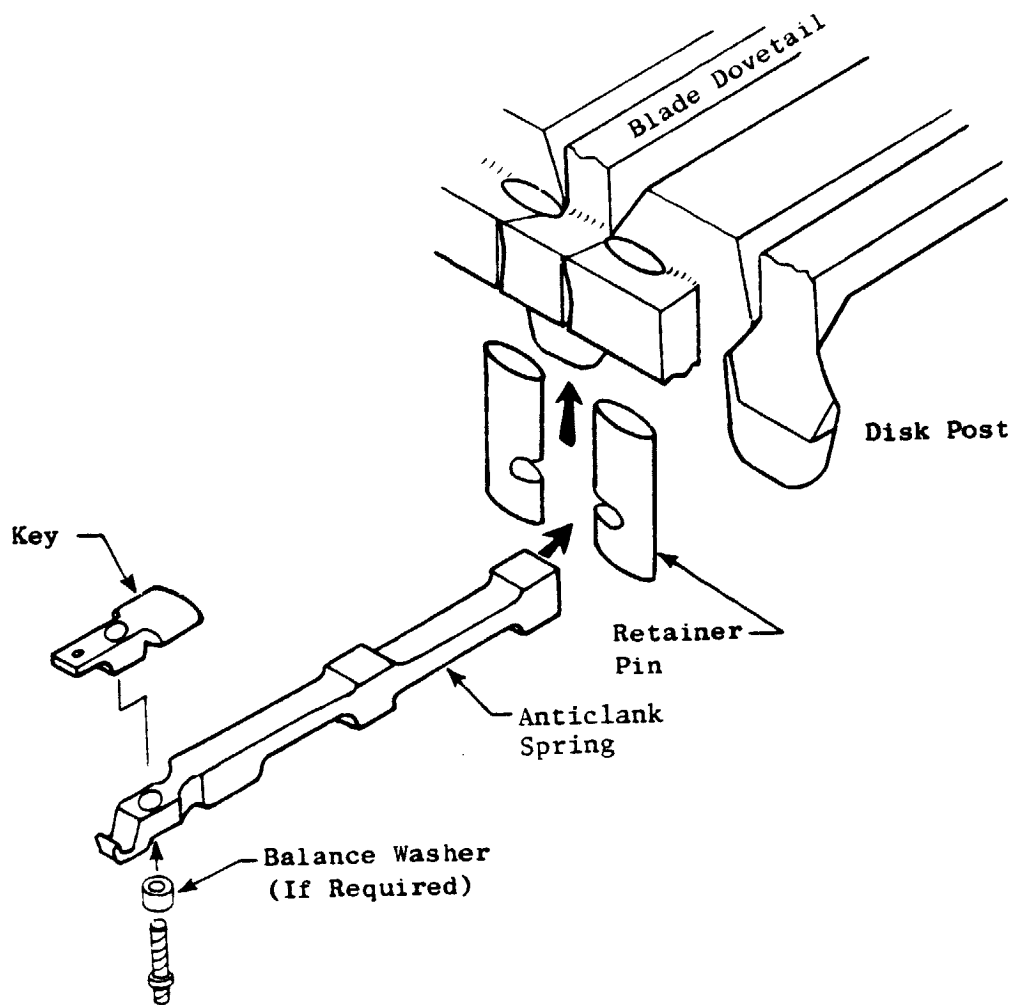
Figure 51.   Fan Blade Retention/Anticlank System.
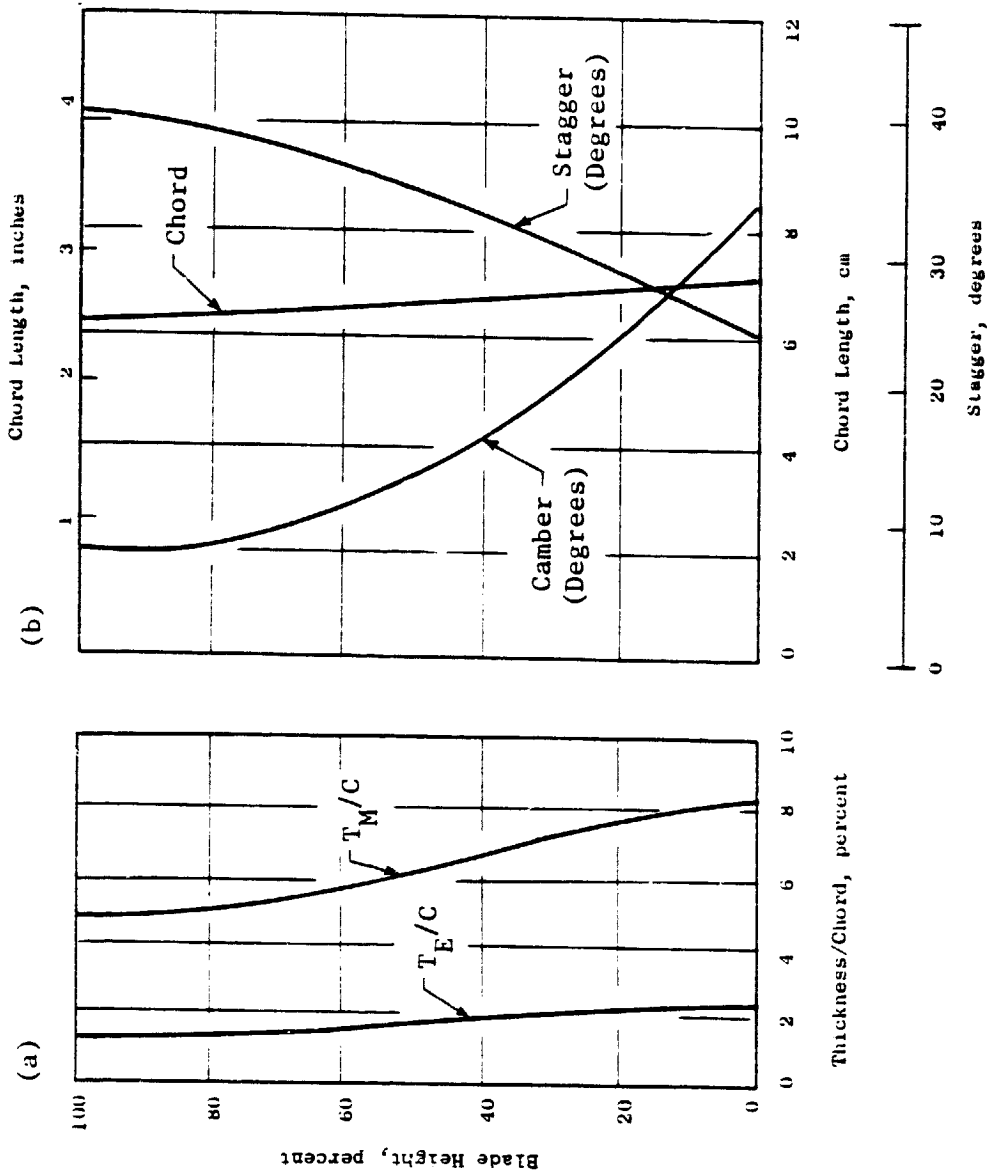
Figure 52. Booster Blade Design Parameters.

63
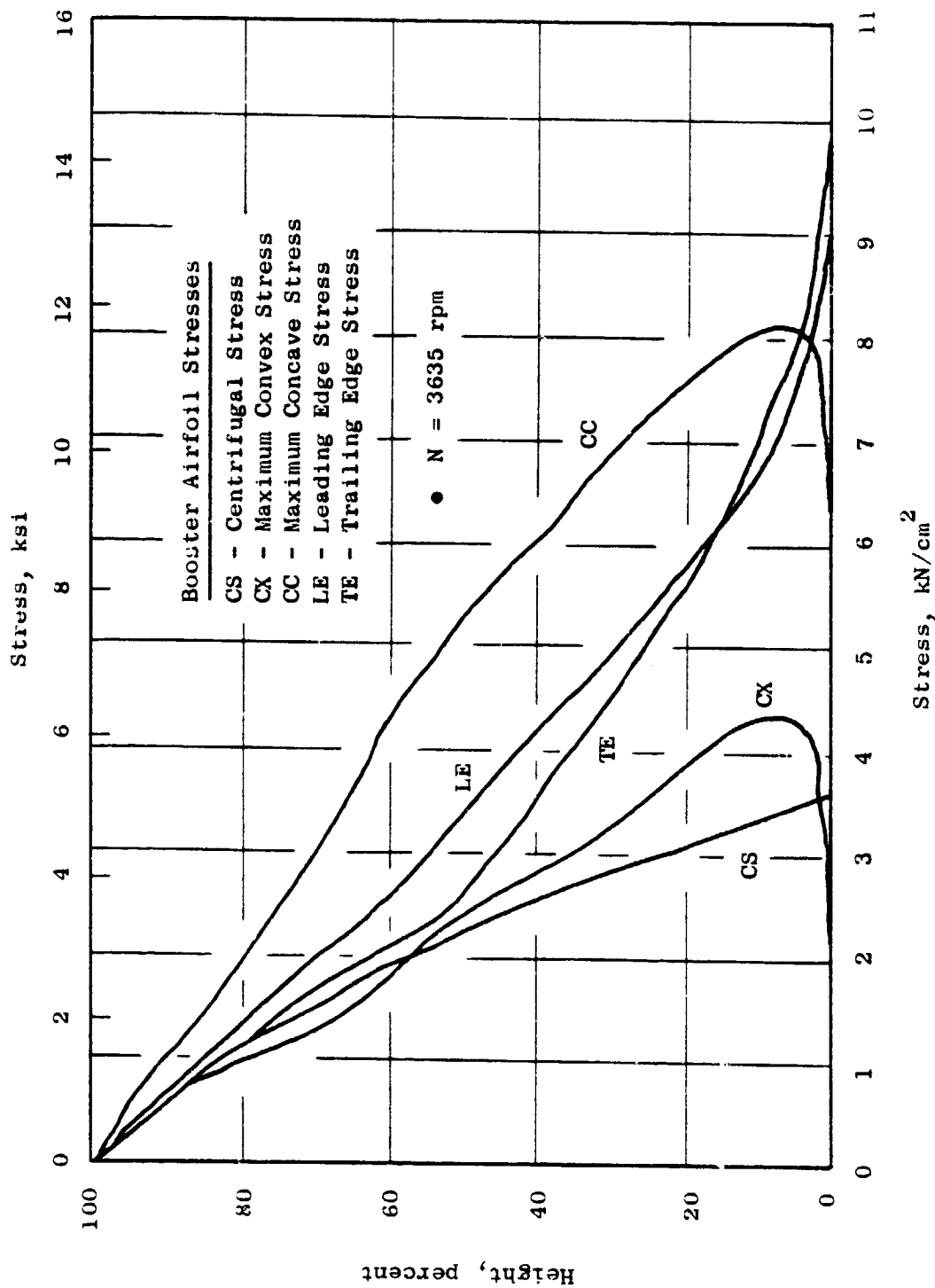
Figure 53. Booster Airfoil Stresses.
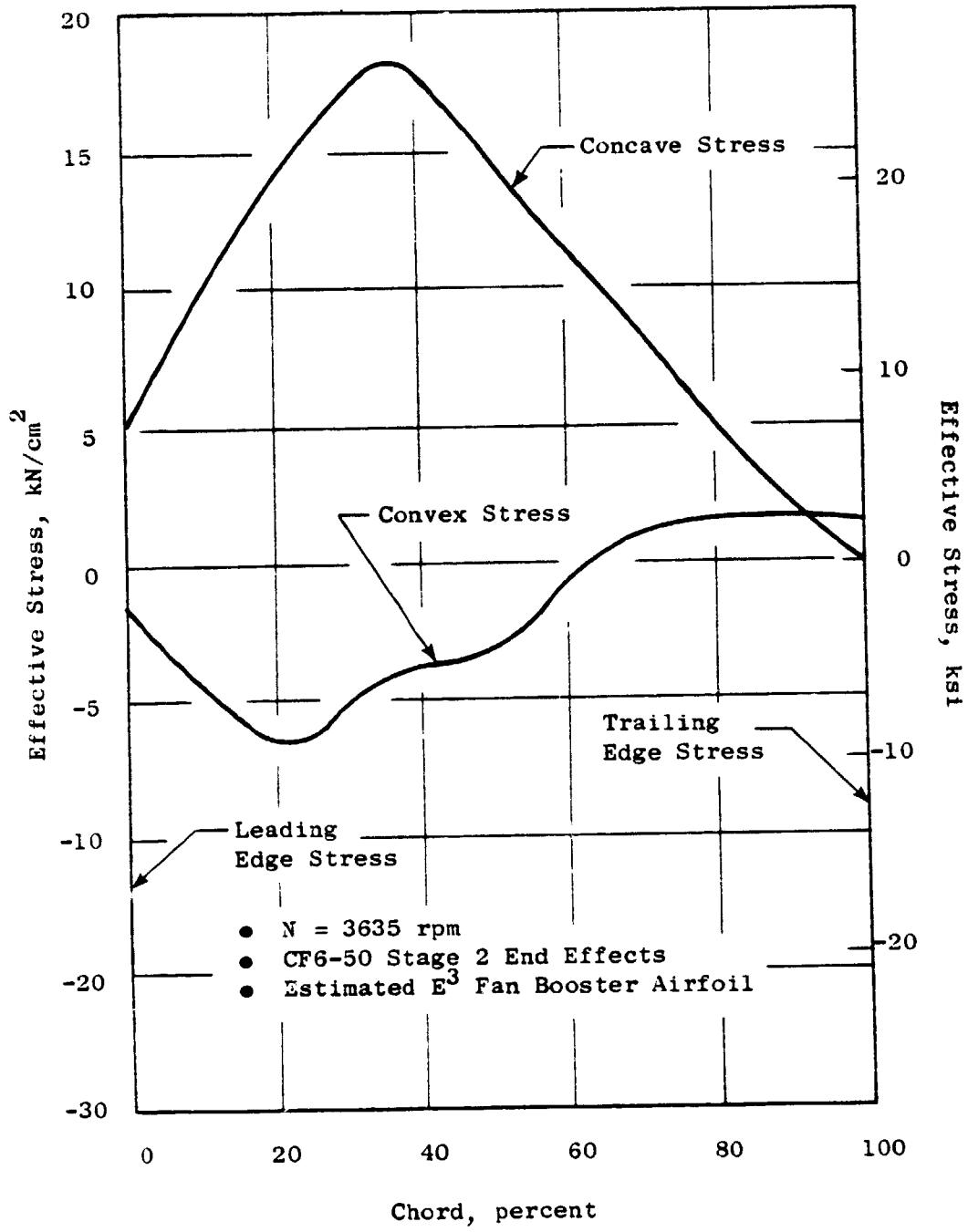
Figure 54. Booster Airfoil Root Stresses.

65
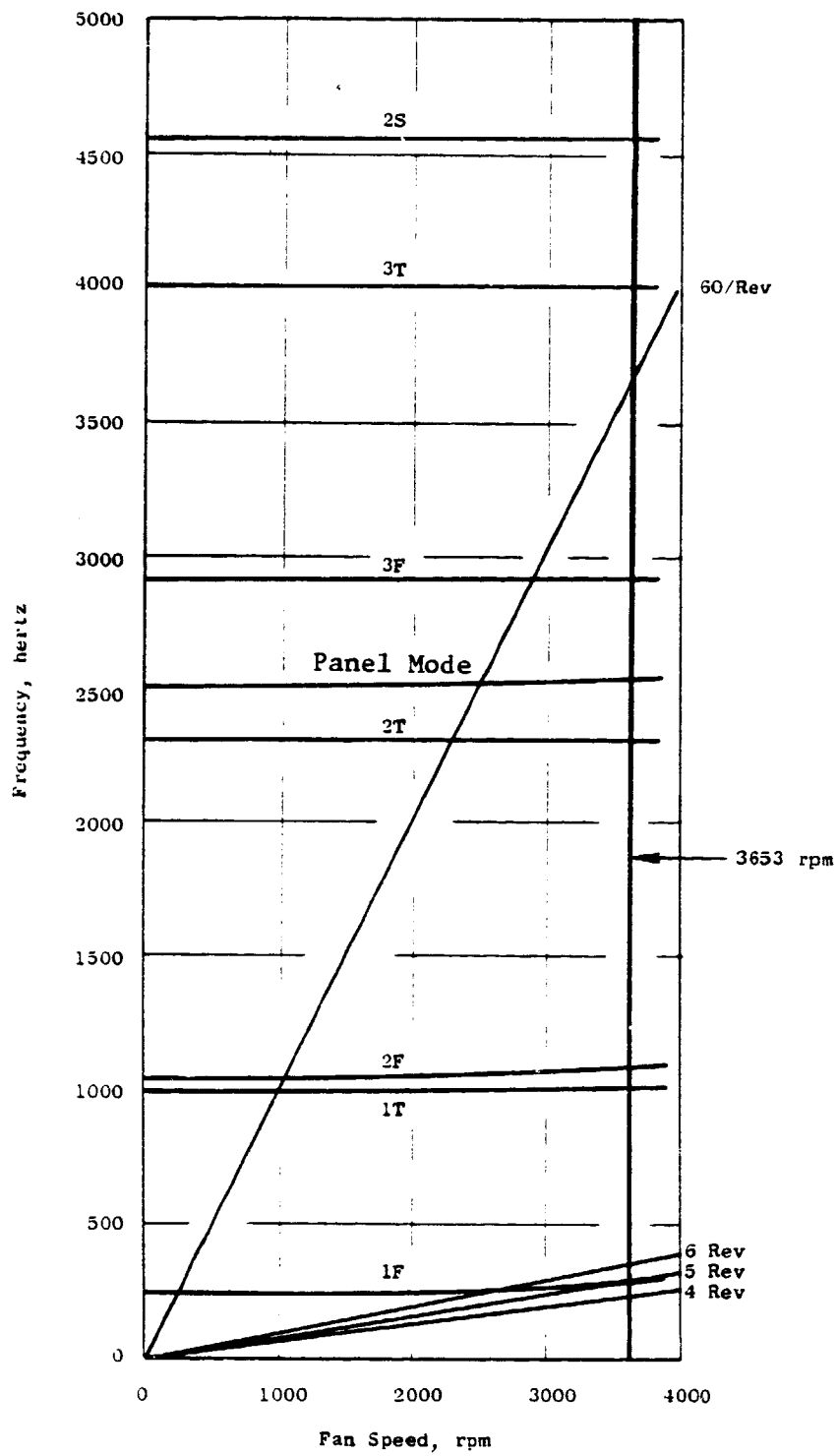
Figure 55. Booster Blade Campbell Diagram.

Forward

Aft

13.7 kN/cm² (19.9 ksi)

13.7 kN/cm² (19.9 ksi)

13.8 kN/cm² (20.0 ksi)

13.8 kN/cm² (20.0 ksi)
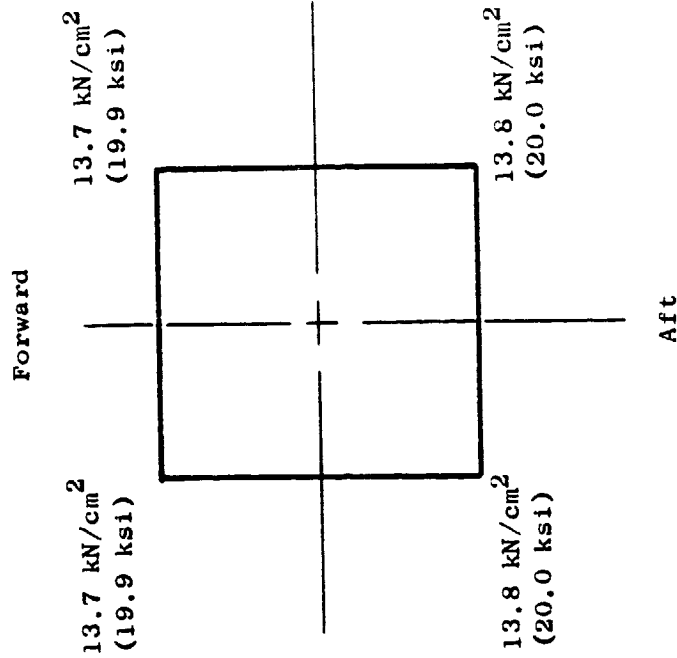
Dovetail Geometry

• Length .... 2.31 cm (0.910 in.)

• Shank Thickness ...... 2.03 cm (0.800 in.)

• Orientation .... 90°

• Flank Angle .... 45°

• Flank Width .... 0.635 cm (0.250 in.)

• Blade Offsets
  Axial .... 0.208 cm (0.082 in.)
  Tangential .... 0.218 cm (0.086 in.)

• Crush Stress .... 16.9 kN/cm² (24.5 ksi)

Figure 56. Booster Dovetail Stresses.

67
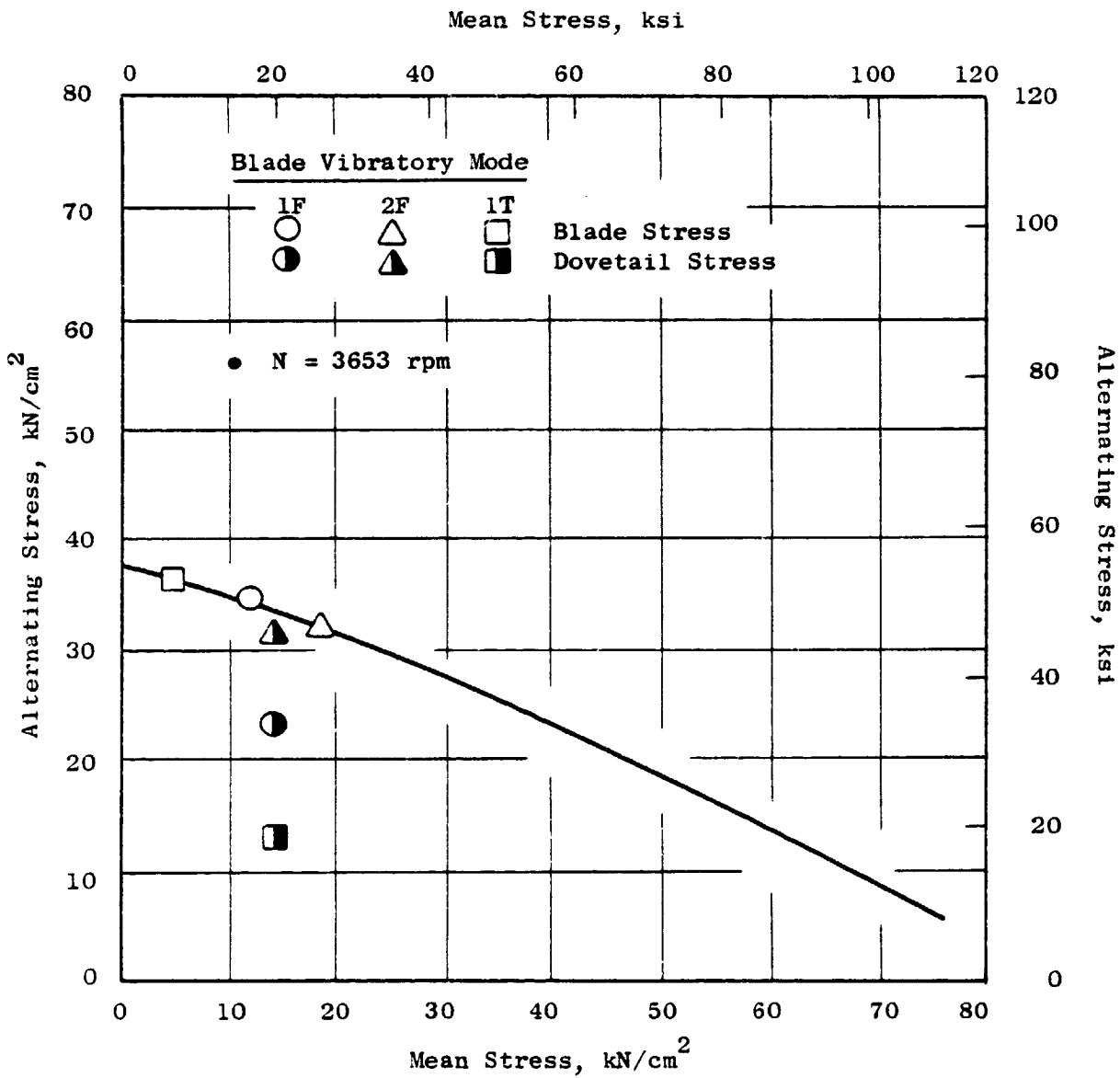
Figure 57.   Booster Dovetail Goodman Diagram.

blade is stall protected against instability in the torsional mode. Balance weights inserted in the booster stage dovetail slot constitute the aft rotor balance plane.

E. Rotor Structure Analysis

The rotor structure was analyzed using the CLASS/MASS thin shell portion of the rotor in combination with AFINE for the analysis of the thick shell Stage 1 and 2 disks. The model breakdown is shown in Figure 58. Radial loads and moments due to the blade stages were input at the disk rims and restraints imposed by the bearings input on the shafting. Rotor deflections from this model were used to establish blade lengths for proper clearance and cold component dimensioning; under operating conditions then, the correct aerodynamic flowpath will be established.

Figure 59 shows in detail the AFINE model used to analyze the disk with the significant stresses and deflections noted around the disk and shaft stub. The disk, being sized for growth capability, is not highly stressed at FPS conditions; and at the rim with the dovetail slot stress concentration applied, cyclic life requirements are easily met. In the curved section of the shaft, the configuration has been carefully contoured to avoid high bending stresses by attenuating the disk deflections over several inches of shaft length. To make most efficient use of the material available, the disk cross section was made nonsymmetrical. Blade loading, because of the shank configuration, the aft positioning of the part span shroud, and gas loading produces a forward moment loading on the disk; the restraint of the forward connection of the shaft induces a moment load in the same direction. Positioning the center of gravity of the disk aft of the blade stacking axis produces a countermoment that can be made to balance disk loadings to essentially neutralize disk rolling. The eccentric contouring was also made to accommodate the No. 1 bearing sump wall to permit closer spacing of the fan centerline to the bearing.

Figure 60 shows the analytical model of the second stage disk and spacer and the associated stresses and deflections. All are well within the acceptable limits. In the disk, the bore projection was positioned to counteract rim moment input by the blade and the spacer connection to minimize disk rotation; the length of the bore was sized to keep vibratory frequencies of the disk out of the fan operating range.

The disk/forward fan shaft bolted joint is shown in Figure 61. The joint utilizes thirty 5/8-inch bolts preloaded sufficiently to transmit fan torque through flange friction rather than shear loading the bolts and working the bolt holes. Using more and smaller bolts allows the flange joint to be lighter and still transmit the required torque. Tight fitting bolts prevent shifting of the joint and minimize bending of the bolt.

Table VI is the weight breakdown of the FPS fan rotor.
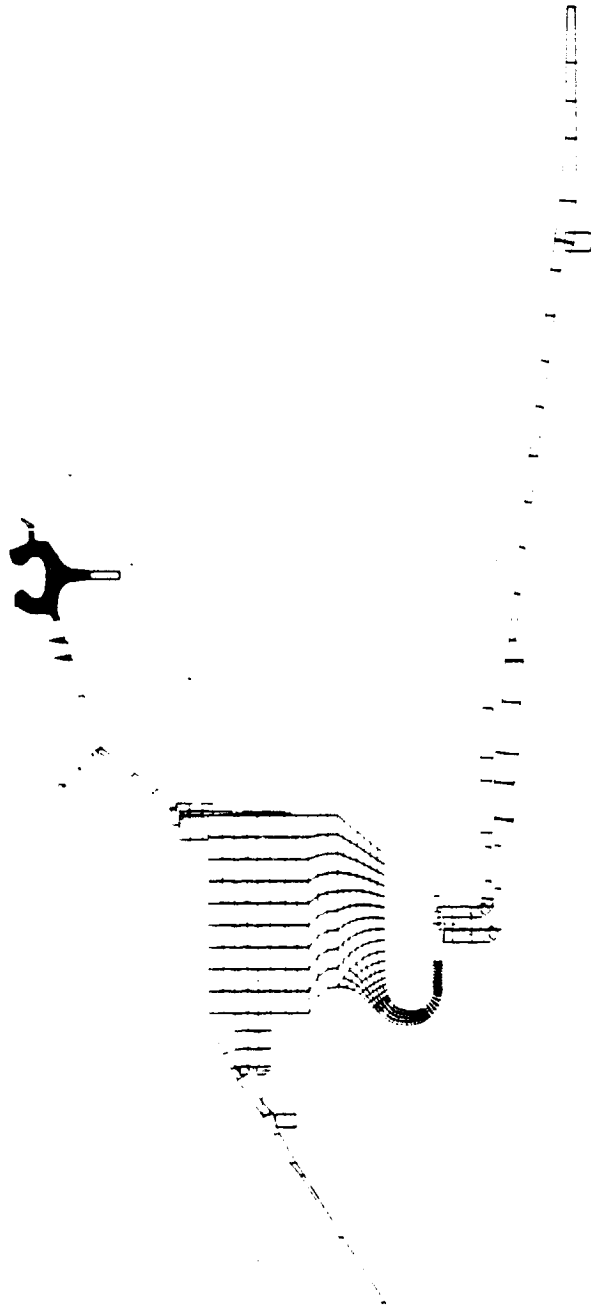
Figure 58. Rotor Structure CLASS/MASS Model.
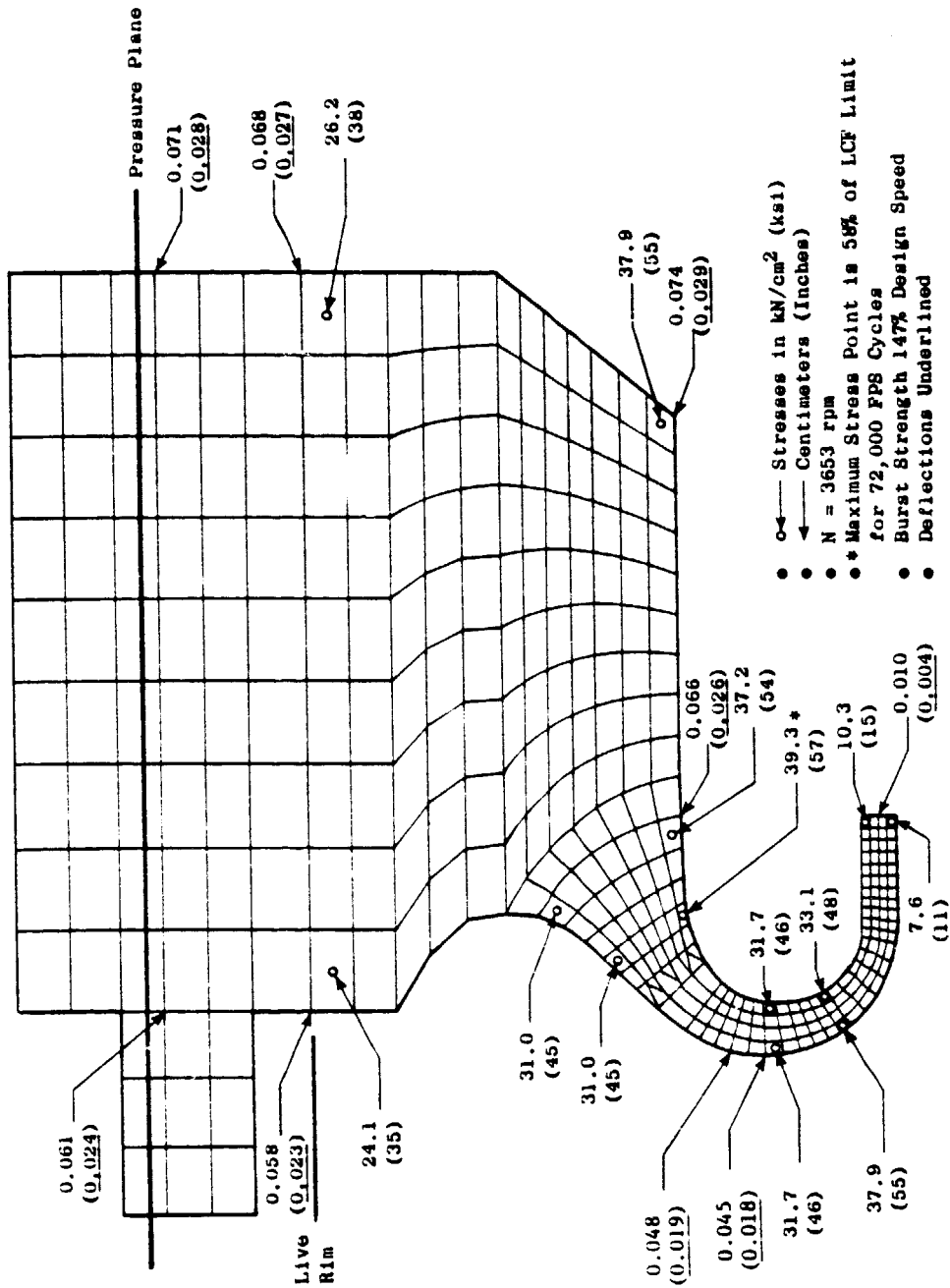
Figure 59. Fan Disk Effective Stresses and Radial Deflections.

0.093 (0.0368)

0.088 (0.0347)

24.8 (36)

17.9 (26)

0.092 (0.0362)

22.1 (32)

23.4 (34)

0.092 (0.0362)

20.7 (30)

0.092 (0.0364)

0.086 (0.0338)

19.3 (28)

17.9 (26)

17.2 (25)

15.8 (23)

11.5 (17)

14.5 (21)

16.5 (24)

24.8 (36)

26.2 (38)

13.1 (19)

13.8 (20)

12.4 (18)

21.4 (31)

• 3653 rpm

• Effective Stresses in kN/cm² (ksi)

• Deflections Underlined cm (in.)
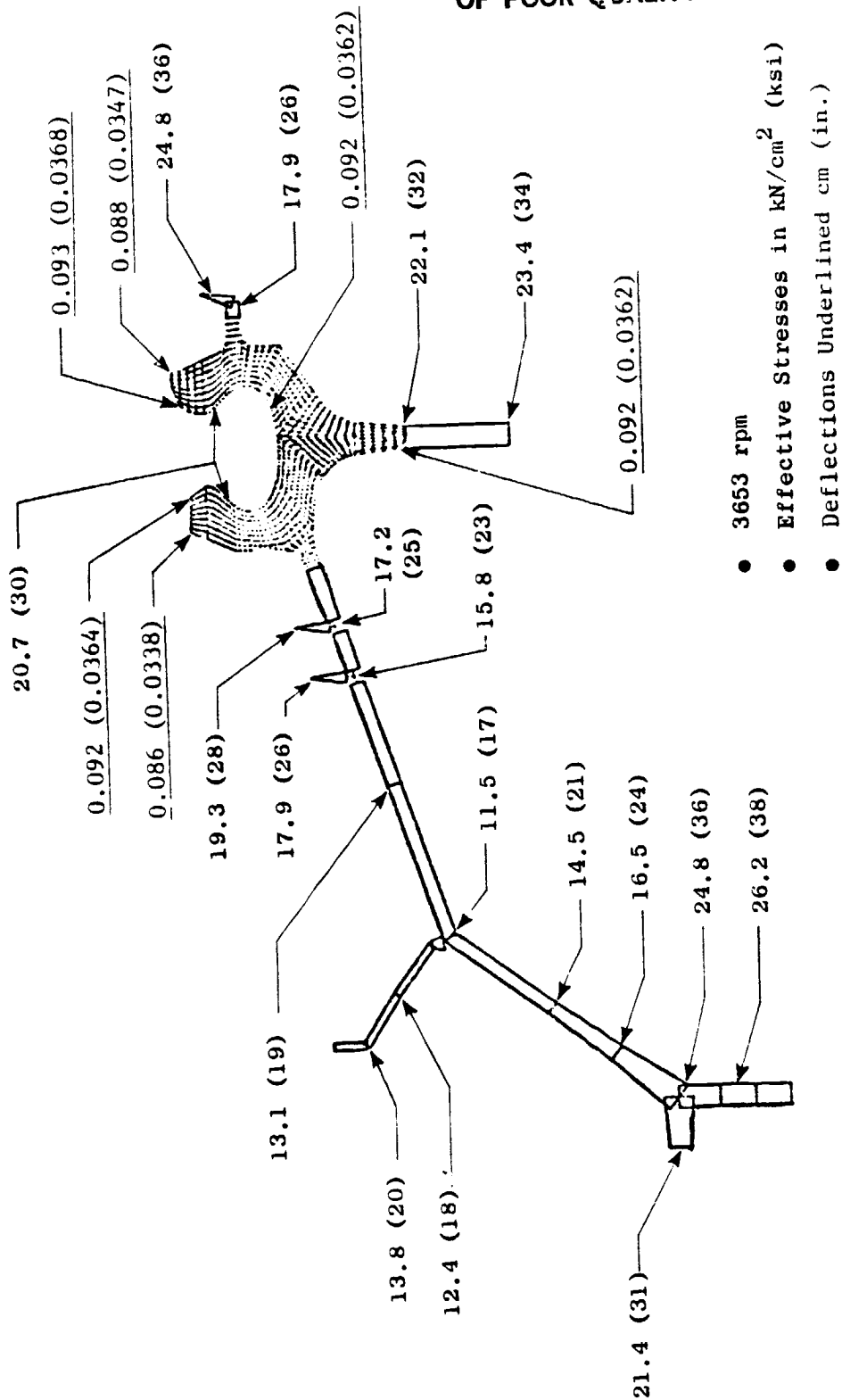
Figure 60. Booster Spool Stresses and Radial Deflections.

72

- 30 5/8 inch Inconel 718 Bolts
- Preload Required to Drive Fan
- Through Flange Friction = 101.9 kN/Bolt (22914 lb/Bolt)
- Coefficient Friction = 0.15

No. 1 Bearing
Net Resultant

LP Turbine

Ti 6-4
Shaft

Fan
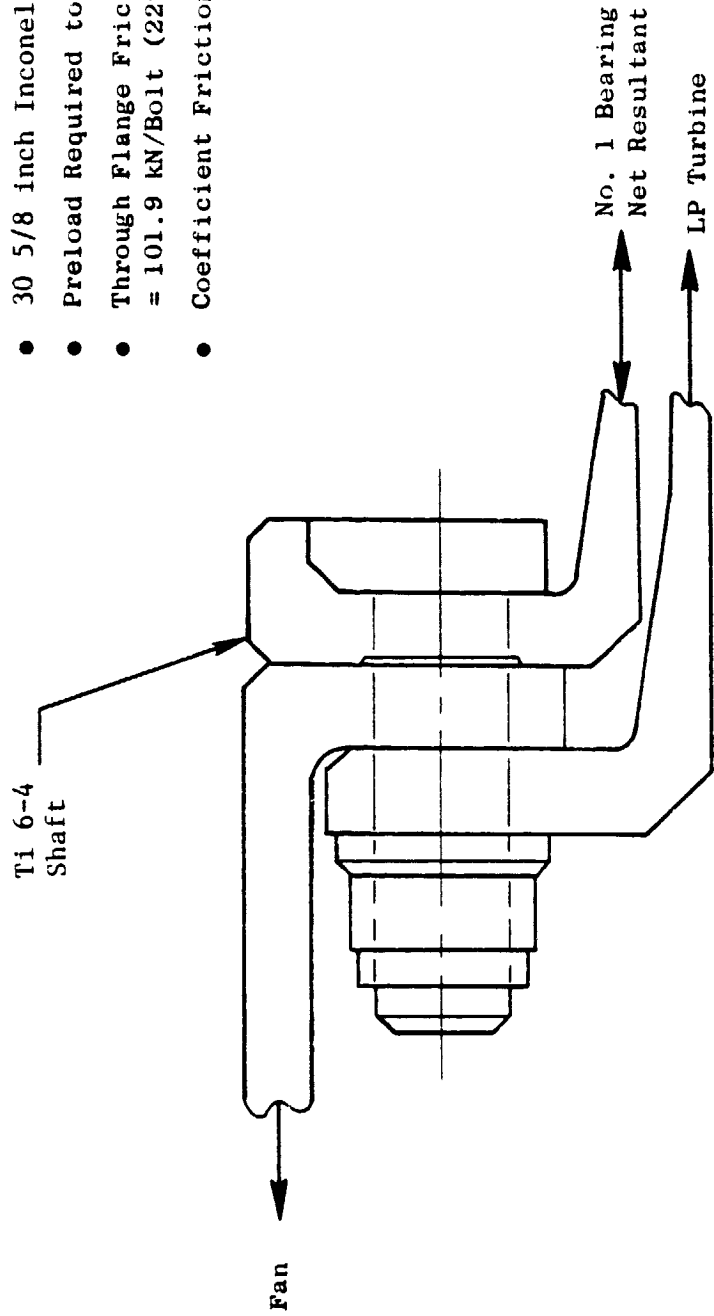
Figure 61. Fan Disk - Low Pressure Shaft Bolted Joint.

Table VI. FPS Fan Weight Status.

	kg	lb
Fan Blades	232.7	513
Fan Disk	137.4	303
Booster Blade	15.9	35
Booster Disk	42.2	93
Spinner	8.6	19
Disk Seal	2.7	6
Retention and Anticlank System	7.7	17
Forward Fan Shaft	34.5	76
Hardware	14.5	32
Total	496.2	1094

IV. FAN STATOR DESIGN

The mechanical design of the E^3 fan stator includes the design of the fan frame, the stator vanes, and the casing/containment structure.

Two different fan frame configurations will be developed in the E^3 Fan Program. One configuration will be utilized for the Full-Scale Fan Component Test (FSFT) and will remain in the fan module for the ICLS turbofan test. The other configuration will represent the conceptual design proposed for the Flight Propulsion System (FPS). All frame configurations will incorporate an integral vane frame design in which the outer bypass vanes provide both an aerodynamic and structural function. The integral vane frame design will feature five different bypass vane configurations in the vane row to correct for circumferential flow distortions that will be caused by the 12 o'clock engine pylon structure. The frame configuration for the FSFT will mount at the bypass case directly to the test facility hardware. Consequently, no engine mounts or hardware for nacelle attachment will be required. Although no radial driveshaft is required for the FSFT, provisions for the driveshaft will be incorporated to reduce the disassembly and rework required to prepare the frame for the ICLS engine test.

For the turbofan engine test (ICLS), the fan frame will provide the forward engine mount locations on the core frame, hardware for the nacelle inner and outer cowl attachment, and a means to include a radial driveshaft to a fan mounted gearbox. The radial driveshaft will be added in the plane of the bypass vanes by modifying the 6 o'clock vane and one vane to either side.

The fan frame design for the FPS is a study only with no hardware requirements. The FPS frame configuration will feature an integral vane frame aerodynamically the same in the bypass as the frame for the FSFT, but the bypass vanes will be a composite design instead of the metal vanes used in the FSFT and ICLS. Additionally, the FPS design will feature an advanced composite containment design based on work being done under a NASA contract to develop advanced composite containment concepts and work done by the U.S. Army on lightweight armor.

The design of the core frame and bypass vane assembly is complete. The core frame is a welded assembly of the eight finish machined struts to finished flowpath rings which are then final machined at the outer and inner flanges and rabbets. The bypass vanes are individual pieces that bolt to the core frame at their ID and bolt to an outer bypass casing at their OD. The stator vanes and hardware for the Stator 1 and core OGV assemblies have been designed as have been the midcase and fan containment case. The containment case design is now a modification to a CF6-50 steel case in order to hold down costs.

A. Fan Stator Configurations

The fan stator configuration (midcase and containment case not shown) that will be used for the FSFT and the ICLS engine test is shown in Figure 62. The solid 17-4 PH steel bypass OGV's and core struts are nonflight-type

360° Casing
17-4 PH

34 Bypass OGV's
17-4 PH

360° Ring
17-4 PH

8 Strut Core Frame
17-4 PH

4-90° Panels
6061-T6

360° Case
2024-T6

360° Fairing
17-4 PH

64 Vanes
7075-T73

60 Vanes
403SS

360° Shroud
17-4 PH

Porous Teflon

360° Shrouds
6061-T6
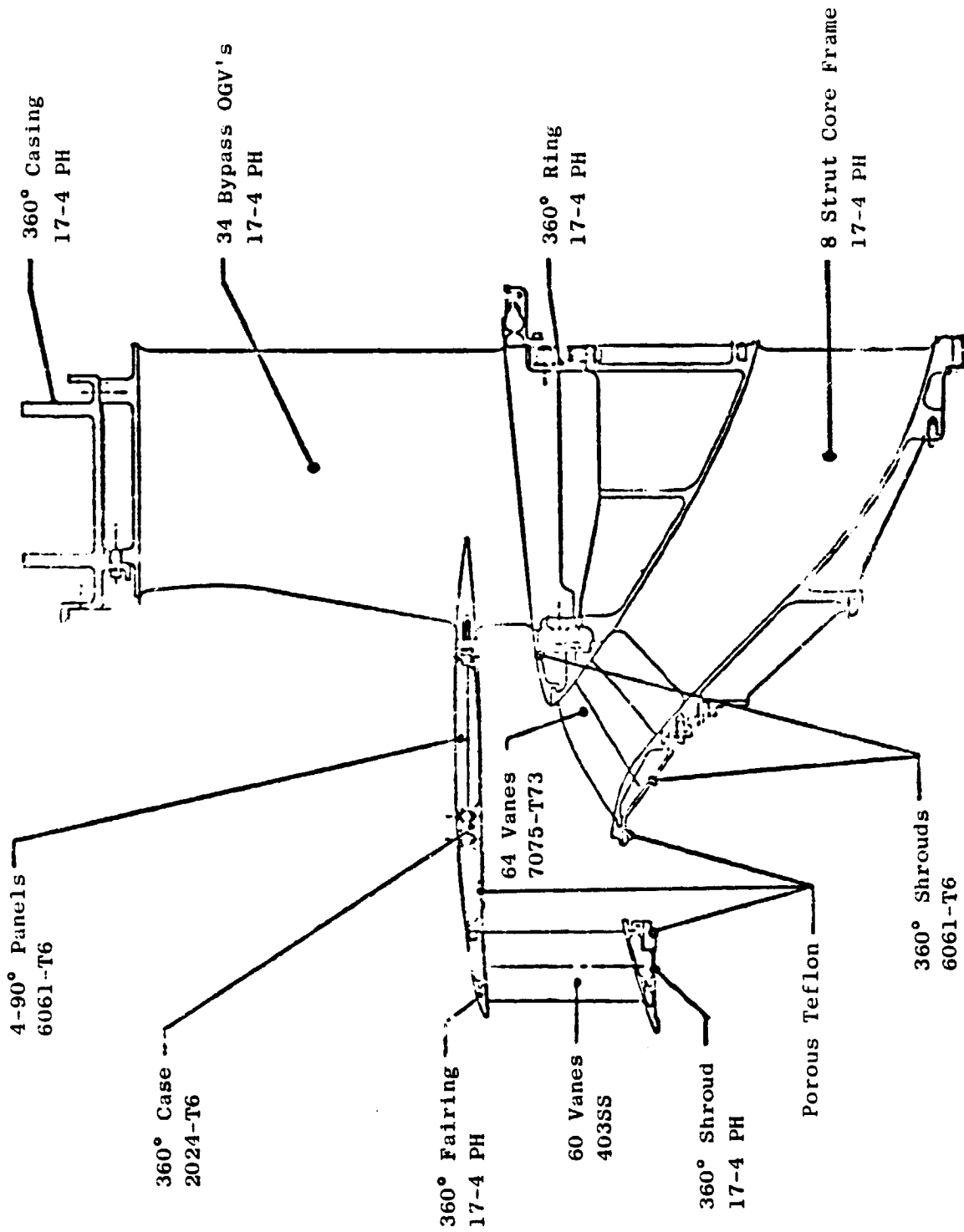
Figure 62. ICLS Fan Stator Configuration.

designs but the Stator 1 and core OGV vane assemblies are representative of flight type hardware. Lightweight 7075 Al will be used for the core OGV's and 6061 Al for the inner and outer shrouds. In the Stator 1 assembly, the flow splitter casing is aluminum with the vanes 403SS (proposed Ti 6-4 for the FPS design) for cost reasons and the inner and outer fairings are steel for FOD protection during the development tests.

The proposed FPS fan stator configuration is shown in Figure 63. This design integrates the fan bypass outer flowpath, the nacelle outer flowpath, and the bypass OGV's as a single structure. The main structure of the casing is a sandwich structure (with graphite/epoxy facings) which forms the outer flowpath of the nacelle. The inner flowpath of the casing is formed by the acoustic treatment and supporting structure. The bypass vanes are formed by graphite/epoxy skins which are bonded to the radial spokes extending from the inner and outer structural wheel rims. The metal core frame is envisioned as a one-piece aluminum casting with the core struts internally stiffened to support the bypass vane/outer casing assembly and the bearing cone loads. This approach is based on technology currently in place on the production TF34 frame. The E^3 core frame will be about twice the diameter but of the same order of casting complexity as the TF34 cast frame. The Stage 1 vanes are shown as Ti 6-4 material for the FPS design as discussed in the ICLS fan stator description.

A cross section of the core frame is shown in Figure 64 with the service requirements for the eight-strut structure listed. The core struts at the +45° location from top vertical will provide attachment points for the forward engine mounts. Seal pressurization air will be provided by air scoops located in the core struts as illustrated in Figure 65. A detail of the bottom core strut is shown in Figure 66 with the direction of the radial driveshaft depicted. Figure 67 shows the proposed modification to the bottom vertical bypass vane and adjacent vanes to incorporate the radial driveshaft to the fan mounted gearbox. A fairing is shown around the shaft to provide a smooth transition to the bypass vane airfoil surfaces and to house the service lines.

One of the ICLS engine fire prevention and fire containment requirements includes the cavity space between the core engine and the fan bypass duct. The current plan to satisfy this requirement is through the method shown in Figure 68. The fan frame will supply a flange to which the core cowl seal support can be attached. As is shown, the core cowl door will provide three scoops around the circumference to gather the purge air which will be directed to the core cavity through holes in the seal support.

B. Fan Frame Analysis

A great deal of analysis has been performed on the fan frame not only for the FPS design but also for the FSFT and ICLS frame designs as well. The slave frame designs for the FSFT/ICLS are studied to ensure compatibility with the other engine components based on static deflection and engine dynamics criteria. Frame flexibility studies have been completed on the preliminary flight frame (FPS) design and the slave frame (FSFT/ICLS) design. Engine mount position
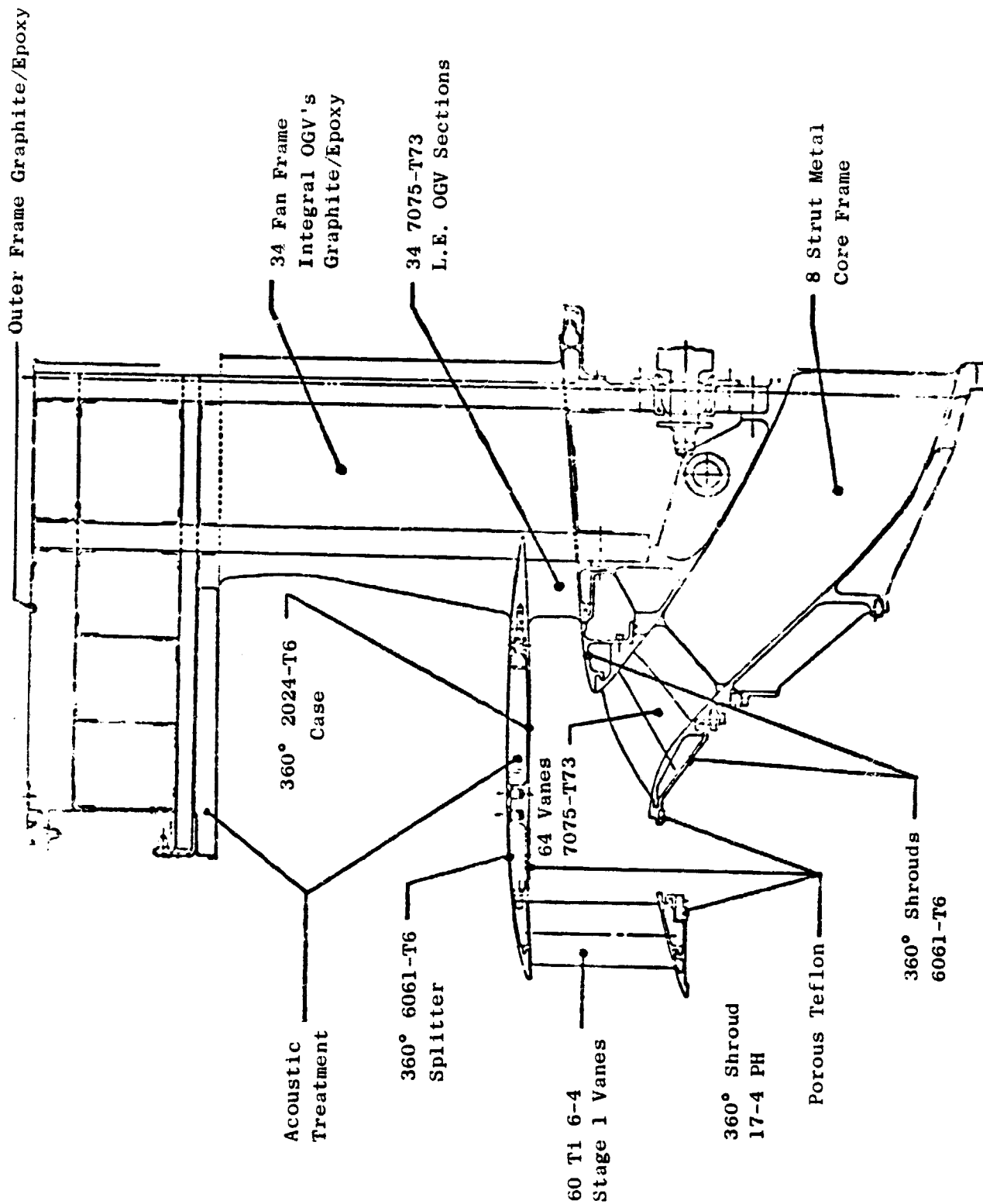
Figure 63. FPS Fan Stator Configuration.

Outer Frame Graphite/Epoxy

34 Fan Frame Integral OGV's Graphite/Epoxy

34 7075-T73 L.E. OGV Sections

8 Strut Metal Core Frame

360° 2024-T6 Case

64 Vanes 7075-T73

Acoustic Treatment

360° 6061-T6 Splitter

60 Ti 6-4 Stage 1 Vanes

360° Shroud 17-4 PH

Porous Teflon

360° Shrouds 6061-T6
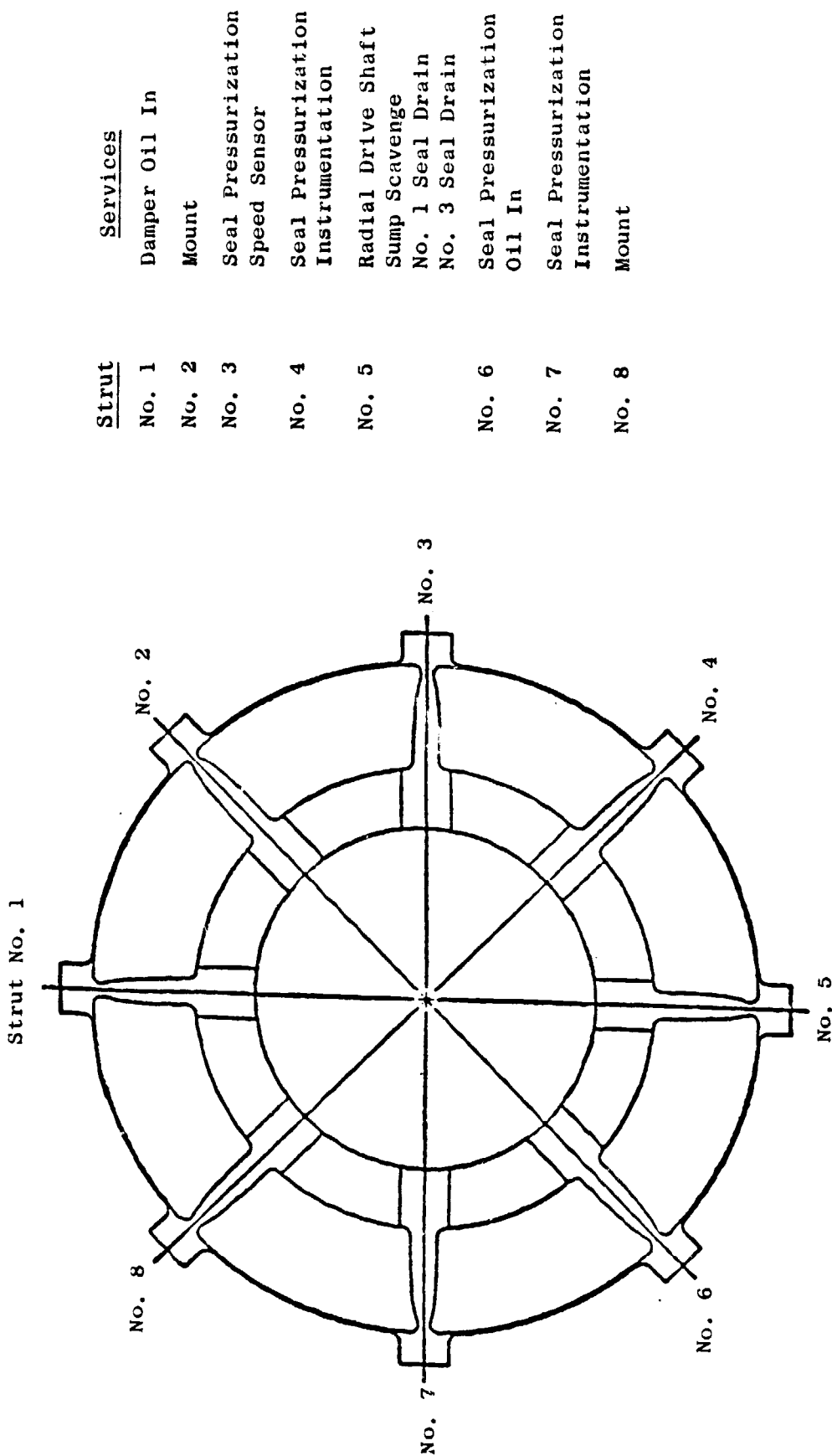
Strut	Services
No. 1	Damper Oil In
No. 2	Mount
No. 3	Seal Pressurization Speed Sensor
No. 4	Seal Pressurization Instrumentation
No. 5	Radial Drive Shaft Sump Scavenge No. 1 Seal Drain No. 3 Seal Drain
No. 6	Seal Pressurization Oil In
No. 7	Seal Pressurization Instrumentation
No. 8	Mount

Aft Looking Forward

Figure 64. Fan Frame Services.

Fan Frame
Section

2.75

0.33

Forward
Looking
Aft

Top View

0.33
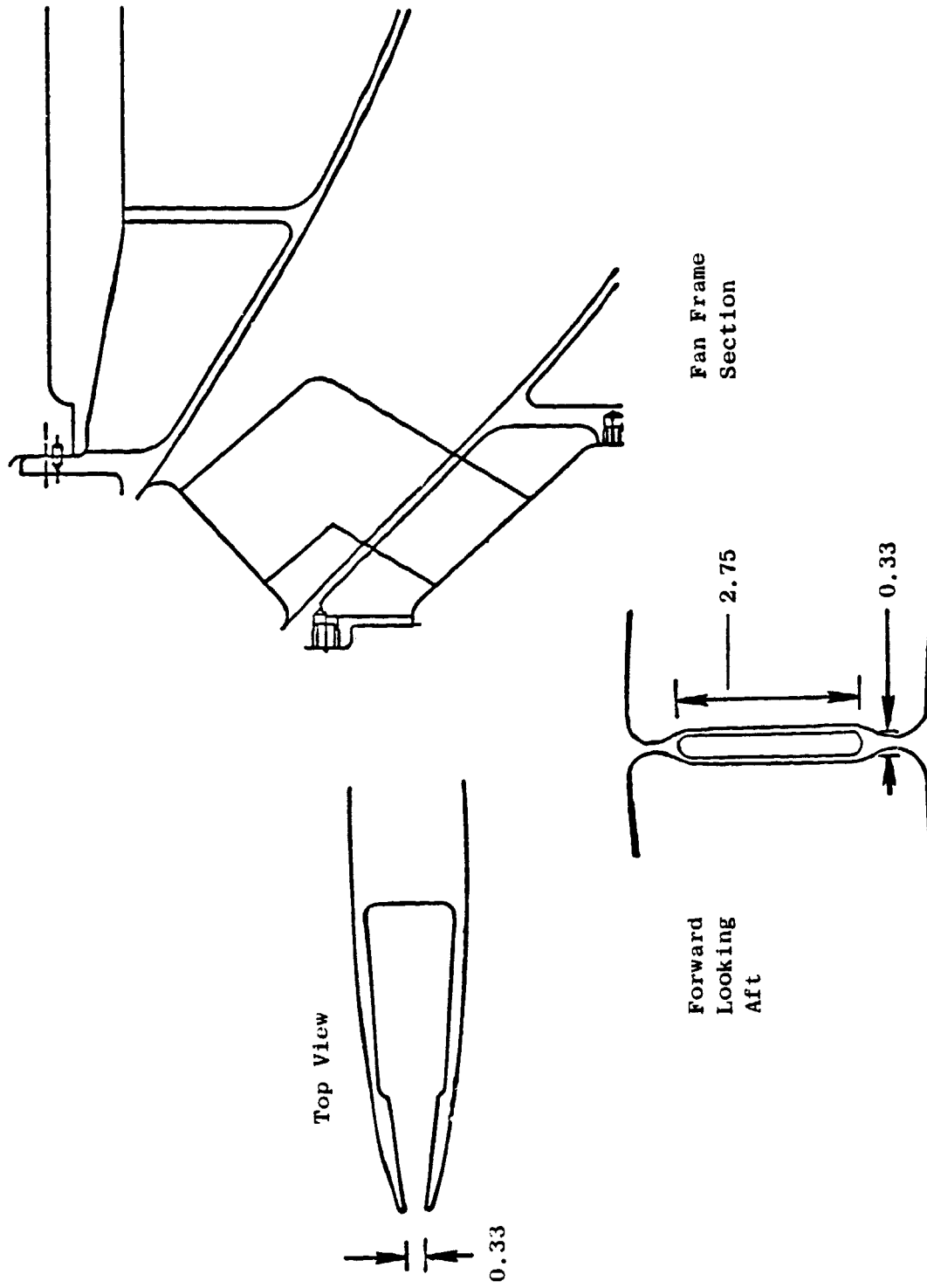
Figure 65. Sump Pressurization Air Scoops Located in Core Struts 3, 4, 6, and 7.

No. 3 Seal
Drain

Radial
Drive

Scavenge
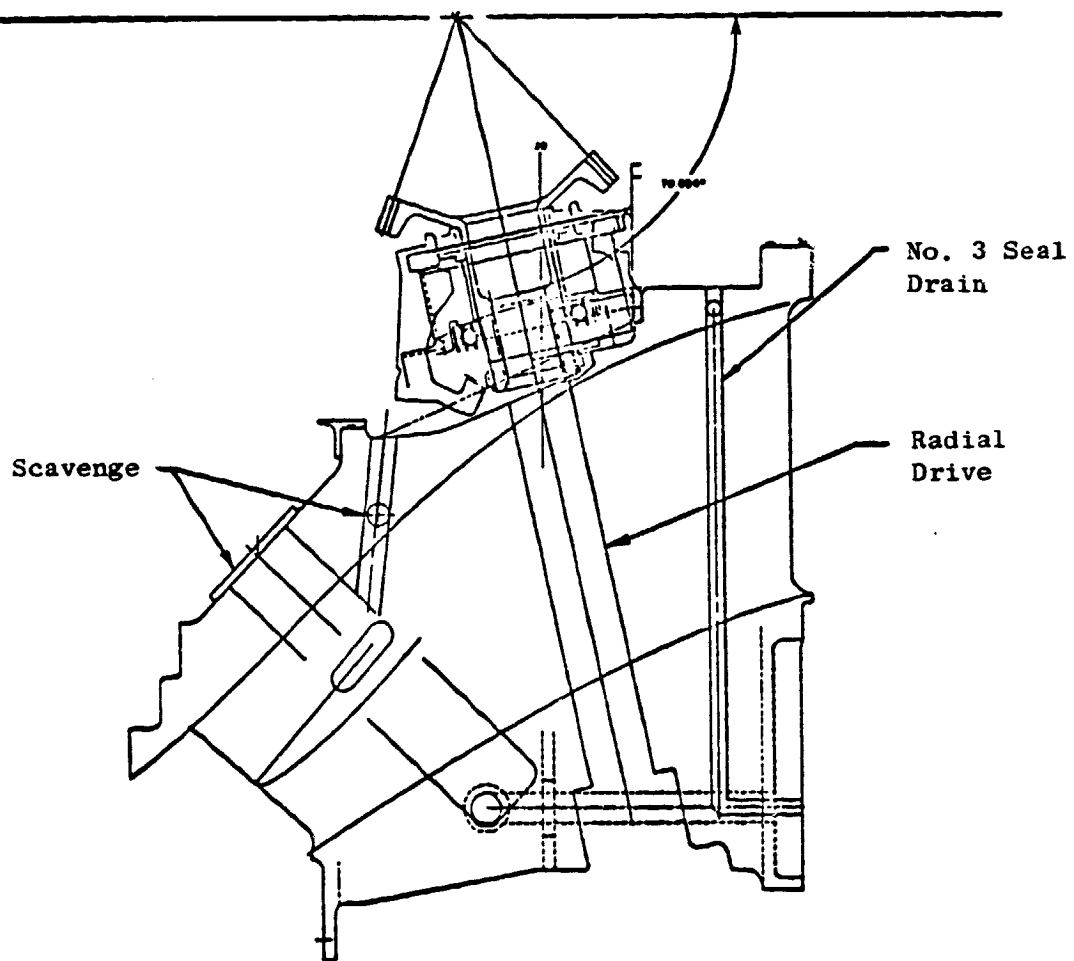
Figure 66.   Fan Frame Bottom Core Strut.
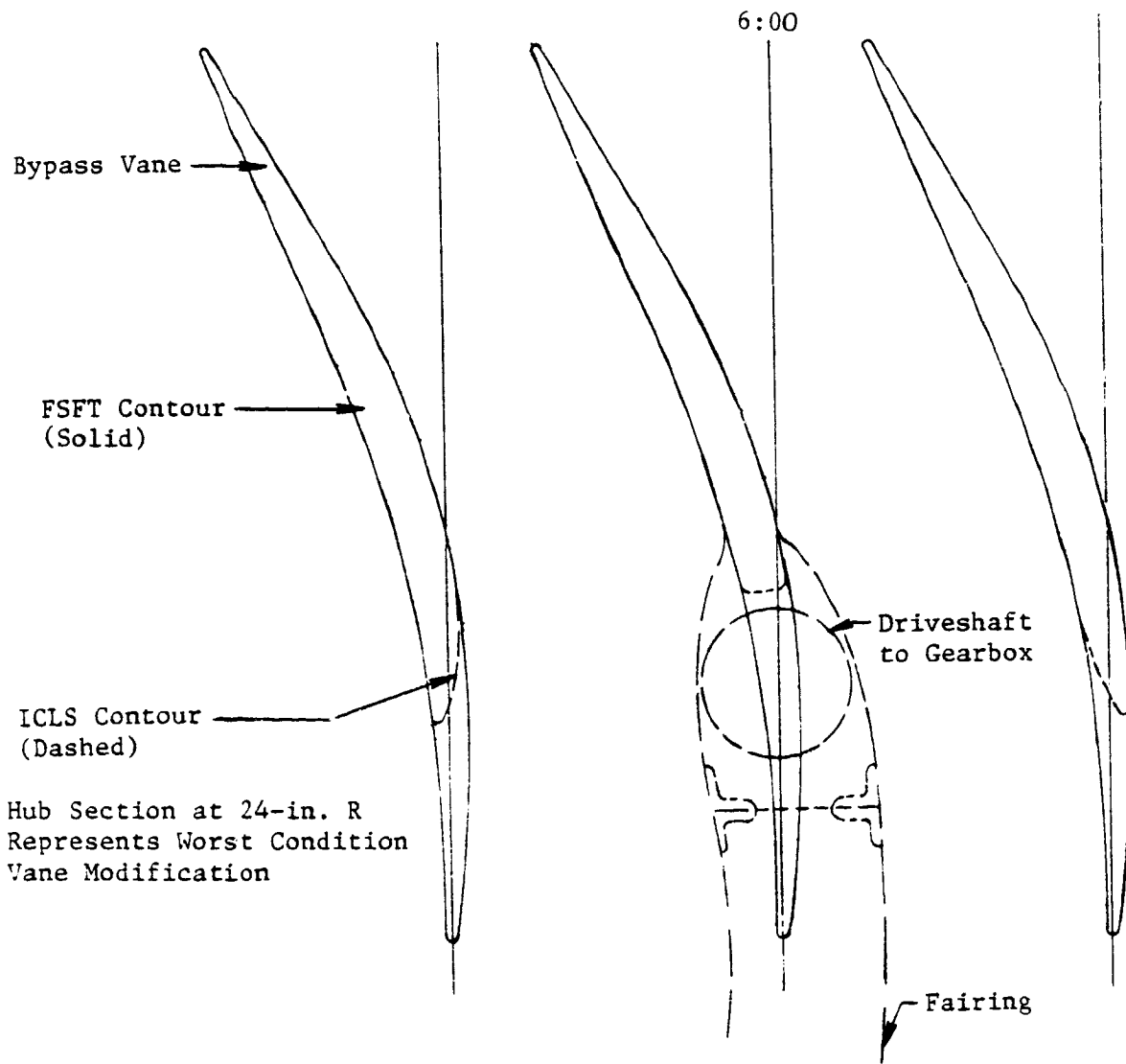
Figure 67. Proposed Modifications for ICLS Driveshaft and Fairings.

Bypass
Vane

Core
Cowl

Seal

Support
Flange

0.25 lb/sec Total

Located 3 Places

0.35 in.

1.25 in.
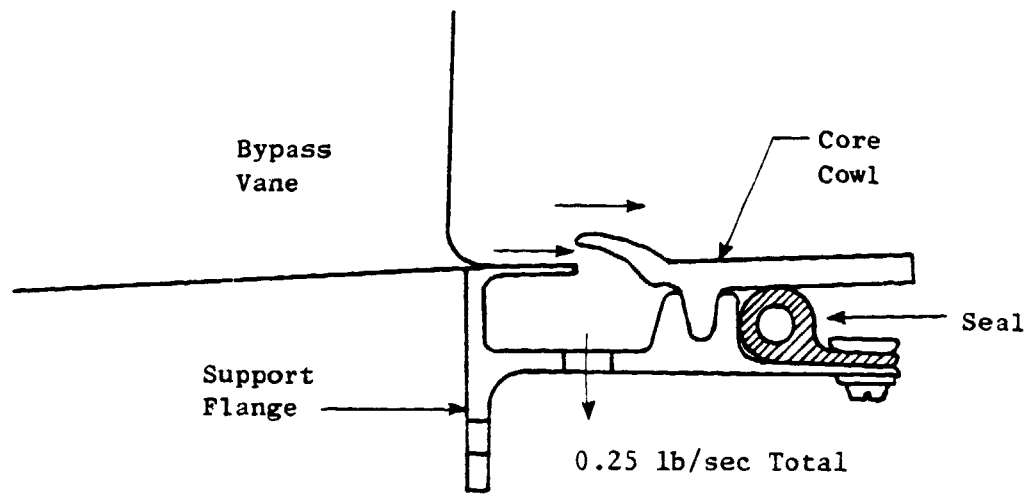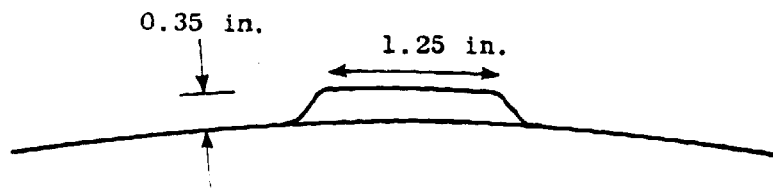
Figure 68.   Forward Core Cowl Support/Purge.

and ovalization studies have also been completed on the FPS design to optimize
the effect of the forward engine mount on compressor clearances. Analyses are
currently in process on the slave frame to cover critical load conditions such
as blade-out and rotor seizure. The normal load design analysis has been com-
pleted on the FSFT/ICLS (slave) frame design with the bolted flange analysis
to be completed. The final design of the FPS frame is currently scheduled for
the late-1980 to mid-1981 time period. The FPS configuration will be optimized
relative to frame flexibilities, operating deflections, stresses, and weight.
The basic design requirements for the FSFT/ICLS fan stator module are

- Represent, where possible, the FPS structure

- Provide adequate stiffness to minimize deflections to satisfy engine
  system dynamics

- Provide design flexibility for acoustic requirements.

Figure 69 illustrates the analytical computer model of the E^3 frame. The
model incorporates the core frame and bypass vane structural elements as
well as the stator assemblies and the outer bypass case. This model was
used to determine frame stiffness values for engine system response calcu-
lations and to evaluate the frame deflections under various loading con-
ditions. Figures 70 and 71 illustrate the frame stiffness values for shear
and overturning moment loading that have been established from the prelimi-
nary FPS frame studies and the current FSFT/ICLS analysis and how these values
effect the engine system response. The stiffness comparison chart shows the
difference between the possible extremes for an FPS frame design utilizing
different materials. The FPS-SOFT values represent an all aluminum structure
whereas the FPS-STIFF values represent an all steel structure. The comparison
shows the solid steel ICLS frame design to be significantly stiffer than the
FPS frames, particularly in the bypass portion of the structure. Figure 71
shows the fan frequency response and the No. 1 bearing load variation with a
given fan unbalance. The figure shows the critical frequency for each frame
design to be outside the maximum operating speed of the fan.

Figure 72 shows the temperature distribution through the fan for the
operating conditions applicable to the FSFT and the ICLS engine aero design
point. Axial deflections at critical locations on the frame assembly are
given in Figure 73 for loading and frame mounting conditions consistent with
the FSFT and ICLS engine test requirements. These deflections are used to
establish rotor/stator clearances.

C. Stator Vane Mechanical Design

A detail of the Stage 1 stator and core OGV assemblies is shown in
Figure 74. Porous Teflon will be utilized at the booster rotor rub tip sur-
face and the rotor seal rub surfaces due to its excellent material properties
and potentially lower cost. The Stator 1 vanes are individual vanes assembled
radially through loading slots into the 360° inner shroud. This assembly
bolts to the 360° cantilevered island casing supported at the bypass vane
leading edge. A 360° outer fairing which bolts radially into the island

84
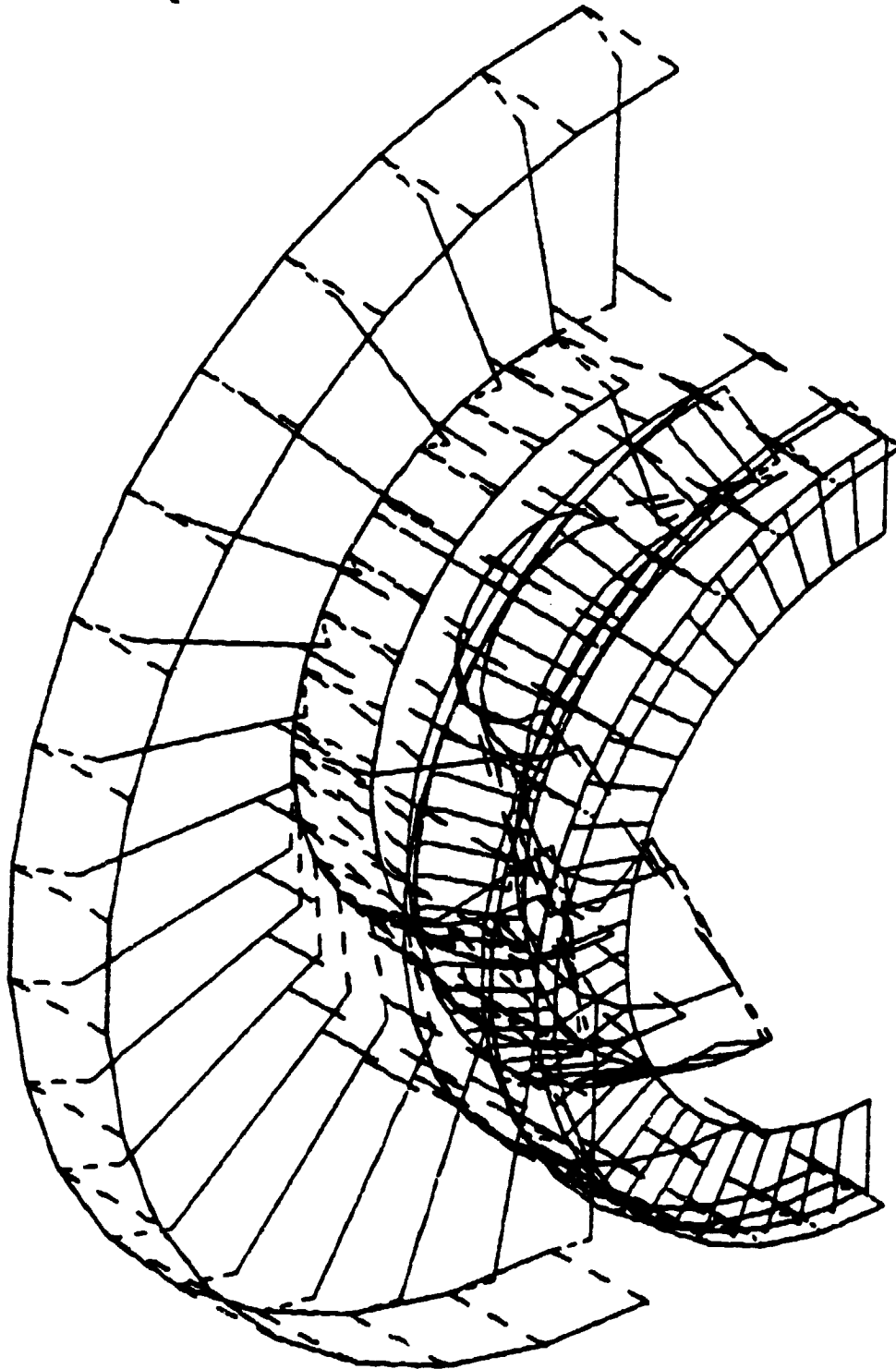
Figure 69.   Fan Frame MASS Analytical Model.

E^3	K_1 (Core)		K_2 (Bypass)	
	P/δ N/m (lb/in.)	M/θ m-N/rad (in.-lb/rad)	P/δ N/m (lb/in.)	M/θ m-N/rad (in.-lb/rad)
FPS - Soft	3.91×10^8 (2.23×10^6)	0.84×10^8 (0.74×10^9)	7.55×10^8 (4.31×10^6)	1.21×10^8 (10.7×10^8)
FPS - Stiff	11.46×10^8 (6.54×10^6)	2.44×10^8 (2.16×10^9)	9.50×10^8 (5.42×10^6)	3.35×10^8 (29.6×10^8)
ICLS	17.31×10^8 (9.88×10^6)	3.15×10^8 (2.79×10^9)	34.32×10^8 (19.59×10^6)	10.94×10^8 (96.8×10^8)
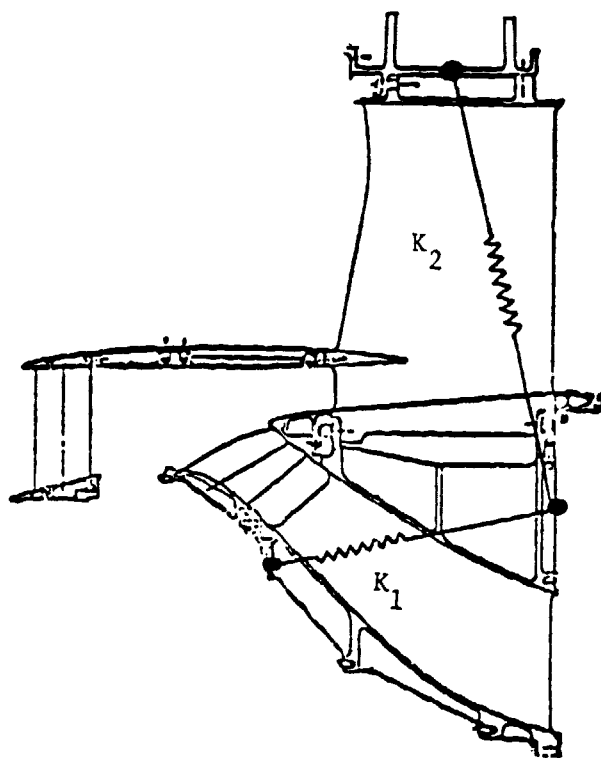
Figure 70. Fan Frame Stiffness Comparison.
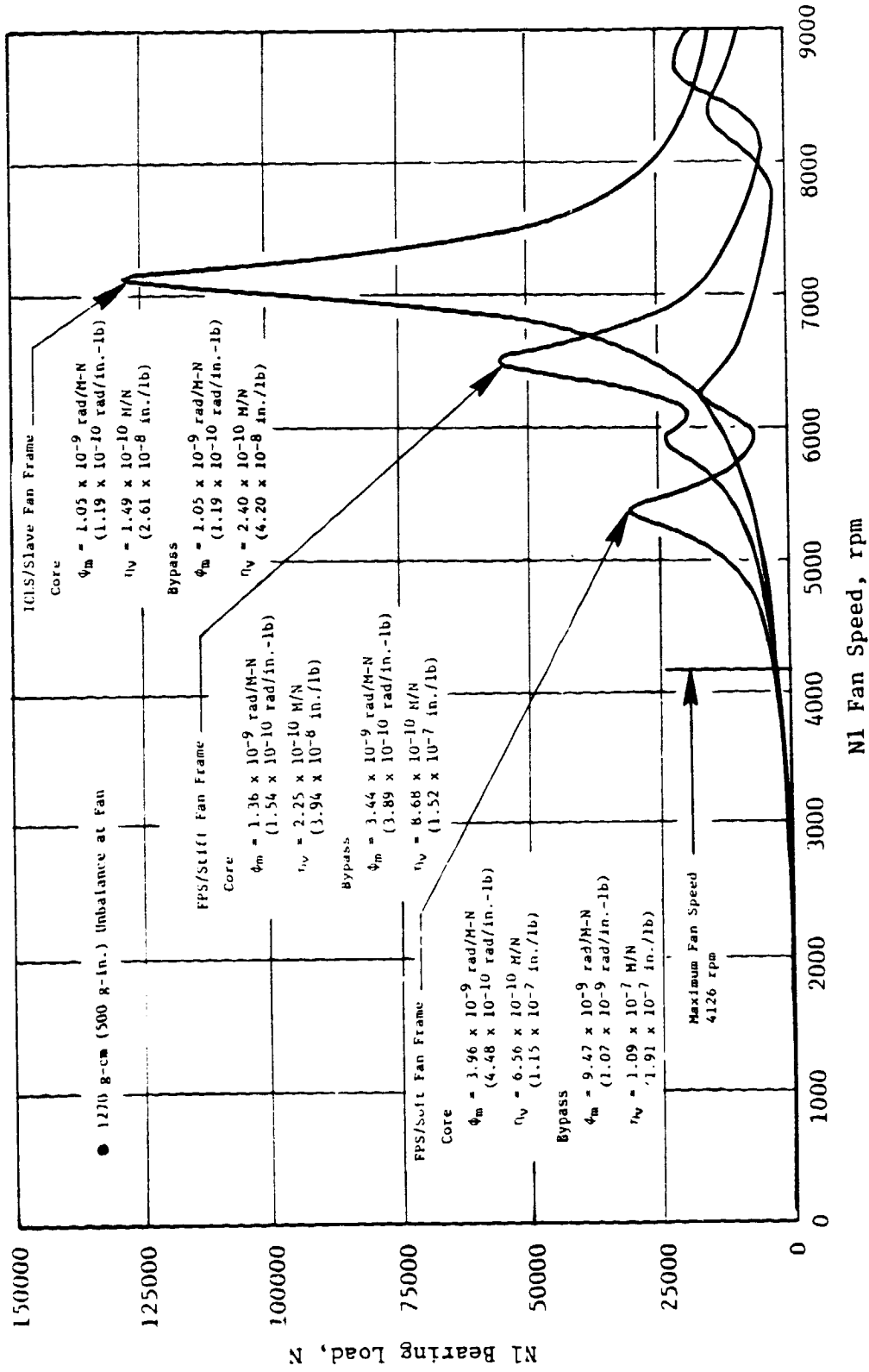
Figure 71. Fan Frequency Response Variation with Frame Stiffness.

87

Figure 72. Fan Temperature Distribution.
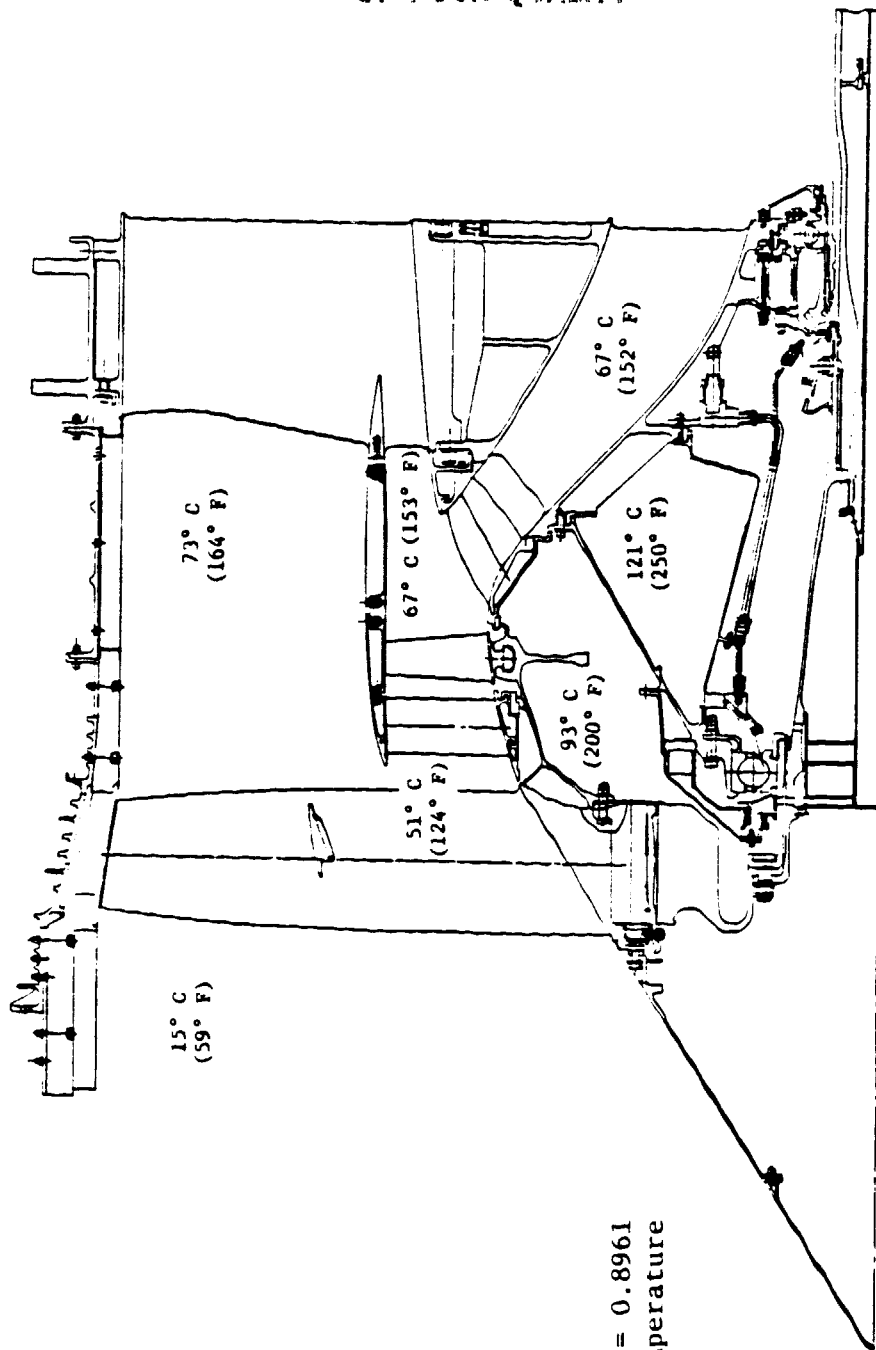
- Ambient Inlet
- 100% Fan Speed
- Case Temperature = 0.8961 x Aero Design Temperature

MASS Model Node	Thermal Loading								External Loading			
	(1) FSFT				(2) ICLS				FSFT Air Loads 100%		ICLS Fan Bearing Thrust Plus Air Loads 100%	
	(3) 100%		(4) Case 41		100%		Case 41					
	cm	in.	cm	in.	cm	in.	cm	in.	cm	in.	cm	in.
300	0.041	0.016	0.028	0.011	0.030	0.012	0.018	0.007	0.003	0.001	-0.003	-0.001
350	0.061	0.024	0.048	0.019	0.035	0.014	0.030	0.012	0.008	0.003	-0.008	-0.003
800	0.061	0.024	0.048	0.019	0.041	0.016	0.033	0.013	0.003	0.001	-0.003	-0.001
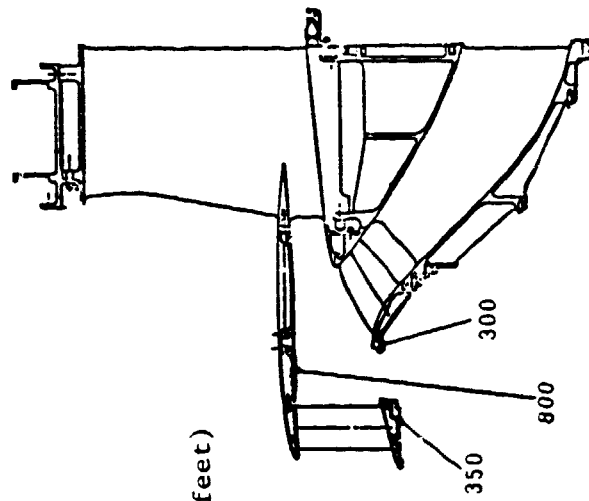
(1) Frame Mounted at Bypass Case

(2) Frame Mounted at Core Frame

(3) Deflections for 100% Fan Speed Ambient Inlet

(4) Deflections for Engine Cycle Case 41 = Mach 0.8/10.7 Km (35,000 feet)

Negative (-) is Aft

Figure 73. FSFT/ICLS Fan Axial Deflections.
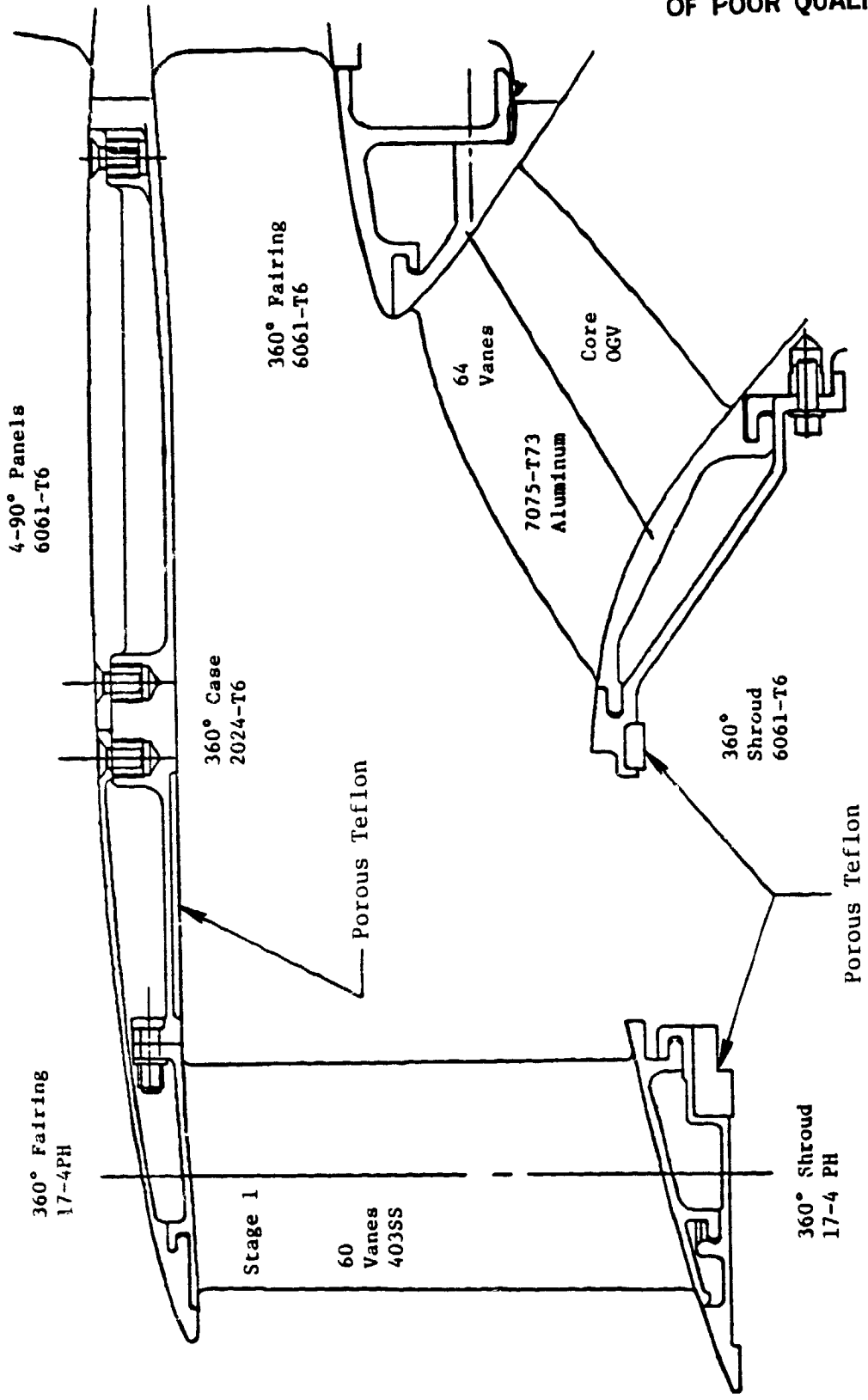
Figure 74. Fan Stator Materials.

360° Fairing
17-4PH

4-90° Panels
6061-T6

360° Fairing
6061-T6

360° Case
2024-T6

Porous Teflon

Stage 1

60
Vanes
403SS

64
Vanes

Core
OGV

7075-T73
Aluminum

360°
Shroud
6061-T6

Porous Teflon

Porous Teflon

360° Shroud
17-4 PH

90

casing attaches to the vane to provide additional support and form the island upper flowpath. The core OGV's are also individual vanes which assemble axially through loading slots into the 360° inner shroud. This assembly bolts to the core frame at the inner shroud with a 360° outer fairing bolting to the vane outer platform and providing the core flow splitter upper flowpath.

Table VII provides a geometry summary for the fan stator vanes. Figures 75 and 76 show the nonlinear tm/c distributions for the Stator 1 vane and core OGV designs which are representative of the proposed FPS designs. The bypass vane distribution is not shown since the design for FSFT/ICLS is a solid steel vane not representative of the hollow composite concept proposed for the FPS design. Figure 77, 78, and 79 represent the finite element analytical models used in the steady state and vibratory analysis of the fan stator vanes. Figures 80, 81, and 82 are the Campbell diagrams for the vanes.

The vane frequencies are shown relative to potential fan blade and booster blade excitations through the fan speed range. The maximum physical fan speed is shown for both the FPS baseline and proposed growth engine cycles. The vane designs for the FSFT/ICLS tests are relative to the baseline fan speed only with the growth engine cycle speed shown for reference. A different vane geometry will be required for a growth engine cycle and will change the vibratory characteristics of the vanes. Therefore, designing the FSFT/ICLS vane geometries to the growth cycle would be an unrealistic requirement.

The diagram for the bypass vane shows the predicted two-stripe (2S) frequency intersecting the 32/rev excitation line near top speed. This is a result of the slave solid vane design representing the desired aerodynamic configuration. The hollow composite vane design proposed for the flight-type design (FPS) will result in a higher two-stripe frequency that can be tuned to avoid vibratory excitation sources. It is felt that the bypass vanes are sufficiently downstream from the fan blade excitation and have sufficient structural section (solid steel) such that the two-stripe mode resonance should not present any problems during the component (FSFT) or engine (ICLS) testing.

The Stage 1 vane Campbell diagram shows adequate margin at maximum speed between the vibratory modes through two-stripe and the fan blade excitation sources, including twice fan blade passing. The core OGV diagram shows a similar distribution of vibratory modes as for Stator 1 with no resonances at maximum speed through the two-stripe mode. The proximity of the fundamental bending and torsion modes makes separating the modes and maintaining adequate margin over fan blade 32/rev and 64/rev excitation frequencies difficult without a major geometry change to the vane which could reduce the aerodynamic performance.

The major excitation source for the core OGV should be the booster rotor 56/rev with the current vane design exhibiting only lower speed resonance. The fan blade once and twice blade passing per rev is marginally close to the vane 1T and 2T modes. But for the reasons mentioned, the vane will be fabricated and bench tested to determine the exact frequency response before any design modification is considered.

91

Table VII. Fan Stator Geometry Summary.

Stator	Nv	Material	
		ICLS	FPS
Stage 1	60	403 SS	Ti 6-4
Inner OGV	64	7075 Al	7075 Al
Bypass	34	17-4 PH	Composite

Geometry

Stator	L cm (in.)	Chord, cm (in.)		tm/c		Stagger, deg.		Camber, deg.		Aspect Ratio
		Root	Tip	Root	Tip	Root	Tip	Root	Tip	
Stage 1	15.67 (6.17)	8.13 (3.20)	8.10 (3.19)	0.485	0.062	20.27	21.51	37.29	35.79	1.935
Inner OGV	11.63 (4.58)	9.25 (3.64)	5.44 (2.14)	0.053	0.062	18.40	21.53	55.38	62.38	1.39
Bypass	43.18 (17.0)	31.27 (12.31)	27.74 (10.92)	0.056	0.073	14.67	14.71	29.20	46.54	2.89
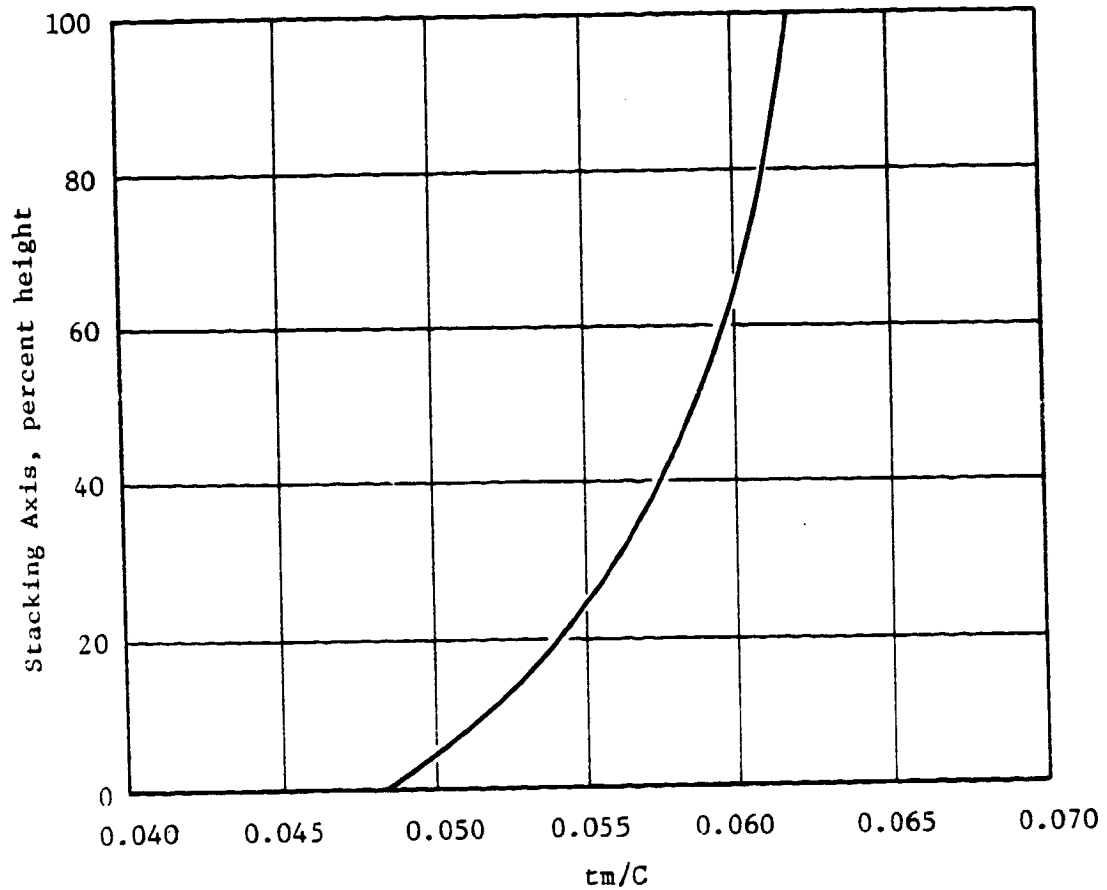
Figure 75.   Fan Stator Stage 1 Vane Tm/c Distribution.
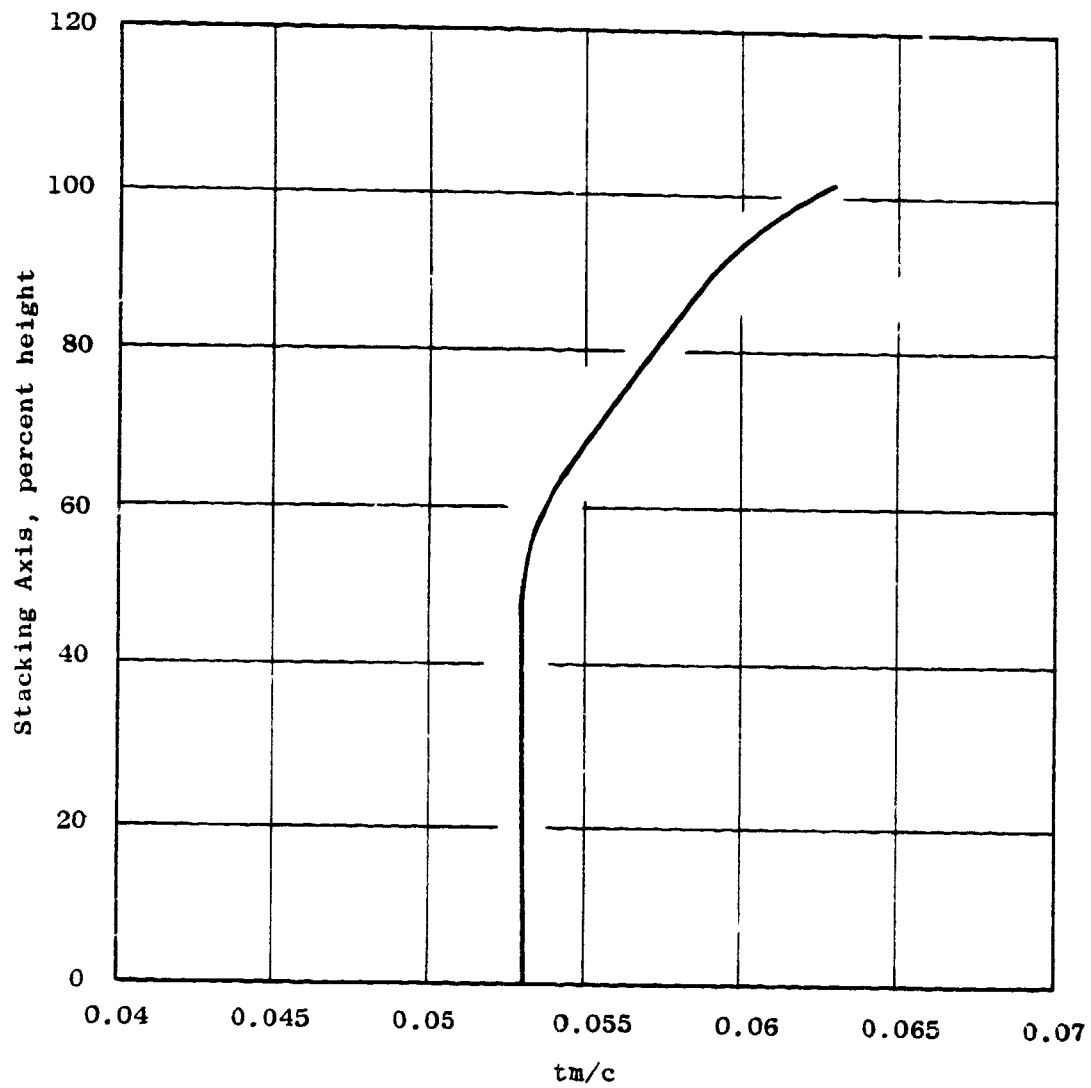
Figure 76.   Fan Stator Core OGV.

94
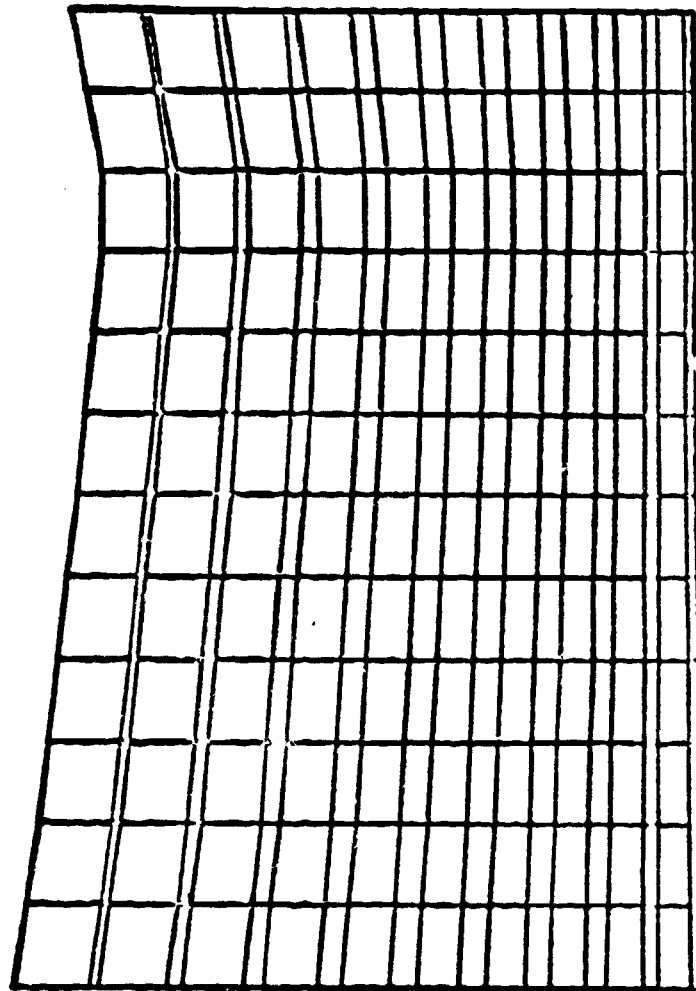
Figure 77. Bypass Vane, SAP-4 Analytical Model.
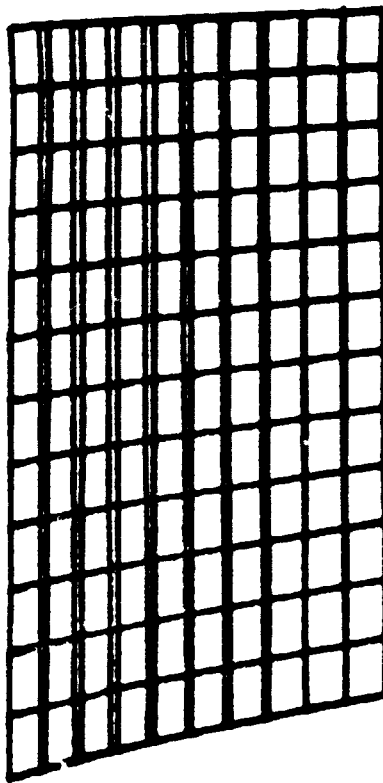
Figure 78.   Stage 1 Vane, SAP-4 Analytical Model.
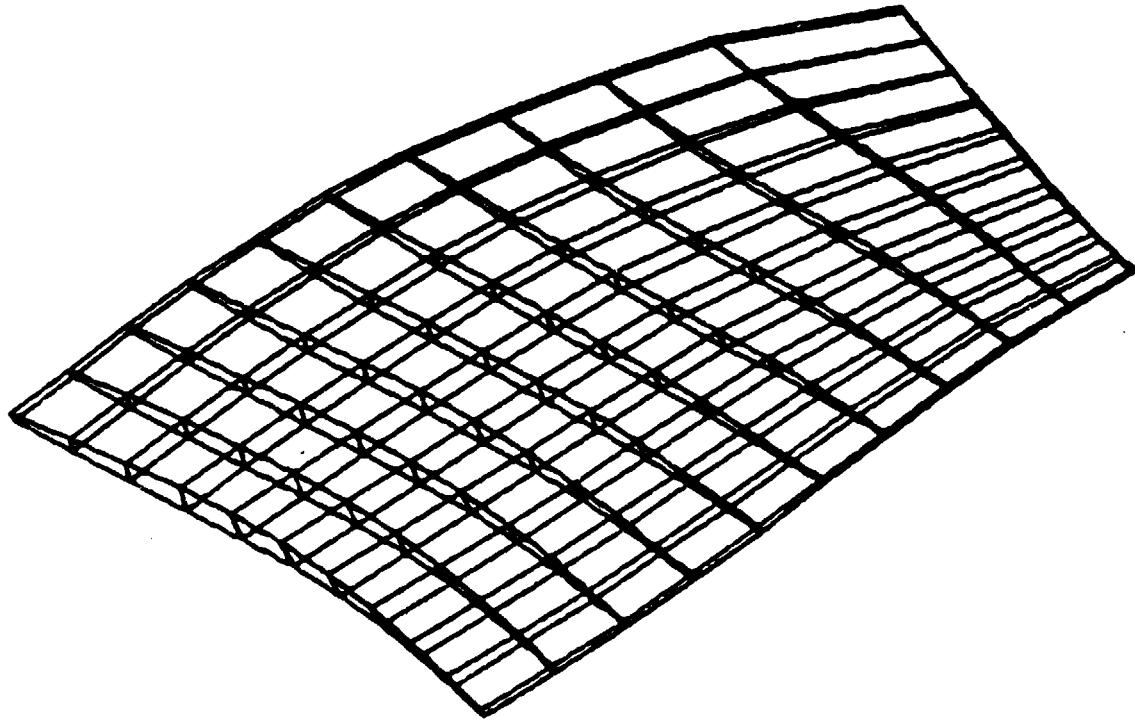
Figure 79.   Core OGV, SAP-4 Analytical Model.
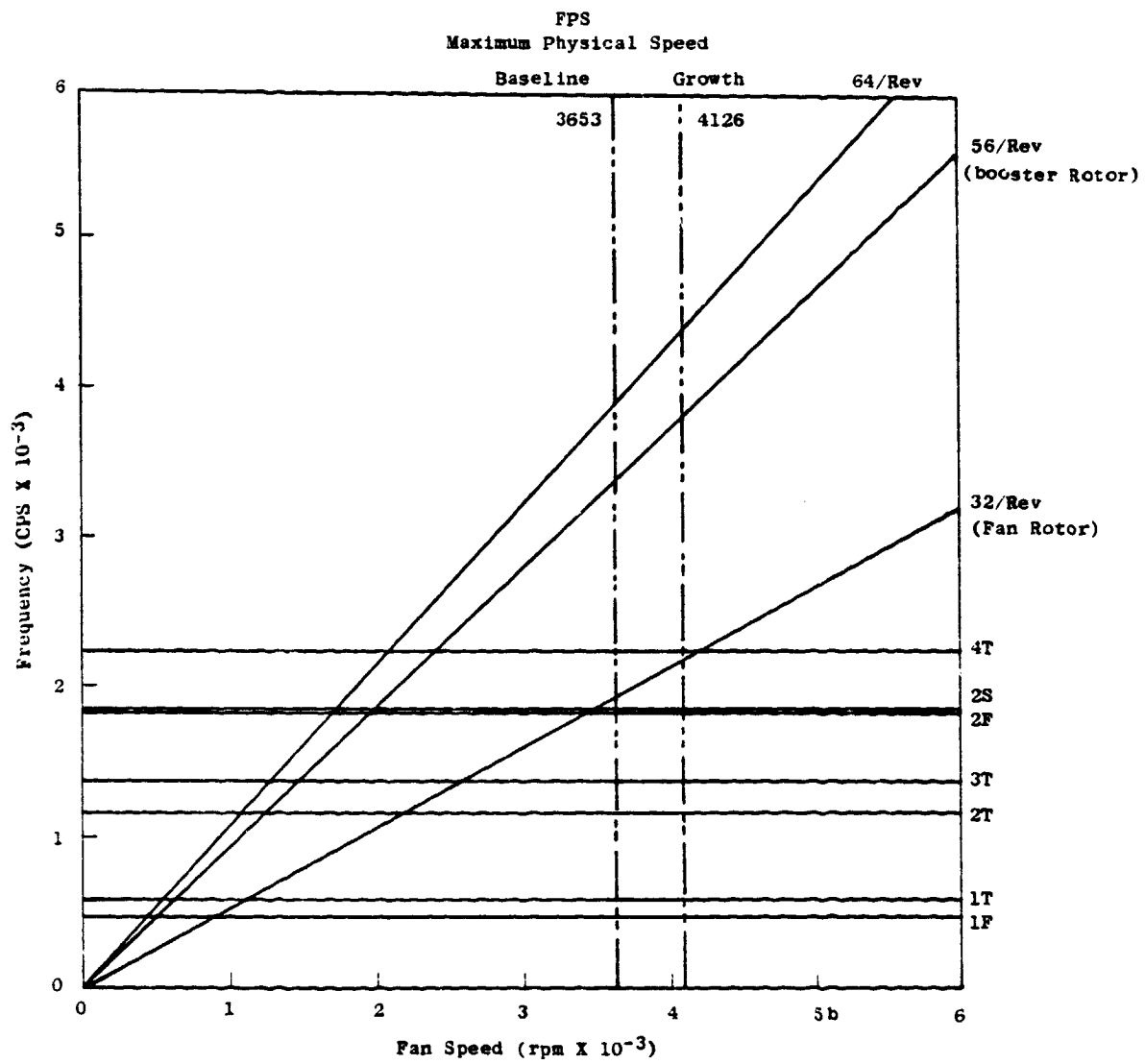
Figure 80. Bypass Vane Campbell Diagram.
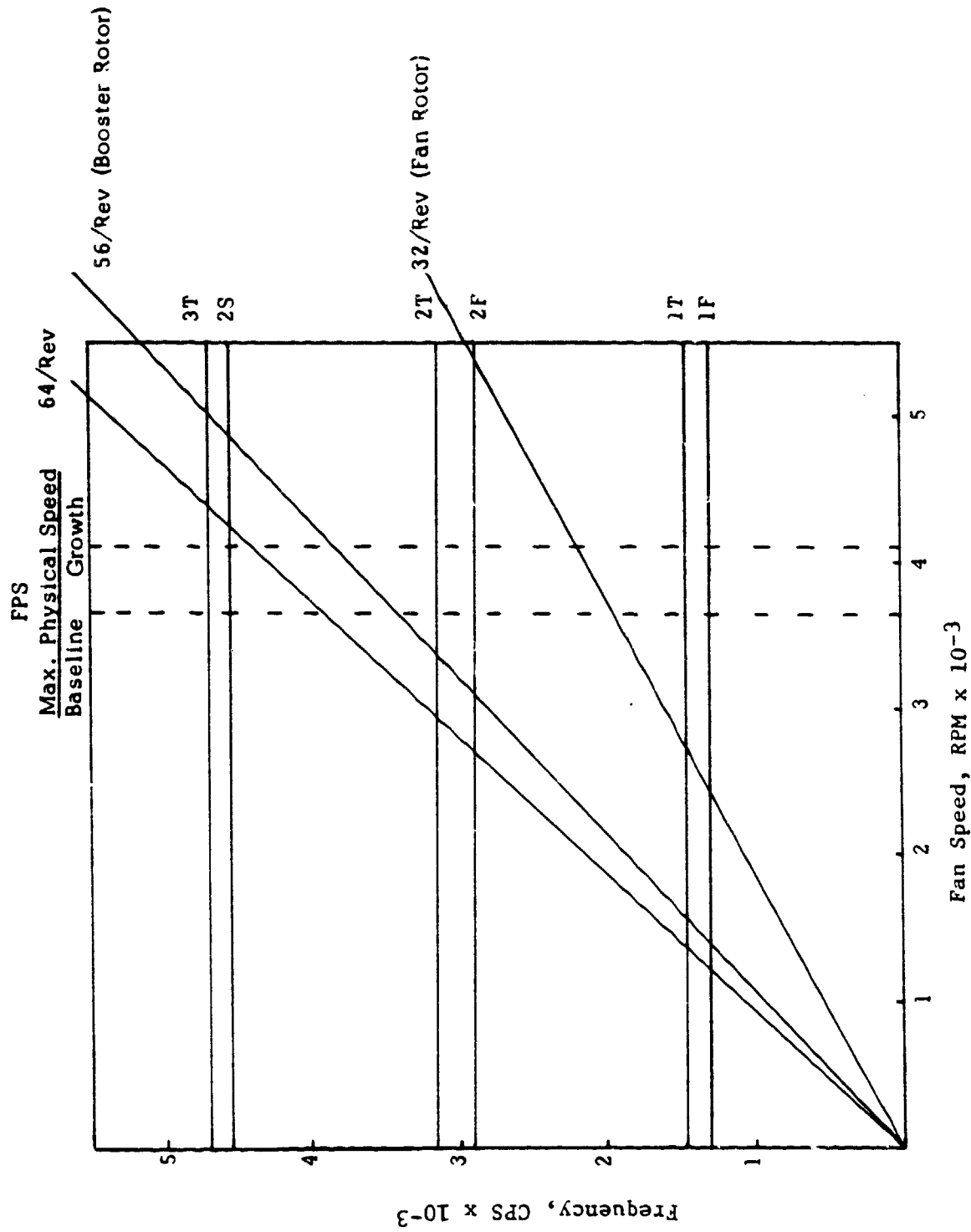
Figure 81. Stage 1 Campbell Diagram.
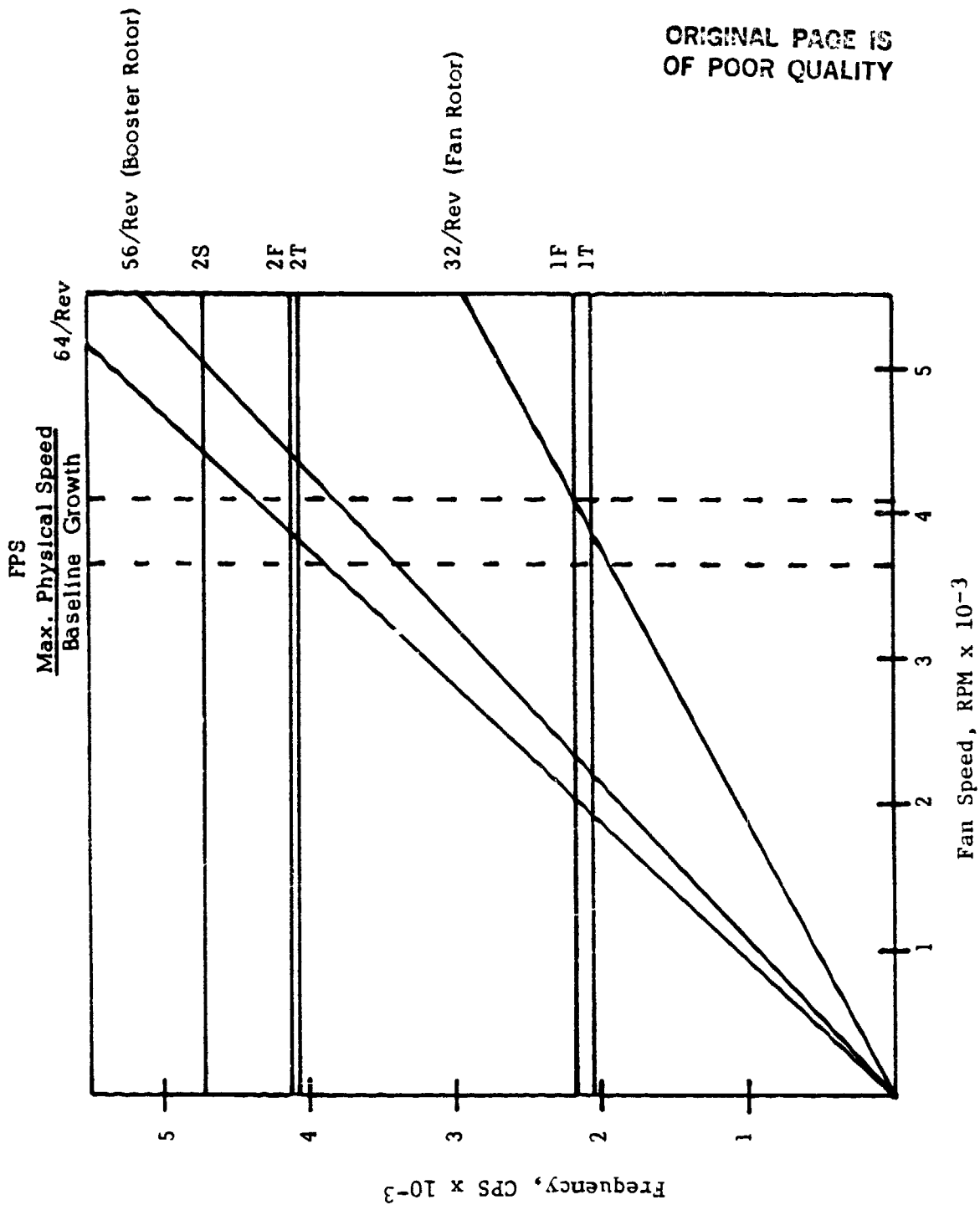
Figure 82. Core OGV Campbell Diagram.

100

The vane airfoil designs have more than adequate incidence angle margin with flexural and torsional instability boundaries.

Table VIII illustrates the vane steady state stress. The table shows the vane designs to be low steady state or mean stressed which improves the vibratory fatigue stress allowable. All the vane designs will be bench tested to determine the actual vibratory strain distribution for each vane frequency and then instrumented for safety monitoring during the component and engine tests. The instrumentation monitoring provides a means of limiting the vane vibratory stress based upon the material allowable to reduce the chance of fatigue failure during testing.

The design of the fan frame and stator assemblies is complete except for the analysis of the modified bypass vanes that are required for the ICLS configuration. The detail drawings for all the vanes and struts have been issued and fabrication has been initiated. The hardware for the Stage 1 and core OGV stator assemblies (shrouds, fairings, etc.) is also on order.

Figures 83 and 84 show the fastener selection for the stator assemblies and for the core frame and bypass vane assembly.

D. FSFT and ICLS Fan Casing/Containment Design

Due to fabrication costs, the FSFT and the ICLS engine test will utilize a slave containment system design instead of the advanced composite containment design proposed for the FPS configuration. The containment system as well as the boilerplate aluminum midcase will provide for both hardwall and acoustic panels required for performance and acoustic testing. The proposed design of the fan frame for the FPS features an integrated nacelle/fan bypass structure which supports the inlet and eliminates inlet loads being carried through the containment structure to the frame. Figure 85 illustrates the advanced composite containment system based on work done under NASA contracts for "Containment of Composite Blades" and "Development of Advanced Lightweight Containment Systems." The design features a structural inner steel shell which should provide a good bearing surface for the fan blades during large rotor excursions during unbalance, etc. and should stop small fragments without major damage. The actual containment system utilizes a honeycomb nesting area backed by the dry Kevlar cloth with a composite cover. The honeycomb nesting also provides stiffness to the structure to prevent fan rotor/casing interaction. Figure 86 shows the interaction frequency curve for the FPS design relative to a CF6-50 engine test. The figure shows the intersection of the fan casing traveling waves and the fan rotor traveling waves beyond both the FPS baseline and growth fan speeds which should ensure safe operation during testing. Figure 87 shows the containment angles proposed for the FPS design based upon CF6 commercial engine containment experience.

The calculation for the E^3 of the blade kinetic energy that has to be contained results in the thickness of the dry Kevlar cloth required. This relationship of kinetic energy to Kevlar thickness is based on data derived from the whirligig testing of the NASA containment programs previously mentioned.

Table VIII. Vibratory Stress Limits for ICLS Fan Frame Vanes.

	Bypass Vanes	Stage 1	Core OGV
Material	17-4 PH	403 SS	7075 - T73 Al
Maximum Design Steady State Stress, MN/m^2 (ksi)	20.7 (3)	203 (29.4)	22.1 (3.2)
Design Margin Alternating Stress For 10^7 Cycles, percent	200	30	150
Temperature of Maximum Allowable Stress, ° C (° F)	121 (250)	121 (250)	93 (200)

128: 1/4 in.-28

64 Vanes

34: 1/4 in.-28

119: 1/4 in.-28
17 Pins: 1/4 in.

120: 1/4 in.-28

90: 1/4 in.-28

120: 1/4 in.-28

60 Vanes
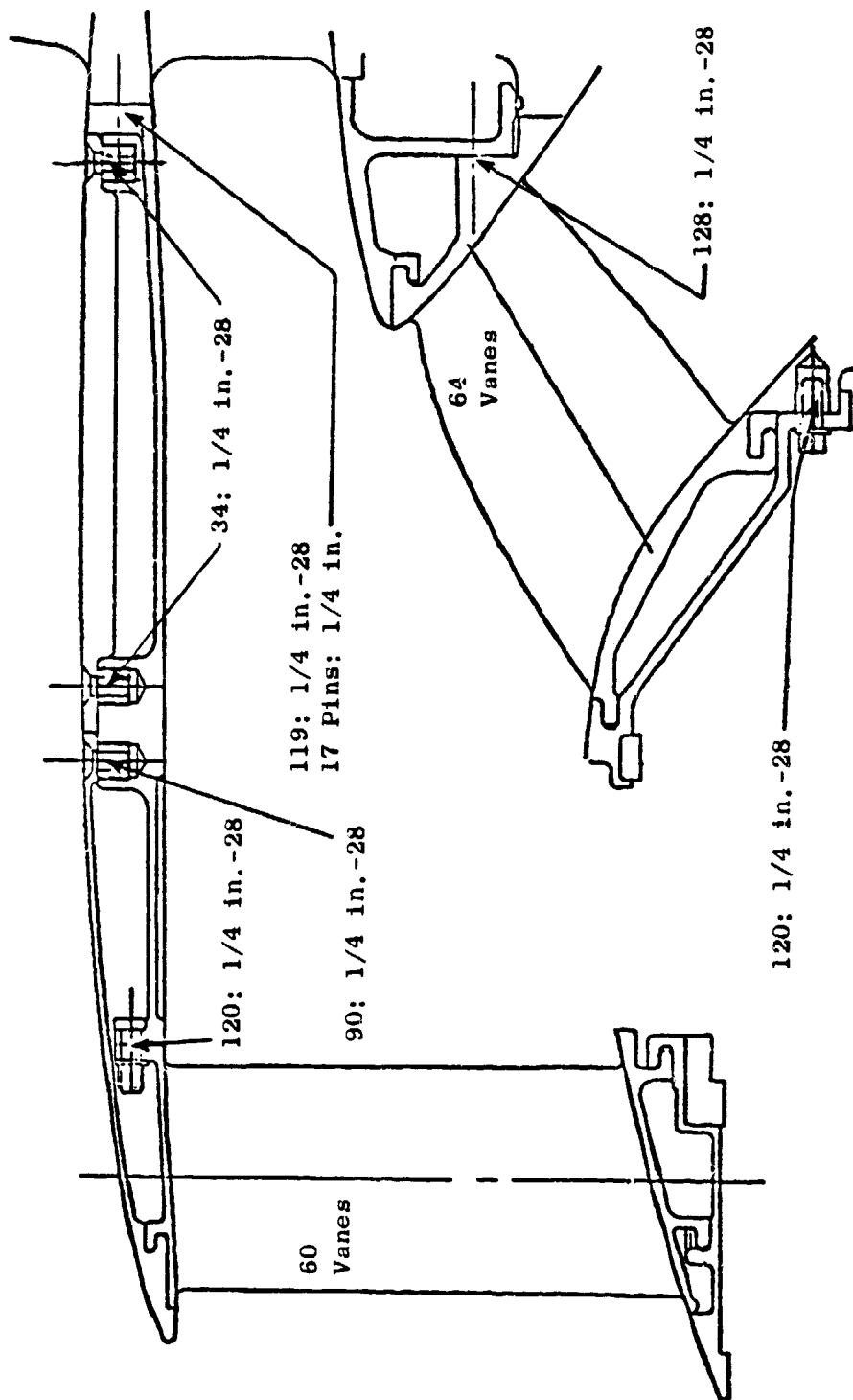
Figure 83. Stage 1 and Core Vane Assembly Fasteners.

120: 0.250-28

170: 0.375-24

170: 0.375-24

170: 0.25-28

68: 0.500-20

68: 0.500-20

86: 0.375-24

96: 0.375-28

94: 0.3125-24

24: 0.250-28

36: 0.250-28

24: 0.250-28
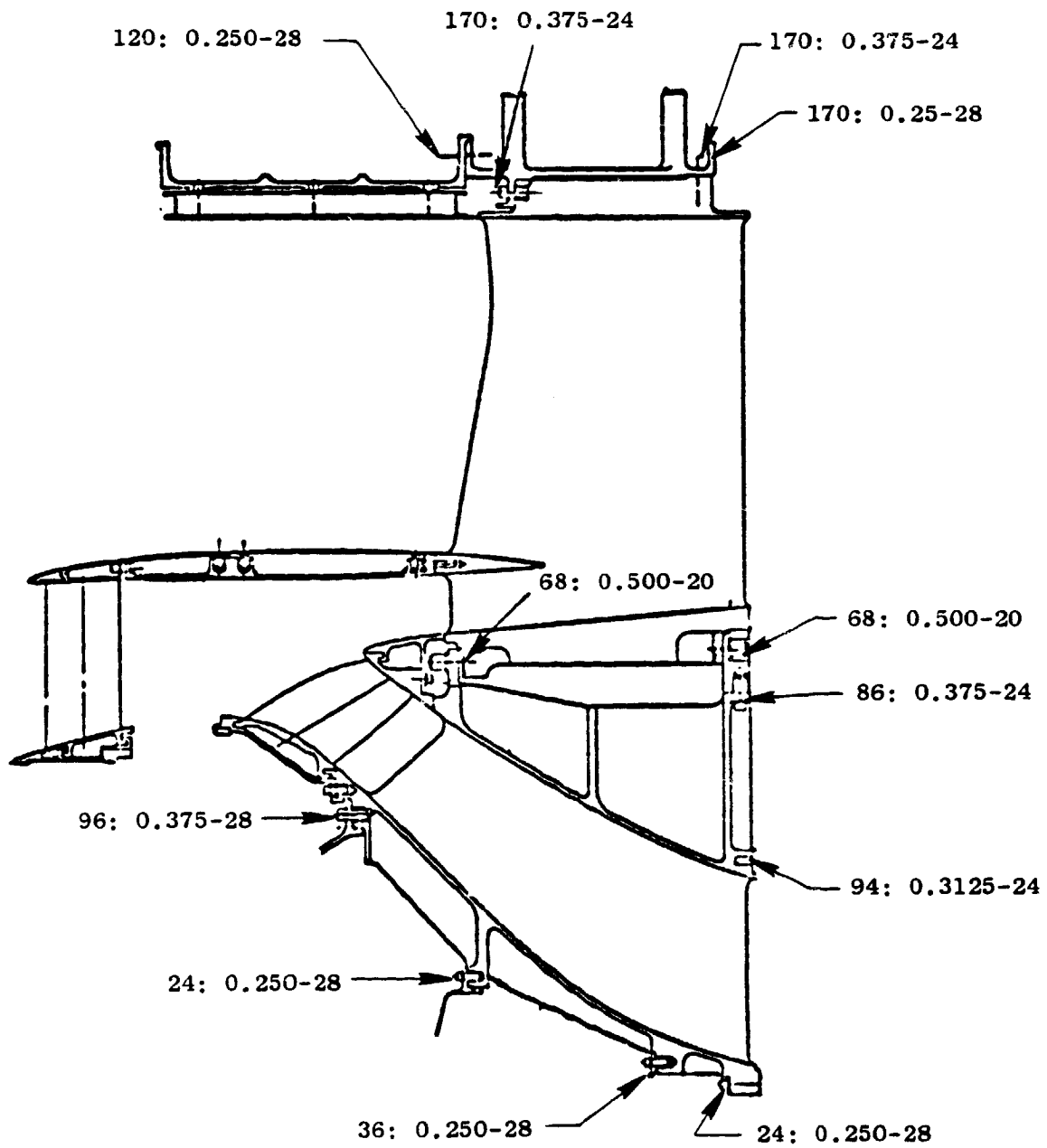
Figure 84.   Slave Frame Bolt Selection.

104

- Primary Containment by Layered Dry Kevlar
- Nesting Space Provided by Lightweight Al Honeycomb
- Normal Loads Resisted by Inner Steel Casing

Kevlar/Epoxy Cover

Kevlar Containment

Al Honeycomb Nesting Area

Inner Steel Case to Prevent Large Rotor Excursions During Unbalance and Stop Small Fragments Without Major Damage

Replaceable Acoustic Panel
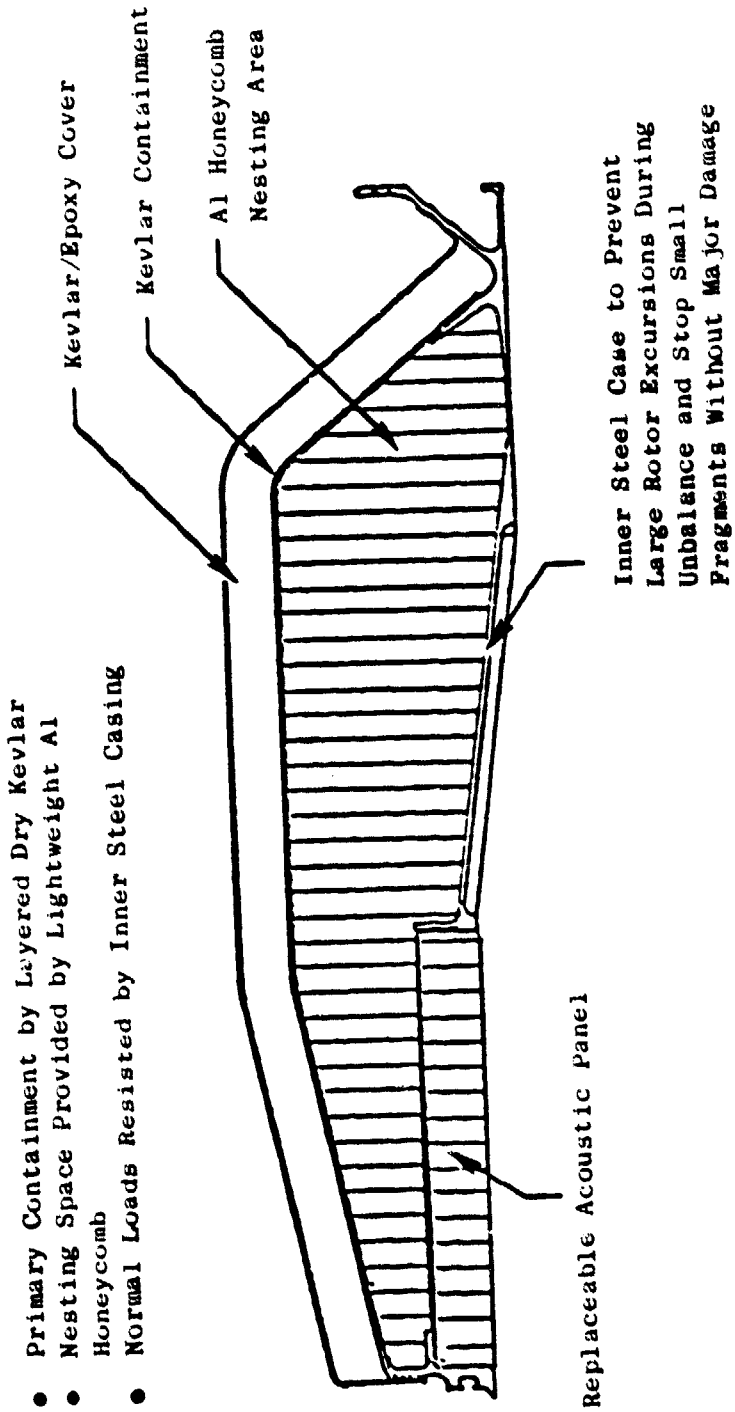
Figure 85. Advanced Composite Containment System.
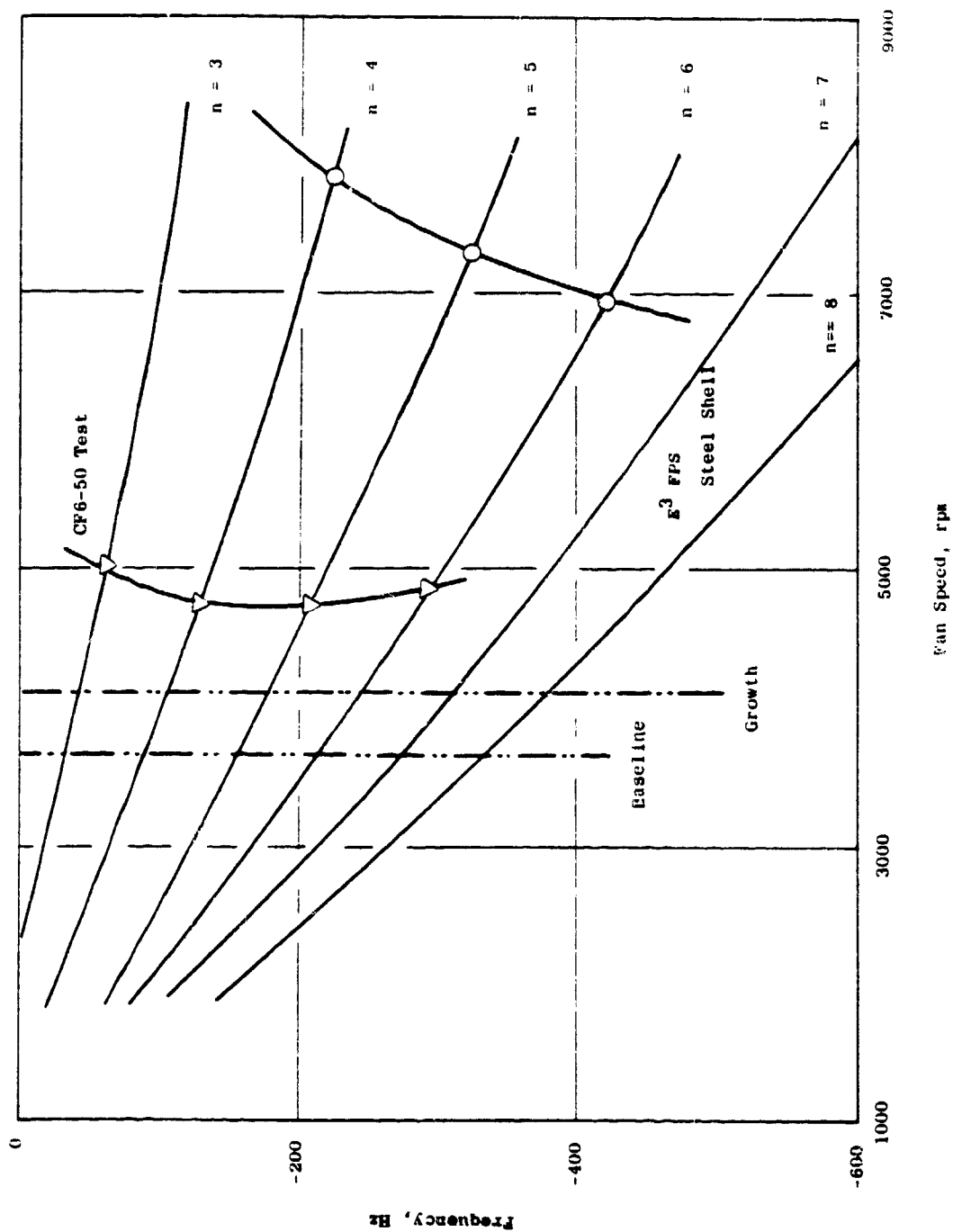
Figure 86. Fan Rotor/Casing Interaction.
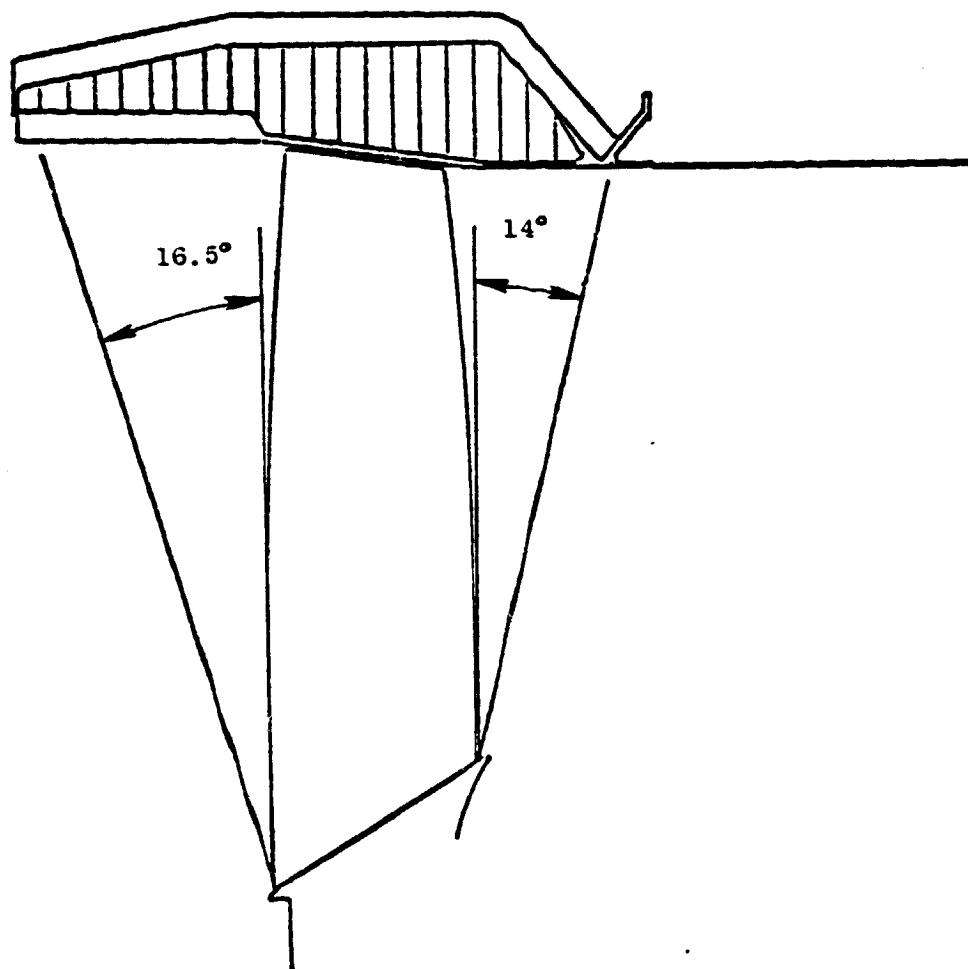
Figure 87.   FPS Containment Angles.

A preliminary calculation of the FPS containment case flange loads based on a fan blade-out condition shows the flange stress under an ultimate load condition to be within the material capabilities of the 304L steel casing.

As previously mentioned, a slave containment system design will be utilized for the FSFT and the ICLS engine test. Figure 8£ shows the low cost modification of a CF6-50 production steel case proposed as the containment system. An aluminum shell will be bolted on the forward end for support of the hardwall and acoustic panels forward of the fan and a steel shell will be welded to the aft end of the CF6-50 case for attachment to the midcase. Shown in phantom are stiffener rings that can be attached to the production case to provide sufficient interaction frequency margin as explained earlier. Figure 86 shows the casing interaction frequencies from a bench test of a CF6-50 case and illustrates that the margin above the E^3 fan operating range should be adequate.

Figure 89 shows the assembly of the outer midcase and containment case for the ICLS configuration to the fan frame slave outer casing.

E. FPS Fan Frame Weight Status

The E^3 FPS fan frame weight status is summarized below. This weight status will be updated as the FPS frame detailed study, scheduled to initiate in late 1980, progresses.

	kg	lbs
• Bypass vane-frame	257	566
• Core frame	129	284
• Core stators/assembly	79	175
• Containment	196	432
	661	1457
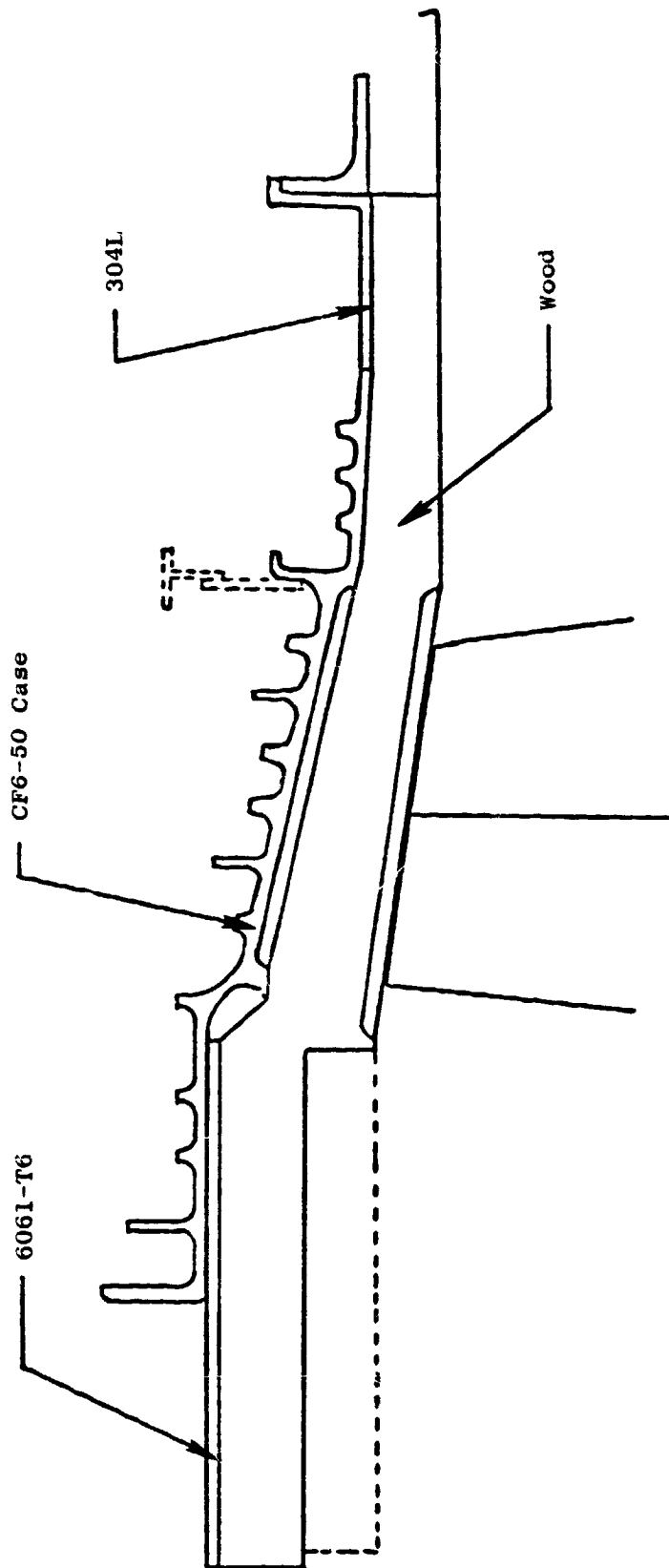
Figure 88. Low Cost Modification of CF6-50 Case.
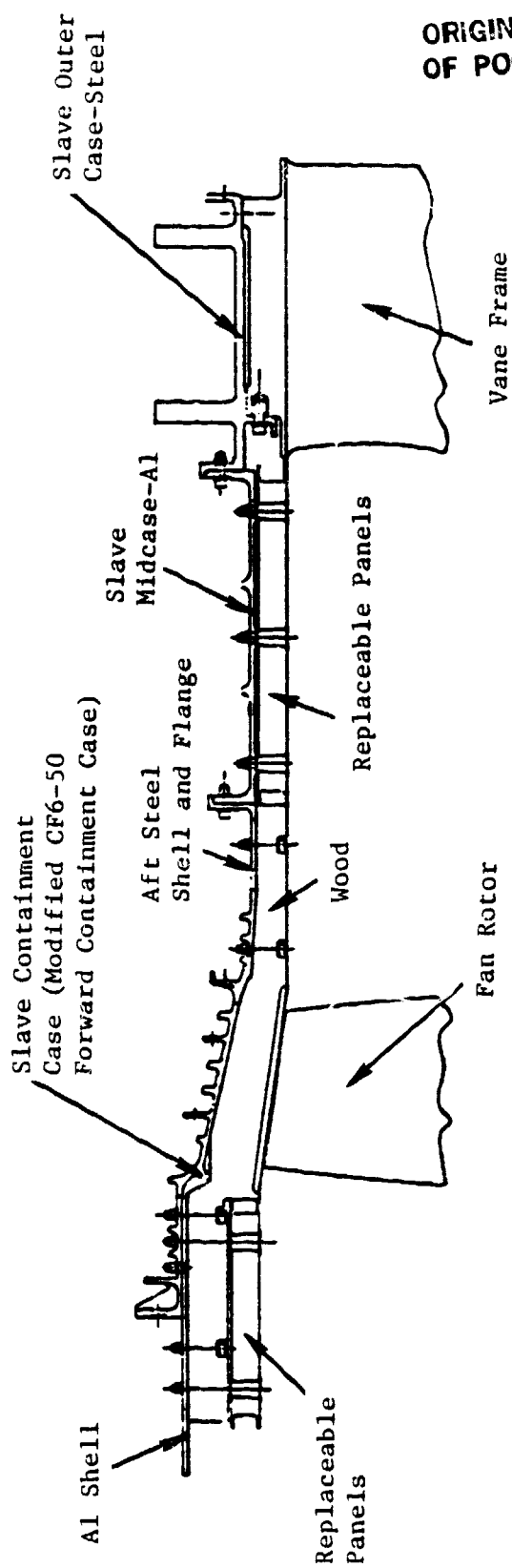
Figure 89. FSFT and ICLS Fan Casings.

REFERENCES

1. Seyler, D.R. and Smith, L.H., Jr., "Single Stage Experimental Evaluation of High Mach Number Compressor Rotor Blading, Part I -- Design of Rotor Blading," NASA CR-54581, April 1967.

2. Monsarrat, N.T., Keenan, M.J., and Tramm, P.C., "Single Stage Evaluation of Highly Loaded, High Mach Number Compressor Stages, Design Report," NASA CR-72562.

3. Reddy, J.L. and Klapproth, J.F., "Advanced Fan Development For High By-pass Engine," AIAA Paper Number 68-563, June 1968.

4. Smith, L.H. and Yeh, Hsuan, "Sweep and Dihedral Effects in Axial Flow Turbomachinery," Journal at Basic Engineering, Transaction of ASME, Series D, Volume 85, 1963.

LIST OF SYMBOLS AND NOMENCLATURE

Symbol	Description	Units
AR	Aspect Ratio $\dfrac{\text{Blade height at stacking axis}}{\text{Chord at 50\% ht.}}$	
C	Blade Chord	cm (in.)
DFACT or D-Factor	Diffusion Factor:	

$$D_{rotor} = 1 - (V'_2/V'_1) + (r_2 V_{\theta_2} - r_1 V_{\theta_1})/(2\,\bar{r}\,\sigma\,V'_1)$$

$$D_{stator} = 1 - (V_2/V_1) + (r_1 V_{\theta_1} - r_2 V_{\theta_2})/(2\,\bar{r}\,\sigma\,V_1)$$

Symbol	Description	Units
d	Diameter	m (ft)
i or INC	Incidence Angle	degrees
IGV	Inlet Guide Vane	---
ID	Inner Diameter	---
M	Mach Number	
N	Engine Speed	rpm
N_B	Number of Blades	
N_V	Number of Vanes	
OD	Outer Diameter	
OGV	Outlet Guide Vane	
P	Static Pressure	Kilo-Pascals (psia)
P/P	Total Pressure Ratio	
P_T	Total Pressure	Kilo-Pascals (psia)
PSI (ψ)	Percent Flow Stream Function	
R or r	Radius	cm (in.)
rpm	Revolutions per Minute	
R1, R2	Rotor 1, Rotor 2, respectively	
$\bar{r}$ or RBAR	Mean Radius	cm (in.)
SA	Stacking Axis	
S1, S2IN	Stator 1, Stator 2, Respectively	
SL	Streamline	

PRECEDING PAGE BLANK NOT FILMED

LIST OF SYMBOLS AND NOMENCLATURE   (Continued)

Symbol	Description	Units

Stall Margin
(%)
$$\dfrac{\left(\dfrac{P/P}{W}\right)_{stall} - \left(\dfrac{P/P}{W}\right)_{operating\ line}}{\left(\dfrac{P/P}{W}\right)_{operating\ line}} \times 100$$

Symbol	Description	Units
T	Temperature	K (° R)
TMC or tm/c	Maximum Thickness-to-Chord Ratio	---
t	Thickness (Blade)	cm (in.)
U	Rotor Speed	m/sec (ft/sec)
V	Velocity	m/sec (ft/sec)
W	Airflow	kg/sec (lbm/sec)
WB	Total Pressure Loss Coefficient	---
Z	Axial Distance	cm
β	Flow Angle	degrees
β^*	Metal Angle	degrees
γ	Specific Heat Ratio	
δ	Pressure Correction ($P_T/1.0133 \times 10^5$ N/m^2)	
δ° (DEV)	Deviation Angle	degrees
ϑ	Temperature Correction ($T_{T_1}/288.15$ K)	
σ	Solidity	
ψ (psi)	Percent Flow Streamfunction	
ϕ (phi)	Slope of Meridional Streamline	degrees
η (eta)	Efficiency	
$\bar{\omega}$ or WB	Total Pressure Loss Coefficient:	

$$\text{Rotor } \bar{\omega} = \frac{P'_{T_{2_{id}}} - P'_{T_2}}{P'_{T_1} - P_\lambda}$$

$$\text{Stator } \bar{\omega} = \frac{P_{T_1} - P_{T_2}}{P_{T_1} - P_1}$$

114

LIST OF SYMBOLS AND NOMENCLATURE (Concluded)

Subscripts

adia	Adiabatic
poly	Polytropic
1 or LE	Leading Edge
2 or TE	Trailing Edge
Sta	Blade Row Station
m or max	Maximum
r	Radial Direction
T	Total Condition
TH	Throat
Z	Axial Direction
θ (Theta)	Tangential Direction
∞	Free Stream
O	Total or Stagnation Conditions

Superscripts

'	Relative to Rotor
°	Degrees

APPENDICES

A. Fan and Quarter-Stage Aerodynamic Design Point Circumferential-Average Flow Solution.

B. Fan Rotor Blade Plane Section Geometry.

C. Stator 1 Plane Section Geometry.

D. Quarter-Stage Rotor Plane Section Geometry.

E. Inner OGV Plane Section Geometry.

F. Bypass OGV Plane Section Geometry.

Appendix A: Fan and Quarter-Stage Aerodynamic Design Point Circumferential
Average Flow Solution.

(METRIC) UNITS *** EEE FAN STATION DATA

BLADE ROW PRINTOUT FOR R1

PCT	EDGE IMM OUT	AXIAL LOC-Z IN	AXIAL LOC-Z OUT	RADIUS IN	RADIUS OUT	STREAM FUNCT IN	STREAM FUNCT OUT	MERID ANGLE IN	MERID ANGLE OUT

BLADE ROW PRINTOUT FOR R1

(METRIC) UNITS *** EEE FAN STATION DATA

PCT IMM	RBAR (INPUT)	INC (INPUT)	X-FACT	DEV (C-R)	TURN	LOSS COEFF	CAMBER	STGR	SOL	TMC	D-FACT	CHORD	AXIAL VEL-R	EFFICIENCY ADIA	POLY	ACC PT RATIO	ACC PT ACC PT RATIO
0.	104.001	5.00	0.	2.48	7.96	0.178	5.43	55.55	1.4062	0.0252	0.435	11.314	0.855	0.775	0.791	1.670	1.2038
7.76	99.267	4.66	0.	2.96	8.99	0.127	7.29	52.69	1.4384	0.0275	0.438	11.030	0.857	0.841	0.863	1.740	1.1940
14.93	94.800	4.95	0.	3.22	8.87	0.087	7.14	50.04	1.4781	0.0295	0.449	10.933	0.824	0.693	0.901	1.719	1.1870
22.32	90.220	6.50	0.	3.43	9.91	0.059	7.84	47.28	1.5132	0.0320	0.456	10.554	0.824	0.929	0.935	1.725	1.1817
30.05	85.419	6.66	0.	3.93	11.31	0.047	9.58	44.42	1.5427	0.0368	0.468	10.187	0.824	0.945	0.949	1.717	1.1769
38.38	80.297	5.70	0.	3.56	12.09	0.047	11.75	41.51	1.5890	0.0403	0.483	9.863	0.820	0.947	0.951	1.694	1.1718
43.56	77.025	5.73	0.	4.90	13.76	0.044	12.93	39.70	1.6221	0.0424	0.488	9.650	0.818	0.951	0.956	1.673	1.1667
45.61	75.754	5.68	0.	5.05	14.11	0.043	13.47	38.99	1.6369	0.0429	0.489	9.586	0.817	0.952	0.956	1.663	1.1645
45.79	75.646	5.65	0.	5.05	14.25	0.042	13.64	38.94	1.6382	0.0430	0.491	9.580	0.814	0.952	0.956	1.663	1.1606
49.31	73.456	5.65	0.	5.26	14.82	0.042	14.43	37.60	1.6546	0.0439	0.492	9.452	0.812	0.954	0.957	1.616	1.1578
52.23	71.641	5.55	0.	5.45	15.38	0.041	15.28	36.64	1.6872	0.0448	0.491	9.344	0.813	0.956	0.958	1.630	1.1508
57.33	68.475	5.00	0.	5.90	16.16	0.039	17.06	35.03	1.7282	0.0463	0.493	9.148	0.849	0.958	0.960	1.602	1.1434
62.79	65.007	4.76	0.	6.27	16.31	0.039	17.82	33.56	1.7731	0.0484	0.507	8.921	0.783	0.958	0.959	1.568	1.1394
65.00	63.169	4.60	0.	6.46	16.91	0.039	18.69	32.50	1.7982	0.0500	0.514	8.781	0.788	0.958	0.959	1.550	1.1394
71.14	59.902	4.65	0.	6.86	19.89	0.039	18.69	32.50	1.8424	0.0531	0.514	8.631	0.788	0.959	0.961	1.525	1.1539
77.94	55.670	4.72	0.	7.48	23.77	0.039	22.10	29.79	1.9140	0.0583	0.497	8.230	0.829	0.960	0.962	1.492	1.1264
81.89	53.223	4.72	0.	7.48	23.77	0.042	26.53	26.40	1.9628	0.0603	0.447	8.258	0.917	0.968	0.962	1.492	1.1226
89.70	49.326	4.80	0.	7.99	25.87	0.077	29.06	24.46	2.1005	0.0618	0.419	8.076	0.966	0.968	0.960	1.474	1.1182
100.00	41.976	3.50	0.	9.58	31.33	0.167	35.66	20.15	2.1976	0.0714	0.369	7.847	1.064	0.931	0.934	1.440	1.1173
				12.63	40.66		49.79	13.72	2.3976	0.0956	0.119	7.700	1.391	0.801	0.806	1.410	

INLET CORR WTFLOW 643.72	PRESS RATIO 1.6342	TEMP RATIO 1.1646	ADIA EFF 0.917	INLET CORR RPM 3727.7	NB 32	AR 2.66

BLADE ROW PRINTOUT FOR S1

(METRIC) UNITS *** EEE FAN STATION DATA

PCT EDGE IMM IN	OUT	AXIAL LOC-Z IN	OUT	RADIUS IN	OUT	STREAM FUNCT IN	OUT	MERID ANGLE IN	OUT	ABS ANGLE IN	OUT	REL ANGLE IN	OUT	TOTAL PRESS IN	OUT	TOTAL TEMP IN	OUT
0.	8.54	22.898	30.444	66.399	66.801	0.	0.100	1.19	2.05	38.30	12.00			156.76	154.44	328.3	328.3
8.44	16.52	22.898	30.452	65.806	65.521	0.100	0.194	4.97	2.58	38.86	11.90			155.79	153.83	327.6	327.6
16.61	20.29	22.885	30.458	63.657	64.324	0.194	0.320	6.74	3.40	38.51	11.50			154.52	152.89	326.7	326.7
20.69	37.26	22.878	30.472	61.680	62.568	0.328	0.427	8.71	4.73	37.91	10.02			152.18	150.75	325.2	325.2
37.69	37.26	22.859	30.484	60.178	61.216	0.427	0.427	9.98	5.78	37.73	10.26			151.18	149.72	324.6	324.6
37.69	48.99	22.859	30.484	60.178	61.216	0.427	0.552	9.98	5.78	37.73	10.26			151.18	149.72	324.6	324.6
49.56	63.56	22.847	30.495	58.218	59.457	0.551	0.700	11.47	7.22	37.38	9.76			149.35	147.78	323.5	323.5
64.21	71.30	22.835	30.507	55.800	57.273	0.700	0.776	13.20	9.03	37.32	9.28			147.04	144.93	322.5	322.5
72.04	84.76	22.831	30.511	54.507	56.100	0.776	0.900	14.10	9.98	37.45	8.89			145.91	143.42	322.2	322.2
85.35	100.00	22.829	30.513	52.318	54.096	0.900	0.990	15.87	11.42	37.88	8.39			144.18	140.83	321.9	321.9
100.00		22.832	30.510	49.892	51.811	1.000	1.000	17.81	12.10	38.79	0.00			142.87	138.57	322.0	322.0

MERID VEL IN	OUT	ABS VEL IN	OUT	REL VEL IN	OUT	TANG VEL IN	OUT	ABS MACH NO IN	OUT	REL MACH NO IN	OUT	BLKG IN	OUT	RCU IN	OUT
196.7	203.1	250.6	207.7			155.3	43.2	0.725	0.591			0.998	0.998	10311	2803
194.2	203.1	249.0	207.5			155.9	42.7	0.721	0.591			0.998	0.998	10134	2901
197.1	202.7	251.2	206.9			155.7	41.5	0.729	0.590			0.998	0.998	9913	2668
200.6	201.3	253.1	205.8			154.4	38.3	0.737	0.586			0.998	0.998	9523	2399
204.1	202.0	256.6	206.0			155.5	36.5	0.749	0.590			0.998	0.998	9358	2236
204.1	202.0	256.6	206.1			155.9	34.6	0.749	0.591			0.998	0.998	9077	2058
208.2	203.1	260.1	205.9			158.3	32.5	0.762	0.592			0.998	0.998	8831	1863
213.2	203.4	265.6	205.9			160.5	31.3	0.784	0.592			0.998	0.998	8749	1758
216.2	203.5	269.2	205.9			166.0	29.4	0.794	0.590			0.998	0.998	8681	1580
221.0	203.0	277.0	205.2			174.1	27.6	0.828	0.590			0.998	0.998	8686	1423
226.5	205.7	285.7	201.0					0.849	0.579						

PCT IMM	RBAR	INC (INPUT)	X-FACT	DEV (C-R)	TURN	LOSS COEFF	CAMBER	STGR	SOL	BLADE SPEED	TMC	D-FACT	CHORD	AXIAL VEL-R	EFFICIENCY ADIA	POLY	ACC PT RATIO	ACC TT RATIO
0.	66.600	0.	0.	7.73	26.30	0.050	34.03	21.20	1.1466		0.0621	0.365	3.148	1.032	0.921	0.925	1.524	1.393
0.49	65.263	0.	0.	7.72	26.97	0.043	34.69	21.52	1.1052		0.0616	0.357	3.109	1.049	0.927	0.932	1.518	1.383
16.57	63.990	0.08	0.	7.68	26.92	0.035	34.45	21.21	1.2097		0.0611	0.363	3.191	1.034	0.933	0.937	1.509	1.369
20.45	62.120	0.15	0.	7.58	27.09	0.031	34.45	20.54	1.2454		0.0604	0.372	3.190	1.012	0.936	0.940	1.488	1.339
37.48	60.697	0.26	0.	7.46	27.47	0.031	34.66	20.14	1.2740		0.0598	0.376	3.188	1.004	0.935	0.939	1.478	1.286
37.48	60.697	0.26	0.	7.46	27.47	0.031	34.66	20.14	1.2740		0.0598	0.376	3.188	1.004	0.935	0.939	1.478	1.264
49.29	58.808	0.40	0.	7.32	27.64	0.035	34.56	19.70	1.3134		0.0587	0.382	3.186	0.987	0.929	0.933	1.458	1.226
63.90	56.537	0.75	0.	7.23	28.12	0.043	34.76	19.34	1.3655		0.0569	0.394	3.183	0.968	0.904	0.909	1.430	1.193
71.73	55.304	0.95	0.	7.22	28.56	0.050	35.03	19.19	1.3960		0.0557	0.403	3.183	0.956	0.885	0.890	1.415	1.182
85.07	53.203	1.50	0.	7.23	29.49	0.065	35.67	19.00	1.4506		0.0531	0.425	3.182	0.933	0.843	0.858	1.390	1.173
100.00	50.851			7.29	30.79	0.080	36.50	19.00	1.5176		0.0487	0.458	3.102	0.902	0.799	0.808	1.360	

INLET CORR WTFLOW	PRESS RATIO	TEMP RATIO	ADIA EFF	INLET CORR RPM	NB	AR
143.74	1.4585	1.1256	0.989	3727.7	60	1.96

BLADE ROW PRINTOUT FOR R2

(METRIC) UNITS *** EEE FAN STATION DATA

PCT EDGE IMM		AXIAL LOC-Z		RADIUS		STREAM FUNCT		MERID ANGLE		BLADE SPEED		ABS MACH NO		ABS ANGLE		REL ANGLE		TOTAL PRESS		TOTAL TEMP	
IN	OUT	IN	OUT	IN	OUT	IN	OUT	IN	OUT	IN	OUT	IN	OUT	IN	OUT	IN	OUT	IN	OUT	IN	OUT
0.	0.	33.617	38.430	66.878	66.878	0.100	0.100	0.69	0.55	261.1	261.1	0.612	0.609	11.60	24.72	46.00	40.71	154.44	170.53	328.3	340.7
8.66	9.31	33.581	38.486	65.617	65.597	0.194	0.194	1.23	-0.72	256.1	256.1	0.613	0.610	11.49	24.00	45.42	40.16	153.83	170.53	327.6	339.3
16.66	17.66	33.542	38.551	64.452	64.448	0.328	0.328	2.15	-0.06	251.6	251.6	0.616	0.611	10.30	23.94	44.88	39.45	152.89	170.53	326.7	338.4
28.40	29.83	33.479	38.655	62.743	62.775	0.427	0.427	2.96	-0.88	245.0	245.0	0.614	0.615	9.75	24.51	44.49	37.05	150.76	170.53	325.2	338.0
37.34	38.99	33.426	38.745	61.442	61.513	0.427	0.427	2.96	-0.88	239.0	240.1	0.618	0.620	9.75	24.79	43.06	36.49	149.72	170.53	324.6	337.9
37.34	38.99	33.426	38.745	61.442	61.513	0.552	0.552	4.12	-0.88	239.0	247.1	0.618	0.628	9.24	24.79	43.06	36.49	149.72	170.53	324.6	337.9
49.02	50.87	33.341	38.749	59.741	59.888	0.552	0.700	4.12	-0.88	233.2	233.7	0.619	0.630	9.24	25.78	43.20	34.14	147.78	170.53	323.5	338.1
63.50	65.31	33.238	39.040	57.632	57.893	0.700	0.700	5.05	-0.50	228.6	226.0	0.610	0.649	8.71	27.27	42.39	30.51	144.93	170.53	322.5	339.0
71.20	72.91	33.184	39.132	56.499	56.848	0.776	0.776	6.91	-0.26	228.6	221.9	0.617	0.663	8.42	28.12	42.00	28.22	143.42	170.53	322.2	339.0
84.61	85.55	33.086	39.289	54.559	55.109	0.900	0.900	8.93	0.32	213.0	215.1	0.611	0.694	7.98	29.56	41.53	23.74	148.03	170.53	321.9	341.7
100.00	100.00	32.969	39.471	52.318	53.128	1.000	1.000	10.93	1.07	204.2	207.4	0.608	0.733	7.63	30.71	41.00	18.65	138.57	170.53	322.0	343.7

MERID VEL		ABS VEL		REL VEL		TANG VEL		BLADE SPEED		REL MACH NO		BLKG		RCU		ACC PT ACC IT	EFFICIENCY		
IN	OUT	IN	OUT	IN	OUT	IN	OUT	IN	OUT	IN	OUT	IN	OUT	IN	OUT	RATIO RATIO	ADIA	POLY	
209.9	197.7	214.3	217.6	302.6	260.8	43.1	91.0	261.1	261.1	0.864	0.730	0.998	0.998	2803	6006	1.683 1.1024	0.800	0.889	
210.3	198.4	214.6	217.3	299.7	259.6	42.7	88.7	256.1	256.1	0.856	0.729	0.998	0.998	2801	5816	1.683 1.1775	0.905	0.911	
210.2	198.6	215.2	217.3	298.0	257.2	41.4	88.2	251.6	251.6	0.853	0.723	0.998	0.998	2668	5602	1.683 1.1745	0.920	0.926	
211.2	198.8	214.4	218.5	295.1	251.7	38.2	90.6	245.0	245.0	0.846	0.700	0.998	0.998	2399	5689	1.683 1.1730	0.928	0.923	
212.0	199.9	215.1	220.2	293.8	248.6	36.4	92.3	239.0	240.1	0.844	0.700	0.998	0.998	2236	5677	1.683 1.1728	0.929	0.934	
212.0	201.3	215.0	220.6	290.0	248.6	36.4	92.3	239.0	247.1	0.836	0.685	0.998	0.998	2058	5822	1.683 1.1734	0.929	0.932	
212.2	201.3	215.0	223.6	298.0	243.3	34.4	97.2	233.2	233.7	0.826	0.670	0.998	0.998	1863	6196	1.683 1.1765	0.916	0.916	
212.1	204.6	214.6	230.2	286.6	237.4	32.3	105.1	228.6	226.0	0.819	0.679	0.998	0.998	1750	6295	1.683 1.1794	0.895	0.903	
211.2	207.2	214.2	234.9	284.2	235.1	31.1	110.7	228.6	221.9	0.805	0.664	0.998	0.998	1500	6677	1.683 1.1859	0.864	0.873	
210.2	213.7	212.2	245.6	279.3	233.4	29.1	121.7	213.0	215.1	0.805	0.659	0.998	0.998	1423	7024	1.683 1.1929	0.833	0.844	
206.8	222.7	208.6	259.0	272.2	235.0	27.2	132.2	204.2	207.4	0.783	0.666								

PCT IMM	RBAR	INC (INPUT)	DEV (C-R)	X-FACT	LOSS COEFF	TURN	CAMBER	STGR	SOL	TMC	D-FACT	CHORD	AXIAL VEL-R
0.	66.878	0.72	3.03	0.	0.080	5.37	7.68	41.52	0.8462	0.0490	0.232	2.508	0.942
8.98	65.607	0.51	2.57	0.	0.052	5.27	7.72	41.05	0.8707	0.0490	0.222	2.523	0.943
17.15	64.450	0.37	3.05	0.	0.037	5.42	8.10	40.45	0.8952	0.0500	0.225	2.540	0.941
29.09	62.759	0.65	3.27	0.	0.031	6.64	9.26	39.21	0.9318	0.0540	0.242	2.583	0.945
38.14	61.478	0.68	3.45	0.	0.030	7.37	10.14	38.11	0.9614	0.0572	0.253	2.611	0.944
38.14	61.478	0.68	3.45	0.	0.030	7.37	10.14	38.11	0.9614	0.0572	0.253	2.611	0.944
49.91	59.811	0.84	3.81	0.	0.030	9.05	12.02	36.35	1.0026	0.0620	0.271	2.649	0.951
64.30	57.762	1.02	4.38	0.	0.033	11.09	15.25	33.75	1.0536	0.0693	0.293	2.688	0.969
72.07	56.673	1.06	4.77	0.	0.037	13.78	17.49	32.20	1.0834	0.0729	0.303	2.712	0.985
85.86	54.034	1.22	5.51	0.	0.050	17.79	22.30	29.26	1.1157	0.0776	0.311	2.751	1.029
100.00	52.219	1.24	6.35	0.	0.064	22.44	27.64	26.87	1.2079	0.0611	0.298	2.813	1.097

INLET CORR WTFLOW	INLET CORR RPM	TEMP RATIO	PRESS RATIO	ADIA EFF	NB	NB	AR
143.74	3727.7	1.1776	1.6830	0.904	56	56	2.10

BLADE ROW PRINTOUT FOR S21N   (METRIC) UNITS *** EEE FAN STATION DATA

PCT EDGE IMM		AXIAL LOC-Z		RADIUS		STREAM FUNCT		MERID ANGLE		ABS ANGLE		REL ANGLE		TOTAL PRESS		TOTAL TEMP	
IN	OUT	IN	OUT	IN	OUT	IN	OUT	IN	OUT	IN	OUT	IN	OUT	IN	OUT	IN	OUT
0.	0.	56.207	60.661	58.593	55.202	0.	0.218	-37.28	-38.78	39.93	2.56			170.53	169.01	337.9	337.9
11.30	21.65	52.995	59.147	57.945	53.713	0.218	0.477	-24.05	-37.10	38.32	2.51			170.53	169.79	339.1	339.1
34.93	44.91	49.526	57.132	56.590	52.113	0.477	0.649	-16.45	-37.31	32.13	2.51			170.53	169.51	339.0	339.8
48.21	67.60	47.992	56.096	56.020	51.241	0.649	0.826	-15.19	-37.39	31.66	2.52			170.53	169.27	339.8	341.7
71.76	78.32	45.706	54.321	54.478	49.815	0.826	0.826	-12.03	-38.10	31.02	2.54			170.53	168.19	341.7	341.7
100.00	100.00	43.217	52.305	52.058	48.324	1.000	1.000	-0.33	-29.82	32.36	2.60			170.53	166.67	343.7	343.7

MERID VEL		ABS VEL		REL VEL		TANG VEL		BLADE SPEED		ABS MACH NO		REL MACH NO		BLKG		RCU	
IN	OUT	IN	OUT	IN	OUT	IN	OUT	IN	OUT	IN	OUT	IN	OUT	IN	OUT	IN	OUT
145.5	163.1	174.8	163.2			96.9	5.7			0.486	0.452			0.990	0.990	5677	314.
140.1	163.0	172.4	163.1			100.5	5.7			0.478	0.451			0.990	0.990	5822	306.
175.1	163.6	209.1	163.7			107.9	5.7			0.586	0.452			0.990	0.990	6105	298.
189.6	163.9	220.6	164.0			112.8	5.7			0.619	0.453			0.990	0.990	6295	293.
200.4	164.6	241.0	164.6			122.6	5.7			0.662	0.453			0.990	0.990	6677	286.
212.0	163.6	250.2	163.7			132.9	5.7			0.706	0.449			0.990	0.990	7024	276.

PCT IMM		INC		DEV		X-FACT	TURN	CAMBER	STGR	SOL	THC	D-FACT	CHORD	AXIAL VEL-R	EFFICIENCY		ACC PT RATIO	ACC TT RATIO
		(INPUT)		(C-R)										ADIA	POLY		
0.	0.	56.897	-12.50	16.00	37.37	2.00	65.95	19.46	1.2910	0.0303	0.275	2.839	1.099	0.912	0.918	1.668	1.1720
16.94	16.94	55.829	-4.96	12.85	35.82	2.00	53.62	16.47	1.3059	0.0334	0.261	2.991	1.022	0.910	0.924	1.676	1.1734
48.37	48.37	54.351	-5.10	10.98	29.61	2.00	45.70	14.38	1.4649	0.0362	0.392	3.077	0.757	0.899	0.906	1.673	1.1765
53.33	53.33	53.635	-4.24	10.56	29.13	2.00	43.93	13.92	1.4920	0.0360	0.427	3.007	0.712	0.802	0.894	1.671	1.1794
76.34	76.34	52.146	-2.43	9.81	28.47	2.00	40.71	13.09	1.5410	0.0372	0.484	3.106	0.634	0.839	0.658	1.660	1.1859
100.00	100.00	50.591	-0.39	9.47	29.75	2.00	39.60	12.94	1.6015	0.0384	0.512	3.132	0.599	0.793	0.807	1.645	1.1929

INLET CORR WTFLOW	PRESS RATIO	TEMP RATIO	ADIA EFF	INLET CORR RPM	NB	AR
82.39	1.6676	1.1791	0.808	3727.7	64	0.03

BLADE ROW PRINTOUT FOR S2OUT

(METRIC) UNITS *** EEE FAN STATION DATA

PCT EDGE IMM IN	OUT	AXIAL LOC-Z IN	OUT	RADIUS IN	OUT	STREAM FUNCT IN	OUT	MERID ANGLE IN	OUT	ABS ANGLE IN	OUT	REL ANGLE IN	OUT	TOTAL PRESS IN	OUT	TOTAL TEMP IN	OUT
0.	0.	64.683	94.996	67.357	69.563	0.	0.234	3.27	4.34	27.91	0.			178.53	166.78	340.7	340.7
24.10	20.75	64.683	94.996	65.897	68.396	0.234	0.455	3.82	4.61	27.29	0.			178.53	166.52	339.3	339.3
45.33	40.65	64.683	94.996	64.619	67.276	0.455	0.769	4.40	4.87	27.22	0.			178.53	166.23	338.4	338.4
76.29	69.75	64.683	94.996	62.745	65.639	0.769	1.000	5.04	5.25	28.00	0.			178.53	165.74	338.0	338.0
100.00	100.00	64.683	94.996	61.318	63.937	1.000		4.94	4.94	28.65	0.			178.53	165.14	337.9	337.9

MERID VEL IN	OUT	ABS VEL IN	OUT	REL VEL IN	OUT	TANG VEL IN	OUT	BLADE SPEED IN	OUT	ABS MACH NO IN	OUT	REL MACH NO IN	OUT	BLKG IN	OUT	RCU IN	OUT
199.7	199.7	193.3	199.7			90.4	0.			0.537	0.556			0.990	0.973	6006.	0.
198.6	198.6	192.9	198.6			88.3	0.			0.537	0.554			0.990	0.973	5817.	0.
197.7	197.7	192.7	197.7			87.9	0.			0.537	0.552			0.990	0.972	5682.	0.
195.6	196.6	193.2	196.6			90.7	0.			0.539	0.549			0.990	0.972	5689.	0.
195.3	195.3	193.7	195.3			92.6	0.			0.541	0.546			0.990	0.971	5677.	0.

PCT IMM	RRAR	INC (INPUT)	DEV (C-R)	TURN	X-FACT	LOSS COEFF	CAMBER	STGR	SOL	TMC	D-FACT	CHORD	AXIAL VEL-R	EFFICIENCY ADIA	POLY	ACC PT RATIO	ACC IT RATIO
0.	68.460	-1.27	4.87	27.91	0.	0.123	34.05	12.15	2.5932	0.0587	0.055	12.916	1.167	0.849	0.851	1.646	1.1024
22.53	67.146	-1.09	4.70	27.29	0.	0.132	33.08	11.84	2.6222	0.0584	0.055	12.810	1.157	0.868	0.870	1.643	1.1775
43.07	65.948	-0.95	4.64	27.22	0.	0.141	32.81	11.77	2.6421	0.0582	0.055	12.677	1.152	0.872	0.300	1.641	1.1745
73.14	64.194	-0.91	4.73	26.00	0.	0.157	33.72	12.13	2.7045	0.0578	0.067	12.631	1.152	0.874	0.002	1.636	1.1730
100.00	62.627	-0.86	4.67	28.65	0.	0.175	34.10	12.42	2.8512	0.0572	0.073	12.992	1.148	0.868	0.877	1.630	1.1728

INLET CORR WTFLOW	PRESS RATIO	TEMP RATIO	ADIA EFF	INLET CORR RPM	NB	AR
61.35	1.6393	1.1755	0.865	3727.7	34	0.18

BLADE ROW PRINTOUT FOR OGV   (METRIC) UNITS *** EEE FAN STATION DATA

PCT EDGE IIM IN	OUT	AXIAL LOC-Z IN	OUT	RADIUS IN	OUT
0.	0.	68.326	94.996	102.743	102.743
13.20	13.20	68.936	95.129	98.366	98.502
24.05	23.73	69.012	95.061	94.768	95.121
35.17	34.53	68.705	94.993	91.079	91.650
46.70	45.77	68.000	94.992	87.254	88.039
59.00	57.77	67.246	94.996	83.173	84.185
72.21	70.88	66.447	94.999	78.793	79.975
77.40	76.23	66.123	94.999	77.046	78.256
77.40	76.23	66.123	94.999	77.046	78.256
79.39	78.20	66.004	94.998	76.412	77.623
86.05	86.04	65.542	94.994	73.938	75.103
94.87	94.90	65.945	94.988	71.276	72.259
100.00	100.00	64.729	94.984	69.576	70.620

MERID VEL IN	OUT	ABS VEL IN	OUT	REL VEL IN	OUT	TANG VEL IN	OUT	STREAM FUNCT IN	OUT	MERID ANGLE IN	OUT	ABS ANGLE IN	OUT
205.0	207.3	252.2	207.3			147.0	0.	0.	0.129	0.	0.	35.65	0.
217.1	215.1	262.0	215.1			146.7	0.	0.129	0.257	0.15	1.01	34.85	0.
223.6	218.2	267.5	218.2			146.8	0.	0.257	0.386	0.25	1.45	33.29	0.
225.8	218.1	269.0	218.1			147.7	0.	0.386	0.515	0.24	1.97	33.20	0.
224.3	214.9	269.9	214.9			150.2	0.	0.515	0.644	0.18	2.54	33.81	0.
220.4	207.9	268.3	207.9			153.0	0.	0.644	0.772	0.20	3.13	34.77	0.
216.3	195.5	264.1	195.5			152.9	0.	0.772	0.828	0.20	3.74	35.38	0.
212.9	189.2	261.0	189.2			152.4	0.	0.828	0.828	0.17	3.97	35.60	0.
212.0	189.2	261.0	189.2			152.1	0.	0.828	0.837	0.16	3.97	35.67	0.
208.4	186.7	257.4	186.7			151.1	0.	0.837	0.901	0.08	4.05	35.94	0.
205.0	176.4	253.5	176.4			149.1	0.	0.901	0.966	-0.32	4.69	36.03	0.
203.0	154.6	251.3	154.6			148.2	0.	0.966	1.000	-0.59	4.73	36.13	0.

BLADE SPEED IN	OUT	ABS MACH NO IN	OUT	REL MACH NO IN	OUT	REL ANGLE IN	OUT	TOTAL PRESS IN	OUT	TOTAL TEMP IN	OUT
	0.	0.749	0.573					169.21	165.54	346.9	346.9
	1.01	0.742	0.599					172.25	169.41	344.3	344.3
	1.45	0.762	0.610					174.21	171.02	342.3	342.3
	1.97	0.771	0.611					174.79	172.57	340.5	340.5
	2.54	0.773	0.603					175.95	171.71	339.1	339.1
	3.13	0.770	0.583					171.64	169.09	337.7	337.7
	3.74	0.768	0.548					167.74	164.56	335.0	335.0
	3.97	0.754	0.531					165.07	162.44	333.0	333.0
	3.97	0.754	0.531					165.87	162.44	333.0	333.0
	4.05	0.752	0.524					165.16	161.61	333.4	333.4
	4.35	0.743	0.495					162.32	158.34	331.6	331.6
	4.69	0.733	0.457					158.95	154.53	329.5	329.5
	4.73	0.727	0.434					156.99	152.32	328.3	328.3

EFFICIENCY ADIA	POLY	BLKG IN	OUT	RCU IN	OUT	ACC PT RATIO	ACC PT RATIO
0.739	0.757	0.998	0.990	15103	0.	1.634	1.2030
0.813	0.826	0.998	0.990	14430	0.	1.672	1.1948
0.869	0.878	0.998	0.955	13911	0.	1.696	1.1870
0.906	0.913	0.998	0.998	13457	0.	1.703	1.1817
0.921	0.927	0.998	0.998	13103	0.	1.695	1.1769
0.918	0.924	0.998	0.998	12727	0.	1.669	1.1718
0.915	0.921	0.998	0.998	12050	0.	1.624	1.1627
0.912	0.918	0.998	0.998	11742	0.	1.601	1.1586
0.912	0.918	0.998	0.998	11742	0.	1.603	1.1586
0.918	0.916	0.998	0.998	11626	0.	1.595	1.1570
0.903	0.909	0.998	0.998	11168	0.	1.563	1.1508
0.895	0.901	0.998	0.998	10626	0.	1.525	1.1435
0.889	0.895	0.998	0.998	10311	0.	1.503	1.1393

PCT IMM	RBAR IN	INC (INPUT)	X-FACT	DEV (C-R)	TURN	LOSS COEFF	CAMBER	STGR	SO!	TMC	D-FACT	CHORD	AXIAL VEL-R
0.	102.743	1.00	0.	8.27	35.65	0.076	42.92	13.19	1.4500	0.0723	0.379	10.039	1.011
13.20	98.434	1.00	0.	8.01	34.85	0.054	40.05	12.62	1.4636	0.0736	0.378	10.401	0.991
23.89	94.944	1.00	0.	7.45	33.29	0.043	39.74	12.42	1.5172	0.0731	0.365	10.480	0.975
34.85	91.365	1.00	0.	7.18	33.20	0.039	39.38	12.51	1.6054	0.0712	0.362	10.671	0.965
46.24	87.646	1.00	0.	7.07	33.01	0.039	39.07	12.87	1.7004	0.0688	0.366	10.894	0.957
58.40	83.679	1.00	0.	7.01	34.77	0.046	40.79	13.38	1.8271	0.0662	0.380	11.124	0.942
71.55	79.384	1.00	0.	6.84	35.38	0.059	41.22	13.77	1.9732	0.0635	0.405	11.396	0.921
76.86	77.651	1.00	0.	6.76	35.60	0.066	41.36	13.92	2.0374	0.0624	0.419	11.511	0.912
76.86	77.651	1.00	0.	6.76	35.60	0.066	41.40	13.92	2.0374	0.0624	0.419	11.511	0.887
78.00	77.017	1.00	0.	6.73	35.67	0.069	41.40	13.97	2.0617	0.0620	0.425	11.553	0.879
86.45	74.520	1.00	0.	6.60	35.94	0.008	41.54	14.17	2.1607	0.0606	0.449	11.715	0.844
94.80	71.760	1.00	0.	6.42	36.03	0.093	41.45	14.30	2.2778	0.0590	0.485	11.894	0.793
100.00	70.098	1.00	0.	6.33	36.13	0.100	41.46	14.48	2.3532	0.0581	0.509	12.002	0.769

INLET CORR WTFLOW 499.98	PRESS RATIO 1.6517	TEMP RATIO 1.1757	ADIA EFF 0.079	INLET CORR RPM 3727.7	NB 34	AR 1.13

124

BLADE ROW PRINTOUT FOR R1

(ENGLISH) UNITS *** EEE FAN STATION DATA

PCT EDGE IMM IN	OUT	AXIAL LOC-Z IN	OUT	RADIUS IN	OUT	STREAM FUNCT IN	OUT	MERID ANGLE IN	OUT	ABS ANGLE IN	OUT	REL ANGLE IN	OUT	TOTAL PRESS IN	OUT	TOTAL TEMP IN	OUT
0.	7.32	0.184	6.292	51.404	40.549	0.	0.	-7.97	-7.97	0.	39.68	63.27	55.32	14.70	24.54	518.7	624.4
0.	14.34	0.020	6.419	39.413	38.758	0.100	0.100	-4.20	-3.89	0.	38.32	61.00	52.01	14.70	24.98	518.7	619.7
0.	21.62	-0.020	6.565	37.504	37.148	0.200	0.200	-1.80	-0.82	0.	38.20	58.56	49.69	14.70	26.27	518.7	616.1
0.	29.30	-0.137	6.713	35.523	35.516	0.300	0.300	0.46	1.55	0.	37.95	56.63	46.71	14.70	26.36	518.7	612.9
0.	37.50	-0.278	6.831	33.434	33.825	0.400	0.400	2.85	3.62	0.	38.42	54.86	43.66	14.70	25.23	518.7	610.4
0.	42.73	-0.389	6.900	31.202	32.823	0.500	0.500	5.13	5.72	0.	39.37	53.00	40.28	14.70	24.89	518.7	607.0
0.	44.77	-0.462	6.952	29.779	30.871	0.560	0.560	6.51	7.26	0.	39.75	51.89	38.13	14.70	24.60	518.7	605.1
0.	44.77	-0.478	6.968	29.226	30.423	0.583	0.583	7.04	8.07	0.	39.84	51.41	37.38	14.70	24.44	518.7	604.6
0.	48.25	-0.487	6.971	29.226	30.338	0.583	0.583	7.04	8.89	0.	40.04	51.41	37.16	14.70	24.44	518.7	604.0
0.	51.14	-0.514	6.995	28.277	29.562	0.620	0.620	8.03	9.89	0.	40.21	50.55	36.72	14.70	24.19	518.7	602.0
0.	56.16	-0.537	7.005	27.492	28.918	0.658	0.658	8.94	11.38	0.	40.23	49.83	34.45	14.70	23.95	518.7	600.1
0.	61.48	-0.562	7.001	26.127	27.791	0.700	0.700	10.68	12.23	0.	41.60	48.56	32.40	14.70	23.54	518.7	596.9
0.	64.48	-0.571	7.001	24.678	26.571	0.750	0.750	12.93	13.77	0.	41.91	47.22	30.91	14.70	23.04	518.7	593.1
0.	69.64	-0.567	7.000	23.863	25.876	0.777	0.777	14.40	14.56	0.	41.91	46.63	29.62	14.70	22.77	518.7	591.0
0.	76.49	-0.567	7.000	23.863	25.876	0.777	0.777	14.40	14.56	0.	41.91	46.53	29.62	14.70	22.77	518.7	591.0
0.	83.54	-0.558	7.027	22.460	24.706	0.820	0.820	17.09	13.19	0.	41.03	45.50	25.61	14.70	22.41	518.7	588.1
0.	90.95	-0.563	7.044	20.596	23.246	0.872	0.872	20.83	15.36	0.	39.63	44.30	20.62	14.70	21.93	518.7	584.2
0.	100.00	-0.563	7.044	20.596	23.246	0.872	0.872	20.83	15.36	0.	39.38	44.30	20.62	14.70	21.93	518.7	584.2
0.		-0.563	7.040	19.484	22.424	0.900	0.900	23.16	16.98	0.	39.38	43.79	17.92	14.70	21.66	518.7	582.3
0.		-0.538	7.041	17.207	20.845	0.950	0.950	28.36	20.71	0.	40.03	43.23	11.90	14.70	21.16	518.7	584.0
0.		-0.500	7.004	14.200	18.852	1.000	1.000	32.50	29.04	0.	39.95	42.12	1.46	14.70	20.72	518.7	579.5

MERID VEL IN	OUT	ABS VEL IN	OUT	REL VEL IN	OUT	BLADE SPEED IN	OUT	ABS MACH NO IN	OUT	REL MACH NO IN	OUT	BLKG IN	OUT	RCU IN	OUT
684.9	585.6	684.9	757.0	1511.0	1022.3	1346.9	1319.1	0.638	0.644	1.407	0.868	0.990	0.990	0.	19586.
712.6	618.2	712.6	777.0	1466.8	989.8	1282.1	1269.5	0.666	0.664	1.370	0.846	0.990	0.990	0.	18644.
746.4	614.8	746.4	782.4	1438.2	958.3	1228.0	1208.4	0.700	0.671	1.342	0.815	0.990	0.990	0.	17973.
761.2	627.6	761.2	795.0	1383.8	915.1	1155.6	1155.3	0.716	0.686	1.301	0.788	0.990	0.990	0.	17380.
766.4	632.1	766.4	806.3	1330.5	871.0	1087.6	1100.3	0.721	0.697	1.252	0.753	0.990	0.990	0.	16927.
765.5	628.6	765.5	811.5	1271.3	821.0	1015.0	1041.7	0.720	0.704	1.196	0.712	0.990	0.990	0.	16436.
764.7	626.2	764.7	811.0	1234.2	793.6	988.7	1004.2	0.719	0.706	1.161	0.698	0.990	0.990	0.	16048.
764.5	626.8	764.5	812.3	1220.0	784.3	968.0	989.6	0.719	0.707	1.147	0.683	0.990	0.990	0.	15948.
764.5	627.0	764.5	813.7	1220.0	782.3	958.7	986.9	0.719	0.708	1.147	0.681	0.990	0.990	0.	15739.
764.2	628.4	764.2	814.3	1196.0	767.1	950.7	961.7	0.719	0.710	1.126	0.669	0.990	0.990	0.	15539.
763.6	625.0	763.6	815.2	1176.3	756.5	919.9	940.7	0.719	0.712	1.106	0.661	0.990	0.990	0.	15361.
762.2	603.4	762.3	812.3	1142.5	734.2	894.3	904.0	0.718	0.712	1.074	0.643	0.990	0.990	0.	15021.
759.8	593.1	761.0	794.0	1107.0	696.0	849.9	864.4	0.717	0.696	1.041	0.611	0.990	0.990	0.	14419.
759.0	593.1	759.8	785.7	1086.2	677.0	802.8	841.7	0.714	0.698	1.021	0.594	0.990	0.990	0.	13717.
751.3	611.7	759.8	785.7	1086.2	677.0	776.3	803.7	0.714	0.699	1.021	0.595	0.990	0.990	0.	13335.
732.4	651.1	751.3	801.7	1048.0	675.0	738.6	756.2	0.705	0.707	0.984	0.595	0.990	0.990	0.	13335.
732.4	651.1	732.4	833.2	992.6	692.6	678.0	756.2	0.686	0.741	0.930	0.616	0.990	0.990	0.	12805.
719.1	668.1	732.4	833.2	992.6	692.6	678.0	729.5	0.686	0.741	0.930	0.616	0.990	0.990	0.	12087.
676.6	689.9	719.1	848.4	958.5	699.3	633.0	729.5	0.672	0.757	0.896	0.624	0.990	0.990	0.	12087.
605.7	812.6	676.6	877.4	878.1	703.2	559.7	674.1	0.629	0.788	0.817	0.631	0.990	0.990	0.	11725.
		605.7	1007.2	761.7	812.8	461.9	613.3	0.559	0.923	0.703	0.746	0.990	0.990	0.	11219.

BLADE ROW PRINTOUT FOR R1

(ENGLISH) UNITS *** EEE FAN STATION DATA

PCT IMM	RBAR	INC (INPUT)	X-FACT	DEV (C-R)	TURN	LOSS COEFF	CAMBER	STGR	SOL	TMC	D-FACT	CHORD	AXIAL VEL-R	EFFICIENCY ADIA	POLY	ACC PT RATIO	ACC TT RATIO
0.	40.917	5.40	0.	2.48	7.96	0.170	5.43	55.55	1.4062	0.0252	0.435	11.314	0.855	0.776	0.791	1.678	1.2038
7.75	39.081	4.66	0.	2.96	8.99	0.127	7.29	52.69	1.4304	0.0275	0.438	11.030	0.857	0.841	0.853	1.708	1.1948
14.93	37.326	4.95	0.	3.22	8.87	0.087	7.14	50.04	1.4781	0.0295	0.449	10.833	0.824	0.893	0.901	1.719	1.1878
22.32	35.528	5.50	0.	3.43	9.91	0.059	7.84	47.28	1.5132	0.0328	0.456	10.554	0.824	0.929	0.935	1.725	1.1817
30.05	33.629	5.06	0.	3.53	11.31	0.047	9.58	44.42	1.5427	0.0350	0.468	10.187	0.824	0.945	0.949	1.717	1.1769
38.30	31.611	5.70	0.	4.56	12.89	0.044	11.75	41.51	1.5890	0.0403	0.483	9.863	0.820	0.947	0.951	1.694	1.1718
43.56	30.325	5.73	0.	4.90	13.76	0.044	12.93	39.78	1.6221	0.0424	0.488	9.658	0.818	0.951	0.955	1.673	1.1667
45.61	29.024	5.60	0.	4.98	14.11	0.043	13.47	38.99	1.6369	0.0429	0.489	9.586	0.817	0.952	0.956	1.663	1.1645
45.79	29.782	5.05	0.	5.05	14.25	0.043	13.64	38.94	1.6382	0.0430	0.491	9.580	0.814	0.954	0.957	1.646	1.1606
49.31	28.920	5.65	0.	5.26	14.82	0.042	14.43	37.68	1.6646	0.0448	0.492	9.452	0.813	0.956	0.958	1.638	1.1578
52.23	28.285	5.55	0.	5.45	15.38	0.041	15.28	36.64	1.6872	0.0463	0.493	9.344	0.809	0.958	0.960	1.602	1.1508
57.33	26.959	5.00	0.	5.90	16.16	0.039	17.06	35.03	1.7282	0.0484	0.507	9.148	0.783	0.958	0.960	1.568	1.1434
62.79	25.625	4.75	0.	6.27	16.31	0.039	17.82	33.56	1.7731	0.0500	0.514	8.921	0.788	0.958	0.960	1.550	1.1394
65.88	24.870	4.68	0.	6.46	16.91	0.039	18.69	32.50	1.7982	0.0500	0.514	8.781	0.788	0.958	0.961	1.550	1.1394
65.88	24.070	4.68	0.	6.46	16.91	0.039	18.69	32.50	1.7982	0.0531	0.497	8.531	0.829	0.959	0.962	1.525	1.1339
71.14	23.583	4.65	0.	6.86	19.89	0.039	22.18	29.79	1.8424	0.0583	0.447	8.238	0.917	0.960	0.962	1.492	1.1264
77.94	21.951	4.72	0.	7.48	23.77	0.039	26.53	26.40	1.9140	0.0583	0.447	8.238	0.917	0.960	0.962	1.492	1.1264
77.94	21.951	4.72	0.	7.48	23.77	0.039	26.53	26.40	1.9140	0.0618	0.419	8.075	0.966	0.958	0.960	1.474	1.1226
81.89	20.954	4.50	0.	7.99	25.07	0.042	29.06	24.46	1.9628	0.0714	0.360	7.847	1.084	0.931	0.934	1.440	1.1162
89.78	19.026	5.25	0.	9.58	31.33	0.077	35.66	20.15	2.1005	0.0955	0.119	7.780	1.391	0.881	0.886	1.410	1.1173
100.00	16.526	3.50	0.	12.63	40.66	0.167	49.79	13.72	2.3976								

AOIA EFF	NB	INLET CORR RPM
0.917	32	3727.7

INLET CORR WTFLOW	PRLSS RATIO	TEMP RATIO
1419.16	1.6342	1.1646

BLADE ROW PRINTOUT FOR S1   (ENGLISH) UNITS *** EEE FAN STATION DATA

PCT EDGE IMM		AXIAL		LOC Z	RADIUS		INFRID ANGLE		ABS ANGLE		REL ANGLE		TOTAL PRESS		TOTAL TEMP	
IN	OUT	IN	OUT	OUT	IN	OUT	IN	OUT	IN	OUT	IN	OUT	IN	OUT	IN	OUT
0.	0.54	9.915	9.912	11.906	26.142	26.308	1.19	2.05	38.30	12.00			22.73	22.40	590.9	590.9
16.61	16.57	9.810	9.810	11.901	25.593	25.795	4.97	2.50	38.86	11.90			22.68	22.31	509.7	509.7
28.59	20.29	9.804	9.804	11.997	25.062	25.124	6.74	3.40	38.51	11.58			22.41	22.18	508.1	508.1
37.69	37.26	8.999	8.999	12.001	24.203	24.638	8.71	4.73	37.91	10.02			22.07	21.86	585.4	585.4
37.69	37.26	8.999	8.999	12.001	23.692	24.101	9.98	5.78	37.73	10.26			21.93	21.71	584.2	584.2
49.56	48.99	8.995	8.995	12.006	23.921	24.101	9.98	5.78	37.73	10.26			21.93	21.71	584.2	584.2
64.21	63.56	8.998	8.998	12.011	21.908	22.549	11.47	7.22	37.38	9.75			21.66	21.42	582.3	502.3
72.04	71.38	8.909	8.909	12.012	21.459	22.087	13.28	9.03	37.32	9.20			21.33	21.02	580.5	580.5
85.35	84.76	8.988	8.988	12.013	20.595	21.298	14.18	9.98	37.45	8.09			21.16	20.80	508.0	508.0
100.00	100.00	8.989	8.989	12.012	19.643	20.398	15.67	11.42	37.88	8.39			20.91	20.43	579.5	579.5
							17.01	12.18	38.79	8.00			20.72	20.10	579.5	579.5

MERID VEL		ABS VEL		REL VEL		STREAM FUNCT		TANG VEL		BLADE SPEED	ABS MACH NO		REL MACH NO		BLKG		RCU	
IN	OUT	IN	OUT	IN	OUT	IN	OUT	IN	OUT	IN	OUT	IN	OUT	IN	OUT	IN	OUT	
645.3	666.5	822.1	601.3			0.	0.	0.100	0.100		0.725	0.591			0.990	0.990	13318	3723
637.1	666.3	817.0	680.9			0.194	0.194	0.194	141.6		0.721	0.591			0.990	0.990	13090	3618
646.6	664.9	824.1	678.7			0.320	0.328	140.2			0.729	0.590			0.990	0.990	12805	3446
658.0	668.6	838.4	672.4			0.427	0.427	136.1			0.737	0.586			0.990	0.990	12301	3098
669.5	665.3	841.7	676.0			0.552	0.552	125.8			0.749	0.598			0.990	0.990	12007	2808
669.5	665.3	841.7	676.0			0.708	0.708	119.8			0.749	0.591			0.990	0.990	11725	2658
683.2	666.4	853.5	676.1			0.776	0.776	113.6			0.762	0.592			0.990	0.990	11407	2406
699.5	667.2	871.2	675.7			0.900	0.900	106.7			0.781	0.592			0.990	0.990	11301	2271
709.2	667.7	803.3	675.5			0.900	0.900	102.8			0.794	0.598			0.990	0.990	11213	2051
727.7	666.1	908.8	673.1			1.000	1.000	96.3			0.828	0.579			0.990	0.990	11219	1838
743.1	656.0	937.3	672.2					90.1			0.849							

PCT IMM	RBAR	INC (INPUT)	X-FACT	DEV (C-R)	TURN	STGR	CAMBER	LOSS COEFF	SOL	TMC	D-FACT	CHORD	AXIAL VEL-R	EFFICIENCY		ACC PT	ACC IF
														ADIA	POLY	RATIO	RATIO
0.	26.221	0.	0.	7.73	26.30	21.28	34.03	0.050	1.1466	0.0621	0.365	3.148	1.032	0.921	0.925	1.524	1.393
0.49	25.694	0.	0.	7.72	26.97	21.52	34.69	0.043	1.1852	0.0616	0.357	3.189	1.049	0.927	0.932	1.518	1.363
16.57	25.193	0.08	0.	7.60	26.92	21.21	34.45	0.035	1.2097	0.0611	0.363	3.191	1.034	0.933	0.937	1.509	1.339
28.45	24.457	0.15	0.	7.50	27.09	20.54	34.45	0.031	1.2454	0.0604	0.372	3.190	1.012	0.936	0.940	1.480	1.286
37.48	23.896	0.26	0.	7.46	27.47	20.14	34.66	0.031	1.2740	0.0590	0.376	3.188	1.004	0.935	0.939	1.470	1.264
49.29	23.164	0.48	0.	7.32	27.64	19.78	34.56	0.035	1.3134	0.0587	0.382	3.186	1.044	0.929	0.933	1.478	1.226
63.90	22.259	0.60	0.	7.23	20.12	19.34	34.76	0.050	1.3655	0.0569	0.394	3.183	0.987	0.904	0.909	1.430	1.191
71.73	21.773	0.75	0.	7.22	28.56	19.19	35.03	0.050	1.3960	0.0557	0.403	3.183	0.968	0.885	0.898	1.415	1.182
85.87	20.946	1.05	0.	7.23	29.49	19.08	35.67	0.065	1.4506	0.0531	0.425	3.182	0.956	0.843	0.858	1.398	1.173
100.00	20.020	1.50	0.	7.29	30.79	19.09	36.58	0.088	1.5176	0.0487	0.458	3.182	0.933	0.799	0.808	1.360	1.173

INLET CORR WTFLOW	INLET CORR RPM	AUIA EFF	TEMP RATIO	PRESS RATIO	NB
316.90	3727.7	0.949	1.1256	1.4505	68

127

BLADE ROW PRINTOUT FOR R2   (ENGLISH) UNITS *** EEE FAN STATION DATA

PCT EDGE ITM		AXIAL LOC-Z		RADIUS		STREAM FUNC		MERID ANGLE		ABS ANGLE		REL ANGLE		TOTAL PRESS		TOTAL TEMP	
IN	OUT	IN	OUT	IN	OUT	IN	OUT	IN	OUT	IN	OUT	IN	OUT	IN	OUT	IN	OUT
0.	0.	13.235	15.130	26.110	26.310	0.	0.100	0.69	-0.55	11.60	24.72	46.00	40.71	22.40	24.73	599.9	613.3
8.66	9.31	13.221	15.152	25.934	26.026	0.100	0.194	1.23	-0.72	11.47	23.94	45.42	40.00	22.31	24.73	509.7	610.0
16.66	17.66	13.206	15.177	25.375	25.373	0.194	0.320	2.15	-0.86	11.49	24.51	44.00	39.45	22.18	24.73	508.1	609.2
28.40	29.83	13.181	15.218	24.702	24.714	0.328	0.427	2.96	-0.08	10.30	24.51	44.49	37.05	21.71	24.73	505.4	608.4
37.34	38.99	13.160	15.254	24.190	24.218	0.427	0.427	2.96	-0.08	9.75	24.79	43.86	36.49	21.71	24.73	504.2	608.3
37.34	38.99	13.160	15.254	24.190	24.218	0.427	0.552	4.12	-0.00	9.24	25.78	43.06	36.49	21.42	24.73	502.3	608.6
49.02	58.87	13.126	15.307	23.528	23.575	0.552	0.700	5.05	-0.58	8.71	27.27	42.39	30.51	21.02	24.73	509.5	608.2
63.50	65.31	13.086	15.370	22.690	22.792	0.700	0.776	6.91	-0.26	8.42	28.12	42.00	28.22	20.80	24.73	510.0	611.7
71.28	72.91	13.064	15.406	22.244	22.381	0.776	0.908	8.93	0.32	7.98	29.56	41.53	23.74	20.43	24.73	5?9.5	615.1
84.61	85.55	13.026	15.468	21.400	21.696	0.908	0.908	8.93	0.32	7.63	30.71	41.00	18.65	20.10	24.73	579.5	610.7
100.00	100.00	12.988	15.540	20.598	20.913	1.000	1.000	10.93	1.07	7.63	30.71	41.00	18.65				

MERID VEL		ABS VEL		REL VEL		TANG VEL		BLADE SPEED		ABS MACH NO		REL MACH NO		AXIAL VEL R	BLKG		RCU		ACC PT RATIO	ACC TT RATIO
IN	OUT	IN	OUT	IN	OUT	IN	OUT	IN	OUT	IN	OUT	IN	OUT		IN	OUT	IN	OUT		
688.7	298.6	703.1	713.9	902.8	855.5	141.4		856.5	856.5	0.612	0.609	0.864	0.738	0.942	0.998	0.998	3723	7861	1.683	1.1824
690.1	290.9	704.2	713.0	903.2	851.7	140.4		840.4	840.4	0.613	0.610	0.856	0.729	0.943	0.998	0.998	3618	7513	1.683	1.1775
692.8	209.2	706.0	712.8	977.6	843.8	135.8		825.5	825.4	0.616	0.611	0.853	0.723	0.941	0.998	0.998	3446	7339	1.683	1.1745
690.8	297.3	702.1	716.7	968.0	825.8	125.4		803.6	804.0	0.614	0.615	0.846	0.708	0.945	0.998	0.998	3098	7348	1.683	1.1738
695.5	302.8	705.7	722.3	964.0	815.6	119.4		786.9	787.8	0.619	0.620	0.844	0.700	0.944	0.998	0.998	2888	7333	1.683	1.1728
695.5	302.8	705.7	722.3	964.0	815.6	119.4		786.9	787.8	0.619	0.630	0.844	0.700	0.944	0.998	0.998	2800	7333	1.603	1.1734
696.3	319.0	705.4	733.5	954.0	798.1	113.0		765.1	766.9	0.618	0.630	0.836	0.605	0.951	0.998	0.998	2658	7520	1.603	1.1734
696.2	346.0	704.0	755.1	940.1	779.0	106.1		738.1	741.4	0.617	0.649	0.819	0.670	0.969	0.998	0.998	2406	7886	1.603	1.1765
695.2	363.3	702.7	778.7	932.5	771.4	102.1		723.6	728.1	0.611	0.663	0.805	0.664	0.969	0.998	0.998	2271	8131	1.603	1.1794
689.6	397.5	696.0	805.9	916.2	765.0	95.5		698.7	705.8	0.611	0.694	0.805	0.659	1.029	0.998	0.998	2051	8625	1.683	1.1859
678.5	433.8	684.4	849.7	893.1	771.1	89.2		678.0	680.3	0.600	0.733	0.783	0.665	1.097	0.998	0.998	1838	9073	1.683	1.1929

										EFFICIENCY	
										ADIA	POLY
										0.888	0.809
										0.905	0.911
										0.928	0.926
										0.929	0.933
										0.929	0.934
										0.926	0.932
										0.910	0.916
										0.905	0.903
										0.864	0.873
										0.833	0.844

PCT IMM	RBAR (INPUT)	INC (INPUT)	X-FACT	DEV (C-R)	TURN	CAMBER	LOSS COEFF	STGR	SOL	TMC	D-FACT	CHORD
0.	26.330	0.72	0.	3.03	5.37	7.68	0.000	41.52	0.8462	0.0490	0.232	2.504
8.98	25.038	0.51	0.	2.97	5.27	7.72	0.052	41.85	0.8707	0.0490	0.222	2.523
17.15	25.374	0.37	0.	3.05	5.42	8.10	0.037	40.45	0.0952	0.0508	0.225	2.548
29.09	24.708	0.65	0.	3.27	6.64	9.26	0.031	39.21	0.9318	0.0540	0.242	2.583
38.14	24.294	0.68	0.	3.45	7.37	10.14	0.030	30.11	0.9614	0.0572	0.253	2.611
38.14	24.204	0.68	0.	3.45	7.37	10.14	0.030	30.11	0.9614	0.0572	0.253	2.611
49.91	23.548	0.84	0.	3.81	9.85	12.02	0.033	33.75	1.0036	0.0493	0.293	2.649
64.38	22.741	1.02	0.	4.18	11.89	15.25	0.033	32.28	1.0034	0.0729	0.303	2.608
72.87	22.312	1.06	0.	4.77	13.78	17.49	0.050	29.26	1.1357	0.0776	0.311	2.751
85.06	21.508	1.22	0.	5.51	17.79	22.08	0.050	29.26	1.2079	0.0011	0.298	2.813
100.00	20.755	1.24	0.	6.35	22.44	27.54	0.064	26.07	1.2079			

INLET CORR WFLOW	INLET CORR RPM	NB
316.98	3727.7	56

PRESS RATIO	TEMP RATIO	ADIA EFF
1.6030	1.1776	0.984

BLADE ROW PRINTOUT FOR SZIN

(ENGLISH) UNITS *** EEE FAN STATION DATA

PCT EDGE IMM IN	OUT	AXIAL LOC-Z IN	OUT	RADIUS IN	OUT	STREAM FUNCT IN	OUT	MERID ANGLE IN	OUT	ABS ANGLE IN	OUT	REL ANGLE IN	OUT	TOTAL PRESS IN	OUT	TOTAL TEMP IN	OUT
0.		22.129	23.882	23.068	21.733	0.	0.	-37.28	-36.78	39.93	2.56			24.73	24.51	630.3	639.3
11.30	21.65	20.864	23.286	22.813	21.147	0.218	0.218	-24.85	-37.10	38.32	2.51			24.73	24.63	600.6	600.6
34.93	44.91	19.499	22.493	22.279	29.517	0.477	0.477	-16.45	-37.31	37.13	2.51			24.73	24.59	610.7	610.2
48.21	57.60	18.895	22.005	21.988	20.173	0.689	0.689	-15.19	-37.39	31.65	2.52			24.73	24.55	611.7	611.7
71.76	78.32	17.995	21.386	21.448	19.612	0.826	0.826	-12.03	-38.18	31.02	2.54			24.73	24.39	615.1	615.1
100.00	100.00	17.015	20.593	20.818	19.025	1.000	1.000	-8.33	-39.82	32.35	2.60			24.73	24.17	618.7	618.7

MERID VEL IN	OUT	ABS VEL IN	OUT	REL VEL IN	OUT	TANG VEL IN	OUT	BLADE SPEED IN	OUT	ABS MACH NO IN	OUT	REL MACH NO IN	OUT	BLKG IN	OUT	RCU IN	OUT
477.3	535.1	573.4	535.5			317.9	18.7			0.485	0.452			0.998	0.998	7333	466.
459.6	534.6	565.5	535.0			329.7	18.7			0.478	0.451			0.998	0.998	7570	395.
587.7	536.6	686.1	536.9			354.0	18.7			0.586	0.452			0.998	0.998	7846	384.
621.9	537.7	723.6	538.0			369.9	18.8			0.619	0.453			0.998	0.998	8131	379.
683.9	539.5	793.3	539.9			402.1	18.8			0.682	0.453			0.998	0.998	8625	370.
695.6	536.8	821.0	537.1			436.0	18.7			0.706	0.449			0.998	0.998	9073	357.

PCT IMM	RBAR	INC (INPUT)	X-FACT	DEV (C-R)	TURN	LOSS COEFF	CAMBER	STGR	SOL	TMC	D-FACT	CHORD	AXIAL VEL-R	EFFICIENCY ADIA	POLY	ACC PT RATIO	ACC TT RATIO
0.	22.401	-12.50	2.00	16.00	37.37	0.060	65.95	19.46	1.2910	0.0301	0.275	2.839	1.099	0.912	0.918	1.668	1.728
16.94	21.980	-4.96	2.00	12.85	35.82	0.030	53.62	16.47	1.3859	0.0334	0.261	2.991	1.022	0.918	0.924	1.676	1.734
40.37	21.398	-5.10	2.00	10.98	29.61	0.029	45.70	14.38	1.4649	0.0352	0.392	3.077	0.757	0.899	0.906	1.673	1.765
53.33	21.077	-4.24	2.00	10.56	29.13	0.032	43.93	13.92	1.4920	0.0360	0.427	3.087	0.712	0.802	0.898	1.671	1.794
75.34	20.538	-2.43	2.00	9.81	28.47	0.051	40.71	13.09	1.5410	0.0372	0.484	3.106	0.634	0.839	0.858	1.660	1.459
100.00	19.918	-0.39	2.00	9.47	29.75	0.080	39.60	12.94	1.6015	0.0384	0.512	3.132	0.599	0.793	0.807	1.645	1.529

INLET CORR VTFLOW	PRESS RATIO	TEMP RATIO	ADIA EFF	INLET CORR RPM	NB
181.65	1.6676	1.1791	0.888	3727.7	64

BLADE ROW PRINTOUT FOR S2OUT   (ENGLISH) UNITS *** EEE FAN STATION DATA

PCT EDGE IMM		AXIAL LOC-Z		RADIUS		STREAM FUNCT		MERID ANGLE		ABS ANGLE		REL ANGLE		TOTAL PRESS		TOTAL TEMP	
IN	OUT	IN	OUT	IN	OUT	IN	OUT	IN	OUT	IN	OUT	IN	OUT	IN	OUT	IN	OUT
Ø.	Ø.	25.466	37.4ØØ	26.519	27.387	Ø.	Ø.	3.27	4.34	27.91	Ø.			24.73	24.19	613.3	613.3
24.18	2Ø.75	25.466	37.4ØØ	25.944	26.927	Ø.234	Ø.234	3.82	4.61	27.29	Ø.			24.73	24.15	61Ø.8	61Ø.8
45.33	4Ø.65	25.466	37.4ØØ	25.441	26.487	Ø.455	Ø.455	4.4Ø	4.87	27.22	Ø.			24.73	24.11	6Ø9.2	6Ø9.2
76.29	65.75	25.466	37.4ØØ	24.7Ø5	25.842	Ø.769	Ø.769	5.Ø4	5.25	28.Ø8	Ø.			24.73	24.Ø4	6Ø8.4	6Ø8.4
1ØØ.ØØ	1ØØ.ØØ	25.466	37.4ØØ	24.141	25.172	1.ØØØ	1.ØØØ	4.94	4.94	28.65	Ø.			24.73	23.95	6Ø8.3	6Ø8.3

MERID VEL		ABS VEL		REL VEL		TANG VEL		BLADE SPEED	ABS MACH NO		REL MACH NO		BLKG		RCU	
IN	OUT	IN	OUT	IN	OUT	IN	OUT	IN	IN	OUT	IN	OUT	IN	OUT	IN	OUT
569.6	655.3	634.2	655.3			296.4	Ø.		Ø.537	Ø.556			Ø.998	Ø.973	7861.	Ø.
562.6	651.6	632.7	651.6			289.6	Ø.		Ø.537	Ø.554			Ø.99Ø	Ø.973	7513.	Ø.
562.4	648.5	632.1	648.5			288.5	Ø.		Ø.537	Ø.552			Ø.99Ø	Ø.972	7339.	Ø.
559.6	645.1	633.7	645.1			297.4	Ø.		Ø.539	Ø.549			Ø.99Ø	Ø.972	7348.	Ø.
558.1	648.9	635.4	648.9			303.8	Ø.		Ø.541	Ø.546			Ø.99Ø	Ø.971	7333.	Ø.

PCT IMM	RBAR	INC (INPUT)	X-FACT	DEV (C-R)	TURN	LOSS COEFF	CAMBER	STGR	SOL	TMC	D-FACT	CHORD	AXIAL VEL-R	EFFICIENCY ADIA	POLY	ACC PT RATIO	ACC TT RATIO
Ø.	26.953	-1.27	Ø.	4.87	27.91	Ø.123	34.Ø5	12.15	2.5932	Ø.Ø587	Ø.Ø55	12.916	1.167	Ø.84Ø	Ø.851	1.646	1.824
22.53	2Ø.436	-1.Ø9	Ø.	4.7Ø	27.29	Ø.132	33.Ø8	11.84	2.6222	Ø.Ø584	Ø.Ø56	12.81Ø	1.157	Ø.86Ø	Ø.87Ø	1.643	1.775
43.Ø7	25.964	-Ø.95	Ø.	4.64	27.22	Ø.141	32.81	11.77	2.6421	Ø.Ø582	Ø.Ø59	12.677	1.152	Ø.872	Ø.88Ø	1.641	1.745
73.14	25.273	-Ø.91	Ø.	4.73	28.Ø8	Ø.157	33.72	12.13	2.7Ø45	Ø.Ø578	Ø.Ø67	12.631	1.152	Ø.874	Ø.882	1.636	1.74Ø
1ØØ.ØØ	24.656	-Ø.86	Ø.	4.67	28.65	Ø.175	34.18	12.42	2.8512	Ø.Ø572	Ø.Ø73	12.992	1.148	Ø.868	Ø.877	1.63Ø	1.7Ø8

INLET CORR WTFLOW	PRESS RATIO	TEMP RATIO	ADIA EFF	INLET CORR RPM	NB
135.25	1.6393	1.1755	Ø.865	3727.7	34

BLADE ROW PRINTOUT FOR OGV   (ENGLISH) UNITS *** EEE FAN STATION DATA

PCT EDGE IMM IN	OUT	AXIAL LOC-Z IN	OUT	RADIUS IN	OUT	MERID ANGLE IN	OUT	STREAM FUNCT IN	OUT	ABS ANGLE IN	OUT	REL ANGLE IN	OUT	TOTAL PRESS IN	OUT	TOTAL TEMP IN	OUT
0.	0.	26.900	37.400	40.450	40.450	0.	0.	0.	0.	35.65	0.			24.54	24.01	624.4	624.4
13.20	13.20	27.140	37.452	38.727	30.788	0.15	1.01	0.129	0.129	34.05	0.			24.98	24.57	619.7	619.7
24.05	23.73	27.170	37.426	37.310	37.449	0.25	1.45	0.257	0.257	33.29	0.			25.27	24.92	616.1	616.1
35.17	34.53	27.049	37.399	35.858	36.003	0.24	1.97	0.386	0.386	33.20	0.			25.35	25.03	612.9	612.9
46.78	45.77	26.772	37.398	34.352	34.661	0.18	2.54	0.515	0.515	33.81	0.			25.23	24.90	618.4	618.4
59.00	57.77	26.475	37.400	32.745	33.114	0.20	3.13	0.644	0.644	34.77	0.			24.89	24.52	607.8	607.8
72.21	70.80	26.168	37.401	31.021	31.486	0.28	3.74	0.772	0.772	35.38	0.			24.33	23.87	603.1	603.1
77.48	76.23	26.033	37.401	30.333	30.809	0.17	3.97	0.820	0.820	35.60	0.			24.06	23.56	600.9	600.9
77.48	76.23	26.033	37.401	30.333	30.809	0.17	3.97	0.820	0.820	35.60	0.			24.06	23.56	600.9	600.9
79.39	78.20	25.986	37.401	30.083	30.568	0.15	4.05	0.837	0.837	35.67	0.			23.95	23.44	600.1	600.1
86.85	86.04	25.804	37.399	29.109	29.568	-0.00	4.35	0.901	0.901	35.94	0.			23.54	22.97	596.9	596.9
94.87	94.90	25.600	37.397	28.062	28.449	-0.32	4.69	0.966	0.966	36.03	0.			23.05	22.41	593.1	593.1
100.00	100.00	25.483	37.395	27.392	27.803	-0.59	4.73	1.000	1.000	36.13	0.			22.77	22.09	590.9	590.9

MERID VEL IN	OUT	ABS VEL IN	OUT	REL VEL IN	OUT	TANG VEL IN	OUT	BLADE SPEED IN	OUT	ABS MACH NO IN	OUT	REL MACH NO IN	OUT	BLKG IN	OUT	RCU IN	OUT
672.5	680.0	827.5	680.0			482.3	0.			0.709	0.573			0.990	0.990	19508	0.
712.3	705.7	859.7	705.7			481.3	0.			0.742	0.599			0.990	0.990	18639	0.
733.5	715.7	877.5	715.7			481.6	0.			0.762	0.610			0.990	0.990	17968	0.
748.7	715.4	885.2	715.4			484.7	0.			0.771	0.611			0.990	0.990	17382	0.
735.0	705.2	885.5	705.2			492.7	0.			0.773	0.603			0.990	0.990	16924	0.
723.0	682.1	880.2	682.1			502.0	0.			0.770	0.583			0.990	0.990	16439	0.
706.4	641.4	866.5	641.4			501.7	0.			0.760	0.548			0.990	0.990	15564	0.
698.4	628.0	859.0	628.0			500.0	0.			0.754	0.531			0.990	0.990	15167	0.
698.4	628.0	859.0	628.0			500.0	0.			0.754	0.531			0.990	0.990	15107	0.
695.4	612.6	856.0	612.6			499.2	0.			0.752	0.524			0.990	0.990	15017	0.
683.7	578.7	844.4	578.7			495.6	0.			0.743	0.495			0.990	0.990	14426	0.
672.5	535.1	831.6	535.1			489.1	0.			0.733	0.457			0.990	0.990	13725	0.
666.0	507.2	824.6	507.2			486.2	0.			0.727	0.434			0.990	0.990	13318	0.

PCT IMM	RBAR	INC (INPUT)	X-FACT	DEV (C-R)	TURN	ADIA EFF	CAMBER	LOSS COEFF	STGR	SOL	TMC	D-FACT	CHORD	AXIAL VEL-R	EFFICIENCY ADIA	POLY	ACC PT RATIO	ACC TT RATIO
0.	40.450	1.00	0.	8.27	35.65	0.879	42.92	0.076	13.19	1.4500	0.0723	0.379	10.839	1.011	0.739	0.757	1.634	1.2038
13.20	38.753	1.00	0.	7.81	34.05		40.85	0.054	12.62	1.4636	0.0736	0.378	10.481	0.991	0.813	0.826	1.672	1.1948
23.89	37.388	1.00	0.	7.45	33.29		39.74	0.043	12.42	1.5172	0.0731	0.365	10.488	0.975	0.868	0.878	1.696	1.1878
34.85	35.978	1.00	0.	7.18	33.20		39.38	0.039	12.51	1.5054	0.0712	0.362	10.671	0.965	0.906	0.913	1.703	1.1817
46.24	34.506	1.00	0.	7.07	33.81		39.87	0.039	12.87	1.7004	0.0680	0.366	10.894	0.957	0.918	0.924	1.695	1.1769
58.40	32.945	1.00	0.	7.01	34.77		40.79	0.046	13.38	1.0271	0.0662	0.388	11.124	0.942	0.918	0.924	1.669	1.1718
71.55	31.254	1.00	0.	6.84	35.38		41.22	0.059	13.77	1.9732	0.0635	0.405	11.396	0.906	0.915	0.921	1.624	1.1627
76.66	30.571	1.00	0.	6.76	35.60		41.36	0.066	13.92	2.0374	0.0624	0.419	11.511	0.887	0.912	0.918	1.603	1.1586
76.86	30.571	1.00	0.	6.76	35.60		41.36	0.066	13.92	2.0374	0.0624	0.419	11.511	0.887	0.912	0.918	1.603	1.1586
78.80	30.322	1.00	0.	6.73	35.67		41.40	0.069	13.97	2.0617	0.0620	0.425	11.553	0.879	0.918	0.916	1.595	1.1549
86.45	29.339	1.00	0.	6.68	35.94		41.54	0.080	14.17	2.1607	0.0606	0.449	11.715	0.844	0.903	0.909	1.563	1.1409
94.88	28.255	1.00	0.	6.42	36.03		41.45	0.093	14.38	2.2778	0.0590	0.405	11.894	0.793	0.895	0.901	1.525	1.1419
100.00	27.598	1.00	0.	6.33	36.13		41.46	0.100	14.40	2.3552	0.0581	0.509	12.002	0.759	0.869	0.895	1.501	1.1441

INLET CORR WTFLOW	INLET CORR RPM	PRESS RATIO	TEMP RATIO	ADIA EFF	NB
1102.26	3727.7	1.6517	1.1757	0.879	34

NOMENCLATURE FOR APPENDIX A

PCT Edge IMM	Percent Immersion from OD
Axial Loc-Z	Axial Location (Z) of Leading and Trailing Edge Station ~ cm (in.)
Radius	Inlet and Exit Radii, cm (in.)
Merid Angle	Inlet and Exit Slope, degrees
Stream Funct	Inlet and Exit Streamline Percent Flow from OD
Merid Angle	Inlet and Exit Meridional Angle of Streamline, degrees
Abs Angle	Inlet and Exit Absolute Air Angle, degrees
Rel Angle	Inlet and Exit Relative Air Angle, degrees
Total Press	Inlet and Exit Total Pressure, Kilo-Pascals (psia)
Total Temp	Inlet and Exit Total Temperature, Degrees Kelvin (° R)
Merid Vel	Inlet and Exit Meridional Velocity, m/sec (ft/sec)
Abs Vel	Inlet and Exit Absolute Velocity, m/sec (ft/sec)
Rel Vel	Inlet and Exit Relative Velocity, m/sec (ft/sec)
Tang Vel	Inlet and Exit Tangential Velocity, m/sec (ft/sec)
Blade Speed	Inlet and Exit Blade Speed, m/sec (ft/sec)
Abs Mach No.	Inlet and Exit Absolute Mach Number
Rel Mach No.	Inlet and Exit Relative Mach Number
Blade Blkg	Inlet and Exit Station Blockage
RCU	Inlet and Exit Radius x Tang Vel, cm-m/sec (in.-ft/sec)
Efficiency Adia	Accumulative Adiabatic Efficiency
Efficiency Poly	Accumulative Polytropic Efficiency
RBAR	Average Radius, cm (in.)
INC	Incidence Angle, degrees
XFACT	Empirical Adjustment Factor to Carter's Rule Deviation, degrees
DEV (C-R)	Carter's Rule Deviation Angle, degrees
TURN	Turning Angle, degrees
Loss Coeff	Total-Pressure Loss Coefficient
CAM	Camber Angle, degrees
STGR	Stagger Angle, degrees
SOL	Solidity
TMC	Maximum Thickness-to-Chord Ratio

132

NOMENCLATURE FOR APPENDIX A (Concluded)

D-FACT	Diffusion Factor
Chord	Airfoil Chord Length, cm (in.)
Axial VEL-R	Exit/Inlet Axial Velocity Ratio
ACC PT Ratio	Accumulative Total Pressure Ratio
ACC TT Ratio	Accumulative Total Temperature Ratio
Inlet Corr Wt_{Flow}	Fan Inlet Corrected Weight Flow, kg/sec (lbm/sec)
Press Ratio	Accumulative Average Total Pressure Ratio
Temp Ratio	Accumulative Average Total Temperature Ratio
ADIA EFF	Accumulative Average Adiabatic Efficiency
Inlet Corr RPM	Fan Inlet Corrected Revolutions Per Minute
NB	Number of Blades

Appendix B: Fan Rotor Blade Plane Section Geometry.

	Percent Blade Ht	Section Ht cm	in.	Chord cm	in.	Stagger deg	Camber deg	Tm/c	β*LE deg	β*TE deg
	-9	-5.690	-2.240	18.771	7.390	-2.67	81.38	0.1286	39.59	-41.80
S.A. ID	0	0	0	19.068	7.507	6.18	69.61	0.1002	39.27	-30.34
	5	3.117	1.227	19.418	7.645	10.79	62.09	0.0852	39.25	-22.84
	10	6.233	2.454	19.881	7.827	15.15	52.80	0.0728	39.42	-13.38
	15	9.350	3.681	20.401	8.032	19.19	44.99	0.0650	39.84	-5.16
	20	12.466	4.908	20.907	8.231	22.65	37.75	0.0603	40.46	2.71
	25	15.583	6.135	21.394	8.423	25.60	31.83	0.0561	41.15	9.32
	30	18.700	7.362	21.928	8.633	28.35	27.49	0.0524	41.87	14.38
	35	21.815	8.589	22.449	8.838	30.92	23.86	0.0494	42.77	18.90
	40	24.931	9.815	22.941	9.032	33.31	20.83	0.0473	43.85	23.02
	45	28.047	11.042	23.449	9.232	35.46	19.31	0.0457	45.02	25.71
	50	31.164	12.269	23.955	9.431	37.46	18.58	0.0443	46.13	27.54
	55	34.280	13.496	24.425	9.616	39.29	17.53	0.0429	47.01	29.48
	60	37.397	14.723	24.925	9.813	41.21	16.42	0.0412	47.94	31.52
	65	40.513	15.950	25.441	10.016	43.23	15.59	0.0387	49.16	33.57
	70	43.630	17.177	25.946	10.215	45.25	14.62	0.0357	50.40	35.78
	75	46.746	18.404	26.469	10.421	47.47	13.24	0.0331	51.57	38.33
	80	49.862	19.631	26.990	10.626	49.81	11.88	0.0310	52.91	41.03
	85	52.979	20.858	27.483	10.820	52.11	10.67	0.0294	54.44	43.77
	90	56.095	22.085	27.935	10.998	54.20	9.48	0.0281	56.02	46.53
	95	59.211	23.312	28.336	11.156	55.99	8.27	0.0267	57.55	49.28
S.A. OD	100	62.328	24.538	28.715	11.305	57.60	6.75	0.0252	58.99	52.25
	102.5	63.653	25.060	28.880	11.370	58.27	6.21	0.0246	59.56	53.35

NB = 32

Stacking Axis:

R_{OD} = 103.901 cm (40.9061 in.)
R_{ID} = 41.757 cm (16.4399 in.)
Z = 8.192 cm (3.2253 in.)

Appendix C: Stator 1 Plane Section Geometry.

Percent Blade Ht	Section Ht cm	Section Ht in.	Chord cm	Chord in.	Stagger deg	Camber deg	Tm/c	β^*_{LE} deg	β^*_{TE} deg
-6.6	-1.037	-0.408	8.103	3.190	19.48	41.48	0.0463	40.88	-0.60
0	0	0	8.103	3.190	19.01	39.17	0.0486	38.92	-0.25
10	1.568	0.617	8.103	3.190	18.53	37.06	0.0518	36.83	-0.23
20	3.136	1.235	8.103	3.190	18.50	36.12	0.0541	36.48	0.36
30	4.704	1.852	8.103	3.190	18.66	35.60	0.0558	36.54	0.94
40	6.271	2.469	8.103	3.190	18.92	35.18	0.0573	36.71	1.53
50	7.839	3.086	8.103	3.190	19.25	34.97	0.0584	37.10	2.13
60	9.407	3.703	8.103	3.190	19.66	34.88	0.0593	37.54	2.66
70	10.975	4.321	8.103	3.190	20.15	34.64	0.0601	37.87	3.23
80	12.542	4.938	8.103	3.190	20.66	34.36	0.0608	38.23	3.87
90	14.110	5.555	8.103	3.190	21.02	34.20	0.0614	38.54	4.34
100	15.679	6.173	8.103	3.190	21.10	33.84	0.0621	38.36	4.52
101.2	15.869	6.248	8.103	3.190	21.10	33.38	0.0622	38.35	4.97

NB = 60

Stacking Axis:

R_{OD} = 66.612 cm (26.2250 in.)
R_{ID} = 50.933 cm (20.0523 in.)
Zsa = 26.671 cm (10.5005 in.)

Appendix D: Quarter-Stage Rotor Plane Section Geometry.

Percent Blade Ht	Section Ht cm	Section Ht in.	Chord cm	Chord in.	Stagger deg	Camber deg	Tm/c	β_{LE}^* deg	β_{TE}^* deg
-5.29	-0.744	-0.293	7.153	2.816	22.65	35.75	0.0826	40.09	4.33
0	0.010	0.004	7.102	2.796	23.91	33.40	0.0813	40.40	7.00
3.74	0.527	0.207	7.069	2.783	24.78	32.00	0.0805	40.47	8.47
12.77	1.796	0.707	6.995	2.754	26.93	27.51	0.0781	40.70	13.19
21.80	3.066	1.207	6.927	2.727	29.04	23.36	0.0752	41.03	17.67
30.83	4.336	1.707	6.861	2.701	31.01	19.60	0.0715	41.41	21.81
39.86	5.606	2.207	6.795	2.675	32.78	16.55	0.0670	41.91	25.37
48.89	6.876	2.707	6.728	2.649	34.45	14.22	0.0624	42.50	28.28
57.92	8.146	3.207	6.657	2.621	36.18	12.23	0.0586	43.05	30.82
66.95	9.416	3.707	6.586	2.593	37.53	10.65	0.0553	43.63	32.98
75.98	10.686	4.207	6.520	2.567	38.63	9.40	0.0525	44.17	34.77
85.01	11.956	4.707	6.452	2.540	39.62	8.53	0.0503	44.61	36.08
94.03	13.226	5.207	6.386	2.514	40.38	8.27	0.0488	45.03	36.76
100.00	14.065	5.537	6.348	2.499	40.79	8.21	0.0490	45.22	37.02

NB = 56

Stacking Axis:
R_{OD} = 66.878 cm (26.330 in.)
R_{ID} = 52.813 cm (20.793 in.)
Z = 39.901 cm (14.134 in.)

Appendix E: Inner OGV Plane Section Geometry.

Percent Blade Ht	Section Ht cm	Section Ht in.	Chord cm	Chord in.	Stagger deg	Camber deg	Tm/c	β_{LE}^* deg	β_{TE}^* deg
-33.0	-3.835	-1.510	9.353	3.682	14.77	57.91	0.0552	52.13	-5.78
-21.8	-2.54	-1.00	9.327	3.672	16.04	57.34	0.0544	52.12	-5.22
-10.9	-1.27	-0.50	9.299	3.661	17.26	56.09	0.0536	51.46	-4.63
0	0	0	9.253	3.643	18.40	55.38	0.0530	51.40	-3.98
10.9	1.27	0.50	9.177	3.613	19.41	55.18	0.0526	51.89	-3.28
21.8	2.54	1.00	9.042	3.560	20.22	55.02	0.0524	52.21	-2.81
32.7	3.81	1.50	8.832	3.477	20.74	53.85	0.0526	52.14	-1.71
43.7	5.08	2.00	8.560	3.370	20.93	53.71	0.0529	52.79	-0.92
54.6	6.35	2.50	8.189	3.224	20.84	54.70	0.0535	53.96	-0.74
65.5	7.62	3.00	7.663	3.017	20.60	56.39	0.0546	54.89	-1.51
76.4	8.89	3.50	7.023	2.765	20.08	57.76	0.0563	55.07	-2.69
87.3	10.16	4.00	6.320	2.488	19.80	59.17	0.0586	54.66	-4.51
100	11.63	4.58	5.433	2.139	21.53	62.38	0.0625	53.79	-8.59
109.1	12.70	5.00	4.785	1.884	24.48	65.46	0.0664	53.78	-11.68

NB = 64

Appendix F: Bypass OGV Plane Section Geometry.

Section Radius cm	in.	Chord cm	in.	Stagger deg	Camber deg	Tm/c	β^*_{LE} deg	β^*_{TE} deg
Vane I								
60.96	24	31.255	12.305	14.52	16.20	0.0561	25.92	9.72
66.04	26	31.103	12.245	13.39	14.56	0.0574	25.40	10.83
68.58	27	31.440	12.378	15.39	24.96	0.0572	35.32	10.37
76.20	30	29.804	11.734	13.87	24.25	0.0619	35.83	11.57
86.36	34	27.722	10.914	12.27	25.53	0.0686	36.49	10.96
93.98	37	26.581	10.465	11.90	28.47	0.0734	37.26	8.78
104.14	41	27.734	10.919	14.78	38.73	0.0725	41.71	2.98
Vane II								
50.96	24	31.262	12.308	14.57	22.40	0.0561	25.91	3.51
66.04	26	31.110	12.248	13.46	20.78	0.0574	25.41	4.63
68.58	27	31.440	12.378	15.39	30.57	0.0572	35.42	4.85
76.20	30	29.804	11.734	13.87	30.22	0.0619	35.88	5.66
86.36	34	27.722	10.914	12.27	32.27	0.0686	36.46	4.19
93.98	37	26.581	10.465	11.90	36.48	0.0734	37.16	0.68
104.14	41	27.734	10.919	14.78	42.14	0.0725	41.43	-0.71
Vane III (nominal)								
60.96	24	31.278	12.314	14.67	29.20	0.0562	25.86	-3.34
66.04	26	31.079	12.236	13.55	27.52	0.0575	25.42	-2.10
68.58	27	31.440	12.378	15.42	36.92	0.0572	35.64	-1.28
76.20	30	29.804	11.734	13.86	37.39	0.0619	35.98	-1.41
53.36	34	27.722	10.914	12.36	39.02	0.0686	36.42	-2.60
93.98	37	26.581	10.465	12.18	41.97	0.0734	36.98	-4.99
104.14	41	27.734	10.919	14.71	46.54	0.0725	41.18	-5.36
Vane IV								
50.96	24	31.295	12.321	14.80	35.83	0.0562	25.85	-9.98
66.04	26	31.140	12.260	13.68	34.06	0.0574	25.43	-8.63
68.58	27	31.440	12.378	15.44	42.98	0.0572	35.71	-7.27
76.20	30	29.804	11.734	13.89	44.06	0.0619	36.03	-8.03
83.36	34	27.722	10.914	12.28	45.80	0.0686	36.37	-9.43
93.98	37	26.581	10.465	11.91	47.55	0.0734	36.87	-10.68
104.14	41	27.734	10.919	14.78	50.83	0.0725	41.06	-9.77
Vane V								
60.96	24	31.300	12.323	14.83	41.90	0.0561	25.89	-16.00
66.04	26	31.145	12.262	13.73	39.85	0.0574	25.39	-14.46
68.58	27	31.440	12.378	15.46	48.37	0.0572	35.84	-12.53
76.20	30	29.804	11.734	13.90	50.19	0.0619	36.09	-14.10
83.36	34	27.722	10.914	12.29	51.91	0.0686	36.31	-15.60
93.98	37	26.581	10.465	11.91	52.62	0.0734	36.68	-15.94
104.14	41	27.734	10.919	14.78	54.82	0.0725	40.88	-13.94

No. of Vanes = 34

Vane Type	Vane No.	Circumferential Location (deg)
I	2-6	10.6 - 52.9
II	7-12	63.5 - 116.5
III	1, 13-23	0, 127.1 - 232.9
IV	24-29	243.5 - 296.5
V	30-34	307.1 - 349.4

END

DATE

FILMED

MAR 29 1983